The Journal of
Gemmology
2013 / Volume 33 / Nos. 7–8

SSEF
SCHWEIZERISCHES GEMMOLOGISCHES INSTITUT
SWISS GEMMOLOGICAL INSTITUTE
INSTITUT SUISSE DE GEMMOLOGIE

Gem-A
THE GEMMOLOGICAL ASSOCIATION OF GREAT BRITAIN

The Gemmological Association of Great Britain

21 Ely Place, London EC1N 6TD, UK
T: +44 (0)20 7404 3334 **F:** +44 (0)20 7404 8843
E: information@gem-a.com **W:** www.gem-a.com

Registered Charity No. 1109555
Registered office: Palladium House, 1–4 Argyll Street, London W1F 7LD

The Journal of Gemmology

The Editor-in-Chief is glad to consider original articles shedding new light on subjects of gemmological interest for publication in *The Journal of Gemmology*. A guide to the preparation of typescripts for publication in *The Journal* is given on our website, or contact the Production Editor at the Gemmological Association of Great Britain.

Any opinions expressed in *The Journal of Gemmology* are understood to be the views of the contributors and not necessarily of the publishers.

Editorial

A fond farewell to Dr Roger Harding

This issue marks a change in the editorship of *The Journal of Gemmology,* with Dr Roger Harding retiring and Brendan Laurs stepping in. Roger has been named Editor Emeritus in recognition of his nearly two decades of editing *The Journal*, and he remains active with proofreading the articles and giving sage advice borne of his long experience.

Roger began editing *The Journal* in 1994, when he succeeded Alan Jobbins, who came after John Chisholm and Gordon Andrews. Roger drew on his academic background in geology and mineralogy to raise the stature of *The Journal* in the scientific community. He recognized that gemmologists everywhere, and laboratory gemmologists in particular, face increasingly complex problems of identification that require more sophisticated solutions. Authors who have worked with Roger will remember his meticulous attention to detail and sympathetic rewriting if English was not the author's first language. This is an ethic which we will endeavour to continue.

On behalf of Gem-A, I would like to thank Roger for his many years of tireless service. Under his leadership *The Journal* became the most-circulated academic journal on gemmology, and with Brendan taking the helm, I'm sure it will continue to grow. A trained gemmologist, Brendan also has a master's degree in geology and 15 years of experience with *Gems & Gemology*, most recently as Editor and Technical Specialist. He has written extensively on the geology of gem deposits and is well known in the international gemmological research community.

James Riley
Gem-A Chief Executive
Executive Editor, *The Journal of Gemmology*

Exciting changes ahead for *The Journal*

I am very pleased to carry forward the legacy of Dr Roger Harding and those who came before him at the helm of *The Journal of Gemmology*. With the support of The Swiss Gemmological Institute SSEF and my colleagues at Gem-A, *The Journal* will evolve in exciting ways to meet the needs of today's gemmologists, researchers and enthusiasts. Starting in 2014, *The Journal* will be printed quarterly (rather than once per year), and digital versions of the articles in PDF format will be more easily accessible via Gem-A's updated website. In addition, readers will enjoy an updated design.

The Journal will continue to publish high-quality peer-reviewed feature articles describing cutting-edge laboratory studies and field research, whilst also introducing new sections that provide readers with announcements of new technological advancements, tips on practical gemmology, conference reports, learning opportunities and more. See *The Journal* on the Gem-A website for more information. A balance of regular columns, occasional sections and feature articles will deliver useful information that will increase readers' knowledge, enjoyment and effectiveness in their gemmological pursuits.

You will notice on the masthead of the present issue that we have expanded the team of Associate Editors. These experts are critical to the peer-review process that is the foundation of *The Journal,* as they ensure the technical accuracy and appropriateness of the feature articles. I feel very fortunate to have their support as we move toward making *The Journal* the preeminent publication of the international gemmological community.

Brendan Laurs
Editor-in-Chief, *The Journal of Gemmology*

SSEF

SCHWEIZERISCHES GEMMOLOGISCHES INSTITUT
SWISS GEMMOLOGICAL INSTITUTE
INSTITUT SUISSE DE GEMMOLOGIE

ORIGIN DETERMINATION · TREATMENT DETECTION

DIAMOND GRADING · PEARL TESTING

EDUCATION · RESEARCH

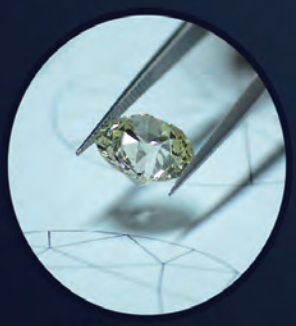

THE SCIENCE OF GEMSTONE TESTING©

28 February - 2 March 2014 Hong Kong Central office
3 - 7 March 2014 Asia World Expo
5 - 9 March 2014 Convention and Exhibition Centre Booth no. 5CON-008
Tel.: **+852 649 649 94** (local)

Falknerstrasse 9 CH-4001 Basel Switzerland Tel. +41 61 262 06 40 Fax + 41 61 262 06 41 admin@ssef.ch www.ssef.ch

Peñas Blancas: An historic Colombian emerald mine

Ron Ringsrud and Edward Boehm

Abstract: The Peñas Blancas emerald mine is part of Colombia's Muzo mining region, an 800 km^2 area that encompasses the famous Muzo, Coscuez and La Pita mines. This is the largest emerald district in Colombia, and it is the most productive and well-known emerald mining region in the world. Peñas Blancas has a fascinating and turbulent history, which sheds light on that of the entire Colombian emerald industry. Just as important, Peñas Blancas is finally accessible after more than 20 years of being closed to outsiders. This article describes the history, geology and gemmology of Peñas Blancas emeralds, and compares this historic mine to other famous producers in the region.

Keywords: Colombia, emerald, geology, inclusions, Peñas Blancas, RI, SG, trapiche

Introduction

From ancient artisanal beginnings with the Chibcha and Muzo Indians, the emerald mines of Colombia have supplied the world with fine material for hundreds of years. When the Spaniards, led by Hernán Cortés, conquered Mexico almost 500 years ago, legend has it that Aztec ruler Montezuma was adorned in gold and emeralds. The Spanish conquistador Francisco Pizarro also found emeralds, now known to be from Colombia, as far south as what are now Ecuador, Peru and Chile. After the conquered treasures made their way to Spain, the Spanish traded the emeralds with the Persians for gold. Thus, Colombian mines have been supplying the world with emeralds since the mid-1500s.

A relatively unknown Colombian emerald deposit is Peñas Blancas, located in the famous Muzo mining district. This mine has rarely been mentioned in gemmological literature except as an historical footnote. Long thought to be depleted, Peñas Blancas closed in the early 1980s because of a decades-long conflict between the two controlling families of the area. This conflict was finally resolved in late 2003, and by March 2004 the Peñas Blancas mine was producing high-quality rough. The authors are aware of one parcel yielding 270 carats of faceted emeralds that sold for US$810,000 ($3,000/ct). The authors first visited the mine in late 2004, and subsequent trips by one of us (RR) revealed good potential for future production, although mining continues slowly in the absence of investment and technology.

Peñas Blancas emeralds are known among local dealers for their exceptional colour and transparency. Although Peñas Blancas is hosted by a geological formation that is somewhat different from the three other Muzo-region mines, the fine quality of the emeralds (e.g., *Figure 1*) is similar to its more famous neighbours. The history of the mine has had a significant impact on the development of the entire Muzo district, and eventually Peñas Blancas may be partially responsible for the revival of this important mining region.

Figure 1: This superb mineral specimen taken from Peñas Blancas in February 2004 beautifully displays a cluster of emeralds that surround a quartz crystal. Quartz is more common in the emerald-mineralized zone at Peñas Blancas than at other Colombian localities. The specimen measures 55×65×90 mm and is courtesy of the Roz and Gene Meieran Collection; photo by Harold and Erica Van Pelt.

Early history

According to general understanding in Bogotá's emerald trade, Peñas Blancas attained significance in 1959 when a large emerald pocket started a bonanza that revived a dormant national industry and launched the careers of many of its principal players. Formerly known as *Peña Blanca*, the mine first appeared on a sketch map published by J. Pogue (1916; see *Figure 2*). At the turn of the 20th century, Pogue along with Charles Olden and Robert Sheibe (Sinkankas, 1981), were among the few geologist-explorers who were adding to the published knowledge about gem occurrences in Colombia. After World War II, Victor Oppenheim was the first of many geologists assessing petroleum and coal deposits in South America, and he briefly mentioned the Peñas Blancas mine: "...Tambrias or Peña Blanca mine — This mine is located some 25 km northeast of Muzo but as is the case of the La Chapa mine, very little is now known of the emeralds there, as the mine has not been worked for a considerable time" (Oppenheim, 1948, p. 37). Apparently, after the passage of many decades and two World Wars, the Peñas Blancas prospect was nearly forgotten.

The rediscovery of Peñas Blancas as a source of fine emeralds is now legendary. Since 1955, San Pablo de Borbur has been the closest town to the Peñas Blancas mine. From Borbur, mules would take locals to the Peñas Blancas area once a week for agricultural work. Those *campesinos* would sometimes find emeralds on the ground and, not knowing what they were, simply give them away. According to a local legend, in 1958 a mule driver showed a Peñas Blancas emerald to one of his relatives in Muzo, and within a few months the rush began.

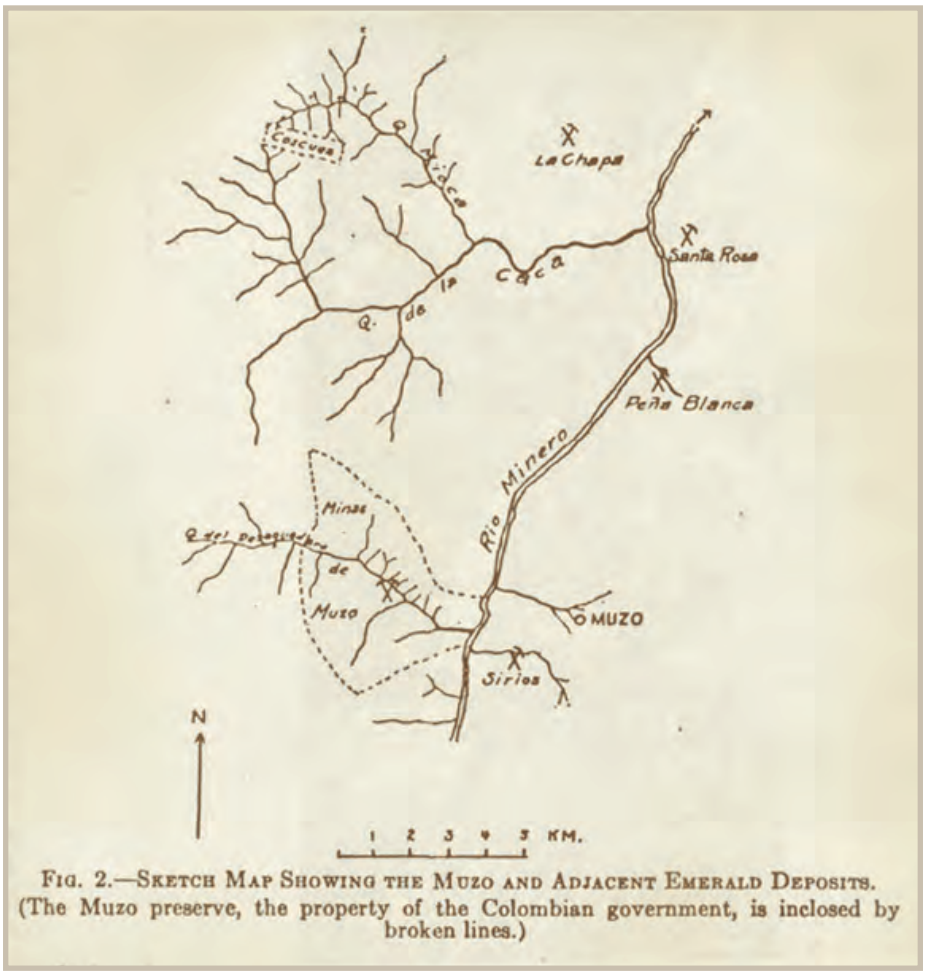

FIG. 2.—SKETCH MAP SHOWING THE MUZO AND ADJACENT EMERALD DEPOSITS. (The Muzo preserve, the property of the Colombian government, is inclosed by broken lines.)

Figure 2: A sketch map of the Muzo mining region by J. Pogue (1916) depicting Peña Blanca (Peñas Blancas) a few kilometres north of the small town of Muzo.

Emeralds were initially found on the surface underneath an overgrowth of vegetation, in a rich vein more than 60 m long (Claver Téllez, 2011). During the initial years of the boom, shallow trenches provided miners with significant quantities of gem-quality rough.

Emeralds from this find eventually reached the Gemological Institute of America (GIA), then located in Los Angeles. An unattributed two-page article titled 'A new emerald find in Colombia' appeared in the Spring 1961 issue of *Gems & Gemology*. The article states (pp 142, 158):

> "Each of the clear, deep-green stones showed prism faces and the two or three with basal pinacoids also had very small bipyramid faces of the same order as the prisms. We understand that production has ranged in size from one carat to about thirty carats. The rich, velvety color of the few we saw was reminiscent of the Muzo product.
>
> "The new find … has been the scene of a wild rush of perhaps fifteen hundred miners. At this writing, the government has not yet determined who should be granted the right to work the property; the army, however, has surrounded the area, to keep order and prevent robbery."

It would be two decades until Peñas Blancas was cited again in the gemmological literature, when John Sinkankas included it in his 'Chronology of Colombian Emerald' section of *Emerald and other Beryls* (Sinkankas, 1981, p. 412). Sinkankas mentioned a new Colombian agency called *Empresa de Esmeraldas* (Emerald Company), formed by the Banco de la República to control the emerald region and to mine emeralds on behalf of the government, "including recently discovered deposits in Boyacá Province" (referring to Peñas Blancas). The government attempt to control the mining region was unsuccessful, and in 1968 the Colombian Ministry of Mines and Petroleum formed the *Empresa Colombiana de Minas* or ECOMINAS (Sinkankas, 1981). ECOMINAS ran the region more efficiently by granting mining

concessions to private companies (Keller, 1981).

Recent history

The vast wealth produced by Peñas Blancas during the 1960s and 1970s allowed aggressive and entrepreneurial leaders not only to launch themselves into the emerald business but also to gain influence in the entire region. In those years, Muzo and Coscuez were stagnating under government control while Peñas Blancas was a relatively new find, uncontrolled by the government, and yielding gems only 6 ft (1.8 m) below the surface. The 1960s were dominated by the irascible Isauro Murcia, whose son Jaime *El Pekinés* later assumed control at Coscuez during the infamous Emerald Wars of 1985–1990 (see below). A powerful syndicate composed of Palermo and Gilberto Molina, Victor Carranza and Juan Beetar consolidated their control of the Colombian emerald industry in the 1970s and 1980s, initially at Peñas Blancas and then at Muzo.

Gilberto Molina is credited with instigating the development in 1986 of a much-needed road from Muzo to Otanche (near the Coscuez mine) and an airstrip in Quípama (near Muzo). Molina was known on occasion to dump quantities of *moralla* (lower-quality emerald rough) into Muzo's Itoco River streambed just before religious holidays like Christmas and Easter. He wanted to assure that the thousands of *guaqueros* (independent diggers) had stones to trade and thereby enjoyed the holidays. In contrast, during the 1970s, the legendary *El Ganso* (The Goose) Humberto Ariza ruled his dominion from horseback, exercising his power daily with a small squadron of armed men based in Coscuez. In the 1980s, Ariza's enemies and rivals were so numerous that he would never stay more than 30 minutes in one location to avoid assassination attempts. Ariza ultimately died in a blaze of bullets. Later, the folklore and history of Peñas Blancas was further embellished by the menacing presence of scar-faced Pacho Vargas and the fearless Quintero brothers.

During the 1980s, the Muzo and Coscuez mines enjoyed strong production while Peñas Blancas was essentially closed and intermittently yielded only small amounts of rough. The Muzo region, while accessible, was strongly territorial with a violent rivalry between groups from Muzo and Coscuez (Angarita and Angarita, 2013). In 1985, the entry of the personal army of drug-lord José Gonzalo Rodríquez Gacha, a partner of Medellín Cartel leader Pablo Escobar, escalated this rivalry into what became known as the Emerald Wars.

This conflict lasted until 1990, with most of the violence localized in the Muzo mining region. Occasionally, shootings would occur in downtown Bogotá in the famous emerald district of Avenida Jiminez and 7th Avenue. Nevertheless, abundant emerald production from the region continued throughout those years, especially at Coscuez (Ringsrud, 1986). To avoid areas of fighting and danger, the routes taken by the gem couriers as they made their way to the cutting centres in Bogotá were extremely circuitous and laboured. Due to the violence, a road between the village of Santa Barbara and the Coscuez mine was closed for more than four years. It became known locally as *El Muro de Berlin* (The Berlin Wall) because no one could cross it and live to tell about it. Curiously, the actual Berlin Wall fell on 9 November 1989, the same week the road to the Coscuez mine was re-opened.

While federal forces of the Colombian government dealt with drug-lord Rodríquez, it was the emerald miners and guards associated with Carranza who finally secured the emerald region. The end of the Emerald Wars was so significant that on 7 November 1989 the Archbishop of Colombia presided over a peace accord that was signed in Chiquinquirá, a major city and religious centre in the province of Boyacá. With Gilberto Molina a casualty of the violence, Carranza and Beetar continued to consolidate their regional power in the 1990s, and controlled the region until Carranza's death in April 2013.

Although Colombia's emerald mines have been quite productive over the past 15 years, the region has remained uninviting to foreign buyers. However, as of this writing, the locals and many of the newer mine owners have expressed a strong desire to replace the violent past with forward-looking openness, productivity and planning. Many locals still remain armed, but there is improved accessibility to the region and a pride in talking about the relative safety of the roads and the lack of fighting during the past decade. There has been a major military presence since 2008, and strongly enforced gun laws. Government-mandated accountability and control at the mines has added to their accessibility. As a result, foreign-owned mining operations have entered the region; Muzo International (known in Colombia as Minería Texas Colombia) now controls the Muzo mine, while additional international companies are actively creating alliances in other districts.

Because the Emerald Wars were prolonged and escalated by groups involved in the drug trade, there remains an on-going regional enmity toward guerrilla- or drug-related groups who try to enter the mining areas. Not only the emerald miners and their families, but also the *campesinos* are vigilant in their efforts to keep out paramilitary groups and guerrillas. In 2004, fields of coca (used for making cocaine) were discovered just 15 km from the villages of Borbur and Otanche. They were uprooted with great fanfare through the cooperation of local emerald miners and the Colombian national police. The talk among farmers of the region is that lucrative crops like stevia (a sugar substitute) and cocoa (for chocolate) will eventually provide better and equally profitable alternatives for export. Fedesmeraldas, the umbrella organization that encompasses the organizations of emerald miners, dealers and exporters, as well as the Colombian Ministry of Mines and Energy, has completed several multi-year projects building clinics, schools and co-ops in the region (see, e.g., www.emeraldmine.com/2012Archive.htm).

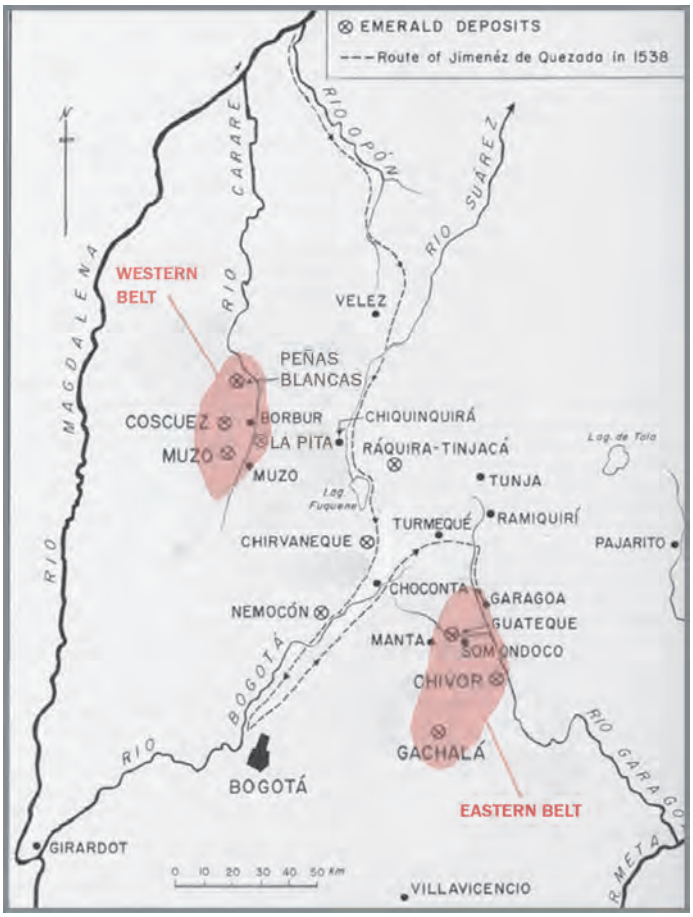

Figure 3: Emerald deposits in Colombia are situated in two belts within a mountain range known as the Eastern Cordillera. The western belt hosts the Peña Blancas, Muzo, Coscuez and La Pita mines, while the Chivor mine is located in the eastern belt. After Sinkankas (1981).

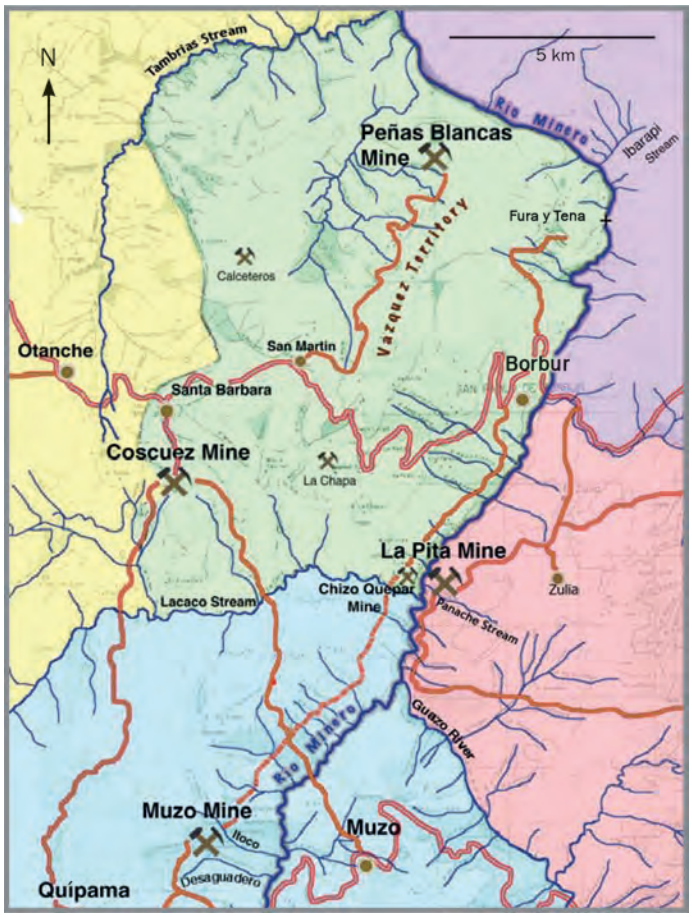

Figure 4: This map depicts the current active mines in the Muzo mining region. Peñas Blancas can be seen at the top, and the Muzo mine is at the bottom of the map. The town of Borbur is located just southeast of Peñas Blancas. Compiled by R. Ringsrud.

Location and access

Colombia's emerald deposits are situated in two belts that are hosted by a mountain range known as the Eastern Cordillera or Cordillera Oriental (e.g., Cheilletz *et al.,* 1994). Within this range, the Peñas Blancas, Muzo, Coscuez and La Pita mines are located in the western belt, while Chivor and others are situated in the eastern belt *(Figure 3)*. All of the mines are located within the state of Boyacá, about a day's drive from Bogotá. Peñas Blancas and the other western-zone mines can be reached by a challenging journey that descends from the capital city of Bogotá (2,600 m) in the central highlands through the lush, semitropical forest to the western flanks bordering the Andes Mountains. After five to six hours of driving on paved and unpaved roads, one reaches the mining region at an altitude of approximately 1,150 m. The area is marked by the twin peaks known as *Fura y Tena* (see Box A). The Peñas Blancas mine (5°43.0'N, 74°4.9'W) is located approximately 40 minutes by off-road vehicle from the town of Borbur (*Figures 4* and *5*). The name *Peña Blanca* that appears on older maps means 'white outcrop', in reference to the limestone layers where emeralds were first discovered. Today locals refer to the mine as *Peñas Blancas*, or simply as *La Peña*.

The village of Borbur lies at about 980 m above sea level, and is still principally a farming and mining town with a population of just over 1,000. The entire municipality surrounding Borbur has a population of almost 11,000. This area, bordered to the east by the Río Minero (Minero River), encompasses Peñas Blancas, Coscuez and part of the La Pita mine. A new road completed in 2011 along the western flank of the Río Minero valley extends from Borbur to the Muzo mine. This road provides direct access through Chizo Quepar to the Muzo mine rather than through the town of Muzo, which is on the other side of the river (see *Figure 4*). Another recent development in this formerly inhospitable region is the arrival of mobile phone coverage to many parts of the mining area. The rapid access to information about new finds enables buyers from Bogotá to respond quickly, making it more difficult and competitive to acquire top-quality gem rough at the mines.

Overall, the Muzo emerald region is rather small; the mines of Muzo, Coscuez, La Pita and Peñas Blancas could all theoretically be visited within a half-day's driving. However, access to any of the

emerald mines is impossible without also having an invitation from a manager, operator or owner of that mine, and visits must be made in the company of locals from each particular mine.

The major mines of Muzo and Coscuez are government-owned, and today access is provided to private companies in 10-year renewable leases from INGEOMINAS, an affiliate of the Colombian Ministry of Mines and Energy. Legal mining claims and filings must be accompanied by environmental permission from two agencies. Peñas Blancas is privately owned, and prospecting of its tunnels is negotiated individually with local strongmen and families from the region, as at other small mines such as Chivor and Gachalá.

Figure 5: The Borbur Cathedral tower is seen here, with the peaks of Fura y Tena in the distance. Photo © Robert Weldon.

Box A: Fura y Tena

Presiding over the lush valley of the Río Minero are the imposing monoliths known as *Fura y Tena (Figure A1)*. These twin peaks dominate the topography of the emerald region, and are visible from Borbur and Coscuez as well as locations close to Muzo and La Pita. The higher peak, Fura (850 m from base to peak), looks like an irregular pyramid topped by a pointed cone, while Tena is a shorter obelisk that reaches only to Fura's shoulder. Río Minero, another significant feature common to all the mines in the Muzo district, runs between the two peaks.

The Fura y Tena are subjects of an indigenous legend dating back to the time of the Muisca and Muzo Indians that dwelled in the area before the Spanish Conquest. The legend speaks of a creator named Ar-e who formed Tena, the first man, and Fura, the first woman, out of the earth. Their life in that land was paradise until Zarve, represented by the Río Minero, tempted and seduced Fura. The infidelity angered the creator, who condemned them to death. Tena, ordained to die first, was turned into stone. Three days later, Fura died at his feet and the god Ar-e sent the torrents of the Zarve River, now called the Minero, to separate them forever. After centuries, the waters purified them and the murmurs of Fura's sadness were converted into the millions of blue butterflies *(Morpho didius)* that populate the region, while her tears became the emeralds. Fura and Tena then became minor deities presiding over the sun's rays, the winds and the underworld.

Figure A1: The peaks of the Fura y Tena dominate the emerald mining region and are visible from the Coscuez mine, Borbur and the La Pita mine. Río Minero, another prominent feature in the mining region, flows between the two peaks. Photo by R. Ringsrud.

Box B: Formation of Colombian emerald deposits

By Terri Ottaway, Museum Curator, Gemological Institute of America, Carlsbad, California, U.S.A.

Colombia's emeralds, arguably the finest in the world, are geologically unique, occurring in organic-rich shales and limestones without the usual association of beryllium-bearing pegmatites. The absence of a well-defined source of Be, the key ingredient in emerald, has long been a perplexing problem for geologists.

In contrast, elsewhere in the world emeralds have formed in environments where pegmatites and related solutions have transected ultramafic country rocks such as serpentinites or amphibolites. Subjected to heat and fluids from the intruding pegmatite, the surrounding country rocks underwent metasomatism to form mica or amphibole schists. Within the schists a mixing zone of pegmatite solutions containing Be, Al and Si, and local solutions containing Cr, V and Fe, resulted in the crystallization of emeralds. For a thorough description of metamorphic emerald environments, see Kazmi and Snee (1989).

Emeralds formed in pegmatite-schist environments are frequently heavily included with mica or amphibole, which reduces the transparency of the crystals and lowers their value as gems. Additionally, Fe can substitute into the emerald structure and negatively affect the colour. Chromium and vanadium not only give the characteristic beautiful blue-green colour to emerald, but they also impart a strong red fluorescence (Nassau, 1983). Although not visible to the naked eye, it may act to enhance the perceived blue-green colour. The presence of Fe in the beryl structure quenches the fluorescence, causing the emerald's colour to appear less intense. Iron can also impart a yellow tinge, resulting in a more 'grass-green' colour. Colombian emeralds are renowned for their intense, velvety blue-green colour and are devoid of inclusions of mica and amphibole, which signifies that their environment of formation differed from the conventional schist-related model.

Despite the lack of evidence, early researchers attempting to explain the formation of emeralds in the black shales of Colombia proposed that emerald-bearing solutions were derived from some hidden igneous activity at depth (Pogue, 1916; Scheibe, 1933; Oppenheim, 1948; Campbell and Bürgl, 1965). Then an intriguing observation was noted that there was a strong spatial association between emerald deposits and evaporites (Oppenheim, 1948; Roedder, 1963; McLaughlin, 1972). Evaporites form through the evaporation of seawater to form large beds of gypsum (hydrous calcium sulphate) and halite (sodium chloride). Their relationship to emeralds becomes all the more evident when one examines the fluid inclusions inside emerald crystals. Fluid inclusions are tiny pockets of the actual solutions from which the emeralds formed that became trapped in tiny cavities during the crystallization process. Over time as the temperature and pressure surrounding the emerald decreased, gases and elements came out of solution to form three-phase (gas-liquid-solid) inclusions. Thus, fluid inclusions represent a geological 'fingerprint'. The presence of halite (salt) crystals within fluid inclusions in all Colombian emeralds indicates the extremely high salinity of the emerald-forming solutions. Perhaps brines from evaporites leached sufficient key elements from the shales and limestones and precipitated them as emeralds (Beus, 1979; Kozlowski *et al.,* 1988; Giuliani *et al.,* 1993).

A geochemical study of the fluid inclusions, isotopes and organic matter of the emeralds, veins and shales at Muzo points to emeralds having formed at approximately 330°C through the interaction of sulphate from incoming evaporitic solutions with the organic-rich shales and limestones (Ottaway, 1991; Ottaway *et al.,* 1994; Giuliani *et al.,* 1995). At certain locations, the sulphate was thermochemically reduced and the organic matter was oxidized to carbon dioxide, releasing organically bound Be, Cr and V. The resulting pressurized solutions were forced into the fractured shales and limestones where they precipitated pyrite, calcite, albite and emerald. The reaction sites where this occurred are distinctively bleached in contrast to the rest of the black shales due to the absence of organic matter. Miners refer to these areas as *cenicero* (ashtray). The abundance of native sulphur in the cenicero further enhances this descriptive term. The peculiar, hexagonally patterned trapiche emeralds are found in the shale surrounding the cenicero. The black shale adjacent to the cenicero also records exposure to a high-temperature event through the elevated reflectance levels as compared to the rest of the shales (Ottaway, 1991).

The removal of Fe from the system in the form of pyrite was critical to the colour of Colombian emeralds. With just Cr and V as chromophores, the emeralds show the renowned intense blue-green colour we value so much.

Emeralds from the Cosquez mine contain fluid inclusions almost identical to those studied at Muzo (Ottaway, 1991; Ottaway *et al.,* 1994). A site visit also confirmed that the greatest concentrations of emeralds were from zones close to bleached areas of shale rich in native sulphur. Indeed, evidence points to the same processes having occurred at the Chivor mine on the eastern flank of the Cordillera Oriental (Ottaway, 1991). Thus, given a favourable environment, the processes of emerald formation presumably occurred over and over, producing all of the known deposits in Colombia, including the emeralds at the Peñas Blancas mine. Although rocks matching the description of the cenicero have not been reported there, it may be that weathering, erosion or mining activity have removed all traces of their existence. Alternatively, it is likely that large emerald-producing areas indicated by reaction sites such as the cenicero are waiting to be discovered.

Geology

The diverse geology of Colombia gives rise to a wealth of varied mineral resources. Petroleum, coal, nickel and emerald are the most important minerals to the Colombian economy. In addition, the Western Cordillera and Central Cordillera are known for gold deposits in granitic rock. The Eastern Cordillera, where the emerald mines are located, consists mainly of sedimentary rock, principally limestones and shales with minor igneous and metamorphic rocks. The major emerald deposits, found as hydrothermal deposits in sedimentary rock, are limited to the western margin (Muzo region) and the eastern margin (Chivor region) of the Eastern Cordillera (again, see *Figure 3*).

Several authors have described the geology of the Muzo district, including Pogue (1916), Schiebe (1933) and Oppenheim (1948). This work is summarized in Keller (1981), Sinkankas (1981) and Ringsrud (1986). A thick layer of black carbonaceous shales and minor amounts of limestone underlies the emerald mining areas. Fossils in these rocks indicate that they are from the Cretaceous Period (approximately 120 million years old). The shales are intensely folded and transected by a number of north-northeast-trending faults that are accompanied by zones of brecciation (fracturing). Mining geologist Cesar Agusto Valencia, working at the Peñas Blancas and La Pita mines, found that fault zones are often rich in emerald, particularly where they intersect and are deformed (C.A. Valencia, pers. comm., 1998). The fault zones can sometimes be identified by changes in the colour or texture of the surrounding rock, or by water seepage. Ottaway *et al.* (1994) state that these fractures in the shales are weaknesses that allowed hydrothermal fluids to infiltrate and deposit calcite, dolomite, emerald, pyrite, quartz and other accompanying minerals such as albite, fluorite, parisite and baryte (for more details, see Box B). This deposition occurred in several episodes involving heat and sometimes violent pulses of pressure (Cheilletz *et al.*, 1994; Ottaway *et al.*, 1994; Giuliani *et al.*, 1995, 2000; Branquet *et al.*, 1999).

Figure 6: The Peñas Blancas mining area is visible in this photo. The green foliated area below and above the mining camp (centre-right) is where past mining yielded many fine-quality trapiche emeralds. At present this area is not being exploited. Photo by R. Ringsrud.

Two rock units are of significance to the emerald deposits: the Paja Formation, in which the mines of Muzo, Coscuez and La Pita are situated; and the Rosablanca Formation, which hosts Peñas Blancas (*Figure 6;* INGEOMINAS, 2005). (The Villeta Formation is also cited by some authors as the host of the emerald deposits.) In contrast to Colombia's other emerald mines, the prominent geological feature of the Rosablanca Formation at Peñas Blancas is its compact and blocky shale. This carbonaceous, fine-grained, argillite shale is penetrated by intersecting white calcite and quartz veins in which the emerald mineralization occurs *(Figure 7)*. By comparison, the Muzo, Coscuez and La Pita areas are characterized by softer, coarser grained, carbonaceous black shales that are highly fractured *(Figure 8)*. Peripheral to the Peñas Blancas exploitation zone, cavities and fissures in the shales give rise to many small, white stalactites of calcium carbonate, which are collected by the locals. Most shops in Borbur have at least one on display, which the locals call *gangas de agua* (water minerals).

Figure 7: The host rock at Peñas Blancas (Rosablanca Formation) is comprised of blocky fine-grained carbonaceous shale penetrated by intersecting white calcite and quartz veins that locally host emerald mineralization. Note the solid compactness of the rock. Photo by R. Ringsrud.

As with other areas in the Muzo mining region, pyrite formation preceded the crystallization of emerald and is one reason for the superior colour of Colombian emerald (see Box B). At Coscuez and Peñas Blancas, pyrite seems to form in thin veins and stock works running through the shales. The pyrite also weathers to form orangy brown iron

Figure 8: All other emerald mines in the Muzo region are located within the Paja Formation, which is characterized by more highly fractured and softer carbonaceous shales (here, being examined by Dr Peter Keller). Compare this with the blocky nature of the shale at Peñas Blancas in Figure 7. Photo by R. Ringsrud.

Figure 10: This large transparent quartz crystal (probably half of a Japan-law twin, 23 cm long) and accompanying emerald crystal were found at Peñas Blancas in 2004. Photo by E. Boehm.

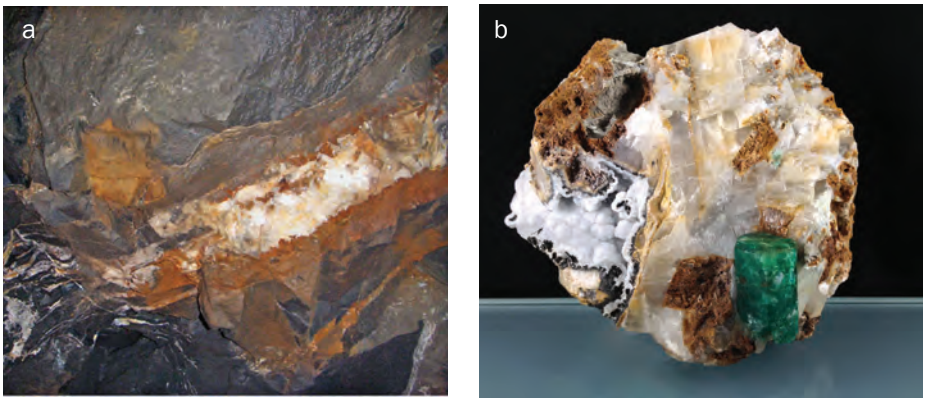

Figure 9: (a) Deep within the tunnels at Peñas Blancas, a white calcite vein (approximately 9 cm wide) shows typical orangy brown iron staining. (b) This mineral specimen from Peñas Blancas features a 2.5-cm-long emerald crystal embedded in the typical matrix of iron-stained calcite with a later secondary coating of botryoidal white calcite. Photos by E. Boehm.

stains along the veins, which are common at Peñas Blancas *(Figure 9)*. In Muzo and La Pita, the pyrite more often forms nodules in the veins or is found as crystals in the shales and veins.

At Peñas Blancas, the mineralized veins range in width from 1 to 30 cm and are usually filled with calcite, dolomite, pyrite and quartz. The emerald crystals occur most frequently attached to the walls of the vein, and are embedded in the vein material. Where the veins are wide enough to form cavities, the emeralds may be larger. Field observations indicate that the best emerald crystals usually occur in the narrower veins (~5 cm thick) and that quartz crystals increase in transparency toward emerald mineralization. Quartz crystals, some quite large and transparent *(Figure 10)*, are commonly found in association with the emeralds (see also *Figure 1*). Quartz found in or near emerald veins is referred to as *cuarzo de veta* (vein quartz), and is typically transparent and very clean, while the more common quartz found elsewhere is known as *cuarzo de tierra* and is not as transparent. The abundance of quartz as a vein mineral differentiates Peñas Blancas from other emerald mines in the area.

Mining

During the bonanza years of 1958–1965, emerald mining at Peñas Blancas consisted of uncovering the surface of *La Culata* (Spanish for gun breech [opening] or a mound, referring to landforms at the mining site) and following productive veins. Miners eventually dug down over 10 m, with intersecting trenches that were subsequently widened with a bulldozer into gullies. What remains of these workings today are four steep mounds separated by wide gullies. The mounds are perforated by prospecting holes and are overgrown with vegetation *(Figure 11)*. One tunnel, *El Tunel de los Dos,* was started in this time period above La Culata and was extremely productive for many years.

When the surface mining operations predominated, terms like *capas buenas* (emerald-bearing layers), *cambiado* (barren zones) and *cama* (breccia-like masses) were used to describe the rocks. These terms helped to orient the miners as they worked the faces of the slopes. Later, such terms fell out of use as mining moved underground, following productive veins with shafts and drifts. After the depletion of the surface-reaching deposits at Peñas Blancas in the early 1970s,

Figure 11: Mining at Peñas Blancas began 50 years ago at the top of these mounds, in an area known as La Culata. Emeralds found at the surface started a bonanza. The miners dug trenches that eventually reached a depth of over 10 m. Photo by E. Boehm.

Figure 12: The authors (RR on left and EB on right) and mine foreman Edilfo Ramírez inspect emerald crystals on matrix from Peñas Blancas. Photo by Willington López.

tunnelling became the only means of following the emerald-rich veins.

At the well-known mines of Muzo, Coscuez, La Pita and Chivor, the brecciated shale host rock provided little resistance to the use of dynamite, and sometimes the force of the explosions passed into the veins, thus damaging the emeralds. Rough stones from these localities sometimes show an indicative whitish percussion mark at the surface that may or may not have accompanying fissures emanating into the stone.

The harder, more blocky shale at Peñas Blancas requires the use of more dynamite than at the other emerald mines, but the uniform compactness of the shale helps insulate the veins from the force of the explosions. If well placed, the dynamite clears away the hard shale without damaging the actual veins, which are then worked manually. The emeralds mined by this process are generally free from percussion fractures caused by dynamite use. They are commonly recovered still embedded in the vein material *(Figure 12)*.

Because of the independent and artisanal nature of the mine workings at Peñas Blancas, there is little money to invest in infrastructure. Even the best-equipped tunnels have only one pump for ventilation and a generator for an electric hammer-drill.

Gemmology

In the authors' experience, Peñas Blancas emeralds are very slightly bluish green (e.g., *Figure 13*), like most Colombian emeralds, but they generally contain less colour zoning and possess a velvety appearance that is highly prized. Also like most Colombian emeralds, the crystals form first-order prisms with flat terminations. However, a unique characteristic of the Peñas Blancas rough material is called *cascocho* by some cutters and dealers. It refers to the tendency of the crystals to have numerous pits and cavities, which hinder the cutting of large stones. They are most likely due to secondary chemical etching after emerald formation.

While visiting Bogotá's downtown emerald market, the authors were fortunate to see two large pieces of rough from Peñas Blancas prior to cutting *(Figure 13)*. The larger crystal weighed 22 g and was faceted into nine stones weighing 32.90 ct (a 30% yield), with the largest being a ~9 ct heart shape *(Figure 14)*. Much sawing was required to remove the cavities from the rough. However, the attraction of Peñas Blancas emerald rough is that beneath the zone of cavities and pits there is sometimes fine material of exceptional purity. The hope of uncovering that fine material, which is not always evident when viewing the surface of the rough, is what often entices cutters and dealers to take risks on emerald

Figure 13: The colour and clarity of some Peñas Blancas emeralds make them highly prized. The 22 g crystal on the left yielded higher-quality material than the smaller crystal on the right. Photo by E. Boehm.

Figure 14: These nine emeralds, faceted from the larger Peñas Blancas crystal in Figure 13, *weigh 32.90 carats in total. The large heart shape weighs ~9 ct. Photo by E. Boehm.*

crystals from this mine. The cutters equate them to the seed of a peach, whose pitted and gnarly exterior *(cascocho)* covers an inner seed or nodule *(la almendra)* that is pure and fine.

The authors studied 10 rough or partially polished emerald samples that they purchased during their late-2004 trip to Peñas Blancas. The emeralds were obtained from an intermediary who bought them at the mine camp. Refractive indices (taken from at least one polished surface or crystal face) obtained with a GIA Duplex II refractometer were consistent with emeralds from the Muzo region (n_o=1.578–1.580, n_e=1.569–1.572; see *Table I*, cf., O'Donoghue, 2006). With the exception of sample 6 (SG=2.68), the hydrostatic specific gravity values were somewhat lower than reported for emeralds from this region (i.e., 2.63–2.67 vs. 2.70; O'Donoghue, 2006). These lower values may be due to the stones' higher 'porosity', resulting in trapped air bubbles, because of etch cavities present in the rough material. Faceted gems without cavities would likely yield higher SG values. Samples 7–10 contained significant fractures and surface cavities that were filled with oil and epoxy resin (e.g., *Figure 15*). These samples would have therefore rendered inaccurate specific gravity readings.

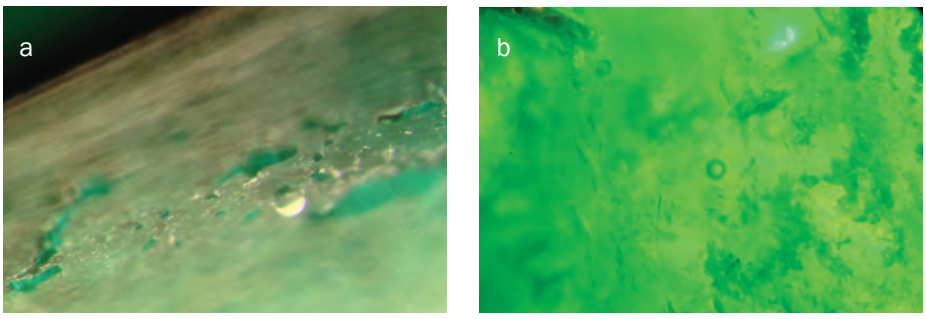

Figure 15: Rough emeralds from Peñas Blancas are sometimes fracture-filled with oil, resin or a combination of these. (a) The pitted surface etching typical of Peñas Blancas emeralds is shown, along with an air bubble that appeared on the surface as a result of the heat generated from the incandescent bulb of the microscope. The heat caused oil in the sample to expand, forcing a bubble and then some oil to the surface. (b) Air bubbles trapped in this emerald's filler could possibly be mistaken for two-phase inclusions. Photomicrographs by E. Boehm, magnified 66× (a) and 50× (b).

Table I: RI and SG values of 10 rough emerald samples from Peñas Blancas, Colombia.

Sample	Weight (ct)	n_o	n_e	SG
1	1.28	1.580	1.570	2.64
2	1.41	1.580	1.572	2.67
3	1.57	1.580	1.572	2.60
4	2.05	1.580	1.570	2.63
5	2.18	1.580	1.572	2.63
6	2.54	1.578	1.569	2.68
7	4.38	1.58	1.57	nd*
8	4.99	1.578	1.570	nd
9	6.88	1.580	1.570	nd
10	22.52	1.578	1.570	nd

* Abbreviation: nd = not determined.

Inclusions in emeralds from this mining area were first described by Dr E.J. Gübelin and J.I. Koivula (1986, p. 250) in samples coming from the 'Burbar' mine which we know today as Borbur, the closest village to Peñas Blancas. Those authors described the "greatly distorted and distended form of the secondary three-phase inclusions" as typical hallmarks of these emeralds *(Figure 16a)*. Similar secondary three-phase inclusions were also observed in the samples examined for this article *(Figure 16b,c)*. Primary or syngenetic three-phase inclusions are also seen in emeralds from Peñas Blancas. Some protogenetic inclusions of pyrite, calcite and quartz were noted, but such crystals are more commonly found as associated minerals within the gem-bearing veins or attached to the surface of the emerald crystals.

Trapiche emeralds

Most gemmologists are familiar with trapiche emeralds from Muzo, in which inclusions of carbonaceous matter form spokes radiating from a hexagonal centre, creating six black 'rays' in the emerald crystal (e.g., Ringsrud, 2009, pp 344–6).

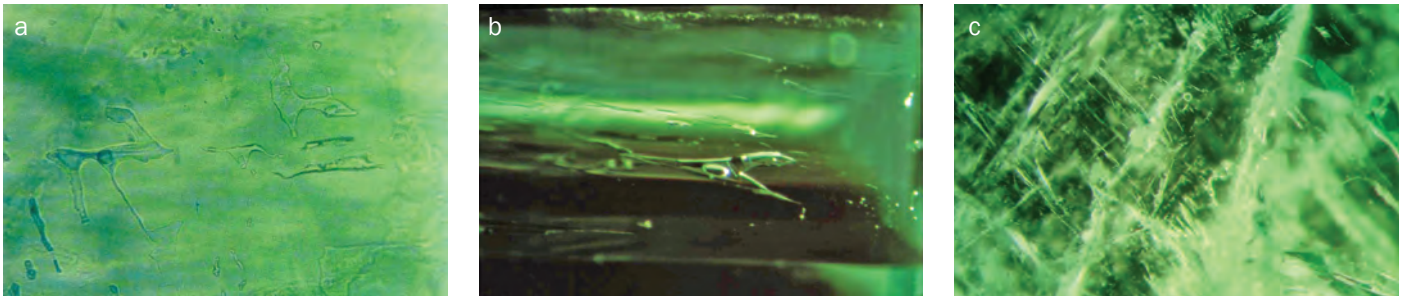

Figure 16: Secondary three-phase inclusions in Peñas Blancas emeralds. (a) Irregular shapes photographed by Dr E.J. Gübelin, magnified 50× (from Gübelin and Koivula, 1986, p. 250). (b) A classic inclusion scene containing a halite crystal, CO_2 gas, and liquid in a 1.41 ct emerald crystal from Peñas Blancas; photomicrograph taken by Dr E.J. Gübelin in 2004; magnified 66×. (c) View parallel to the basal plane of an emerald crystal with a small three-phase inclusion in the top-centre; photomicrograph by E. Boehm, magnified 50×.

The Spaniards called these peculiar emeralds *trapiche* because of their resemblance to the cogs and gears with which sugarcane was crushed. Trapiches are usually cut into cabochons to show off this cog-wheel pattern.

In the 1960s and 1970s, many well-formed large trapiches from Peñas Blancas with white (albite) or black (carbonaceous) interstitial material found their way into collections all over the world (e.g., *Figure 17*). Unfortunately, their size and abundance was also the cause of their destruction: the rays of the trapiche were often sawn through and the six transparent gem segments were then cut into calibrated stones. Rare chatoyant sections were polished into cabochons to form cat's-eyes. Trapiches are no longer being mined at Peñas Blancas. During our visit in 2004, the locals indicated the 'trapiche zone' was found in a steep area overgrown with vegetation (again, see *Figure 6*).

Conclusion and future potential

Since its rediscovery in 1958, the turbulent history of the Peñas Blancas mine demonstrates the necessity of not only solving the geological and engineering aspects of emerald extraction but also understanding the inherent social factors at play in the area. After the initial bonanza, the best emerald production at Peñas Blancas occurred during the presence of loyal, trained security forces headed by strong, undisputed leaders. The current trend of pacification, organization and investment in Boyaca's rich emerald region may allow Peñas Blancas to once again become a significant emerald producer.

Recent exploration at Peñas Blancas has consisted of little more than locals digging shallow test pits, of which only a few have shown potential. The lower trapiche zone could provide additional production, along with the upper area known as La Culata. However, as is the case elsewhere in the subtropical Boyacá mining region, heavy overgrowth has inhibited proper geologic exploration. Prospecting also has been hindered by the area's remoteness, steep topography and challenging social climate. However, it seems probable that more sources of fine Colombian emeralds will be found. One example is provided by the La Pita mine *(Figure 18)*. After two decades of dormancy, in 1998 the La Pita mine suddenly became a major producer in the region (Michelou, 2001). This gives an indication of the possible future of Peñas Blancas and the surrounding region.

However, for Peñas Blancas to realize its full potential, it must first become attractive to outside investment. A decade after the authors' initial visit, the road to Peñas Blancas is still barely passable. The original bonanza left behind a mining

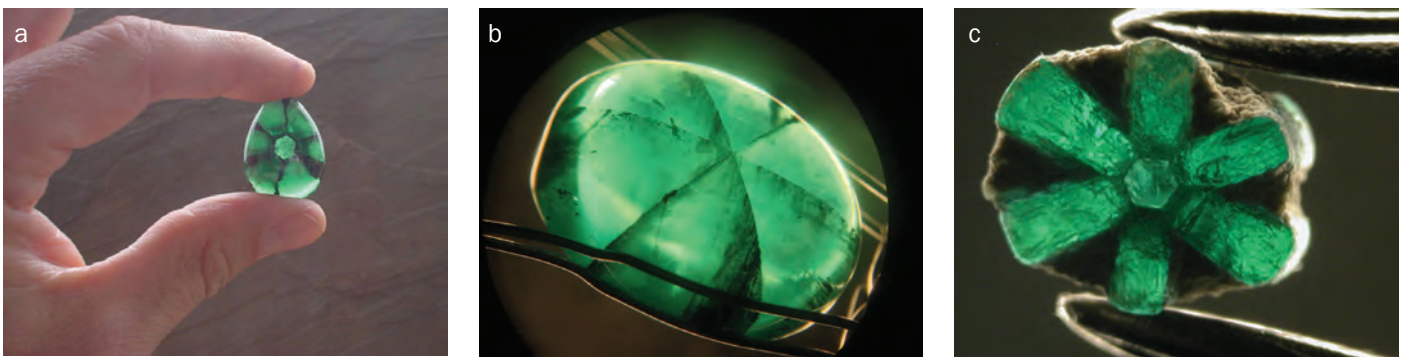

Figure 17: Trapiche emeralds from Peñas Blancas entered the market in the 1960s and 1970s. (a) The most common trapiche variety consists of emerald material intersected by spokes of dark carbonaceous inclusions (28 ct; courtesy of RareSource, photo by E. Boehm). (b) This 25 ct trapiche cabochon displays chatoyant segments, although any cat's-eye emeralds cut from them would be rather small; photomicrograph by E. Boehm, magnified 8×. (c) A 'reverse trapiche' example in which the spokes are formed by straight segments of emerald with albite or shale in between (here, 7 mm in diameter; photo by R. Ringsrud). This type of trapiche, now quite rare in the market, has been found in relatively large sizes (up to 20 ct).

Figure 18: The La Pita emerald mine (left-centre) had its own bonanza in the late 1990s. Continued steady production has elevated the La Pita to the legendary status of Muzo and Coscuez as one of the premier mines in the Muzo region. Photo by R. Ringsrud.

area full of potential but needing serious infrastructure improvements to make it worthy of exploitation.

Even after almost five centuries of supplying fine emeralds to the world, the Muzo region still shows no signs of exhaustion. World emerald demand will only increase, and it is expected that exploration and production in Colombia's premier mining region will grow to meet the demand. With the colour green in fashion and Hollywood actresses wearing more and more emeralds, the future importance of Peñas Blancas, and all emerald mines, will only grow.

Acknowledgements

The authors are grateful to Camilo Mora, Leonel Mendieta, Wellington López, Wilson Obando and Carolina Quintana for their assistance with fieldwork at Peñas Blancas. César Augusto Valencia is thanked for helpful discussions.

References

Angarita, G., and Angarita, M., 2013. Carranza: The myth and the industry. *InColor,* Summer, **23**, 20–4

Beus, A.A., 1979. Sodium — a geochemical indicator of emerald mineralization in the Cordillera Oriental, Colombia. *Journal of Geochemical Exploration,* **11**, 195–208

Branquet, Y., Laumonier, B., Cheilletz, A., and Giuliani, G., 1999. Emerald in the Eastern Cordillera: Two tectonic settings for one mineralization. *Geology,* **27**, 597–600

Campbell, C.J., and Bürgl, H., 1965. Section through the Eastern Cordillera of Colombia, South America. *Geological Society of America Bulletin,* **76**, 569–90

Cheilletz, A., Féraud, G., Giuliani, G., and Rodriguez, C.T., 1994. Time-pressure and temperature constraints on the formation of Colombian emeralds: An $^{40}Ar/^{39}Ar$ laser microprobe and fluid inclusion study. *Economic Geology,* **89**, 361–80

Claver Téllez, P., 2011. *Verde, La Historia Secreta de la Guerra Entre los Esmeralderos.* Intermedio Editores, Bogotá, Colombia

Giuliani, G., Cheilletz, A., Dubessy, J., and Rodriguez, C.T., 1993. Chemical composition of fluid inclusions in Colombian emerald deposits. In: Y.T. Maurice, Ed., *Proceedings of the Eighth Quadrennial IAGOD Symposium,* Ottawa, Canada, 12–18 August 1990. E. Schweizerbart'sche Verlagsbuchandlung, Stuttgart, Germany, 159–68

Giuliani, G., Cheilletz, A., Arboleda, C., Carrillo, V., Rueda, F., and Baker, J., 1995. An evaporitic origin of the parent brines of the Colombian emeralds: Fluid inclusions and sulfur isotope evidence. *European Journal of Mineralogy,* **7**, 151–65

Giuliani, G., France-Lanord, C., Cheilletz, A., Coget, P., Branquet, Y., and Laumonier, B., 2000. Sulfate reduction by organic matter in Colombian emerald deposits: chemical and stable isotope (C, O, H) evidence. *Economic Geology,* **95**, 1129–53

Gübelin, E., and Koivula, J.I., 1986. *Photoatlas of Inclusions in Gemstones.* Opinio Publishers, Basel, Switzerland

INGEOMINAS, 2005. *Levantamiento de Información Estratigrafica.* Informe

No. 2160, Instituto Colombiano de Geología y Minería, Bogotá, Colombia, May

Kazmi, A.H., and Snee, L.W., Eds., 1989. *Emeralds of Pakistan*. Van Nostrand Reinhold, New York, USA

Keller, P.C., 1981. Emeralds of Colombia. *Gems & Gemology,* **17**(2), 80–92

Kozlowski, A., Metz, P., and Jaramillo, H.A.E., 1988. Emeralds from Somondoco, Colombia: Chemical composition, fluid inclusions and origin. *Neues Jahrbuch für Mineralogie, Abhandlungen,* **159**(1), 23–49

McLaughlin, D.H., 1972. Evaporite deposits of Bogota area, Cordillera Oriental, Colombia. *American Association of Petroleum Geologists Bulletin,* **56**(11), 2240–59

Michelou J.C., 2001. Les nouvelles minas de La Pita, Part I. *Revue de Gemmologie,* **143**, 9–14

Nassau, K., 1983. *The Physics and Chemistry of Color: The Fifteen Causes of Color*. John Wiley & Sons, Toronto, Canada, 454 pp

A New Emerald Find in Colombia, 1961. *Gems & Gemology,* **10**(5), 142, 158

O'Donoghue, M., Ed., 2006. *Gems,* 6th edn. Butterworth-Heinemann, Oxford, p. 154

Oppenheim, V., 1948. The Muzo emerald zone, Colombia, South America. *Economic Geology,* **43**, 31–8

Ottaway, T.L., 1991. The geochemistry of the Muzo emerald deposit, Colombia. Master's thesis, University of Toronto, Canada

Ottaway, T.L., Wicks, F.J., Bryndzia, L.T., Kyser, T.K., and Spooner, E.T.C., 1994. Formation of the Muzo hydrothermal emerald deposit in Colombia. *Nature,* **369**, 552–4

Pogue, J., 1916. The emerald deposits of Muzo, Colombia. *Transactions of the American Institute of Mining and Metallurgical Engineers,* **55**, 810–34

Ringsrud, R., 1986. The Coscuez mine, a major source of Colombian emeralds. *Gems & Gemology,* **17**(2), 67–79

Ringsrud, R., 2009. *Emeralds: A Passionate Guide*. Green View Press, Oxnard, California, USA

Roedder, E.J., 1963. Studies of fluid inclusions II: Freezing data and their interpretation. *Economic Geology,* **58**, 167–200

Scheibe, R., 1933. Informe geológico sobre la mina de esmeraldas de Muzo. *Compilación de los Estudios Geológicos Oficiales en Colombia,* **1**(4), 169–98

Sinkankas J., 1981. *Emerald and Other Beryls*. Chilton Book Co., Radnor, PA, USA

The Authors

Ron Ringsrud
Muzo International, 40 Rue du Rhone, Geneva, Switzerland
email: ronald.ringsrud@muzoemerald.com

Edward Boehm
RareSource, P.O. Box 4009, Chattanooga TN 37405 USA
email: edward@raresource.com

Greek, Etruscan and Roman garnets in the antiquities collection of the J. Paul Getty Museum

Lisbet Thoresen and Karl Schmetzer

Abstract: The results of quantitative electron microprobe analyses and observations of gemmological properties and microscopic features are presented for 11 garnets of ancient Greek, Etruscan and Roman manufacture. In addition to chemical data, the gemmological properties of the Getty Museum garnets are presented, including refractive index, density and inclusions. According to their chemical composition and gemmological properties, the 11 garnets were subdivided into four groups: Cr-poor pyrope, Mn-rich almandine, Ca-rich almandine and intermediate pyrope-almandine. Combining the data of the 11 Getty garnets with published analyses of 26 Greek and Roman garnets from ancient jewellery and glyptic, the chemical distribution pattern of all 37 garnets expanded the boundaries of the established four groups and added a fifth garnet group comprising Mn-poor almandine. The compositional fields for these five groups are compared with data reported for Early Medieval garnets, mostly from Merovingian cloisonné jewellery. The chemical composition and physical properties of the garnets yield insights into possible sources of rough gem material, networks of trade/transmission in the ancient world, and associations between finished objects now dispersed in different collections.

Keywords: antiquities, carved gems, electron microprobe analysis, garnet, inclusions, optical spectra, pyrope-almandine

A late Hellenistic (323–30 BC) almandine carbuncle engraved with winged Eros carrying the attributes of Herakles, gem no. 5 of the present study (14.7×12.1 mm). The J. Paul Getty Museum, Villa Collection, Malibu, California. Photo by Harold and Erica Van Pelt.

Introduction

The use of red garnets in ancient craft industries, primarily as beads, is attested in Egypt from the Predynastic period through the New Kingdom (i.e., 4th–2nd millennium BC; Aston *et al.*, 2000), and in some Western Asiatic and Near Eastern cultures of the 2nd–1st millennium BC (Moorey, 1994). Their early use was sporadic at best, but trade in gems from distant sources, including garnets, proliferated in the Hellenistic era (323–30 BC) under the successors of Alexander the Great, or *Diadochi*, who divided his empire. Among them, the Seleucids, who ruled Western Asia, and the Ptolemies, who ruled Egypt and territories in the Eastern Mediterranean, were able to control the overland and sea trade, respectively. The development of luxury arts, including glyptic (i.e., the art of gem carving), flourished under their patronage and garnets became the premier gem during the Hellenistic era. In workshops throughout the ancient world — from countries around the Mediterranean to the Black Sea region and Western and Central Asia — garnets were used to make intaglios, cameos, beads and jewellery inlays (e.g., *Figure 1*).

Greek, Etruscan and Roman garnets in the antiquities collection of the J. Paul Getty Museum

Figure 1: A Hellenistic necklace from a jewellery hoard, dated 230–210 BC, found in ca. *1900 in a tomb in Taranto, southern Italy. The necklace consists of a chain of looped links of gold alternating with carved pyrope, and a Herakles knot clasp inlaid with pieces of pyrope (17 mm long). Orange cornelians with a tapered cone shape are set on either side of the Herakles knot centrepiece. © Antikensammlung, Staatliche Museen zu Berlin. Photo by Johannes Laurentius.*

The popularity of garnets continued into the Roman Imperial era, but waned over time, and then enjoyed a resurgence in the Severan (AD 193–225) and Constantinian (AD 313–363) dynasties in the later Roman Empire. Polychromy and garnet inlays in cloisonné metalwork emerged as an altogether new expression in jewellery of the Byzantine East and persisted through the Medieval period. Originating with tribes of the Pontic-Caspian steppes and Central Asia, these distinctive artistic conceptions and objects spread across Western Europe and around the Mediterranean, as far as northwestern Africa. During this 'Garnet Millennium' (Adams, 2011) — from the Hellenistic era through the Early Medieval period (about AD 500–700) — ancient texts, gems and jewellery found in archaeological contexts, and also carved gems extant in modern collections, all attest to the availability of garnets from different sources occurring in a wide variety of colours, sizes and qualities.

Adams (2011) gave an excellent overview of the occurrence and distribution of garnets in disparate cultures throughout the ancient world from the late 4th century BC to the 7th century AD, including a discussion of nomenclature and garnet sources as described in ancient texts and in recent analytical provenance studies. Detailed discussions of Hellenistic engraved garnets were given by Spier (1989) and Plantzos (1999).

Traditionally, glyptic has been characterized, dated and attributed to a culture, workshop or individual artist based primarily on stylistic criteria such as subject/motif, shape of the fashioned gem, choice of gem materials and tool work. A strong reliance is placed on the jewellery setting to help narrow the date and sometimes likely place of manufacture. However, many ancient intaglios and cameos that survive to the present day lack their original mounting, and most such gems in modern collections — private or public — came from the art market, so their connection to a precise cultural horizon has been broken.

Complementing the tools at the disposal of scholars for attributing gems — comparanda (gems and settings that are stylistically or typologically similar), ancient texts and inscriptions, and archaeological context — the physical and chemical properties of the gems themselves provide additional criteria potentially useful to archaeologists for determining the period and place of production and tracing the materials to their original sources, which in turn may illuminate facts related to transmission and intercultural contacts in the ancient world.

Chemical composition and other properties such as inclusions may be helpful in identifying the geographic origin of gems. For example, using these criteria, some sapphires and rubies may be attributed to a gem-producing region or even a specific locality with a high degree of probability. However, localizing many otherwise distinctive gem materials to their sources can be difficult, because their geological environment often can be very similar in different regions. This is true of emeralds, for example, where they may occur in phlogopite or biotite schists in various countries; as such they are associated with similar minerals and may have similar inclusions and trace-element compositions, thus making difficult an unambiguous determination of origin.

Garnets are common gem materials, particularly metamorphic almandine and igneous/metamorphic pyrope. Fortunately, garnets have a chemical complexity that makes them at least partly distinctive, and it is sometimes possible to link specific garnets to a particular type of host rock and even to a specific source.

Historically, the identification of most garnets used in ancient glyptic (4th/3rd century BC to 5th century AD) has been based on visual observation of colour and seldom according to the stones' chemical composition as represented by garnet end-member percentages. Despite the numerous garnets extant in ancient Greek and Roman jewellery, only a few studies on a small number of stones have been published.

This article adds chemical data and gemmological properties of 11 ancient garnet intaglios and cameos from the J. Paul Getty Museum, Villa Collection, Malibu, California. Their chemical compositions are discussed in relation to the published analyses of a small number of other ancient Greek and Roman garnets, as well as additional data published on garnets belonging to the Early Medieval era. Although a

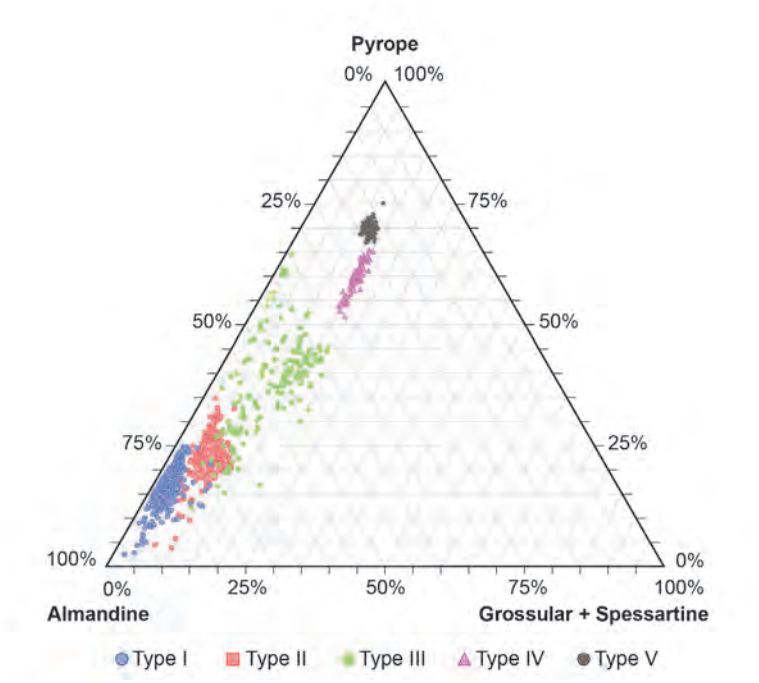

Figure 2: Ternary diagram of pyrope–almandine–(grossular+spessartine) end member compositions of garnet inlays in Early Medieval cloisonné metalwork, after Calligaro et al. *(2006–2007). The garnets were subdivided into five different types, some with partly overlapping compositional ranges.*

comparison with the later-dated garnets is not precisely parallel, they represent the nearest temporal association with Graeco-Roman garnets available currently.

Analytical provenance studies of Early Medieval garnets

Beginning about the 1970s, various analytical techniques were used to determine the geographical provenance of garnets mounted in objects produced during the Early Medieval period, including Anglo-Saxon, Frankish, Scandinavian and South Russian artefacts. Typically, the jewellery and other functional objects contained thinly sliced garnet inlays mounted in cells with metal bases and partitions or boundaries (i.e., cloisons).

Methods such as powder X-ray diffraction (Löfgren, 1973; Arrhenius, 1985) or Raman spectroscopy (Adams *et al.,* 2011), in general, may enable the subdividing of garnet samples of unknown origin and composition into pyrope-rich and almandine-rich groups. The application of X-ray fluorescence (XRF) analysis in air usually precludes quantitative determination of lighter elements such as Mg and Al (Bimson *et al.,* 1982; Greiff, 1998) and presents difficulties in comparing results of different researchers, because complete quantitative analyses (necessary to calculate the percentages of the garnet end members) are not available.

A recent study initiated at the British Museum included qualitative nondestructive analyses of 19 engraved garnets of Eastern manufacture (i.e., cultures of Central and South Asia) — Sasanian, Kushan and Hunnic (Adams *et al.,* 2011). Produced between the 1st and 6th century AD, these garnets were differentiated by colour and segregated into two groups by Raman spectroscopy: almandine with a low pyrope content and almandine with a somewhat greater pyrope content.

To obtain full quantitative analyses of ancient garnets, various nondestructive methods have been used, such as electron microprobe analysis (Löfgren, 1973; Rösch *et al.,* 1997; Quast and Schüssler, 2000), scanning electron microscopy–energy dispersive spectroscopy (SEM-EDS; Greiff, 1998; Mannerstrand and Lundqvist, 2003) or proton-induced X-ray emission (PIXE) analysis (Farges, 1998; Calligaro *et al.,* 2002). In addition, a combination of XRF and PIXE (Pappalardo *et al.,* 2005) or a combination of XRF and Raman spectroscopy (Gilg and Gast, 2012) have been used to obtain full quantitative data of garnets.

Additional analytical studies of Hellenistic and Roman garnets were published by Formigli and Heilmeyer (1990), Gartzke (2004) and Gliozzo *et al.* (2011), and data on Early Medieval garnets were published by Calligaro *et al.* (2006–2007; 2009), Pèrin and Calligaro (2007), Mathis *et al.* (2008), Gilg *et al.* (2010), and Horváth and Bendö (2011). To date, more than 2,000 full analyses have been published (or shown in comparative diagrams) on garnets of the Early Medieval period, and interpretation of these data has been discussed intensively. According to their chemical composition, these garnets (dating from the 5th to 7th century AD) reportedly originated mainly from areas known today as the Czech Republic, France, Germany, Belgium, Hungary, Italy and Spain. Most were identified as members of the pyrope-almandine solid-solution series, many also with spessartine and grossular components. Some contained up to several weight percent of Cr_2O_3, representing the uvarovite or knorringite end member of the garnet group.

The Medieval garnets in some of these studies were subdivided into five different types (*Figure 2;* see Calligaro *et al.,* 2006–2007). These subdivisions comprise two types of almandine, two varieties of pyrope with different Cr contents and one intermediate pyrope-almandine type. By contrast, in a later study by Gilg *et al.* (2010), garnets were divided into four clusters (representing four of Calligaro's types) plus one intermediate group X (nearly identical to Calligaro's intermediate pyrope-almandine type). Gilg *et al.'s* group X represents specimens with widely varying properties and compositions. Calcium-rich intermediate pyrope-almandine from Sweden and Denmark, mostly dating to the 8th century or later, forms another type (not shown in *Figure 2*) and is related mainly to Scandinavian deposits (Lundström, 1973; Mannerstrand and Lundqvist, 2003).

Greek, Etruscan and Roman garnets in the antiquities collection of the J. Paul Getty Museum

Table I: Description of 11 ancient garnets from the J. Paul Getty Museum, Villa Collection.

Gem no.	Identification	Description, inventory no., primary references and source	Culture/era (and location, if known)	Period
1	Cr-poor pyrope	Scarab, large corner winglets of diamond shape and ridge carination. On the flat side is engraved a helmeted head in profile. Inv. no. 81.AN.76.142 (13.3×9.4×8.1 mm). Boardman (1975), pp 34, 106, no. 142.	Etruscan	Late 4th–3rd century BC
2	Intermediate almandine-rich pyrope-almandine	Cameo portrait head of a woman in profile and wearing a veil. Inv. no. 81.AN.76.59 (19.1×12.9×6.2 mm). Boardman (1975), pp 92–93, no. 59. Possibly Berenike (d. *ca.* 222 BC); although Spier (1989) and Plantzos (1999) suggest that she is probably Arsinoë II (d. 270 BC), the sister-wife of Ptolemy II, and they concur on a probable date of manufacture in the second half of the 3rd century BC. Spier (1989), p. 30, no. 34, p. 35, fig. 36; Spier (1992), p. 157; and Plantzos (1999), p. 51, no. 87 and p. 64, pl. 90.9.	Hellenistic (Ptolemaic)	3rd century BC
3	Mn-rich almandine	Oval intaglio ring-stone, obverse highly convex, reverse flat. A woman wearing a himation swathed around her legs and over her arm; she rests her elbow on a column and holds a flower. Inv. no. 81.AN.76.56 (21.9×11.7×5.9 mm). Boardman (1975), pp 19, 92, no. 56.	Hellenistic	3rd century BC
4	Mn-rich almandine	Intaglio, obverse convex, reverse slightly concave, engraved with a man lifting a child onto his shoulder. Inv. no. 81.AN.76.54 (14.1×9.9×4.6 mm). Boardman (1975), p. 92, no. 54.	Hellenistic	2nd century BC
5	Mn-rich almandine	Intaglio, obverse highly convex, reverse concave, engraved with Eros with the attributes of Herakles; he carries a club, a lion skin, and a bow case. Inv. no. 85.AN.370.41 (14.7×12.1×6.6 mm). Spier (1992), p. 90, no. 213.	Hellenistic; Eastern, from Greece	2nd–1st century BC
6	Mn-rich almandine	Intaglio, obverse highly convex, reverse flat, engraved with Eros standing on and holding the reins of a flying butterfly. Inv. no. 83.AN.256.7 (11.4×7.7×4.9 mm). Spier (1992), p. 91, no. 214. Bequest of Eli Djeddah.	Hellenistic; Eastern	2nd–1st century BC
7	Mn-rich almandine	Intaglio, obverse highly convex, reverse flat, engraved female comic mask. Inv. no. 84.AN.1.53 (8.5×6.5×3.9 mm). Spier (1992), p. 92, no. 216.	Hellenistic; Eastern	2nd–1st century BC
8	Ca-rich almandine	Oval intaglio, obverse flat, reverse convex, engraved with head of Dionysos wearing an ivy wreath. Inv. no. 85.AN.444.22 (16.0×13.0×4.4 mm). Spier (1989), no. 48, 29, 33, fig. 31; Spier (1992), p. 21, no. 21; Plantzos (1999), pp 81, 125, no. 349, pl. 53. Gift of Jonathan H. Kagan.	Hellenistic (Ptolemaic); from Iran	Late 2nd–1st century BC
9	Ca-rich almandine	Oval intaglio ring-stone, obverse slightly convex, reverse slightly concave, mounted in a thin gold wire setting, possibly from a ring; engraved with bust of Hermes wearing a petasos. Inv. no. 83.AN.437.28 (8.1×6.8×2.7 mm). Spier (1992), p. 92, no. 217. Gift of Damon Mezzacappa and Jonathan H. Kagan.	Hellenistic; from Asia Minor	1st century BC
10	Intermediate almandine-rich pyrope-almandine	Intaglio, obverse flat, reverse convex, engraved with Minerva seated, holding a branch and sceptre; a shield is at her feet. Inv. no. 82.AN.162.90 (16.1×12.6×4.9 mm). Unpublished. Gift of Stanley Ungar.	Roman Imperial	1st century BC – 1st century AD
11	Cr-poor pyrope	Cameo carving of head of Eros, circled by a ridge or plaque. Inv. no. 83.AN.437.42 (11.7×9.5×5.5 mm). Spier (1992), p. 157, no. 434. Gift of Damon Mezzacappa and Jonathan H. Kagan.	Roman Imperial; from Asia Minor	1st century AD

Figure 3: Ten of the 11 garnet intaglios and cameos in the Getty Museum's Villa Collection are the products of Greek and Roman Imperial workshops. Top: a pyrope-almandine cameo (gem no. 2) and five almandine intaglios with high convex oval or 'carbuncle' shapes (nos. 6, 5, 4, 7 and 3). Bottom: a small round almandine intaglio encircled in a gold hoop (no. 9), an asteriated pyrope-almandine intaglio (no. 10), an almandine intaglio (no. 8) and a pyrope cameo (no. 11). The gems range in dimensions from 8.1×6.8 mm (no. 9) to 21.9×11.7 mm (no. 3). The J. Paul Getty Museum, Villa Collection, Malibu, California. Photo by Harold and Erica Van Pelt.

Gemmological and chemical study of ancient garnets from the J. Paul Getty Museum

Samples

Eleven garnet intaglios and cameos from the J. Paul Getty Museum, Villa Collection, were studied (*Figures 3* and *4*). The objects are catalogued in *Table I* and consist of one Etruscan scarab (late 4th–3rd century BC), a Hellenistic group of one cameo and seven intaglios (3rd–1st century BC), and a Roman group of one intaglio and one cameo (1st century BC – 1st century AD). Detailed descriptions of all these carved gems, except no. 10, were published by Boardman (1975), Spier (1989, 1992) and Plantzos (1999).

Methods

Electron microprobe analysis was performed on all 11 garnets at the Division of Geology and Planetary Sciences, California Institute of Technology, Pasadena, California. For this technique, a specimen must be stable in a 10^{-5} torr vacuum environment. Typically, garnets are durable and subjecting them to vacuum in a microprobe poses no special risk. Fractured stones, however, should not be subjected to vacuum.

The gems were mounted with Elmer's brand white glue in specially machined brass templates with die-cut bevelled apertures of various sizes. A reasonably flat, polished surface was located on each specimen and positioned on the masking plate over an aperture of appropriate size. Four intaglios could be mounted on a single template. A carbon coating with a thickness of about 225 Å was deposited over the exposed gem surfaces in a carbon evaporator. After analysis,

Figure 4: Gem no. 1, a pyrope (13.3×9.4 mm), is the earliest dated and only Etruscan gem in the present study. It is carved in the form of a scarab, with a flat side that contains an engraving of a helmeted head in profile. It appears opaque black in reflected light and red in strong transmitted light. While the scarab shape is characteristic of Etruscan glyptic, the use of garnet as a carving material is rare. The J. Paul Getty Museum, Villa Collection, Malibu. Composite photo by Ellen Rosenbery.

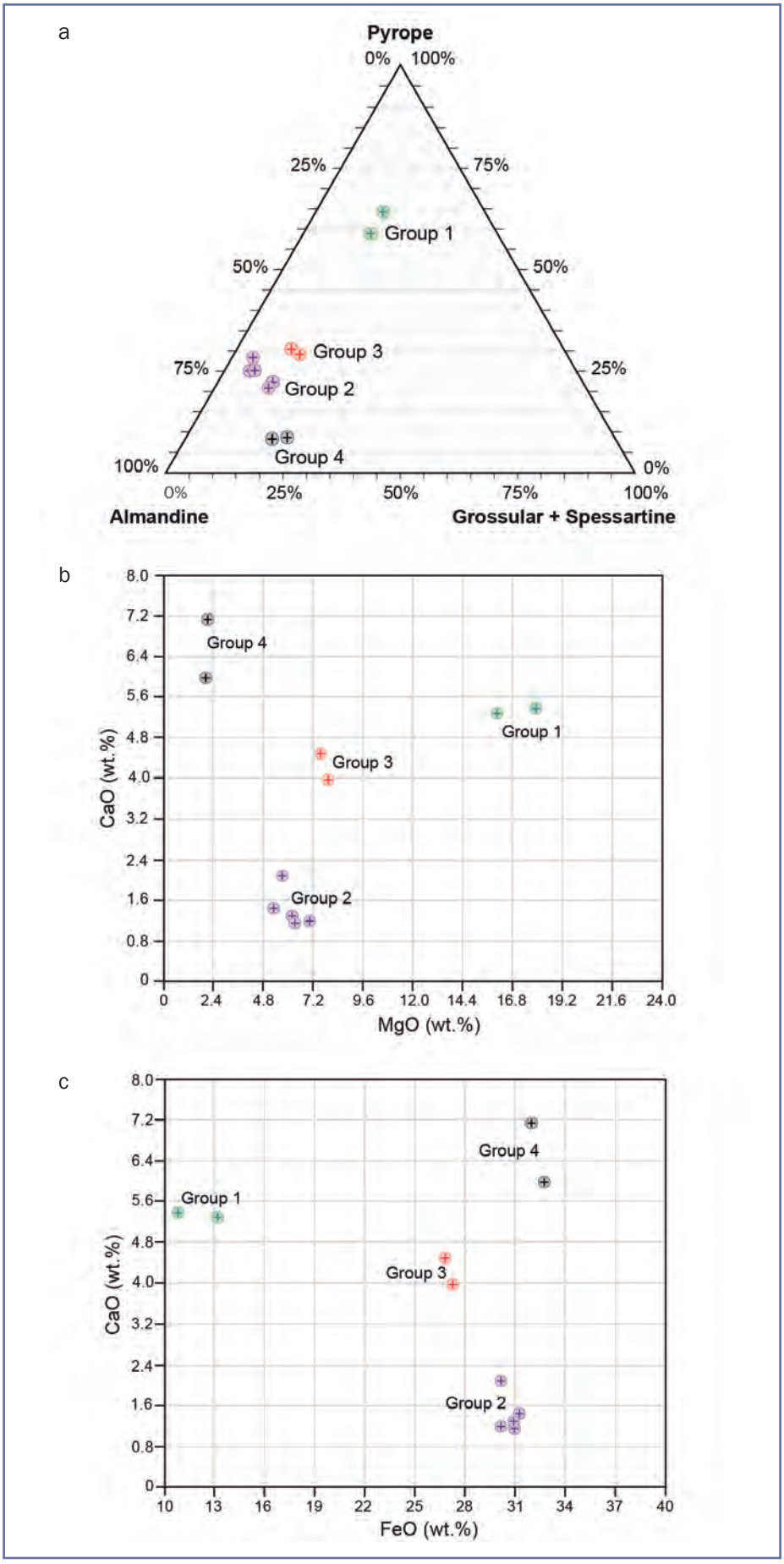

Figure 5: Compositional plots of 11 Etruscan, Greek and Roman garnets from the J. Paul Getty Museum, Villa Collection: (a) ternary diagram of end member compositions; (b) binary MgO–CaO diagram; (c) binary FeO–CaO diagram. The 11 garnets are subdivided into four groups according to their chemical composition: Cr-poor pyrope (Group 1), Mn-rich almandine (Group 2), intermediate pyrope-almandine (Group 3), and Ca-rich almandine (Group 4).

soaking the mounted garnets in warm water easily removed the white glue and the carbon coating was cleaned from the flat, polished surfaces by swabbing with ethanol. (Removal of the carbon from porous or engraved areas can be difficult, so coating of these areas was avoided.)

In successive runs, each template holding the mounted and coated garnets was placed in the chamber of a JEOL JXA-733 electron microprobe. This instrument was equipped with five wavelength-dispersive spectrometers, a Tracor Northern TN-5600 energy-dispersive spectrometer and a TN-5000 X-ray analyser. Surface-reaching inclusions in several of the garnets were identified using the energy-dispersive system of the microprobe.

The microprobe analyses were performed using well-characterized oxide and mineral standards, with a 15 keV accelerating voltage and 25 nA probe current. At least two sample sites on each gem were analysed and then averaged. Data correction was accomplished using CITZAF software. Total iron was taken as FeO, because the electron microprobe cannot discriminate the valence state of Fe^{2+} from Fe^{3+}. The detection limit of trace elements in the garnets was approximately 100 parts per million by weight. The proportion of end-member molecules was calculated from the chemical analyses using the methods of Rickwood (1968) and Locock (2008). However, because the calculated andradite components are very small and the measured Cr contents are low (if present at all), for the simplicity of the discussion we present the composition only as the four dominant end members pyrope, grossular, spessartine and almandine.

Physical and spectroscopic properties were determined using classical gemmological techniques or calculated from chemical composition. Densities for most samples were measured by hydrostatic weighing. However, the density for gem no. 1, the Etruscan scarab, was calculated because undercuts in the carving and the presence of a drill hole made the evacuation of air difficult. Density was also calculated for gem no. 9 because it was mounted in a gold hoop. Density calculations were performed after the method of Skinner (1956), using the percentages of the four end members shown in *Table II* and the physical constants of pure synthetic garnet end members. RI data were obtained using a refractometer and represent average values from measurements made independently by three gemmologists. Due to the poor polish and curved surfaces of some of the gems, RI values could only be measured to the hundredths. All stones were observed with a binocular gemmological microscope and a Beck prism spectroscope.

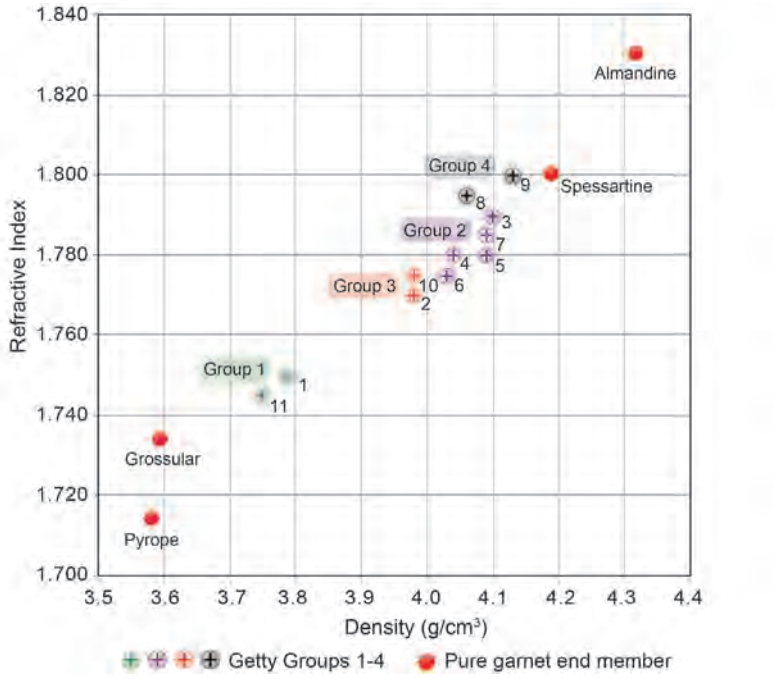

Figure 6: Refractive index versus density of the 11 Getty Museum garnets. The individual data are given in Table III*, and values for some pure end members of the garnet solid-solution series are also depicted. The values for both density and refractive index increase from Cr-poor pyrope (Group 1), to intermediate pyrope-almandine (Group 3) and Mn-rich almandine (Group 2), to Ca-rich almandine (Group 4).*

Chemical composition and molecular percentages of end members

The compositional range of the 11 Getty Museum garnets *(Table II)* shows they are members of the pyrope-almandine solid-solution series. Two of the garnets are pyrope, each containing 14% grossular and 1% spessartine. Nine garnets are almandine, containing 3–20% grossular and 1–7% spessartine. Compositional plots *(Figure 5)* show distinct separation between the pyrope (Group 1) and the various Fe-rich almandine samples, which can be subdivided into three groups described as Mn-rich almandine (Group 2), intermediate pyrope-almandine (Group 3) and Ca-rich almandine (Group 4).

Gemmological characteristics

The physical properties of the Getty Museum garnets, including RI, density, colour and internal features, are presented in *Table III*. A plot of density vs. RI *(Figure 6)* again shows the clear separation of pyrope (Group 1) from almandine (Groups 2 and 4) and the corresponding increase in both values with greater almandine content. The two intermediate pyrope-almandine samples (Group 3) have slightly lower RI and density values than the almandines of Groups 2 and 4.

The two Group 1 pyropes are dark coloured with internal features that are difficult to resolve, even with strong transmitted illumination. The Roman gem

Table II. Electron microprobe analysis and percentages of end members calculated for 11 ancient garnets in the J. Paul Getty Museum, Villa Collection.

Group	Group 1 Pyrope		Group 2 Mn-bearing almandine					Group 3 Intermediate pyrope-almandine		Group 4 Ca-rich almandine	
Oxide (wt.%) / Gem no.	1	11	3	4	5	6	7	2	10	8	9
P_2O_5	0.04	0.02	0.03	0.08	0.15	0.11	0.08	0.03	0.02	0.05	0.03
SiO_2	42.10	43.00	38.51	39.10	37.96	38.78	38.85	39.81	39.82	38.03	37.90
TiO_2	0.45	0.37	nd[a]	0.03	0.02	0.03	0.02	nd	0.02	0.04	0.05
Al_2O_3	23.51	24.06	22.00	22.29	21.53	21.96	22.19	22.57	22.63	21.53	21.40
V_2O_3	nd	0.02	nd	nd	nd	0.03	0.01	0.02	nd	0.03	0.01
Cr_2O_3	nd	0.03	nd	nd	nd	0.01	nd	nd	nd	nd	nd
FeO[b]	13.20	10.82	31.23	30.14	30.90	30.97	30.14	27.25	26.77	31.98	32.74
MnO	0.36	0.31	3.42	0.42	0.61	1.35	2.58	0.34	0.81	0.67	0.54
ZnO	nd	0.01	0.02	0.01	0.02	0.05	0.02	0.04	0.02	0.02	0.01
MgO	16.05	17.91	5.32	7.03	6.18	6.32	5.70	7.93	7.55	2.16	2.03
CaO	5.27	5.37	1.44	1.19	1.29	1.14	2.08	3.96	4.48	7.12	5.97
Na_2O	0.06	0.02	0.02	0.08	0.12	0.11	0.07	0.03	0.01	0.04	0.04
Total[c]	**101.06**	**101.94**	**102.03**	**100.37**	**98.80**	**100.85**	**101.72**	**101.98**	**102.13**	**101.68**	**100.73**
Cations per 12 oxygens											
P	0.002	0.001	0.002	0.005	0.010	0.007	0.005	0.002	0.001	0.003	0.002
Si	3.016	3.018	2.990	3.023	3.008	3.011	3.002	3.008	3.008	2.992	3.008
Sum Z	**3.018**	**3.019**	**2.992**	**3.028**	**3.018**	**3.018**	**3.007**	**3.010**	**3.009**	**2.995**	**3.010**
Ti	0.024	0.020	nd	0.001	0.001	0.001	0.001	nd	0.001	0.002	0.004
Al	1.985	1.990	2.013	2.031	2.011	2.010	2.020	2.010	2.014	1.996	1.998
V	nd	0.001	nd	nd	nd	0.002	0.001	0.001	nd	0.002	0.002
Cr	nd	0.002	nd	nd	nd	0.001	nd	nd	nd	nd	nd
Sum Y	**2.009**	**2.013**	**2.013**	**2.032**	**2.012**	**2.014**	**2.022**	**2.011**	**2.015**	**2.000**	**2.004**
Fe	0.791	0.635	2.028	1.949	2.048	2.011	1.947	1.722	1.691	2.104	2.173
Mn	0.022	0.019	0.225	0.027	0.041	0.089	0.169	0.022	0.052	0.045	0.034
Zn	nd	0.001	0.001	0.001	0.001	0.003	0.001	0.002	0.001	0.001	0.001
Mg	1.714	1.874	0.616	0.811	0.730	0.732	0.657	0.893	0.851	0.254	0.242
Ca	0.404	0.404	0.120	0.099	0.110	0.095	0.172	0.321	0.363	0.600	0.520
Na	0.009	0.003	0.003	0.012	0.019	0.017	0.010	0.004	0.001	0.006	0.007
Sum X	**2.940**	**2.936**	**2.993**	**2.899**	**2.949**	**2.947**	**2.956**	**2.964**	**2.959**	**3.010**	**2.977**
End member percentages[d]											
Pyrope	58.49	63.91	20.60	28.09	24.92	25.01	22.30	30.19	28.78	8.45	8.16
Grossular	13.79	13.79	4.02	3.42	3.74	3.24	5.84	10.84	12.28	19.98	17.51
Spessartine	0.75	0.63	7.52	0.95	1.41	3.03	5.73	0.75	1.74	1.50	1.14
Almandine	26.97	21.67	67.86	67.54	69.93	68.72	66.13	58.22	57.20	70.07	73.19

[a] Abbreviation: nd = not detected.

[b] Total iron as FeO.

[c] Slightly high totals for some analyses are due to the fact that the ancient garnets did not have perfectly flat polished surfaces that could be oriented exactly perpendicular to the electron beam. Nevertheless, the sum of cations at the X, Y and Z sites indicates that all of the analyses are of high quality.

[d] Percentages of end members were calculated as the four end-members pyrope ($Mg_3Al_2Si_3O_{12}$), grossular ($Ca_3Al_2Si_3O_{12}$), spessartine ($Mn_3Al_2Si_3O_{12}$) and almandine ($Fe^{2+}_3Al_2Si_3O_{12}$). The end members uvarovite ($Ca_3Cr_2Si_3O_{12}$), andradite ($Ca_3Fe^{3+}_2Si_3O_{12}$), and knorringite ($Mg_3Cr_2Si_3O_{12}$) were not included because the amounts were negligible.

Greek, Etruscan and Roman garnets in the antiquities collection of the J. Paul Getty Museum

Table III: Gemmological properties of 11 ancient garnets from the J. Paul Getty Museum, Villa Collection.

Gem no.	RI	D (g/cm^3)	Colour and diaphaneity	Internal features
Group 1: Cr-poor pyrope ($Py_{58-64}Gro_{14}Sp_1Alm_{22-27}$)				
1	1.75	3.79 (calc.)	Very dark red, nearly black in reflected light; semitransparent	Difficult to resolve, due to the stone's dark colour and roiled internal appearance
11	1.745	3.75	Dark orange-brown to reddish brown; thinner parts of carving around edges appear yellowish brown in transmitted light; semitransparent	Roiled appearance; fractures in front surface, in the right cheek, and across back of the plaque; and scattered, fine tubes (some curved or bent), tapering to a point into the body of the stone
Group 2: Mn-rich almandine ($Py_{21-28}Gro_{3-6}Sp_{1-8}Alm_{66-70}$)				
3	1.79	4.10	Vivid reddish purple; transparent	Numerous transparent crystals (zircon and/or monazite), some with colour zoning, some with brown strain halos; irregularly shaped transparent colourless crystals (probably quartz), which, in turn, contain opaque black inclusions; metamict zircon* crystals; angular transparent inclusions (possibly quartz); rutile needles oriented at 70° and 110°; small transparent rods with rounded ends (probably apatite); and long, curved transparent colourless crystals (probably sillimanite)
4	1.78	4.04	Medium to dark reddish purple; transparent	Strong ADR; transparent zircon(?) and monazite* crystals with strain halos; irregularly shaped two-phase inclusions arranged in a plane; angular transparent inclusions, probably quartz; rutile needles oriented at 70° and 110°; and small transparent rods with rounded ends, probably apatite
5	1.78	4.09	Medium to dark reddish purple; transparent	Strong ADR; numerous zircon* crystals with strain halos; transparent colourless crystals with strain halos, possibly monazite and/or zircon; rutile needles oriented at 70° and 110°; small transparent rods with rounded ends, probably apatite; long, curved transparent crystals, probably sillimanite; numerous large, irregularly shaped transparent crystals, probably quartz; large, irregularly shaped black inclusions of ilmenite, some flat; high-relief crystals (rutile?); opaque black crystals (rutile or ilmenite?); transparent colourless crystals containing unidentified inclusions, some agglomerated in masses of opaque black crystals of corroded ilmenite; and a stained fracture
6	1.775	4.03	Medium to dark reddish purple; transparent	Numerous stained fractures; zircon(?) and brownish stained, transparent monazite* crystals; and quartz*, including numerous aggregates of irregularly shaped transparent crystals
7	1.785	4.09	Vivid pinkish purple; transparent	Few inclusions overall; transparent crystals of zircon and monazite with strain halos; metamict zircons*; a fracture; and several transparent stubby, rod-shaped crystals with rounded ends, probably apatite
Group 3: Intermediate pyrope-almandine ($Py_{29-30}Gro_{11-12}Sp_{1-2}Alm_{57-58}$)				
2	1.77	3.98	Light red-purple, with very slight brownish/greyish cast and flashes of orange when turned under a light; transparent	Stained micaceous flakes; irregularly shaped transparent colourless crystals, probably quartz, included with opaque black corroded crystals, probably ilmenite; rutile with a cottony/silky appearance; dashes and dots; small transparent rods with rounded ends, probably apatite; several transparent crystals of zircon and/or monazite, surrounded by strain halos; a fracture; and surface-reaching, blocky black inclusions, probably rutile or ilmenite
10	1.775	3.98	Reddish orange with brownish purple cast; semitransparent	Turbid, zoned, heavily fractured and asteriated; corroded, opaque black inclusions of various sizes; stained fractures; flat, irregularly shaped, transparent, colourless crystals, probably quartz, included with black corroded crystals, probably ilmenite; zircon*; transparent crystals intersecting irregularly shaped opaque black inclusions; a dense arrangement of short rutile needles with a silky appearance; dots and dashes; and numerous minute micaceous flakes scattered throughout
Group 4: Ca-rich almandine ($Py_8Gro_{17-20}Sp_1Alm_{70-73}$)				
8	1.795	4.06	Medium to dark brownish red; semitransparent	Numerous partially healed fractures and wispy, minute two-phase inclusions arranged in stained planes; and several zircon crystals surrounded by tension haloes
9	1.80	4.13 (calc.)	Medium orange-brown; transparent	Partially healed fractures, stained and showing high relief; tattered micaceous(?) flakes and blocky and irregularly shaped, opaque black inclusions, variable in size; and minute inclusions (some appear two-phase)

* This inclusion was identified by energy-dispersive spectroscopy; otherwise inclusions were identified visually and not confirmed by analytical instrumentation.

Greek, Etruscan and Roman garnets in the antiquities collection of the J. Paul Getty Museum

(no. 11) appears yellowish brown around the edges where it is thin — a feature sometimes observed in pyrope *(Figure 7)*. It contains fine tubes that terminate in tapered points *(Figure 8)*.

The five Hellenistic intaglios comprising Group 2 (Mn-rich almandine) all exhibit the vivid, saturated reddish purple to purple colour *(Figure 9)* that is typically associated with rhodolite or 'Grape garnet'. However, they show a compositional range and physical properties that are different from rhodolite (i.e., pyrope-almandine: Stockton and Manson, 1985; Webster, 1994; Lind *et al.*, 1998; Hanneman, 2000; Adamo *et al.*, 2007). All five of the ancient gems have relatively high RI and density values due to their large almandine component. Gem nos. 3 and 7 are the two brightest stones in Group 2. They also have the greatest spessartine content of all the garnets studied, at 7.5 and 5.7 mol%, respectively *(Table II)*. Gem nos. 4, 5, and 6 have a more turbid appearance and all show a darker, more purple hue. The inclusions exposed at the surface of the Group 2 garnets were identified using EDS as quartz, zircon, metamict zircon (in which radioactive elements were detected) and monazite (*Figures 10–12)*.

Tension halos surround both zircon and monazite crystallites *(Figures 10a–c)*. Some of these halos are stained brown, as expected for those surrounding monazite (J.I. Koivula, pers. comm., 2013). Other internal features include oriented rutile needles *(Figure 10d)* and irregularly shaped quartz *(Figures 11* and *12)*. Additional inclusions that were identified by their visual appearance include apatite rods *(Figure 12)*; long, slender sillimanite with a fibrous or tubular appearance *(Figure 13)*; transparent crystals (quartz and/or apatite) agglomerated with opaque black material, possibly decomposed ilmenite *(Figure 14)*; and ilmenite *(Figure 15)*.

The two intermediate pyrope-almandines of Group 3 (gem nos. 2 and 10; *Figures 16* and *17*) are very close in chemical composition, RI and density *(Tables II* and *III)*. However, they are quite different in appearance and belong to different periods of production. Gem

Figure 7: Gem no. 11 (11.7×9.5 mm) is a Roman pyrope cameo encircled by a flat plaque; it is semitransparent and dark orange-brown to reddish brown. The front-facing head of Eros was a popular motif carved in garnets and other gems during the Roman Imperial era. The J. Paul Getty Museum, Villa Collection, Malibu, California, gift of Damon Mezzacappa and Jonathan H. Kagan. Photo by Ellen Rosenbery.

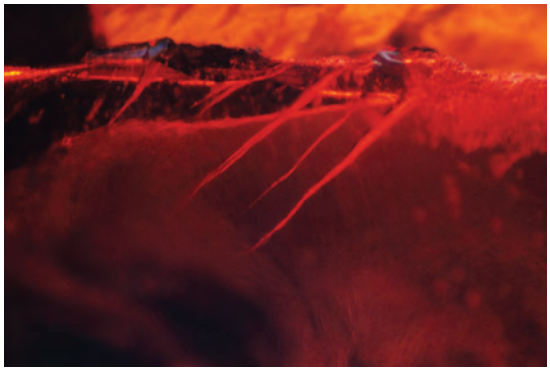

Figure 8: Fine tubes originating at a surface-reaching fracture taper into the body of gem no. 11, a Roman pyrope cameo carving. Photomicrograph by Lisbet Thoresen; magnified 50×.

Figure 9: These five almandine intaglios, representing the Getty Group 2 garnets, all share very similar optical properties, chemical composition and a saturated reddish purple to purple colour. They are cut en cabochon *with the engraved sides highly convex. The shapes of the stones and the subjects depicted are characteristic signatures of Hellenistic glyptic. Clockwise from left: gem nos. 3 (21.9×11.7 mm), 7, 4, 6 and 5. The J. Paul Getty Museum, Villa Collection. Photo by Ellen Rosenbery.*

Greek, Etruscan and Roman garnets in the antiquities collection of the J. Paul Getty Museum

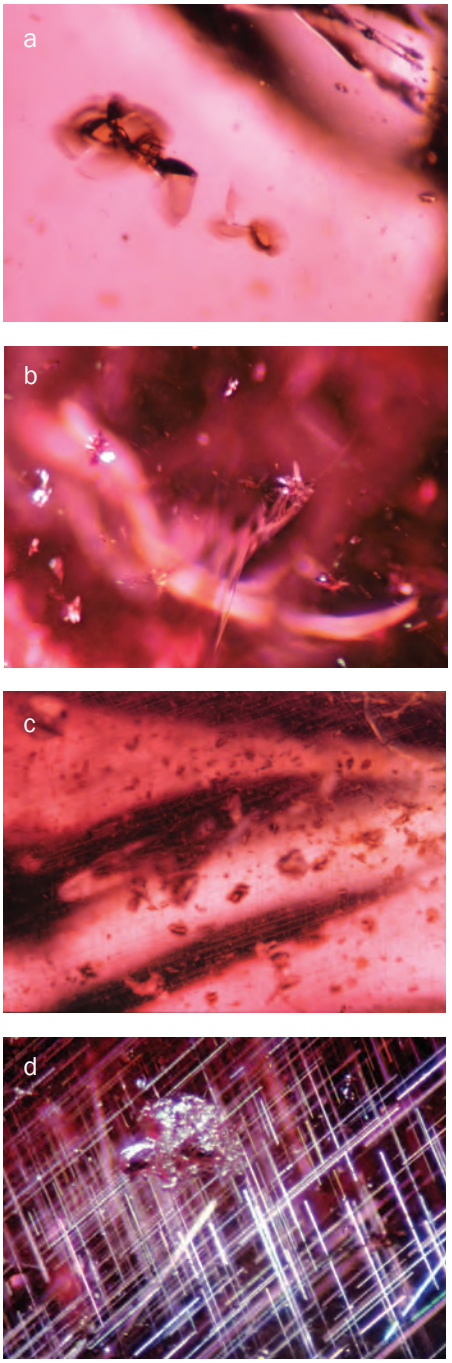

Figure 10: (a) Tension halos around zircon inclusions (here, in gem no. 4).
(b) Scattered zircon crystals surrounded by tension halos (here, gem no. 7).
(c) Monazite inclusions with brown-stained strain halos, visible against a background of oriented fine rutile needles in gem no. 4.
(d) Radioactive elements contained in its crystal lattice caused this metamict zircon crystal to rupture in its almandine host (gem no. 3). In the background, acicular crystals of rutile are oriented in two directions, forming angles of 70.5° and 109.5°.
Photomicrographs by John I. Koivula; magnified 85× (a), 52× (b), 63× (c) and 50× (d).

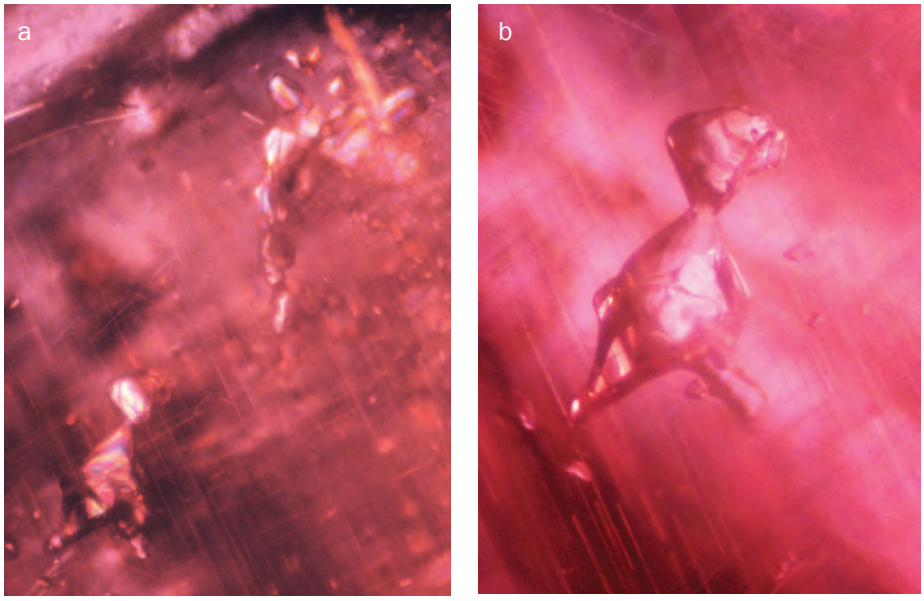

Figure 11: Relatively large, blocky crystal inclusions of irregular shape in the garnets are often quartz, as in these images of gem no. 5. Viewed with crossed polarizing filters (a), the inclusions exhibit spectral colours. Photomicrographs by Lisbet Thoresen (a, magnified 50×) and John I. Koivula (b, magnified 110×).

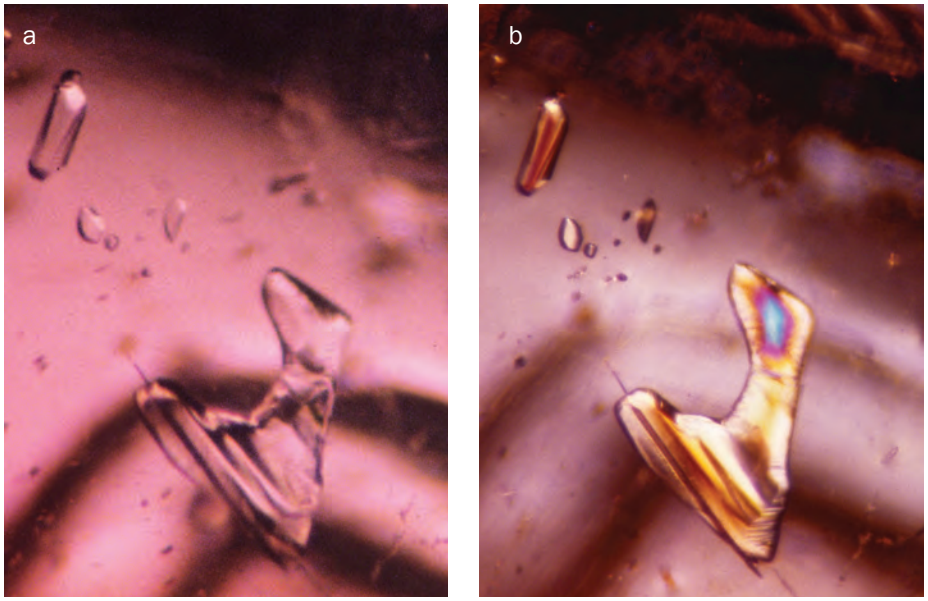

Figure 12: The transparent rod-shaped inclusion (at top left) observed in almandine gem no. 4 under plane polarized light (a) and crossed polarizers (b) appears to be apatite. Also seen is a large irregularly shaped crystal, probably quartz, with a rutile needle captured along its lower edge. Photomicrographs by John I. Koivula and Lisbet Thoresen; magnified 50×.

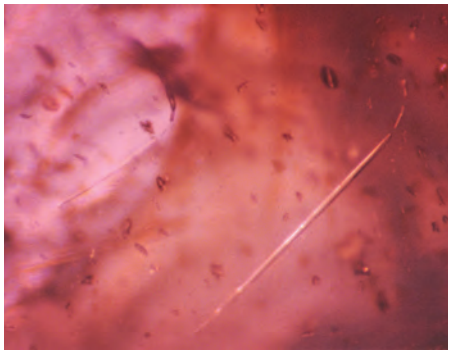

Figure 13: Slender tubular-shaped inclusions, both curved and straight, such as the one seen here in gem no. 5 (magnified 46×) were observed in several of the Group 2 almandines. They are probably sillimanite. Also present are monazite inclusions hovering in the background. Photomicrograph by Lisbet Thoresen.

Greek, Etruscan and Roman garnets in the antiquities collection of the J. Paul Getty Museum

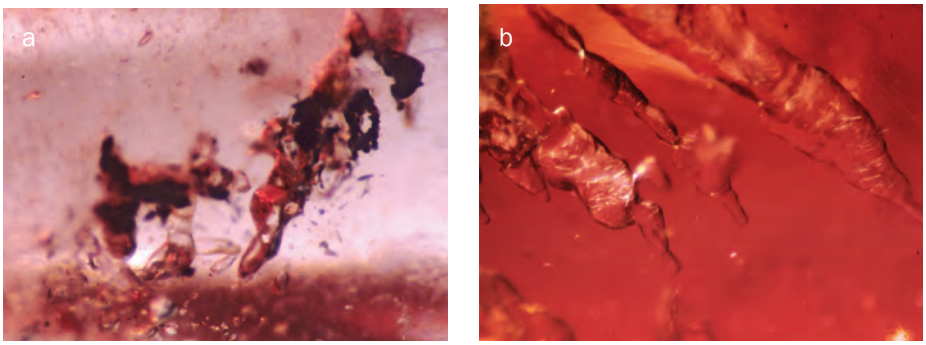

Figure 14: (a) Irregularly shaped, high-relief crystals, probably quartz with opaque black inclusions (ilmenite and/or rutile?), like the ones seen here in gem no. 10, are typical of several of the Groups 2 and 3 garnets. (b) Large irregularly shaped transparent crystals (probably quartz) contain randomly oriented inclusions having the appearance of small fibres or rods, seen here in gem no. 10. Photomicrographs by Lisbet Thoresen (a, magnified 30×) and John I. Koivula (b, magnified 65×).

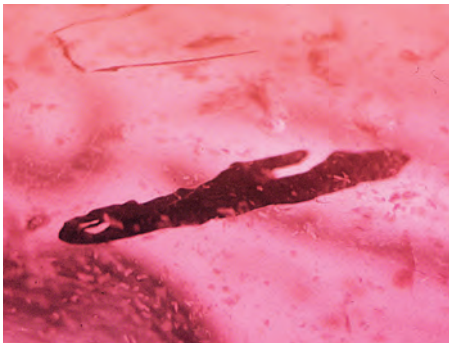

Figure 15: Irregularly shaped opaque black inclusions (ilmenite?), such as the one seen here in gem no. 5, can be observed in several Group 2 and 3 garnets. Photomicrograph by John I. Koivula; magnified 40×.

no. 2 is a Hellenistic cameo portrait of a Ptolemaic queen that exhibits lower saturation and brightness than the Group 2 almandines, but its appearance is otherwise very similar to gem nos. 3 and 7. It is relatively clean internally and contains inclusions similar to those seen in the Group 2 garnets. Gem no. 10 is a Roman intaglio that appears turbid and is predominantly reddish orange with a brownish purple cast. It is unique among the Getty Museum garnets for its colour and moderate asterism caused by a dense arrangement of silky rutile. Other internal features include transparent blocky crystals with black material (possibly decomposed ilmenite, *Figure 14a*), and several large irregularly shaped crystals (probably quartz) that in turn contain inclusions resembling stubby rods or thick fibres *(Figure 14b)*.

Figure 16 (left): Portrait bust, probably Queen Arsinoë II (d. 270 BC), the deified sister-wife of Ptolemy II. This fine cameo (gem no. 2, 19.1×12.9 mm) was cut from a large piece of pyrope-almandine of exceptional clarity. It has a light red-purple colour that weakly flashes an orange hue when turned under a light. The J. Paul Getty Museum, Villa Collection. Photo by Ellen Rosenbery.

Figure 17: An early Roman Imperial intaglio (gem no. 10, 16.1×12.6 mm) depicting the goddess Minerva seated and facing front, engraved in the flat side of an asteriated pyrope-almandine cabochon. The J. Paul Getty Museum, Villa Collection, gift of Stanley Ungar. Photo by Ellen Rosenbery.

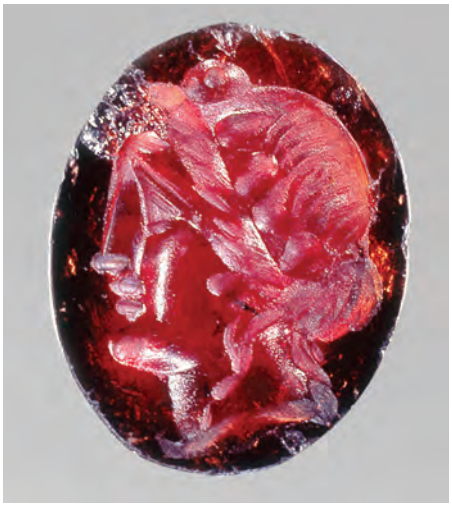

Figure 18 (left): The Hellenistic Group 4 almandines include a Ptolemaic (2nd–1st century BC) intaglio engraved with the profile head of Dionysos (gem no. 8, 16.0×13.0 mm) on the flat face, from Iran. The J. Paul Getty Museum, Villa Collection, gift of Jonathan H. Kagan. Photo by Ellen Rosenbery.

Figure 19: A late Hellenistic (1st century BC) ring-stone mounted in a gold hoop depicting a profile bust of Hermes (gem no. 9, 8.1×6.8 mm), from Asia Minor. The J. Paul Getty Museum, Villa Collection, gift of Damon Mezzacappa and Jonathan H. Kagan. Photo by Ellen Rosenbery.

The two Ca-rich almandines of Group 4, both Hellenistic intaglios (gem nos. 8 and 9; *Figures 18* and *19*), are characterized by significant grossular components of 20 and 17.5 mol%, respectively. They have the greatest almandine components of the Getty Museum garnets — above 70% — so their RI and density values are correspondingly high *(Table III)*. Gem no. 8 is semitransparent and medium to dark brownish red, while no. 9 is medium orange-brown and transparent. Both gems contain high-relief partially healed fractures, but the latter stone also contains blocky, irregularly shaped black inclusions, as well as micaceous(?) flakes. These intaglios belong to two different periods of manufacture and have no typological association, but they are both purported to be of eastern origin (i.e., Iran and Asia Minor).

Spectroscopic properties

Optical spectra of the Getty Museum garnets are illustrated in *Figure 20*. Both pyropes of Group 1 show strong absorption through most of the visible range in the spectroscope, and individual absorption bands are difficult to resolve. All garnets of Groups 2–4 show a clear line spectrum consisting of four absorption bands: A at 610 nm, B in the range between 570 and 590 nm, C

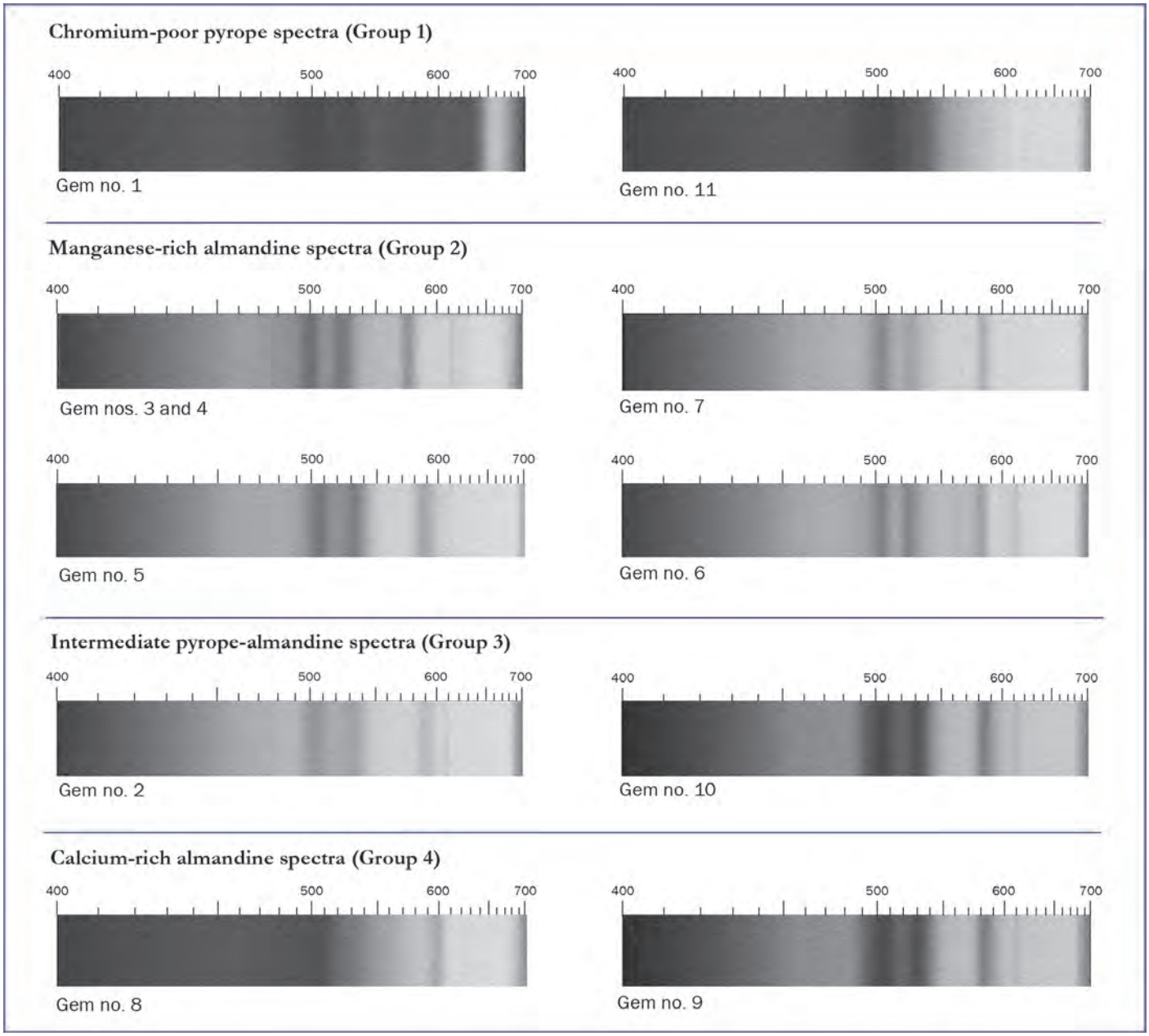

Figure 20: Optical spectra of the 11 garnets in the J. Paul Getty Museum, Villa Collection. The Group 1 pyropes show strong absorption through most of the visible range, while the Groups 2–4 garnets show a clear line spectrum consisting of four absorption bands assigned to bivalent iron (Fe^{2+}) in the garnet structure.

Table IV: Description of 26 Greek and Roman garnets analysed in five studies.

Gem no.	Identification	Description[a]	Culture / period
Antikensammlung, Staatliche Museen zu Berlin (Formigli and Heilmeyer, 1990), electron microprobe analysis			
12, 13	Cr-poor pyrope	Two inlays in a Herakles knot centrepiece belonging to a gold and garnet chain necklace *(Figure 1)*; no. 1980.17	Hellenistic, 230–210 BC; all belong to a jewellery hoard from a tomb in Taranto, southern Italy (excavated *ca.* 1900)
14	Cr-poor pyrope	One garnet carved in the form of a chain link in a gold and garnet chain necklace (with Herakles knot centrepiece; *Figure 1*); no. 1980.17	
15	Cr-poor pyrope	One small plain cabochon in a gold hairnet *(Figure 24)*; no. 1980.22	
Museum für Kunst und Gewerbe, Hamburg (Gartzke, 2004; Gartzke *et al.,* 2004), electron microprobe analysis			
16, 17 18, 19	Mn-rich almandine Mn-poor almandine	Two plain cabochons (7.0×6.0 and 9.5×8.0 mm) Two small beads (All set in a gold earring, no. 1918.58; *Figure 22a*)	Hellenistic, 3rd–1st century BC; although manufactured at different times, all belong to a jewellery hoard from a tomb at Palaiokastro in Thessaly, northern Greece (excavated 1909)
20, 21 22	Mn-rich almandine Mn-poor almandine	One plain cabochon and one small bead One small bead (All set in a gold earring, no. 1918.59; *Figure 22a*)	
23, 24, 25 26	Ca-rich almandine Cr-poor pyrope	Three small beads One small bead (All set in a gold earring, no. 1918.60; *Figure 22b*)	
27	Ca-rich almandine	One plain cabochon (9.8×7.7 mm) set in a gold mount; no. 1917.206	
28	Ca-rich almandine	One plain cabochon (14.4×11.6 mm) set in a gold mount; no. 1918.63	
29	Intermediate almandine-rich pyrope-almandine	One plain cabochon (11.0×8.5 mm) set in a gold mount; no. 1917.205	
Benaki Museum, Athens (Pappalardo *et al.,* 2005), PIXE combined with XRF analysis[b]			
30	Ca-rich almandine	One inlay in a gold diadem; no. 1548	Hellenistic, early 2nd century BC; from Thessaly, northern Greece
31	Cr-poor pyrope	One large oval cabochon engraved with Nike driving a biga, set in a gold finger ring; no. 1551	Hellenistic, *ca.* 200 BC; from Thessaly, northern Greece
Museo Palatino, Rome (Gliozzo *et al.,* 2011), PIXE analysis			
32	Ca-rich almandine	One oval garnet (20×16×5 mm) engraved with a male head in profile surrounded by a taenia; no. 473579	Flavian, AD 69–96; from the Vigna Barberini at Palatine Hill, Rome (excavated 1985–1998)
Staatliche Antikensammlungen und Glyptothek, James Loeb Collection, Munich (Gilg and Gast, 2012), Raman spectroscopy combined with XRF analysis			
33	Cr-poor pyrope	One high-domed oval cabochon (12.0×7.7 mm) engraved with Eros standing in a three-quarter frontal pose and holding a lyre to the side, set in a gold finger ring; no. 632	Hellenistic, end 2nd/1st half of 1st century BC
34	Ca-rich almandine	One high-domed oval cabochon (15.6×11.8 mm) engraved with Tyche/Fortuna wearing a diadem, perhaps in the guise of the Ptolemaic Queen Kleopatra VII. She holds a rudder in the lowered right hand and a double cornucopia raised in the left, set in a gold finger ring; no. 636	Early Roman Imperial, 2nd half of 1st century BC
35	Ca-rich almandine	One oval cabochon (21.4×15.2 mm) engraved with symbolic iconography related to Apollo connoting support of Cassius and Brutus in the aftermath of Julius Caesar's assassination, set in a gold finger ring; no. 637	Roman Republican, 42 BC
36	Ca-rich almandine	One flat oval garnet (20.6×12.8 mm) engraved on the flat front with a thyrsos with fillets, set in a gold finger ring; no. 638	Early Roman Imperial, 2nd half of 1st century BC
37	Intermediate pyrope-rich pyrope-almandine	One plain round (*ca.* 9.9 mm) cabochon set in a gold finger ring; no. 630	Late Roman Empire, 3rd/4th century AD

[a] Only approximate dimensions are given for mounted gems, and no dimensions were reported for gem nos 12–15, 18–26 and 30–31.
[b] Specimen no. 1562 with 4.7 wt.% Na_2O was omitted.

in the range of 523–533 nm and D at 503 nm. All four bands are assigned to bivalent iron (Fe^{2+}) in the garnet structure, and no additional bands of bivalent manganese (Mn^{2+}) or trivalent iron (Fe^{3+}) are detectable. (For the assignment of iron and manganese bands in garnets, refer to Lind *et al.,* 1998, Schmetzer *et al.,* 2009 and the references therein.) These spectral features are consistent with the chemical analyses. While a prism spectroscope is useful for identifying garnets in general (e.g., in a museum setting), it is inadequate for differentiating pyrope-almandine garnets according to different types.

Comparison of chemical composition of Graeco-Roman and Early Medieval garnets

Only limited chemical data for garnets used in ancient glyptic are available presently from a total of 26 stones: 16 beads, inlays and small cabochons set in jewellery, four unengraved cabochons set in a finger ring and other gold mounts, five intaglios set in finger rings and one loose intaglio (Formigli and Heilmeyer, 1990; Gartzke, 2004; Gartzke *et al.,* 2004; Pappalardo *et al.,* 2005; Gliozzo *et al.,* 2011; Gilg and Gast, 2012). A description of these objects and their cultural attributions is given in *Table IV*.

Plots of chemical composition *(Figure 21)* show that the 26 carved gems from the published literature lie within similar compositional ranges as given for the 11 Getty Museum stones. It is difficult to clearly delineate the boundaries of distribution fields for the different groups, especially given the limited number (37) of analysed stones with properties that are so variable; however, the plots show that the compositional ranges of most of the garnets segregate into four different clusters:

- Cr-poor pyrope
- Mn-rich almandine

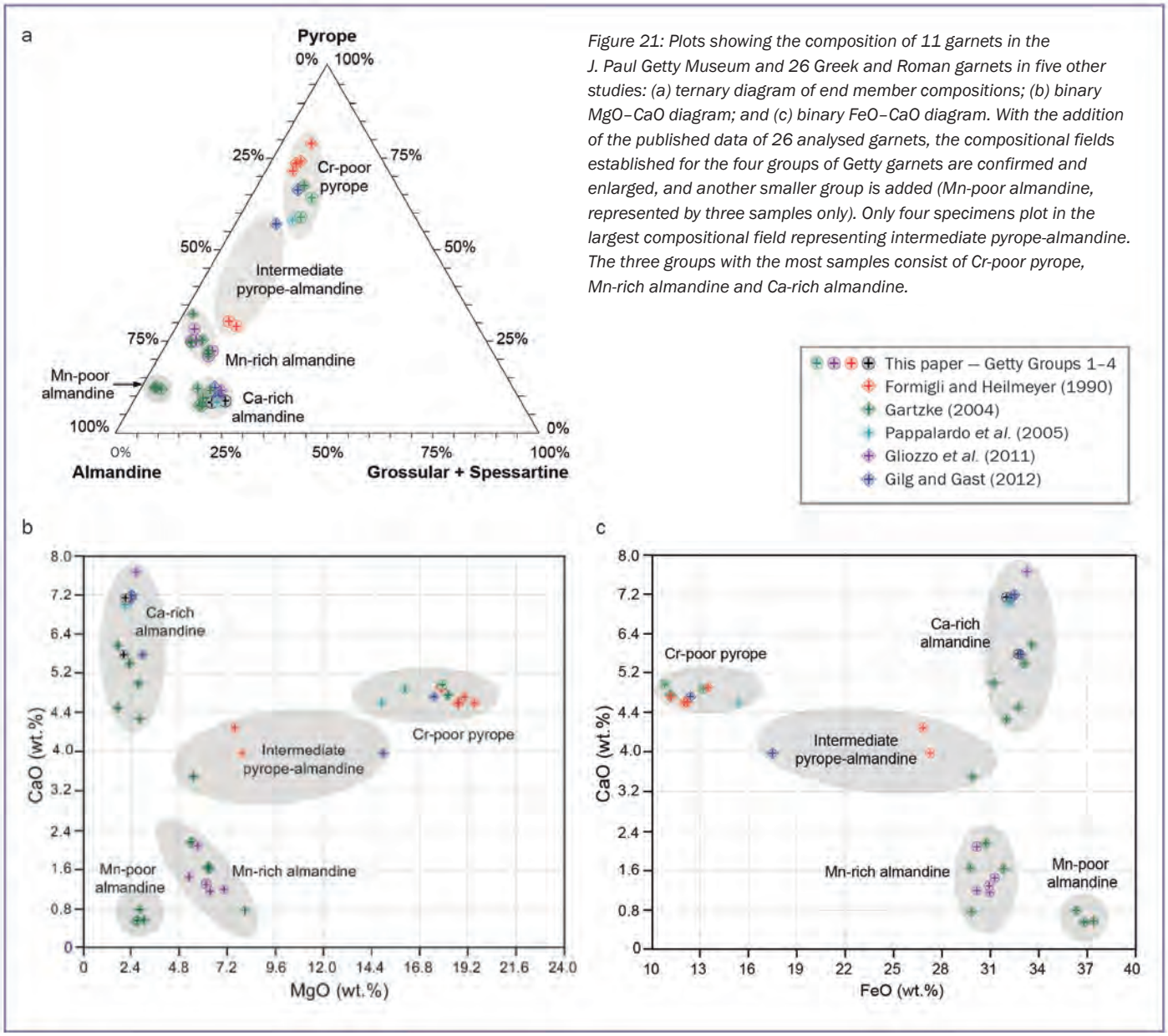

Figure 21: Plots showing the composition of 11 garnets in the J. Paul Getty Museum and 26 Greek and Roman garnets in five other studies: (a) ternary diagram of end member compositions; (b) binary MgO–CaO diagram; and (c) binary FeO–CaO diagram. With the addition of the published data of 26 analysed garnets, the compositional fields established for the four groups of Getty garnets are confirmed and enlarged, and another smaller group is added (Mn-poor almandine, represented by three samples only). Only four specimens plot in the largest compositional field representing intermediate pyrope-almandine. The three groups with the most samples consist of Cr-poor pyrope, Mn-rich almandine and Ca-rich almandine.

Greek, Etruscan and Roman garnets in the antiquities collection of the J. Paul Getty Museum

*Figure 22: Three earrings from a Hellenistic jewellery hoard found in a tomb at Palaiokastro in Thessaly, northern Greece. (a) Pair of gold earrings (approximately 8.1–8.2 cm long) adorned with two winged Erotes suspended between two chains, each terminating in a garnet bead and surmounted by bezel-set gems, including pearls and garnet cabochons (*Table IV, *nos. 16–22). The green stone was analysed by Gartzke (2004) and identified as Cr-bearing mica. (b) Single gold earring (10.2 cm long) adorned with garnets carved as small beads (*Table IV, *nos. 23–26) and suspended from chains, surmounted by a round plaque with a helmeted bust of Athena in gold repoussé. Courtesy of F. Hildebrandt, © Museum für Kunst und Gewerbe, Hamburg; photos by Maria Thrun.*

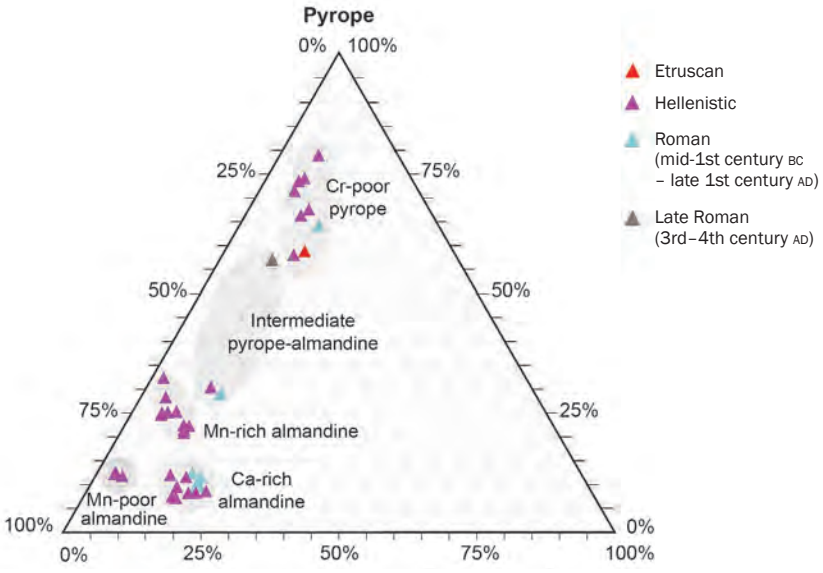

Figure 23: Ternary diagram of end-member compositions of 11 Greek, Etruscan and Roman garnets in the J. Paul Getty Museum and 26 ancient Greek and Roman garnets from the literature, relating compositions to different cultural attributions. The three largest-populated groups are represented by Cr-poor pyrope, Mn-rich almandine and Ca-rich almandine. Garnets of all different chemically separated groups were used in the Hellenistic era. Less heterogeneity of types is seen in the earlier-dated Roman garnets (late 1st century BC to late 1st century AD).

- Ca-rich almandine
- Intermediate pyrope-almandine

One additional field consists of Mn-poor almandine documented by Gartzke (2004), but such compositions were not found in the 11 Getty Museum stones. Stones in this field correspond to three small beads (nos. 18, 19 and 22 in *Table IV*) set in gold earrings from Palaiokastro, in Thessaly, northern Greece *(Figure 22)*. Most contain less Ca than the neighbouring group of Mn-rich almandine.

In the binary diagrams of *Figure 21*, the two Getty Group 3 intermediate pyrope-almandines plot near a mounted garnet cabochon (no. 29 in *Table IV*) analysed by Gartzke (2004). (Note that when plotting no. 29 in the ternary diagram, it overlaps the field of Mn-rich almandine as a result of calculating for [grossular+spessartine], while in the binary diagrams it clearly plots in the pyrope-almandine field. This underscores

the importance of gemmological properties and not only chemical composition for assigning the correct type/cluster/group.) A plain garnet cabochon set in a late Roman gold finger ring (no. 37 in *Table IV*; Gilg and Gast, 2012) also plots within the intermediate pyrope-almandine distribution field. These four garnet analyses are the only data of intermediate pyrope-almandine from the Greek and Roman era that have been published to date. However, in Merovingian cloisonné jewellery of the Early Medieval period, intermediate pyrope-almandine garnets with variable composition are common. In addition, several garnets dating to the Byzantine era (beginning in the 5th century AD) plot within this intermediate group (A. Gilg, pers. comm., 2013). Due to the variable composition of these garnets, it is evident that this heterogeneous group contains gems from different host rocks and/or origins.

The distribution of the ancient garnets having different cultural attributions *(Figure 23)* shows that garnets from all the groups were used in the Hellenistic era. Less heterogeneity of types is seen in the Roman garnets (mid-1st century BC to late 1st century AD). To date, the majority of garnets found within this era are Ca-rich almandine (represented by the two Getty Group 4 garnets and 12 others).

The data published by Gartzke (2004) and Gartzke *et al.* (2004) show that the Hellenistic garnets set in three earrings are different types of garnets and therefore did not originate from the same source. One pair of earrings *(Figure 22a)* contains several Mn-rich almandine cabochons and one small bead (nos. 16, 17, 20 and 21 in *Table IV*), in addition to three beads of Mn-poor almandine (nos. 18, 19 and 22 in *Table IV*). Suspended from gold tassels in a third earring *(Figure 22b)* are three small beads of Ca-rich almandine (nos. 23, 24 and 25 in *Table IV*) and one pyrope (no. 26 in *Table IV*). These observations of different types of garnets set within one item of jewellery are consistent with similar variability in numerous items of cloisonné metalwork containing garnet inlays produced in the Early Medieval period.

In contrast to the variable composition of the garnets in the Hellenistic gold jewellery belonging to the hoard from Palaiokastro in northern Greece, the garnets mounted in the gold necklace and hairnet belonging to the Hellenistic hoard from Taranto, Italy, appear to be homogeneous in composition (Formigli and Heilmeyer, 1990; *Figures 1* and *24*). Analyses performed on four stones characterized all of them as Cr-poor pyrope.

In *Figure 25*, the chemical compositions of earlier Greek and Roman garnets are compared against those of the Early Medieval garnets in the Calligaro *et al.* (2006–2007) study. The nomenclature of different 'types' or 'clusters' used by different researchers is shown in *Table V*. Two of the three main types of Greek and Roman garnets *(Figure 21)* plot within the distribution field of the garnets used in the Early Medieval period:

Figure 24: A Hellenistic gold hairnet with small pyrope cabochons (1.65–4.40 mm in diameter) from a jewellery hoard, dated 230–210 BC, found in ca. 1900 in a tomb in Taranto, southern Italy. The medallion in the centre is 4.1 cm in diameter. © Antikensammlung, Staatliche Museen zu Berlin; photo by Johannes Laurentius.

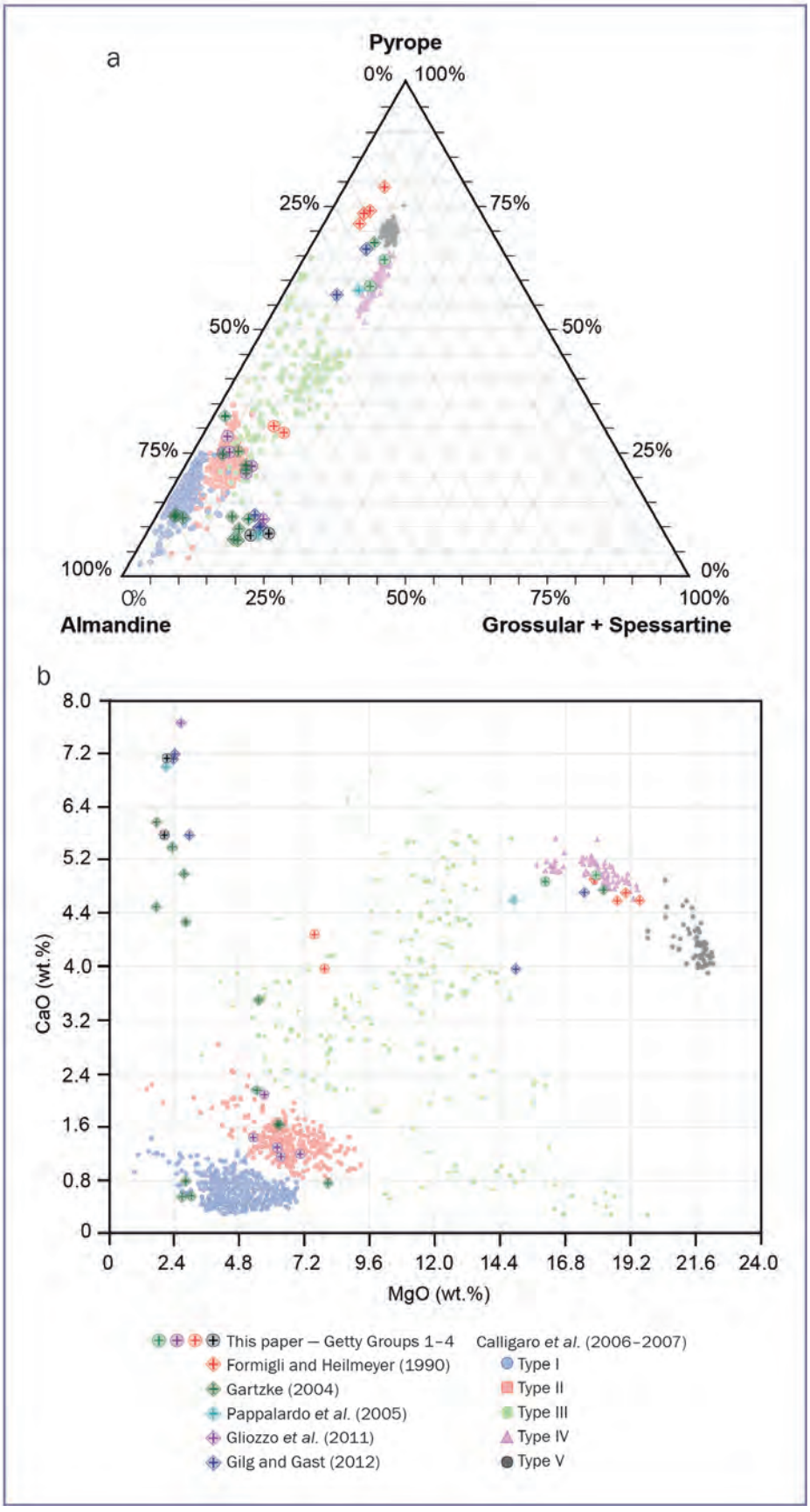

Figure 25: Data from 11 Graeco-Roman garnets in the current study and 26 garnets in five other studies overlaying the data of Early Medieval garnets from Calligaro et al. *(2006–2007). (a) Ternary diagram of end-member compositions, (b) binary MgO–CaO diagram.*

- Mn-rich almandine plots with almandine of Type II of Calligaro *et al.* (2006–2007), identical to Cluster A of Gilg *et al.* (2010).
- Cr-poor pyrope plots with pyrope of Type IV of Calligaro *et al.* (2006–2007), which is identical to Cluster D of Gilg *et al.* (2010) and Gilg and Gast (2012).

Cr-rich pyrope used in later-dated cloisonné metalwork was not represented among the Graeco-Roman garnets analysed. The third cluster of stones found among the Greek and Roman garnet groups, namely Ca-rich almandine, was not found among the garnets analysed in Early Medieval objects. The three almandines with low Ca and Mg contents analysed by Gartzke (2004) plot within the distribution field of Type I almandine of Calligaro *et al.* (2006–2007) or the Cluster B field of Gilg *et al.* (2010). The analyses of Gartzke's Hellenistic specimens, however, show somewhat higher Mn than the comparable group of Medieval garnets. Further work is needed to ascertain whether or not the earlier-dated garnets originated from the same locality represented in the Early Medieval jewellery.

Discussion and conclusions

Considerable analytical data are available on garnets used in the Early Medieval era (5th–7th century AD), primarily in cloisonné metalwork, and a limited number of specimens have been examined together with their gemmological properties (e.g., inclusions). For garnets used in Hellenistic and Roman jewellery, a comparatively small number of analyses were performed and published before 2010, and the inclusion features of most of these specimens were not reported. The first nearly complete data, including identification of inclusions, some confirmed by chemical analyses, were presented by Gilg and Gast (2012) on five ancient Greek and Roman garnets in the James Loeb Collection in the Staatliche Antikensammlungen und Glyptothek in Munich, Germany. The present article provides additional data for 11 Greek, Etruscan and Roman garnets in the J. Paul Getty Museum, Villa Collection.

Table V: Nomenclature and distribution of various garnet types in Merovingian, Hellenistic and Roman glyptic and jewellery.

Period / References	Chemical characteristics and designation of garnet species					
	Mn-poor, Cr-free almandine	Mn-rich, Cr-bearing almandine	Ca-rich almandine	Intermediate pyrope-almandine	Cr-poor pyrope	Cr-rich pyrope
Merovingian (5th to 7th century AD)[a]						
Calligaro *et al.* (2002; 2006–2007), Périn and Calligaro (2007)	Type I almandine	Type II almandine	–	Type III 'rhodolite'	Type IV pyrope	Type V pyrope
Gilg *et al.* (2010)[b]	Cluster B almandine	Cluster A almandine	–	Group X intermediate between pyrope and almandine	Cluster D pyrope	Cluster E pyrope
Hellenistic (3rd to 1st century BC) and Roman (1st century BC to 4th century AD)						
Gilg and Gast (2012)	–	–	Cluster Z	Group X	Cluster D	–
This paper, Getty Museum	–	Group 2	Group 4	Group 3	Group 1	–
Number of specimens (from 11 Getty Museum garnets and 26 garnets in other studies)	3	9	12	3 (almandine-rich) + 1 (pyrope-rich)	9	–

[a] See also Rösch *et al.* (1997), Farges (1998), Greiff (1998), Quast and Schüssler (2000), Mathis *et al.* (2008), and Horváth and Bendö (2011).

[b] Cluster C representing Ca- and Mg-rich almandine from Scandinavia is omitted.

The data from the five earlier studies and the results of the present study help to characterize garnets used in Classical antiquity and differentiate them from one another and also from later-dated stones, specifically Early Medieval garnets and material from the modern market. Unfortunately, because of the lack of quantitative chemical data, the stones examined by Adams *et al.* (2011) cannot be compared directly with our groups and plotted within our diagrams. It appears likely that additional groupings will emerge in future studies, particularly for garnets originating from Western and Central Asia; however, data are needed on reference samples from these regions. Comparison with chemical data available on garnets of the Early Medieval period may reveal distinctive patterns that illuminate details about sources of garnets in antiquity and the ancient gem trade, in general.

Some recent studies lack detailed descriptions of inclusions in the garnets. Inclusion studies may not have been performed, and some garnets such as pyrope frequently do not contain mineral inclusions observable with available magnification. Also, some of the garnets used in antiquity are only semitransparent and/or are mounted in closed-back jewellery settings, which can make observation of inclusions difficult.

According to chemical data from the Getty Museum specimens, four groups of garnets were identified. Comparing our data with published analyses for other Graeco-Roman garnets, these four groups were confirmed and their compositional ranges were enlarged. A fifth group of ancient garnets, also documented among Medieval garnets, is limited to three small beads set in earrings *(Figure 22a)* from Palaiokastro in northern Greece (Gartzke, 2004; Gartzke *et al.,* 2004). Cr-poor pyropes were identified in the Hellenistic necklace and hairnet (*Figures 1* and *24*) belonging to the Taranto Hoard (Formigli and Heilmeyer, 1990), and their uniformity contrasts against the heterogeneity of the Palaiokastro hoard, which suggests that a single source supplied sufficient quantities of raw material for construction of the jewellery found in the tomb at Taranto.

The compositional range of Graeco-Roman garnets in the studies published to date show some overlap of four of the five groups with the different fields of Early Medieval garnets *(Figure 25)*. Ca-rich almandine represented among the ancient Greek and Roman garnets was not found in cloisonné jewellery of the Merovingian period. Cr-rich pyrope, which is documented among Medieval garnets, was not identified among the Greek and Roman gems.

Previously, other researchers have classified Merovingian garnets according to different types *(Table V)*, and they have suggested several possible origins for the Medieval-era stones. The data for the Cr-rich pyrope fit well with the data for Bohemian garnets, which are still mined today in the Czech Republic. For the two types of almandine found frequently in cloisonné metalwork of the Early Medieval period, various localities in India (especially in Rajasthan) have been suggested as possible origins and Sri Lanka has been postulated as a source of intermediate pyrope-almandine (Calligaro *et al.,* 2002, 2006–2007; Gilg *et al.,* 2010; see also Quast and Schüssler, 2000). The data for some ancient pyropes fit with those from Nigeria and Portugal (Cachão *et al.,* 2010; Gilg and Gast, 2012). Some of the ancient garnets published to date,

including the Getty Museum garnets, fall into the distribution fields for some of these gem-producing regions.

A discussion of the sources of ancient garnets is outside the scope of this paper, as it requires a detailed examination in relation to archaeological evidence and ancient texts, as well as comparison of the compositional ranges of ancient garnets against analyses performed on material recently mined (e.g., since 1900), especially from the modern gem trade. Nevertheless, a preliminary comparison of such data suggests that some deposits used in antiquity were different from deposits used later. The distinctive compositions of some ancient Greek and Roman garnets indicate that some stones may have originated from the same source during the same periods of production, although the source may be unknown currently. Relating chemical compositions and gemmological properties, especially inclusions, to stylistic features may help to corroborate attributions to workshops or individual artists.

In workshops of any culture or period, lapidary artists will have had in their inventories of raw materials gems originating from disparate sources. Patrons commissioning custom-made jewellery might also supply their own stones. Blanks or pre-formed rough-outs were prepared in lapidary centres specifically for export and also for use in local workshops. Zwierlein-Diehl (2007) produced a comprehensive reference on glyptic production and workshops in Classical antiquity; for garnets, specifically, see also Spier (1989) and Plantzos (1999). A survey of bead-making industries and a discussion of lapidary centres in the Near East, South Asia (including Sri Lanka) and Southeast Asia (i.e., Oc Eo, Vietnam), from which raw materials and finished garnet beads were exported to Western markets, was given by Francis (2002), with a discussion of garnet beads (almandine and brown grossular) from the Roman colony at Arikamēdu on India's eastern seaboard.

The scope of this discussion precludes considering the myriad correlations between the compositional ranges of ancient Greek and Roman garnets and those of garnets from deposits mined during the past century. For some gems grouped according to composition, more than one locality fits as a prospective source in the ancient world, but the data are far from unequivocal, as noted previously. Also, they are an incomplete representation of the major regions where gems may have originated in antiquity. Specimens from localities in Anatolia, the Levantine littoral to the Iranian Plateau, and more localities in west-northwest Africa and also East Africa are of particular interest. It would not be surprising to see more overlapping of chemical composition, inclusions and other physical properties as additional data from more localities are published. To better differentiate the distribution fields, more detailed characterization — particularly the zonation within garnet specimens, which was not undertaken in this study — will be an important consideration.

This paper has focused on integrating the data for the Getty Museum garnets into a framework that relates isolated analytical studies. The efficacy of such studies lies in their application to a critical re-examination of gemstone origins, their transmission, and their uses or occurrence in the ancient world. Based on a growing body of data from analytical provenance studies published to date, it is clear that complete gemmological characterization and chemical composition provide useful criteria to complement the methods used traditionally in ancient gem studies by archaeologists, historians, connoisseurs, and philologists.

Acknowledgements

Our grateful thanks are given to Prof. George R. Rossman (California Institute of Technology, Pasadena, California), who supported the study and supervised the analyses performed on the Getty Museum garnets; Paul Carpenter (formerly of Caltech), who performed the analyses; Dr Thomas Calligaro (Centre de Recherche et de Restauration des Musées de France, Paris), who shared two of his original diagrams; John I. Koivula (Gemological Institute of America, Carlsbad, California), who read the manuscript, examined the Getty Museum garnets and helped with the identification and characterization of inclusions; Prof. James A. Harrell (University of Toledo, Ohio), who read the manuscript and made useful suggestions; and Prof. H. Albert Gilg (Technical University of Munich, Germany), who kindly supplied several references and discussed various topics.

References

Adamo, I., Pavese, A., Prosperi, L., Diella, V., and Ajò, D., 2007. Gem-quality garnets: Correlations between gemmological properties, chemical composition and infrared spectroscopy. *Journal of Gemmology,* **30**(5/6), 307–19

Adams, N., 2011. The garnet millennium: The role of seal stones in garnet studies. In: C. Entwistle and N. Adams, Eds, *'Gems of Heaven': Recent Research on Engraved Gemstones in Late Antiquity c. AD 200–600.* British Museum Research Publication 177, The British Museum, London, 10–24

Adams, N., Lüle, Ç., and Passmore, E., 2011. Lithóis Indikois: Preliminary characterization of garnet seal stones from Central and South Asia. In: C. Entwistle and N. Adams, Eds, *'Gems of Heaven': Recent Research on Engraved Gemstones in Late Antiquity c.AD 200–600.* British Museum Research Publication 177, The British Museum, London, 25–38

Aston, B.G., Harrell, J.A., and Shaw, I., 2000. Chapter 2: Stones. In: P.T. Nicholson, and I. Shaw, Eds, *Ancient Egyptian Materials and Technology.* Cambridge Univ. Press, Cambridge, 5–77

Arrhenius, B., 1985. *Merovingian Garnet Jewellery, Emergence and Social Implications.* Kungliga Vitterhets Historie och Antikvitets Akademien, Almqvist & Wiksell, Stockholm, Sweden, 227 pp

Bimson, M., La Niece, S., and Leese, M., 1982. The characterization of mounted garnets. *Archaeometry,* **24**(1), 51–8

Greek, Etruscan and Roman garnets in the antiquities collection of the J. Paul Getty Museum

Boardman, J., 1975. *Intaglios and Rings: Greek, Etruscan and Roman, from a Private Collection*. Thames & Hudson, London, 118 pp

Cachão, M., Fonseca, P.E., de Carvalho, R.G., de Carvalho, C.N., Oliveira, R., Fonseca, M.M., and Mata., J., 2010. A mina de granadas do Monte Suímo: de Plínio-o-Velho e Paul Choffat à actualidade. *e-Terra,* **18**(20), 1–4

Calligaro, T., Colinart, S., Poirot, J.-P., and Sudres, C., 2002. Combined external-beam PIXE and μ-Raman characterization of garnets used in Merovingian jewellery. *Nuclear Instruments and Methods in Physics Research B,* **189**(1–4), 320–7

Calligaro, T., Perin, P., Vallet, F., and Poirot, J.-P., 2006–2007. Contribution á l'étude des grenats mérovingiens (Basilique de saint-Denis et autres collections du musée d'Archéologie nationale, diverses collections publiques et objects de fouilles récentes). *Antiquités Nationales,* **38**, 111–44

Calligaro, T., Perin, P., and Sudres, C., 2009. À propos du "trésor de grenats de Carthage", attribué à l'époque vandale. *Antiquités Nationales,* **40**, 155–65

Farges, F., 1998. Mineralogy of the Louvres Merovingian garnet cloisonné jewelry: Origins of the gems of the first kings of France. *American Mineralogist,* **83**(3–4), 323–30

Formigli, E., and Heilmeyer, W.-D., 1990. *Tarentiner Goldschmuck in Berlin*. Walter de Gruyter, Berlin, Germany, 100 pp

Francis Jr., P., 2002. *Asia's Maritime Bead Trade: 300 BC to the Present*. University of Hawai'i Press, Honolulu, Hawaii, 305 pp

Gartzke, E., 2004. *Methoden zur materialkundlichen Untersuchung antiker Schmuckstücke*. Master's thesis, University of Würzburg, Germany, 196 pp

Gartzke, E., Schüssler, U., Schmitt, M., and Hoffmann, A., 2004. Der Schatzfund von Palaiokastron im Lichte goldschmiedetechnischer Betrachtungen sowie mikrosondenanalytischer und ramanspektroskopischer Untersuchungen. www.mineralogie.uni-wuerzburg.de/schuessler/Palaiokastron.pdf

Gilg, H.A., and Gast, N., 2012. Naturwissenschaftliche Unter-suchungen an Granatgemmen der Sammlung James Loeb. In: F. Knauß, Ed., *Die Gemmen der Sammlung James Loeb. Forschungen der Staatlichen Antikensammlungen und Glyptothek, Supplement zu Band 1*. Kunstverlag J. Fink, Lindenberg im Allgäu, 48–57, 62–3

Gilg, H.A., Gast, N., and Calligaro, T., 2010. Vom Karfunkelstein. In: L. Wamser, Ed., *Karfunkelstein und Seide*. Ausstellungskataloge der Archäologischen Staatssammlung, München, Band 37, 87–100

Gliozzo, E., Grassi, N., Bonanni, P., Meneghini, C., and Tomei, M.A., 2011. Gemstones from Vigna Barberini at the Palatine Hill (Rome, Italy). *Archaeometry,* **53**(3), 469–89

Greiff, S., 1998. Naturwissenschaftliche Untersuchungen zur Frage der Rohsteinquellen für frühmittelalterlichen Almandingranatschmuck rheinfränkischer Provenienz. *Jahrbuch des Römisch-Germanischen Zentralmuseums Mainz,* **45**, 599–646

Hanneman, W., 2000. *Naming Gem Garnets*. Hanneman Gemmological Products, Poulsbo, Washington, 103 pp

Horváth, E., and Bendö, Z., 2011. Provenance study on a collection of loose garnets from a Gepidic period grave in northeast Hungary. *Archeometriai Mübely,* **2011**(1), 17–32

Lind, Th., Henn, U., and Milisenda, C.C., 1998. Vergleichende Untersuchungen an Rhodolithen verschiedener Provenienz. *Gemmologie: Zeitschrift der Deutschen Gemmologischen Gesellschaft,* **47**(1), 53–9

Locock, A.J., 2008. An Excel spreadsheet to recast analyses of garnet into end-member components, and a synopsis of the crystal chemistry of natural silicate garnets. *Computers & Geosciences,* **34**(12), 1769–80

Löfgren, J., 1973. Die mineralogische Untersuchung der Granaten von Paviken auf Gotland. *Early Medieval Studies,* **6**, 78–96

Lundström, P., 1973. Almandingranaten von Paviken auf Gotland. *Early Medieval Studies,* **6**, 67–77

Mannerstrand, M., and Lundqvist, L., 2003. Garnet chemistry from the Slöinge excavation, Halland and additional Swedish and Danish excavations – Comparisons with garnet, occurring in a rock context. *Journal of Archaeological Science,* **30**(2), 169–83

Mathis, F., Vrielynck, O., Laclavetine, K., Chêne, G., and Strivay, D., 2008. Study of the provenance of Belgian Merovingian garnets by PIXE at IPNAS cyclotron. *Nuclear Instruments and Methods in Physics Research B,* **266**(10), 2348–52

Moorey, P.R.S., 1994. *Ancient Mesopotamian Materials and Industries: The Archaeological Evidence*. Clarendon Press, Oxford, 414 pp

Pappalardo, L., Karydas, A.G., Kotzamani, N., Pappalardo, G., Romano, F.P., and Zarkadas, Ch., 2005. Complementary use of PIXE-alpha and XRF portable systems for the non-destructive and *in situ* characterization of gemstones in museums. *Nuclear Instruments and Methods in Physics Research B,* **239**(1–2), 114–21

Pèrin, P., and Calligaro, T., 2007. Neue Erkenntnisse zum Arnegundegrab. Ergebnisse der Metallanalysen und der Untersuchungen organischer Überreste aus Sarkophag 49 aus der Basilika von Saint-Denis. *Acta Praehistorica et Archaeologica,* **39**, 147–79

Plantzos, D., 1999. *Hellenistic Engraved Gems*. Clarendon Press, Oxford, 244 pp

Quast, D., and Schüssler, U., 2000. Mineralogische Untersuchungen zur Herkunft der Granate merowinger-zeitlicher Cloisonnéarbeiten. *Germania,* **78**(1), 75–96

Rickwood, P.C., 1968. On recasting analyses of garnet into end-member molecules. *Contributions to Mineralogy and Petrology,* **18**(2), 175–98

Rösch, C., Hock, R., Schüssler, U., Yule, P., and Hannibal, A., 1997. Electron microprobe analysis and X-ray diffraction methods in archaeometry:

Investigations on ancient beads from Sultanate of Oman and from Sri Lanka. *European Journal of Mineralogy,* **9**(4), 763–83

Schmetzer, K., Bernhardt, H.-J., Bosshart, G., and Hainschwang, T., 2009. Colour-change garnets from Madagascar: Variation of chemical, spectroscopic and colourimetric properties. *Journal of Gemmology,* **31**(5–8), 235–82

Skinner, B.J., 1956. Physical properties of end-members of the garnet group. *American Mineralogist,* **41**(5–6), 428–36

Spier, J., 1989. A group of Ptolemaic engraved garnets. *Journal of the Walters Art Gallery,* **47**, 21–38

Spier, J., 1992. *Ancient Gems and Finger Rings: Catalogue of the Collections, The J. Paul Getty Museum*. J. Paul Getty Museum, Malibu, California, 184 pp

Stockton, C.M., and Manson, D.V., 1985. A proposed new classification for gem-quality garnets. *Gems & Gemology,* **21**(4), 205–18

Webster, R., rev. by Read, P.G., 1994. *Gems: Their Sources, Descriptions and Identification, 5th edn*. Butterworth-Heinemann, Boston, 1026 pp

Zwierlein-Diehl, E., 2007. *Antike Gemmen und ihr Nachleben*. Walter de Gruyter, Berlin, Germany, 567 pp

The Authors

Lisbet Thoresen
Beverly Hills, California 90213, U.S.A.
email: lisbet@lthoresen.com

Dr Karl Schmetzer
85238 Petershausen, Germany
email: SchmetzerKarl@hotmail.com

Natural and synthetic vanadium-bearing chrysoberyl

Karl Schmetzer, Michael S. Krzemnicki, Thomas Hainschwang and Heinz-Jürgen Bernhardt

Abstract: Mineralogical and gemmological properties of natural and synthetic V-bearing chrysoberyls are described. The natural samples originate from four sources (Tunduru in Tanzania, Ilakaka in Madagascar, Sri Lanka and Mogok in Myanmar) and the synthetic material was produced by Kyocera Corporation in Japan. The natural crystals show tabular habit with one of the pinacoids **a** {100} or **b** {010} as dominant crystal forms. Their morphology is consistent with internal growth structures determined in the immersion microscope. A few samples contain mineral inclusions of apatite, feldspar, or calcite. Dominant colour-causing trace elements are either V (Tunduru and Ilakaka) or a combination of V and Cr (Sri Lanka and Myanmar). Iron is present in samples from Tunduru, Ilakaka and Sri Lanka, but not from Mogok. Other trace elements such as Ga and Sn were detected in most of the natural samples and were absent from the synthetics.

UV-Vis spectra show superimposed V^{3+} and Cr^{3+} absorptions, as well as minor Fe^{3+} bands. According to the specific V:Cr ratio of the samples, the major ν_1 absorption band in the visible range is shifted from the red-orange (~607 nm) for Cr-free or almost Cr-free non-phenomenal chrysoberyls to the orange range (~589 nm) for a sample with the greatest Cr contents (0.24 wt.% Cr_2O_3). In comparison, colour-change Cr-dominant alexandrites show this major absorption band in the greenish yellow range (about 576–573 nm).

Diagnostic features of V-bearing natural chrysoberyl are compared with their synthetic Kyoc–era counterparts and with samples produced in Russia by flux growth and the horizontally oriented crystallization (HOC) technique. A distinction of natural from synthetic samples is possible by evaluating a combination of chemical, spectroscopic and microscopic features.

Keywords: chromium, colorimetry, crystal habit, inclusions, Madagascar, microprobe analyses, Myanmar, pleochroism, Sri Lanka, Tanzania, UV-Vis spectra, vanadium, X-ray fluorescence analysis

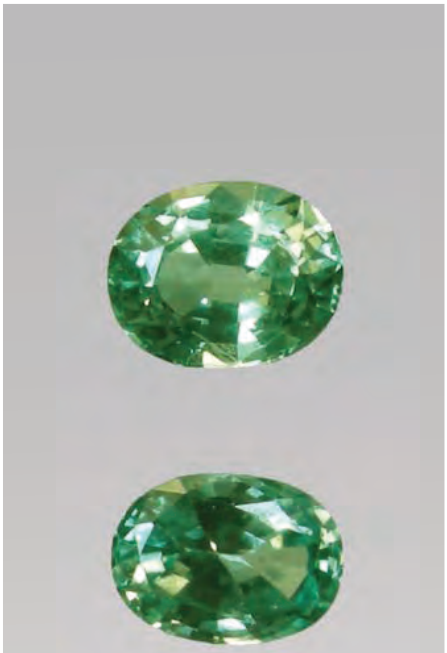

In the mid-1990s, V-bearing synthetic chrysoberyl was grown by Kyocera Corporation as a synthetic counterpart to material discovered at Tunduru, Tanzania. Shown here are a 1.53 ct V-bearing chrysoberyl from Tunduru (top) and a 1.06 ct synthetic chrysoberyl grown by Kyocera (bottom, 7.0×5.0 mm). Photo by K. Schmetzer.

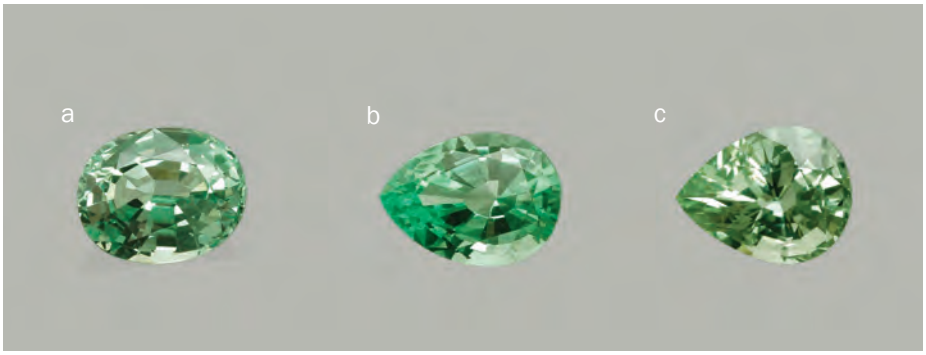

Figure 1: (a) Vanadium-bearing chrysoberyl was first discovered at Tunduru, Tanzania, which is the source of this 1.53 ct oval cut (7.8×6.2 mm). (b) Its synthetic counterpart was grown by Kyocera Corporation (here, 1.12 ct or 7.6×5.7 mm). (c) The Ilakaka area in Madagascar is also a source of V-bearing chrysoberyl; this sample weighs 2.09 ct and measures 9.1×7.2 mm. Composite photo by M. S. Krzemnicki (not to scale).

Introduction

In the mid-1990s, some new bright green chrysoberyls (e.g., *Figure 1a*) found their way to gemmological laboratories worldwide (Johnson and Koivula, 1996; Bank *et al.,* 1997; McClure, 1998; also see Hänni, 2010, who also gives a summary of the different varieties of chrysoberyl). The first faceted stones were extremely clean and thus a synthetic origin was considered possible. Mainly trace-element analysis was applied to establish criteria to distinguish these samples from synthetic counterparts known at that time. The natural samples reportedly originated from the large alluvial mining area of Tunduru in southern Tanzania. Faceted samples of this 'mint' green chrysoberyl variety are considered rare and valuable gems (Mayerson, 2003). Their coloration was found to be due to vanadium and they contained very little or no chromium. Furthermore, no distinct colour change was observed between daylight and incandescent light, as it is commonly seen for Cr-bearing chrysoberyl (alexandrite).

Most alexandrites from various natural sources with a clear colour change (i.e., from green or bluish green in daylight to a colour ranging from violet-purple and reddish purple to purplish red in incandescent light) show distinctly higher Cr than V contents (Schmetzer and Malsy, 2011). Chrysoberyl with almost equal amounts of V and Cr (e.g., from Orissa or Andhra Pradesh, India) also appears green in daylight, but changes in incandescent light only to a pale greyish green (Schmetzer and Bosshart, 2010).

The first synthetic alexandrite, grown by Creative Crystals and marketed since the early 1970s, contained Cr and Fe as the only significant colour-causing trace elements (Cline and Patterson, 1975; Schmetzer *et al.,* 2012). To improve the colour and grow samples that were *"*comparable to natural alexandrite from the Ural mountain region*"*, distinct amounts of V were added, in addition to various quantities of Cr (Machida and Yoshibara, 1980, 1981). Distinct V contents were also found in some flux-grown synthetic alexandrite trillings produced in Novosibirsk, USSR, and some flux-grown single crystals with V>Cr also were reported (Schmetzer *et al.,* 1996). Furthermore, distinct amounts of V have been recorded in some samples of Russian synthetic alexandrite grown from the melt by the Czochralski technique, as well as by the HOC method (horizontally oriented crystallization, a horizontal floating zone technique; see Schmetzer and Bosshart, 2010; Malsy and Armbruster, 2012; Schmetzer *et al.,* 2013a).

In the patent documents by Machida and Yoshibara (1980, 1981) mentioned previously, which were assigned to Kyoto Ceramic Corporation (Kyocera) from Kyoto, Japan, the growth of almost Cr-free, V-bearing synthetic chrysoberyl was also reported. This material is comparable to the non-phenomenal V-bearing green synthetic chrysoberyl that was grown at the same time by the Czochralski method in Novosibirsk (Bukin *et al.,* 1980). Another type of non-phenomenal green synthetic chrysoberyl was grown some years later by Tairus in Novosibirsk using the HOC method (Koivula *et al.,* 1994).

Subsequent to the discovery of V-bearing gem chrysoberyl in Tunduru in the mid-1990s (see above), another

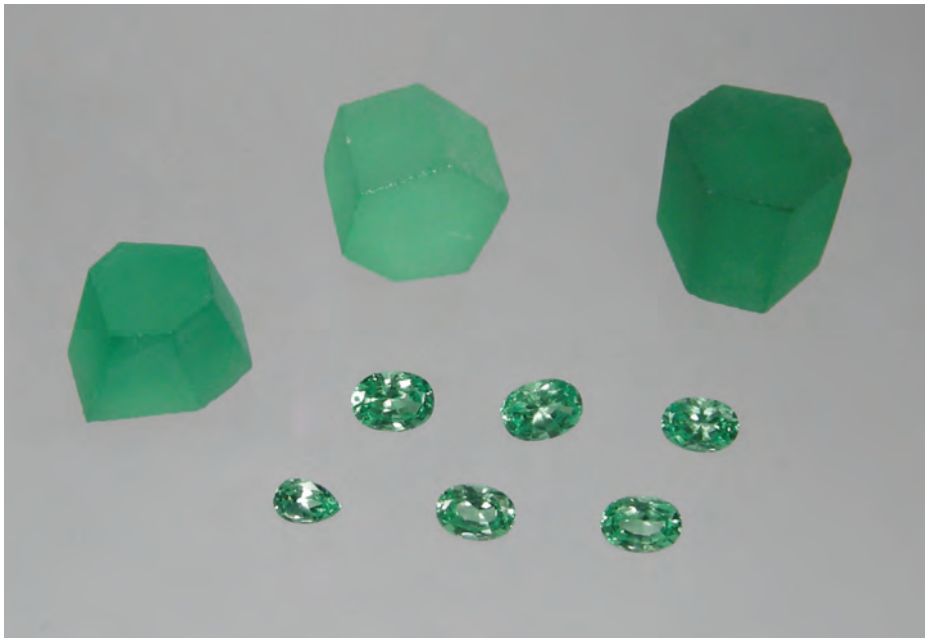

Figure 2: Rough and cut V-bearing synthetic chrysoberyl grown by Kyocera Corporation. The top-right piece weighs 10.5 g and measures 15.5×15.5×14.4 mm; the faceted samples weigh 0.49–1.33 ct. Photo by K. Schmetzer.

patent application was filed by Kyocera in Japan that described the production of the V-bearing counterpart of this gem material (Nishigaki and Mochizuki, 1998). This material was probably of the same type as the samples described briefly by Krzemnicki and Kiefert (1999; see also *Figure 1b*), and also those donated to the Bavarian State Collection for Mineralogy in Munich, Germany *(Figure 2)*.

To the knowledge of the present authors, only one polarized spectrum of a Czochralski-grown V-bearing chrysoberyl is published and it appears in an article that is difficult to access (Bukin *et al.,* 1980). Furthermore, pleochroism and colour were not mentioned in that paper, and descriptions of natural V-bearing chrysoberyl are often vague. This is due to the difficulty in orienting faceted chrysoberyl properly for spectroscopy in relation to the crystallographic axes. There is also a lack of published data on V-bearing non-phenomenal chrysoberyl from sources other than Tunduru, such as from Ilakaka, Madagascar *(Figure 1c)*. The present paper investigates the coloration and other gemmological and mineralogical properties of non-phenomenal natural and synthetic V-bearing chrysoberyl, and aims to fill some of the gaps mentioned above.

Samples

For the synthetics, we examined three pieces of rough and 12 faceted samples from Kyocera. All the rough and nine of the cut stones had been donated by Kyocera Germany to the Bavarian State Collection for Mineralogy in Munich. The other faceted samples were donated by Kyocera Corp. to the Swiss Gemmological Institute SSEF, Basel, Switzerland.

The natural samples consisted of 27 rough and faceted chrysoberyls with V>Cr. They originated from the large placers at Tunduru (14 samples) and Ilakaka (6), as well as from secondary deposits in Sri Lanka (5) and unspecified sources in Mogok (2). Many of the samples were obtained from the H.A. Hänni gemstone collection, which is housed as a reference collection at SSEF. Four rough pieces from Tunduru were obtained in Tanzania by S. Pfenninger for her diploma thesis (2000). Several samples were also obtained from museums or private collections and from the trade. The two chrysoberyls from Mogok were loaned from public or private collections in England where they had been housed since the 1970s (for further details, see Schmetzer *et al.,* 2013b).

In addition to these chrysoberyls from known sources, we also examined five faceted samples from private collections and from the trade with unspecified origins. The data from these samples, which revealed V>Cr by microprobe analysis, are not specifically included in the present study, but notably their chemical and spectroscopic properties all fell within the ranges determined for the larger group of 27 chrysoberyls from known localities. Furthermore, data from 12 light green samples that were found to contain Cr>V (e.g., from Ilakaka and Sri Lanka) are not presented in this study, since such material has already been described elsewhere (see, e.g., Schmetzer *et al.,* 2002).

Table I. Trace element contents, colour, pleochroism, and spectroscopic properties of V-bearing synthetic chrysoberyl grown by Kyocera Corp. in Japan.

Colour and pleochroism[a]

Orientation	X||a	Y||b	Z||c
Daylight	Yellowish green	Green	Bluish green
Incandescent	Yellowish green	Green	Bluish green

Spectroscopic properties

Property	Polarization, position (nm)			Assignment in all three directions of polarization
Orientation	X||a	Y||b	Z||c	
Maxima	607	618	608	V^{3+} first absorption band (ν_1)
	408	411	418	V^{3+} first absorption band (ν_2)
Minima	510	518	498	

Chemical properties (wt.%)

Sample	Ky1	Ky2	Ky3	Ky4	Ky5	Ky6	Ky7
No. analyses[b]	10	10	10	10	1	1	1
TiO_2	<0.01	<0.01	<0.01	<0.01	0.002	0.001	0.002
V_2O_3	0.11	0.12	0.13	0.12	0.115	0.119	0.081
Cr_2O_3	<0.01	<0.01	<0.01	<0.01	nd[c]	0.004	0.006
MnO	<0.01	<0.01	<0.01	<0.01	nd	nd	nd
Fe_2O_3	<0.01	<0.01	<0.01	<0.01	0.002	0.001	0.002

[a] Based on a morphological cell with a = 4.42, b = 9.39 and c = 5.47 Å.
[b] One analysis = EDXRF, 10 analyses (averaged) = electron microprobe.
[c] nd = not detected.

Instrumentation and methods

Gemmological and microscopic properties were determined for all the samples using standard instrumentation. The determination of growth structures and crystal morphology was detailed by Schmetzer (2011). Six samples that contained inclusions of measurable size were studied with a Renishaw InVia Raman microspectrometer, using an argon laser (514 nm) in confocal mode coupled with an Olympus microscope.

Quantitative chemical data for all samples were obtained by electron microprobe (JEOL JXA-8600 and Cameca Camebax SX 50 instruments) or energy-dispersive X-ray fluorescence (EDXRF) spectroscopy using Spectrace 5000 Tracor X-ray and ThermoScientific Quant'X instruments. In addition to the trace elements given in *Tables I* and *II*, aluminium contents were also measured as normal and used as a control value for

the quality of data (since BeO cannot be measured reliably by electron microprobe and EDXRF analyses). Furthermore for all samples semi-quantitative data for Ga and Sn were obtained by one of the analytical techniques mentioned above.

Absorption spectra were recorded with a CCD-type Czerny-Turner spectrometer in combination with an integrating sphere (for further details, see Schmetzer *et al.,* 2013a). Non-polarized spectra were obtained for 12 synthetic and 25 natural samples from known sources as well as for five chrysoberyls from unknown localities. In addition, polarized spectra were performed for about half of these samples. Colorimetric data were obtained in transmission mode for 15 samples with a Zeiss MCS 311 multichannel colour spectrometer (see Schmetzer *et al.,* 2009; Schmetzer and Bosshart, 2010).

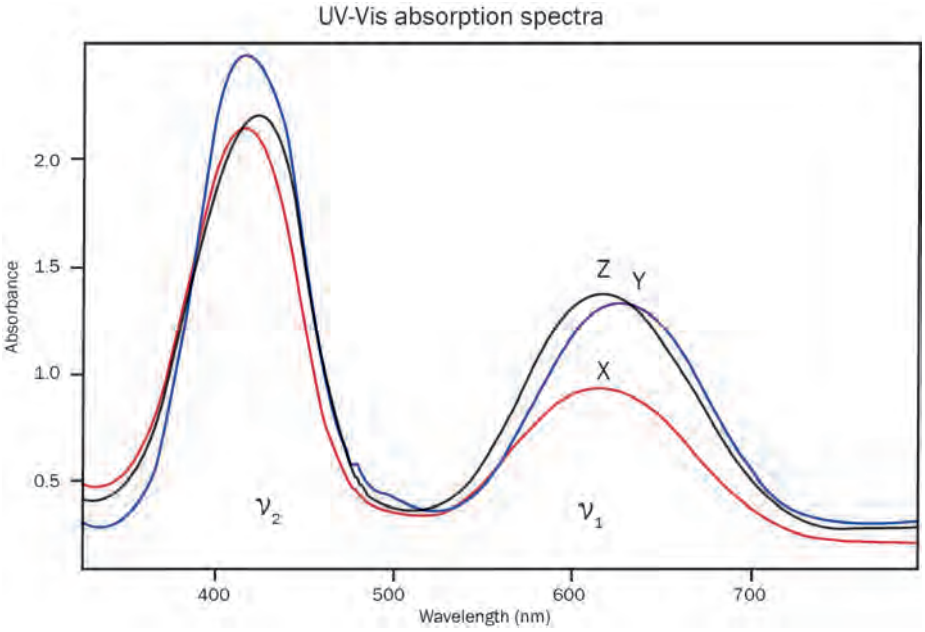

Figure 3: Polarized absorption spectrum of a V-bearing synthetic chrysoberyl grown by Kyocera Corp., with X || a, Y || b and Z || c. The dominant absorption bands are designated ν_1 and ν_2 (see Table I*).*

Kyocera synthetic V-bearing chrysoberyl

The rough samples consisted of two somewhat irregular pseudo-hexagonal cylinders and one pseudo-hexagonal pyramid *(Figure 2)*. They had been sawn from Czochralski-grown crystals, and their upper and lower bases as well as the side faces were roughly polished to clean the surfaces and to give a better visual impression. The faceted gems were cut without specific orientation.

The overall colour of the samples was bright green in both daylight and incandescent light. Pleochroism was weak in the faceted samples but clearly observed in the rough pieces, with X = yellowish green, Y = green and Z = bluish green, independent of lighting.

The dominant colour-causing trace element in this group of samples is vanadium (0.08–0.13 wt.% V_2O_3; *Table I*). Other trace elements were, in general, below the detection limits of the electron microprobe, with small traces of Cr and Fe observed occasionally by EDXRF (see *Table I*).

Polarized absorption spectra of the rough samples showed two strong absorption bands in the red-orange range (~610 nm, designated as first strong absorption band ν_1) and in the violet area (~415 nm, designated as second strong absorption band ν_2) for X, Y and Z, with some variation in maxima positions and intensities *(Table I, Figure 3)*. These absorption bands in the visible range are assigned to V^{3+} which replaces Al^{3+} in the chrysoberyl structure. These absorption features are similar to those depicted by Bukin *et al.* (1980). Also, the non-polarized spectra from the faceted synthetics which are mostly randomly orientated *(Figure 4)* are consistent with these data.

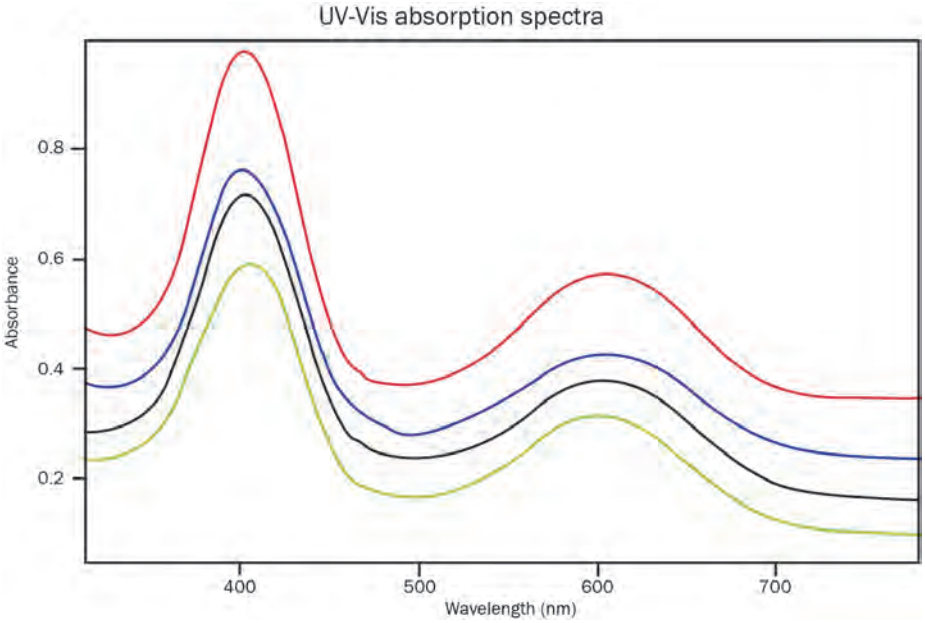

Figure 4: Absorption spectra of four faceted V-bearing synthetic chrysoberyls in random orientation. The top three spectra are displaced vertically for clarity.

The ν_1 absorption bands for Y and Z have approximately the same intensity, but due to the different position of their absorption maxima (618 and 608 nm, respectively), the minimum for Y at 518 nm is in the green range of the spectrum, while the minimum for Z at 498 nm is in the bluish green range. Thus, the different colours of Y and Z are understandable. The ν_1 absorption band in the X spectrum

Table II. Trace-element contents (wt.%), colour, and pleochroism of V-bearing chrysoberyl.

Source	Tunduru, Tanzania								
Colour	Pale to moderate intense green (Type 1)					Intense to very intense green (Type 2)			
Pleochroism[a] X Y Z	Not observed or very weak					Yellowish green Green Bluish green			
Sample	Tu1	Tu2	Tu3	Tu4	Tu5	Tu6	Tu7	Tu8	Tu9
No. of analyses[b]	10	16	8	10	1	1	7	20	15
TiO_2	0.01	0.08	0.01	0.01	0.001	0.007	0.15	0.11	0.01
V_2O_3	0.04	0.06	0.06	0.06	0.103	0.166	0.18	0.21	0.30
Cr_2O_3	0.01	0.01	0.01	0.01	0.004	0.038	0.03	0.03	0.04
MnO	nd[c]	nd	nd	0.01	nd	nd	nd	nd	nd
Fe_2O_3	0.17	0.13	0.10	0.24	0.317	0.227	0.08	0.09	0.20

Source	Ilakaka, Madagascar					Sri Lanka				Mogok, Myanmar
Colour	Pale to moderate intense green				Intense green	Moderate yellowish green				Intense bluish green
Pleochroism[a] X Y Z	Not observed or very weak				Yellowish green Green Bluish green	Not observed or very weak		Yellowish green Green Green		Greyish violet Yellowish green Intense blue-green
Sample	Il1	Il2	Il3	Il4	Il5	SL1	SL2	SL3	SL4	M1
No. of analyses[b]	8	10	10	9	10	10	10	10	10	12
TiO_2	0.01	0.05	0.02	0.01	0.01	0.05	0.01	0.11	0.10	0.08
V_2O_3	0.03	0.04	0.06	0.08	0.15	0.05	0.07	0.08	0.11	0.38
Cr_2O_3	<0.01	<0.01	<0.01	<0.01	<0.01	0.03	0.02	0.05	0.10	0.24
MnO	0.01	0.01	0.01	0.01	0.01	0.01	0.01	0.01	0.01	nd
Fe_2O_3	0.55	0.11	0.23	0.50	0.17	0.90	0.47	0.82	0.65	<0.01

[a] Daylight, based on a morphological cell with a = 4.42, b = 9.39, c = 5.47 Å, and X||a, Y||b, Z||c.
[b] One analysis = EDXRF, 7–20 analyses (averaged) = electron microprobe.
[c] nd = not detected.

is weaker than in Y and Z, which explains the somewhat more yellowish green colour of X.

Microscopic examination of faceted samples revealed no inclusions, growth striations, or clearly visible gas bubbles. Furthermore, gas bubbles were easily observed in only one of the rough pieces *(Figure 5)*.

Natural V-bearing chrysoberyl

Morphology of the rough and internal growth structures

Due to their origin from secondary deposits, most of the rough samples from Tunduru, Ilakaka and Sri Lanka were heavily waterworn and broken. Thus, we could determine the complete morphology only for a few samples *(Figure 6)* by goniometric measurements in combination with the examination of internal growth structures. *Figure 7* shows some examples of internal growth patterns seen in a crystal from Ilakaka, a faceted stone from Tunduru, a crystal from Mogok and a twinned crystal from Sri Lanka.

The crystal forms noted in our samples are well-known and seen frequently in natural chrysoberyl: the pinacoids **a** {100}, **b** {010} and **c** {001}; the prisms **i** {011}, **k** {021}, **m** {110}, **s** {120}, **r** {130} and **x** {101}; and the dipyramids **o** {111}, **n** {121} and **w** {122}. (For further details on chrysoberyl morphology and identification of crystal faces, see Schmetzer, 2011.) Idealized crystal drawings representing all four localities, for which a complete habit determination was possible, are presented

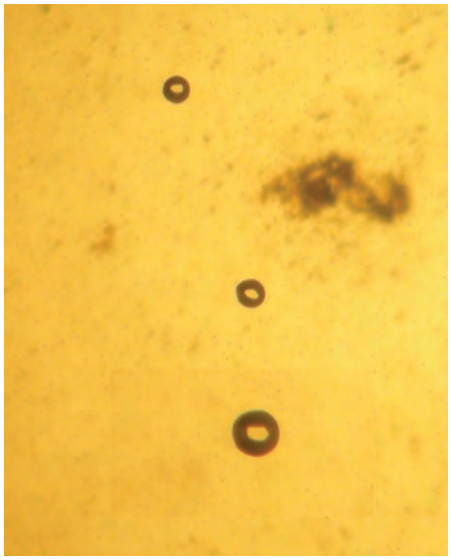

Figure 5: Gas bubbles are rarely seen in synthetic V-bearing chrysoberyl from Kyocera. Immersion, field of view 2.0×2.7 mm. Photo by K. Schmetzer.

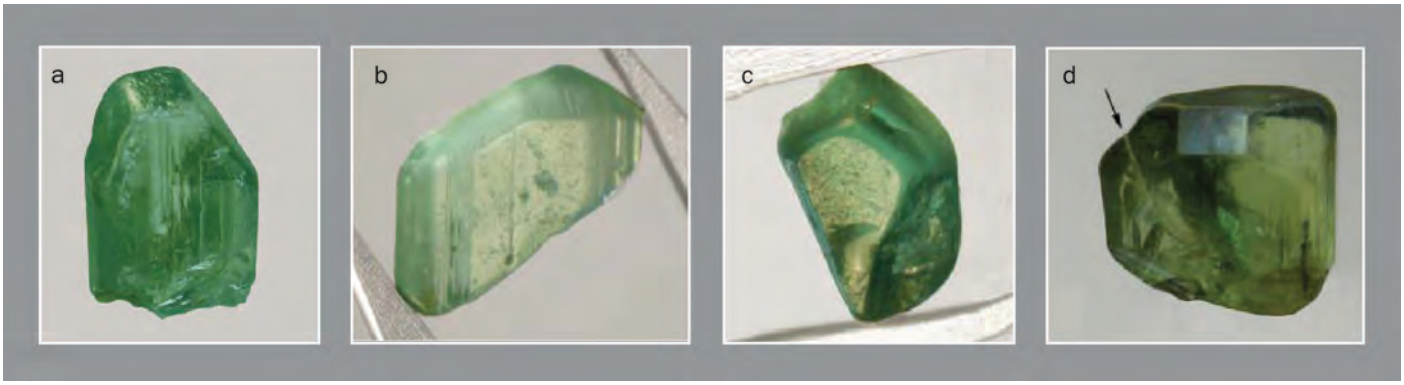

*Figure 6: Morphology of V-bearing chrysoberyl crystals. (a) Ilakaka, 12.7×8.4 mm, tabular parallel to **b** {010}; (b) Ilakaka, 7.4×6.5 mm, tabular parallel to **a** {100}; (c) Tunduru, 5.2×3.1 mm, tabular parallel to **a** {100}; (d) twinned crystal from Sri Lanka, 6.9×6.1 mm, the largest face is **a** (100), and the arrow indicates the twin boundary. Photos by K. Schmetzer.*

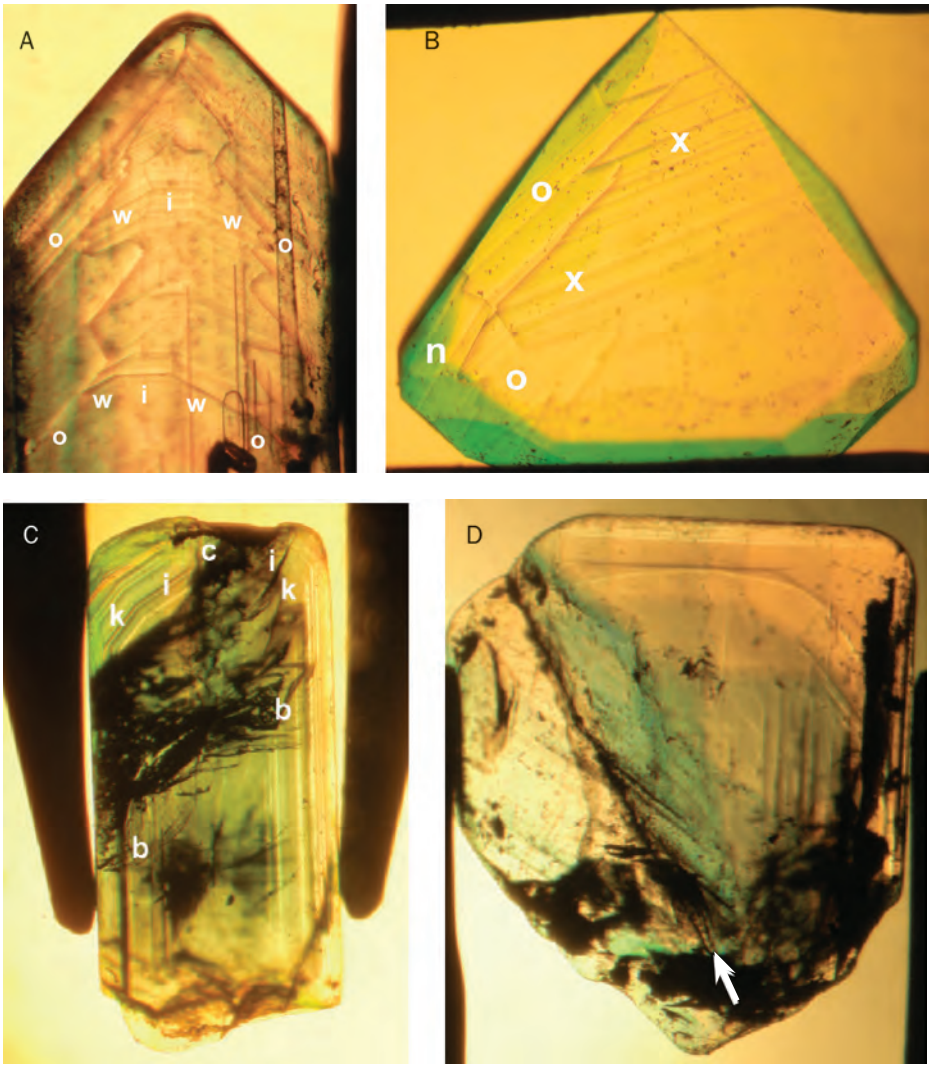

Figure 7: Growth structures in V-bearing chrysoberyl. (A) Crystal from Ilakaka (see Figure 6b*), tabular parallel to **a** {100}; view inclined to the c-axis, showing growth faces parallel to the prism **i** and to the dipyramids **w** and **o**; field of view 2.4×3.2 mm. (B) Cut stone from Tunduru, showing growth zoning parallel to the prism **x** and to the dipyramids **n** and **o**; field of view 5.1×4.7 mm. (C) Crystal from Mogok; view parallel to the a-axis, showing growth faces associated with colour zoning parallel to the pinacoids **b** and **c** and to the prism faces **i** and **k**; field of view 5.3×7.1 mm. (D) Crystal from Sri Lanka (see* Figure 6d*); the largest face is **a** (100) and the arrow points at the twin boundary; field of view 6.7×7.7 mm. Photos in immersion by K. Schmetzer.*

in *Figure 8*. Most samples consisted of untwinned single crystals with variable morphology, but two specific habits were frequently seen, both of which were elongated along the c-axis: tabular with a dominant **b** pinacoid (*Figures 6a* and *8A,D*), or tabular with a dominant **a** pinacoid (*Figures 6b,c* and *8B,C*).

Although twinning was rarely observed, *Figures 6d* and *7D* depict a sample from Sri Lanka that consists of a dominant crystal with a smaller second crystal in twin position. The morphology of the larger crystal is depicted in *Figure 8E*.

Colour, pleochroism and colour-causing trace elements

An overview of the chemical properties and coloration of selected samples from all four sources examined is given in *Table II*, and *Figure 9* provides a comparison of the coloration of the faceted natural and synthetic samples. Vanadium-bearing chrysoberyl from Ilakaka *(Figure 10a)* and Tunduru *(Figure 10b)* ranged from pale to very intense green, in very light to medium-light tones. In lighter green chrysoberyl from both sources, pleochroism was not observed or was very weak. All intense or very intense green stones showed identical pleochroic colours with X = yellowish green, Y = green and Z = bluish green, comparable to the pleochroism observed in the synthetic rough from Kyocera (*Tables I* and *II*). Colour intensity is dependent on and directly correlated with V concentration, which was found

Natural and synthetic vanadium-bearing chrysoberyl

to vary between 0.03 and 0.15 wt.% V_2O_3 in chrysoberyl from Ilakaka and between 0.04 and 0.30 wt.% V_2O_3 from Tunduru. Chromium contents in the Ilakaka samples were <0.01 wt.% Cr_2O_3. The pale to moderately intense green samples from Tunduru (designated Type 1 in this study) also showed very low Cr contents in the range of 0.01 wt.% Cr_2O_3, while the more intensely coloured samples with higher V contents (designated Type 2) had somewhat greater Cr contents in the range of 0.03–0.04 wt.% Cr_2O_3 *(Table II)*. Iron contents were between 0.08 and 0.32 wt.% Fe_2O_3 for samples from Tunduru, with somewhat higher amounts in chrysoberyls from Ilakaka (0.11–0.55 wt.% Fe_2O_3).

Vanadium-bearing chrysoberyls from Sri Lanka *(Figure 10c)* were yellowish green with moderate saturation. The more intensely coloured samples showed pleochroism with X = yellowish green, Y = green and Z = green. Vanadium contents ranged from 0.05 to 0.11 wt.% V_2O_3, and Cr varied between 0.02 and 0.10 wt.% Cr_2O_3 (i.e., somewhat higher Cr than samples from Ilakaka and Tunduru). Iron ranged from 0.47 to 0.90 wt.% Fe_2O_3.

The intense bluish green samples from Myanmar (e.g., *Figure 10d*) showed strong pleochroism with X = greyish violet, Y = yellowish green and Z = intense blue green. The sample analysed by microprobe had the highest V and Cr contents of our chrysoberyls (0.38 wt.% V_2O_3 and 0.24 wt.% Cr_2O_3), with Fe below the detection limit.

The chemical properties of V-bearing natural and synthetic chrysoberyls given in *Tables I* and *II* are plotted in *Figure*

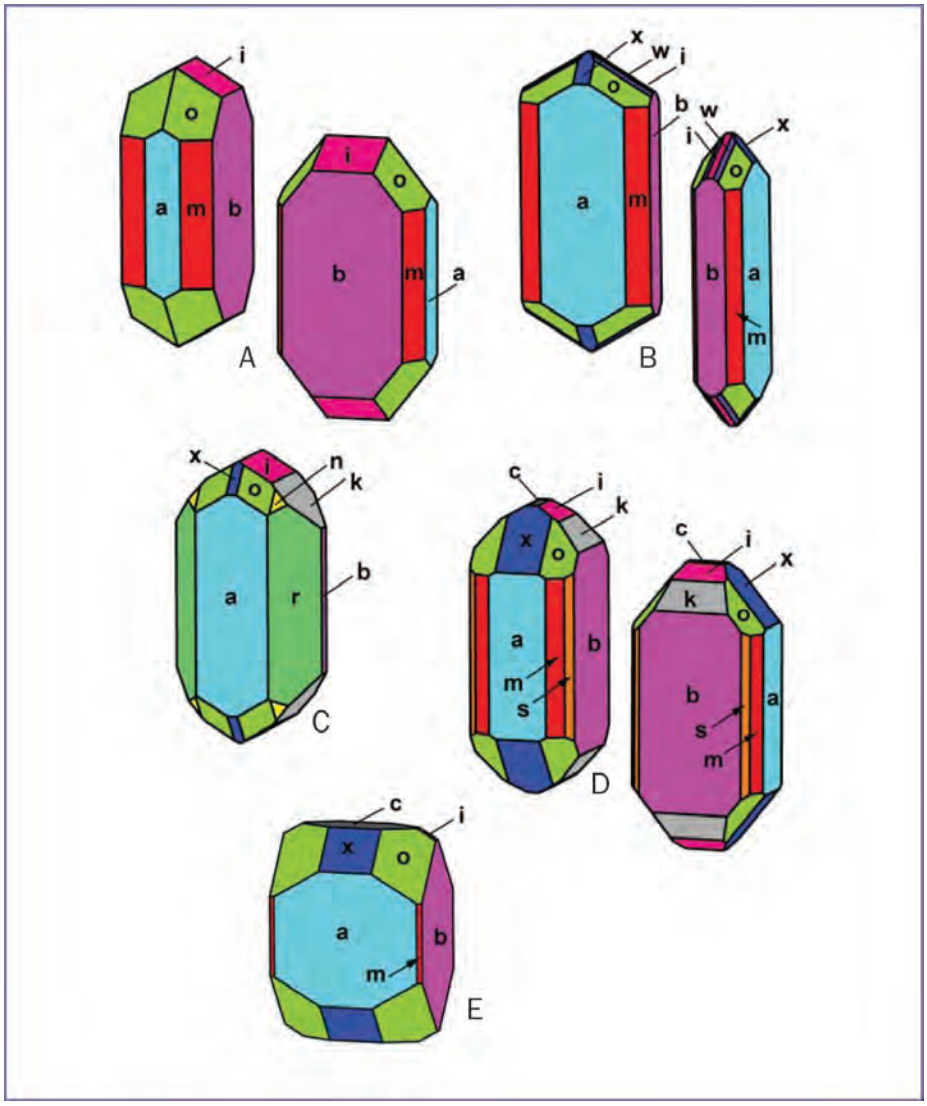

Figure 8: Idealized drawings (clinographic projections) showing the morphology of V-bearing chrysoberyl crystals from various localities; all equivalent crystal faces have the same colour. (A) Ilakaka, views parallel to the a-axis (left) and b-axis (right); the sample (see Figure 6a*) is tabular parallel to* ***b*** *{010}; (B) Ilakaka, views parallel to the a-axis (left) and b-axis (right); the sample (see* Figures 6b *and* 7A*) is tabular parallel to* ***a*** *{100}; (C) Tunduru, view parallel to the a-axis, the sample (see* Figure 6c*) is tabular parallel to* ***a*** *{100}; (D) Mogok, views parallel to the a-axis (left) and b-axis (right); the sample (see* Figure 7C*) is tabular parallel to* ***b*** *{010}; (E) Sri Lanka, view parallel to the a-axis; the drawing represents the larger part of the twin depicted in* Figures 6d *and* 7D*, and the largest face is* ***a*** *(100). Crystal drawings by K. Schmetzer.*

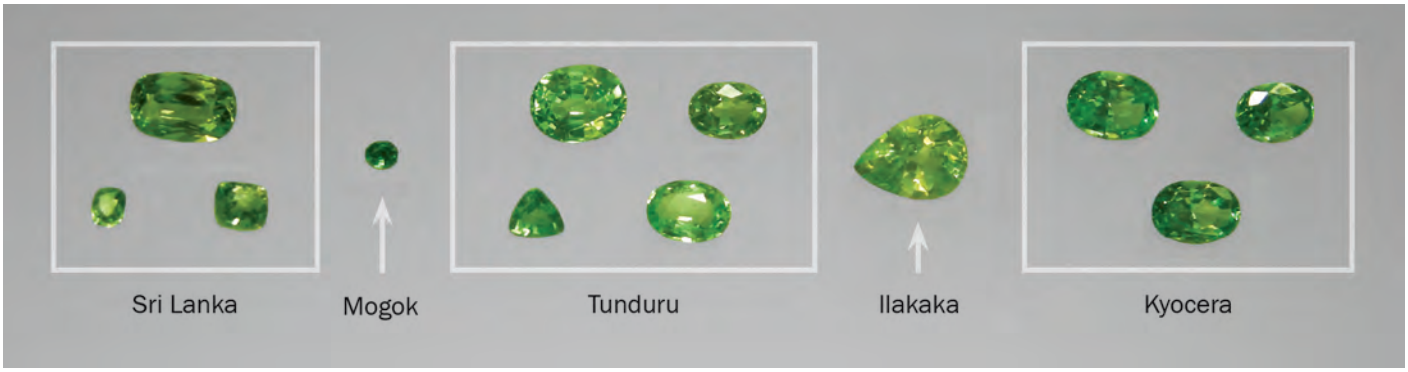

Figure 9: Colour comparison of faceted V-bearing chrysoberyl from various localities and synthetic chrysoberyl grown by Kyocera Corp. The chrysoberyl from Ilakaka weighs 2.09 ct and measures 9.1×7.2 mm. Photo by K. Schmetzer.

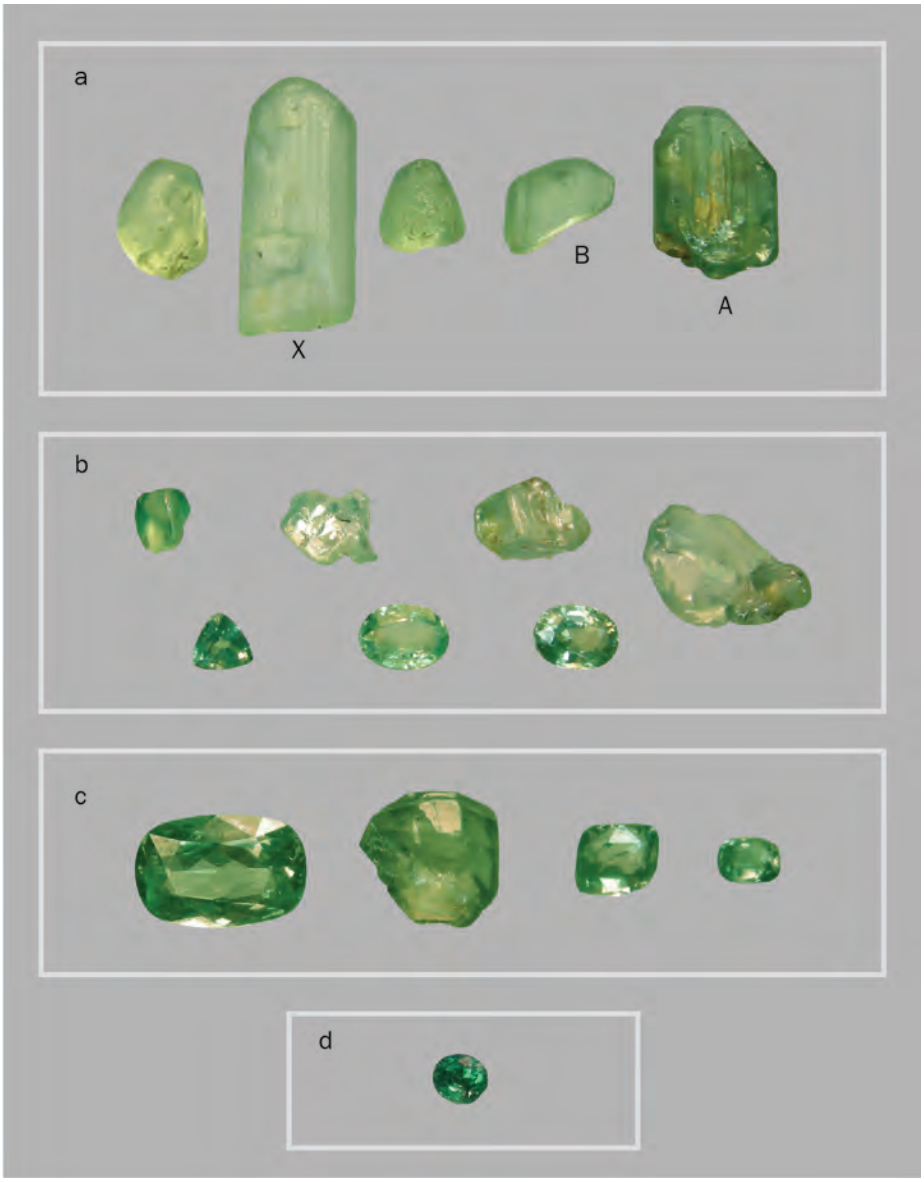

*Figure 10: Vanadium-bearing chrysoberyl from various localities. (a) Ilakaka: for the three labelled single crystals, the external morphologies are: sample X (17.9×7.6 mm), tabular parallel to **b** {010}; sample B (7.4×6.5 mm), tabular parallel to **a** {100}; and sample A (12.7×8.4 mm), tabular parallel to **b** {010}. (b) Tunduru: the faceted samples weigh 0.38 ct (4.3×4.2 mm) to 0.89 ct. (c) Sri Lanka: the cut stones weigh 1.44 ct (8.4×5.6 mm), 0.53 ct and 0.13 ct. (d) Mogok: the sample weighs 0.08 ct and measures 2.6×2.3 mm. Photos by K. Schmetzer (*Figures a–d *not to scale).*

11. The V and Cr contents are similar in the synthetic chrysoberyl from Kyocera and the natural samples from Ilakaka and Tunduru Type 1. In contrast, the more intense green Tunduru Type 2 samples revealed higher V and Cr contents, and the stones from Sri Lanka showed greater Cr and Fe. The bright bluish green stone from Mogok was unique according to its highly enriched amounts of both colour-causing trace elements, V and Cr *(Figure 11a)*. Iron contents were variable: the synthetic material from Kyocera and the Mogok sample were Fe-free, while moderate Fe contents (0.05–0.35 wt.% Fe_2O_3) were found in chrysoberyl from Tunduru and in some of the Ilakaka samples. Greater Fe values were found in the stones from Sri Lanka and in some of the Ilakaka material *(Figure 11b)*.

Gallium and tin as trace elements

Gallium and tin are common trace elements in natural alexandrite from various sources (Ottemann, 1965; Ottemann *et al.,* 1978). It was no surprise that quantitative or semi-quantitative chemical analyses showed significant amounts of Ga in all samples from the four sources examined in this study. The characteristic X-ray lines of Sn were seen in all of the chrysoberyls from Ilakaka and Sri Lanka, and in most samples from Tunduru. No Sn lines were observed in two of the Tunduru Type 2 gems or in the chrysoberyls from Mogok.

Spectroscopic properties and colour variation under different light sources

Polarized absorption spectra were recorded for rough crystals with tabular habit showing dominant **a** (100) or **b** (010) pinacoids (see *Figures 6, 8* and *10*) and for a few faceted samples that were cut with the tables more or less parallel to one of those pinacoids. None of the faceted stones had the table facet oriented parallel to **c** (001). Due to the morphology of the crystals and the table orientations of the faceted stones, we normally could measure only two of the three possible polarized spectra X, Y and Z for each sample. Therefore, we recorded polarized spectra for X and Z (beam parallel to the b-axis) or for Y and Z (beam parallel to the a-axis); example spectra are depicted in *Figure 12*.

Even with these restrictions, it was evident that the positions of absorption maxima and intensity ratios of absorption bands of V^{3+} (in Cr-free or almost Cr-free samples) are consistent with those observed in the Kyocera synthetics (see *Table I*). In most natural samples, the V^{3+}-related features are superimposed on the known Fe^{3+} spectrum of chrysoberyl. The main absorption maxima assigned to Fe^{3+} are located at 365, 375–376 and 439 nm, with somewhat weaker absorption bands or shoulders at 357, 381 and 430 nm. Only the main absorption band showed a slight polarization dependency, with the maximum at 375 nm for X and Z, and at 376 nm for Y. The Fe^{3+} absorption bands we recorded are consistent for chrysoberyl in the literature (Farrell and Newnham, 1965).

A comparison of non-polarized spectra from the four localities *(Figure 13)* shows

Natural and synthetic vanadium-bearing chrysoberyl

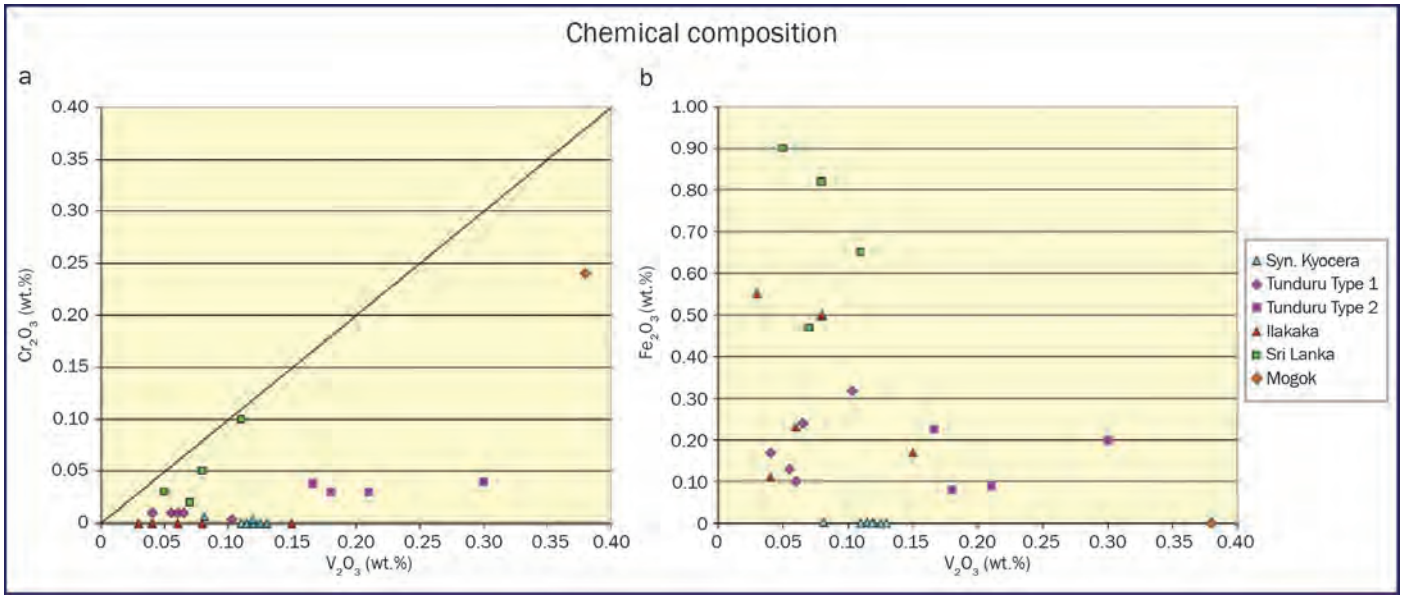

Figure 11: Chemical plots of synthetic chrysoberyl from Kyocera and natural samples from various sources. (a) V_2O_3 versus Cr_2O_3: All points are below the diagonal, as the gems contain more V than Cr. Trace-element contents in the Tunduru Type 1 and Ilakaka stones are similar to the Kyocera material. The Tunduru Type 2 samples reveal higher V and Cr contents, and the chrysoberyls from Sri Lanka also have greater Cr. The sample from Mogok shows highly enriched contents of both trace elements. (b) V_2O_3 versus Fe_2O_3: The Kyocera synthetics and the bright green stone from Mogok are Fe-free, while samples from Tunduru, Ilakaka and Sri Lanka show variable Fe.

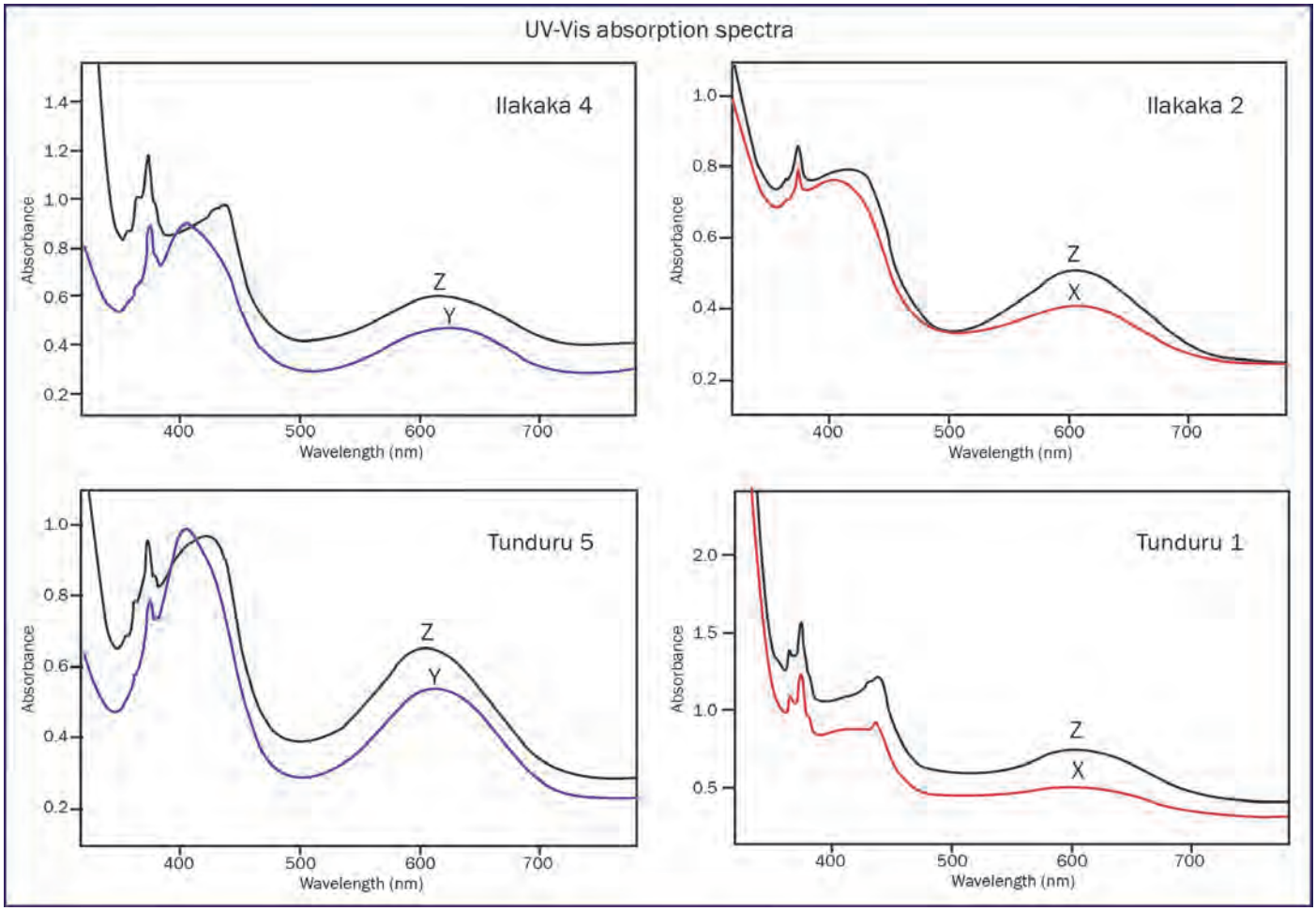

Figure 12: Polarized UV-Vis absorption spectra of one faceted sample and three V-bearing chrysoberyl crystals from Ilakaka and Tunduru, with X || a, Y || b and Z || c. According to the morphology of the samples, polarized spectra were recorded either with the beam parallel to the a-axis (Y and Z polarizations) or parallel to the b-axis (X and Z polarizations). Thickness of samples: Ilakaka 4 = 2.3 mm; Ilakaka 2 = 3.2 mm; Tunduru 5 (faceted) = 3.1 mm; Tunduru 1 = 3.8 mm.

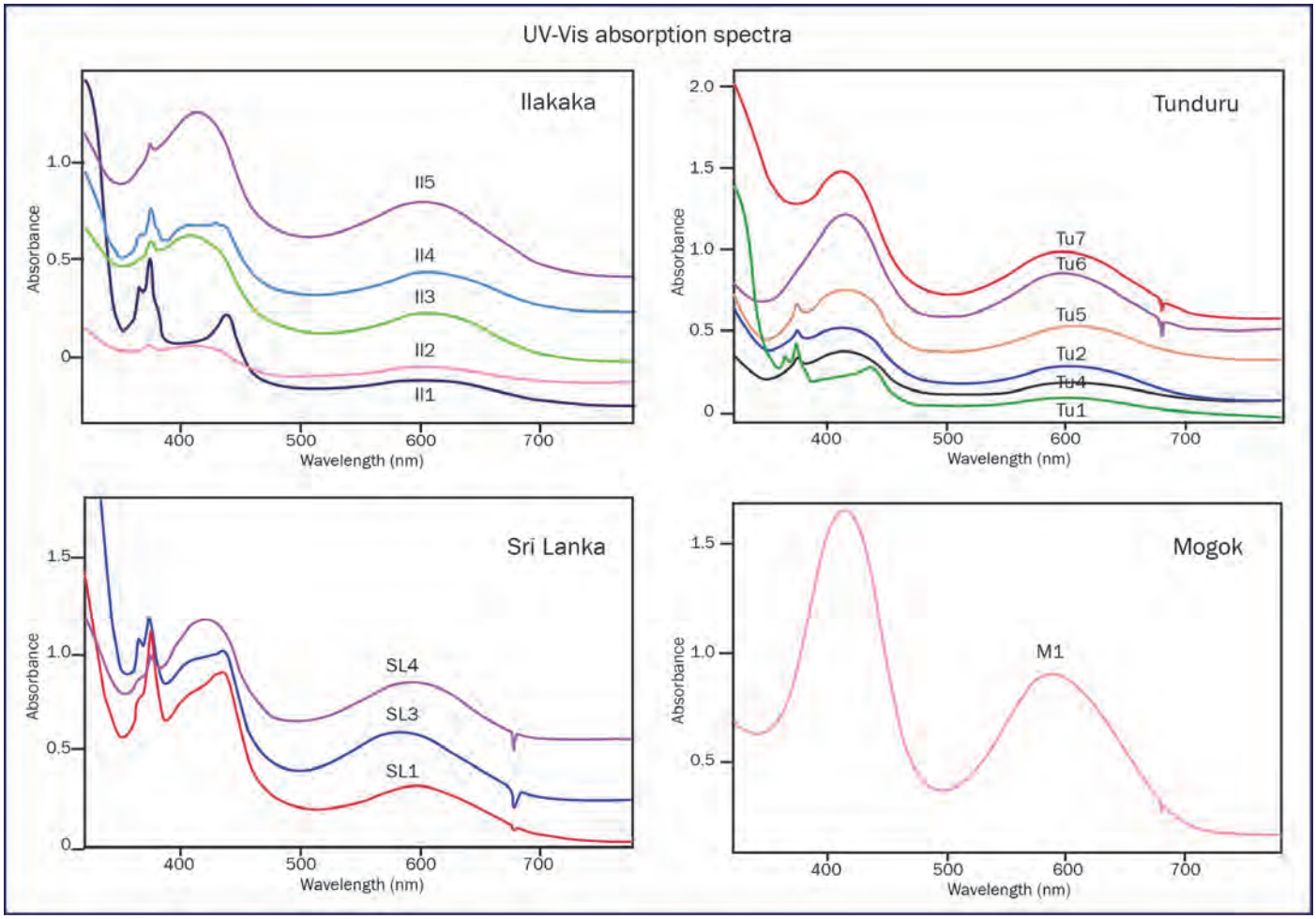

Figure 13: Non-polarized UV-Vis spectra of V-bearing chrysoberyl show absorption bands of V^{3+} and Fe^{3+} (Ilakaka and Tunduru), of V^{3+} and Cr^{3+} (Mogok), and of V^{3+}, Cr^{3+}, and Fe^{3+} (Sri Lanka). Sharp Cr^{3+} lines at ~ 680 nm are recorded for some of the samples only (Tunduru Type 2 [Tu6, Tu7], Sri Lanka and Mogok). The spectra of samples Il2–Il5, Tu2–Tu7, and SL3–SL4 are displaced vertically for clarity; the chemical properties of the samples are given in Table II.

that samples from Ilakaka and some of those from Tunduru do not show the two sharp Cr^{3+} lines at 680 and 678 nm. The Cr contents of these samples are low (<0.01 wt.% Cr_2O_3). In contrast, Cr^{3+} lines were observed in higher-Cr Tunduru samples and in those from Sri Lanka and Myanmar. Due to the experimental conditions, these Cr^{3+} lines are shown in the spectra as 'negative' luminescence peaks (see details in Schmetzer *et al.,* 2013a). Depending on the iron contents of the individual samples, the Fe^{3+} bands described above are also seen with variable intensity in the samples from Ilakaka, Tunduru and Sri Lanka.

In non-polarized spectra (see again *Figure 13*), the position of the first strong V^{3+} absorption band (ν_1) was recorded in the red-orange range at 608–606 nm for Cr-free or almost Cr-free chrysoberyls. Although there is some influence of sample orientation, it is clear that this strong absorption band shifts towards shorter wavelengths with greater Cr contents and with increasing Cr:V ratios *(Figure 14)*. For both samples from Myanmar (Cr:V ratio near 1:1.6), the position of this strong absorption band was recorded in the orange region at 589 nm. For Cr-dominant natural and synthetic alexandrites, this absorption band was shifted further to the greenish yellow range at about 576–573 nm *(Figure 14, Table III)*.

To compare polarized spectra of V-bearing, Cr-free synthetic chrysoberyl with V-free, Cr-bearing synthetic alexandrite, we selected samples grown by Kyocera Corp. (this study) and Creative Crystals (Schmetzer *et al.,* 2012), respectively. As already mentioned for V-bearing synthetic chrysoberyl, the polarized spectra for both trace elements, Cr and V, consist of two strong absorption maxima which are located in the greenish yellow to red-orange range (first maximum, ν_1) and in the blue-violet to violet range (second maximum, ν_2). In *Figure 15* these absorption maxima are shown in all three polarizations. For ν_1, in all three polarization directions the absorption bands for V^{3+} are located at higher wavelengths than for Cr^{3+} *(Table III)*. For this discussion, the Fe^{3+} bands of the synthetic alexandrite are neglected because they are all below 500 nm and therefore not within the range of the ν_1 band. In contrast, the ν_2 bands are much closer to one another in all three polarization directions for both V^{3+} and Cr^{3+}.

For all V- and Cr-bearing chrysoberyls, the V^{3+} and Cr^{3+} absorption bands are superimposed and, in general, no separation in absorption maxima are recorded for these two chromophores. Depending on the Cr:V ratio of an individual sample, the position of ν_1 is

shifted from the red-orange at about 608–606 nm (for Cr-free or almost Cr-free samples) towards lower wavelengths (for Cr-bearing samples, see *Table III*). For V-free or almost V-free natural alexandrite, the maximum of ν_1 is observed in the greenish yellow range at 576–573 nm *(Figure 14)*. This shift in the position of the ν_1 band is responsible for the variable coloration of V-dominant chrysoberyl from different sources. It is also responsible for the colour change seen in Cr-dominant alexandrite.

Colorimetric measurements confirm the visual impressions. For V-bearing samples without Cr (e.g., Kyocera synthetic chrysoberyl), a slight variation from green to bluish green is measured from daylight to incandescent light, and for V- and Cr-bearing chrysoberyls with distinct Fe contents (e.g., from Sri Lanka), a small variation from yellowish green to yellow-green is detected *(Figure 16)*. This different colour behaviour is due to the greater Cr as well as the somewhat higher Fe content (see again *Figure 11b*), which in general increases the yellowness of chrysoberyls. Samples with somewhat higher Cr than V (e.g., from Ilakaka) have been described as yellowish green or green (Schmetzer *et al.,* 2002).

These colour variations within V-bearing samples from various sources are quite different from the characteristically distinct colour change seen in Cr-bearing chrysoberyl (alexandrite) between daylight and incandescent light (see, e.g., Schmetzer *et al.,* 2012, 2013a). In alexandrite, the colour change is normally observed in two of the three polarization directions, X and Y. The third direction, Z, remains green or bluish green under both illumination sources. These observations can be explained by the different positions of the ν_1 absorption maxima (see again *Table III*), with X at 570 (greenish yellow) and Y at 564 nm (yellow-green), while Z is at somewhat higher wavelengths (~586 nm) in the orange range. For vanadium all three maxima are above 600 nm in the red-orange range and therefore none of the polarization directions shows a distinct colour change (rather, only a slight colour variation). Consequently, V-bearing chrysoberyl does not show distinct colour change behaviour (for further details on V- and Cr-bearing samples, especially from Myanmar, see Schmetzer *et al.,* 2013b).

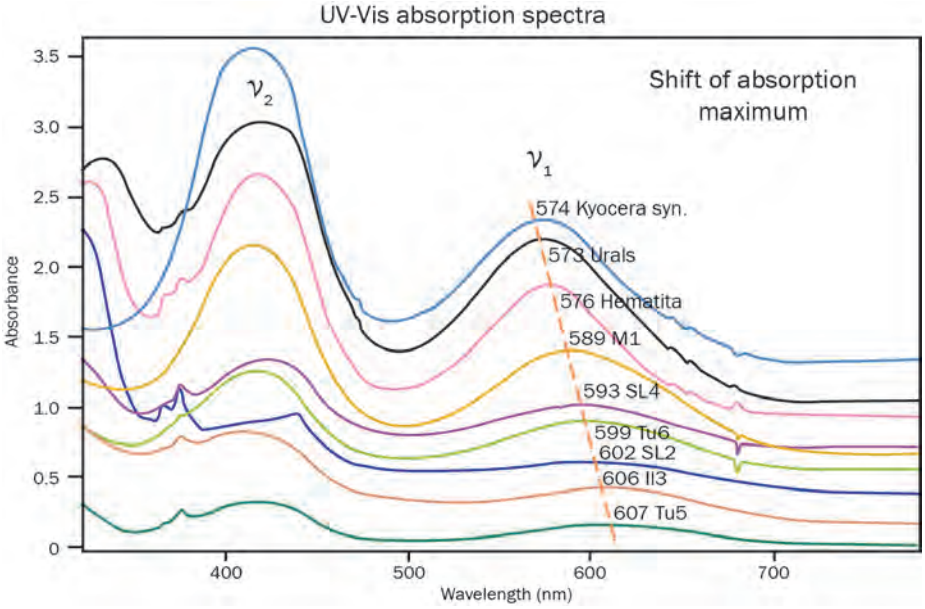

Figure 14: Non-polarized UV-Vis absorption spectra of V-bearing chrysoberyl from various sources (Il = Ilakaka; Tu = Tunduru; SL = Sri Lanka and M = Mogok), together with Cr-bearing alexandrite from Hematita (Brazil) and the Ural Mountains (Russia), as well as synthetic alexandrite grown by Kyocera. Increasing Cr contents cause a shift of the ν_1 absorption maxima towards lower wavelengths. With the exception of sample Tu5, the spectra are displaced vertically for clarity.

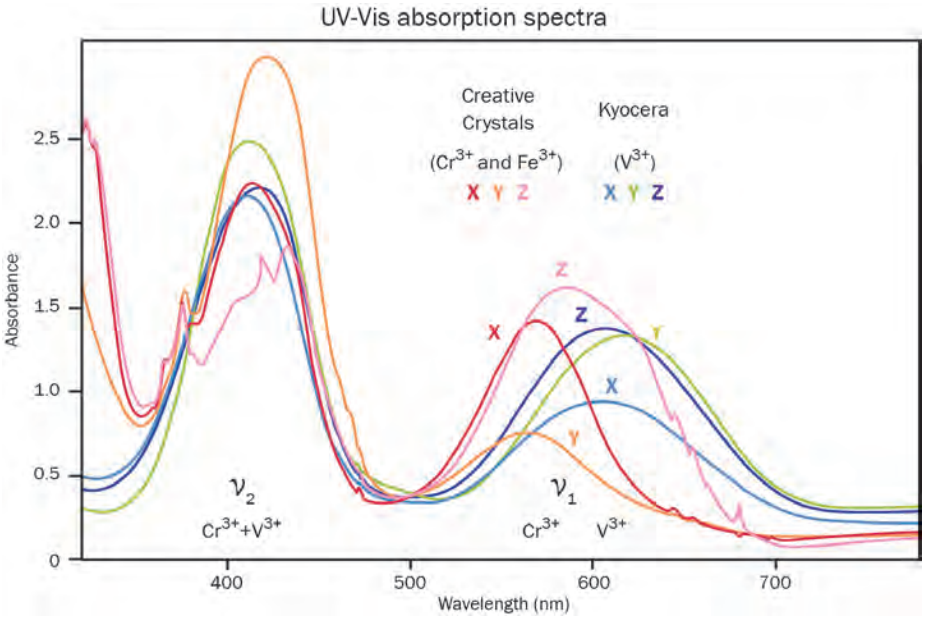

Figure 15: A plot of the polarized UV-Vis absorption spectra of V^{3+} in synthetic chrysoberyl from Kyocera (this paper) and Cr^{3+} in synthetic alexandrite from Creative Crystals (taken from Schmetzer et al., *2012) shows the position of absorption maxima for all three polarization directions (X, Y and Z). The positions of the absorption bands of Cr^{3+} and V^{3+} are close to one another, which explains why separate bands for these ions are not observed in visible-range spectra for samples containing both V and Cr.*

Inclusions

Consistent with previous descriptions of V-bearing natural chrysoberyl from Tunduru, most of our samples from this locality were clean and did not show any mineral inclusions. However, in two Type

1 chrysoberyls we identified numerous tiny apatite crystals *(Figure 17a)* that were partly associated with cavities or growth tubes oriented parallel to the c-axis *(Figure 17b,c)*. Raman analysis of the fluid phase within these elongated cavities showed characteristic peaks of CO_2. A third Type 1 chrysoberyl contained isolated tubes running parallel to the c-axis *(Figure 17d)* and a tiny negative crystal that also was found to contain liquid CO_2. In addition, small partially healed fractures were observed in some samples *(Figure 17e)*. In contrast to this inclusion pattern, one Tunduru Type 2 stone contained numerous minute inclusions identified as feldspar, with Raman spectra indicative of orthoclase (K-feldspar).

A light green chrysoberyl from Ilakaka showed an inclusion pattern consistent with that seen in the Tunduru Type 1 samples. It showed numerous tiny, birefringent, isolated crystals *(Figure 17f)* that were identified as apatite. Some of these apatite inclusions were connected to elongated tubes running parallel to the c-axis of the host. The other samples from Ilakaka did not contain any mineral inclusions.

In the faceted chrysoberyl from Mogok we identified several small mineral inclusions as calcite. Some of these calcites were part of two- or multi-phase inclusions with a fluid component also showing the Raman lines of CO_2.

In the V-bearing chrysoberyl from Sri Lanka we were unable to identify any characteristic mineral inclusions by Raman spectroscopy.

Table III. Absorption maxima (nm) of the first absorption band (ν_1) in V- and Cr-bearing chrysoberyl and alexandrite.

Property	Polarization			Without polarization
	X || a	Y || b	Z || c	
V-bearing, Cr-free synthetic chrysoberyl from Kyocera	607	618	608	608–606
V- and Cr-bearing chrysoberyl, Mogok[a]	570[b]	599	593	589
Cr-bearing, V-free synthetic alexandrite from Creative Crystals[c]	570[b]	564[b]	586	576–573[b]

[a] Cr:V = 1:1.6.
[b] These directions show a colour change between daylight and incandescent light.
[c] From Schmetzer *et al.* (2012).

Characteristic features and distinction of synthetic and natural V-bearing chrysoberyls

Two types of V-bearing synthetic chrysoberyl were produced in the 1990s, by Kyocera in Japan and at various institutes in Novosibirsk, USSR (Academy of Science and/or Tairus). The Kyocera material was characterized for this report and its properties are compared to natural V-bearing chrysoberyl in *Table IV*. The Russian synthetics were examined by H. A. Hänni and K. Schmetzer (Johnson and Koivula, 1996, 1997; see *Figure 18a*) and found to contain extremely high

Table IV. Diagnostic properties of some natural and synthetic V-bearing chrysoberyl[a].

Feature	Characteristic	Kyocera synthetic	Tunduru		Ilakaka	Sri Lanka	Mogok[b]
			Type 1	Type 2			
Chemical	Chromophores	V	V, Fe	V>>Cr, Fe	V, Fe	V>Cr, Fe	V>Cr
	Other trace elements	Not observed	Ga, Sn	Ga or Ga, Sn	Ga, Sn	Ga, Sn	Ga
Microscopic	Growth structures	Not observed	Growth patterns in various directions	Growth patterns in various directions	Growth patterns in various directions	Growth patterns in various directions	Growth patterns in various directions
	Mineral inclusions	Not observed	Apatite, occasionally associated with growth tubes	K-feldspar	Apatite, occasionally associated with growth tubes	Not observed	Calcite
	Other inclusions	Gas bubbles	Negative crystals with CO_2, isolated growth tubes		Isolated growth tubes		Fluid inclusions with CO_2
Spectroscopic	Absorption bands	V	V, Fe	V, Fe	V, Fe	V, Cr, Fe	V, Cr
	Sharp Cr lines	Not observed	Not observed	Present	Not observed	Present	Present

[a] For diagnostic properties of V- and Cr-bearing synthetic chrysoberyl and alexandrite grown by the floating zone method (HOC), see Johnson and Koivula (1996, 1997) and Schmetzer *et al.* (2013a); for diagnostic properties of V- and Cr-bearing synthetic chrysoberyl and alexandrite grown by the flux method, see Schmetzer *et al.* (1996, 2012).
[b] For further details, see Schmetzer *et al.* (2013b).

Natural and synthetic vanadium-bearing chrysoberyl

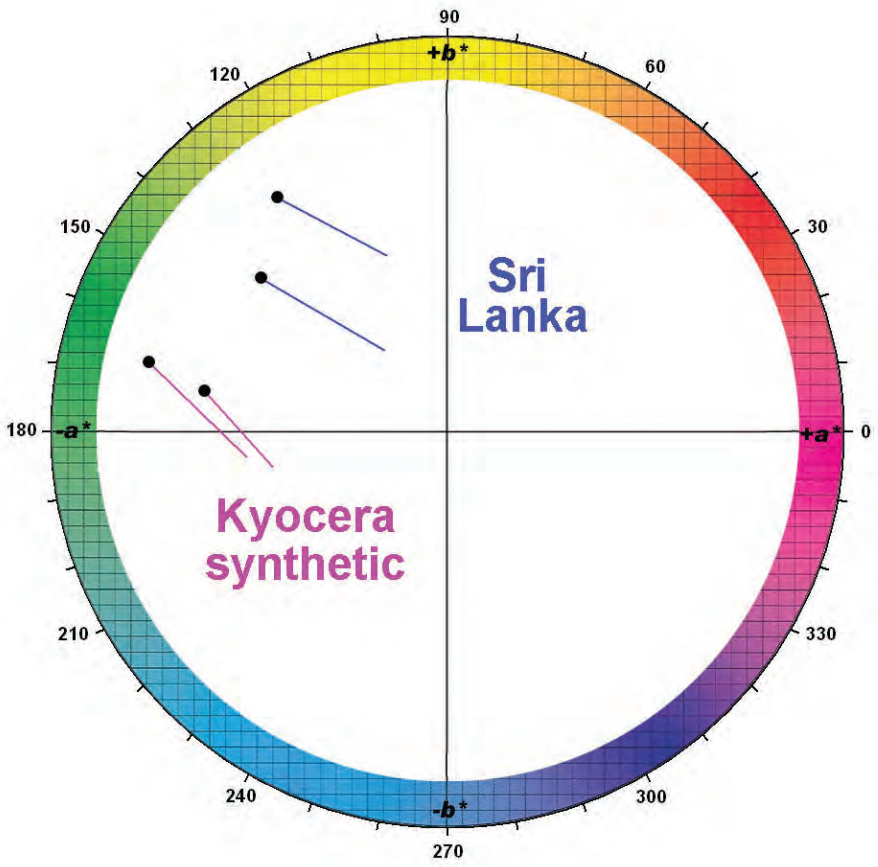

*Figure 16: Colorimetric parameters for two V- and Cr-bearing, Fe-rich chrysoberyls from Sri Lanka (with V>Cr), and V-bearing, Fe- and Cr-free synthetic chrysoberyl from Kyocera are plotted for daylight and incandescent light in the CIELAB colour circle. The neutral point (white point) is in the centre of the a*b* coordinate system and the outer circle represents a chroma of 40. The black circles plot the colour coordinates in daylight D_{65} and the other ends of the differently coloured bars represent the coordinates of the same samples in tungsten light A. The V-, Cr- and Fe-bearing chrysoberyls from Sri Lanka show a small colour variation from yellow green to greenish yellow, whilst the V-bearing, Fe- and Cr-free synthetic chrysoberyls from Kyocera shift slightly from green to bluish green.*

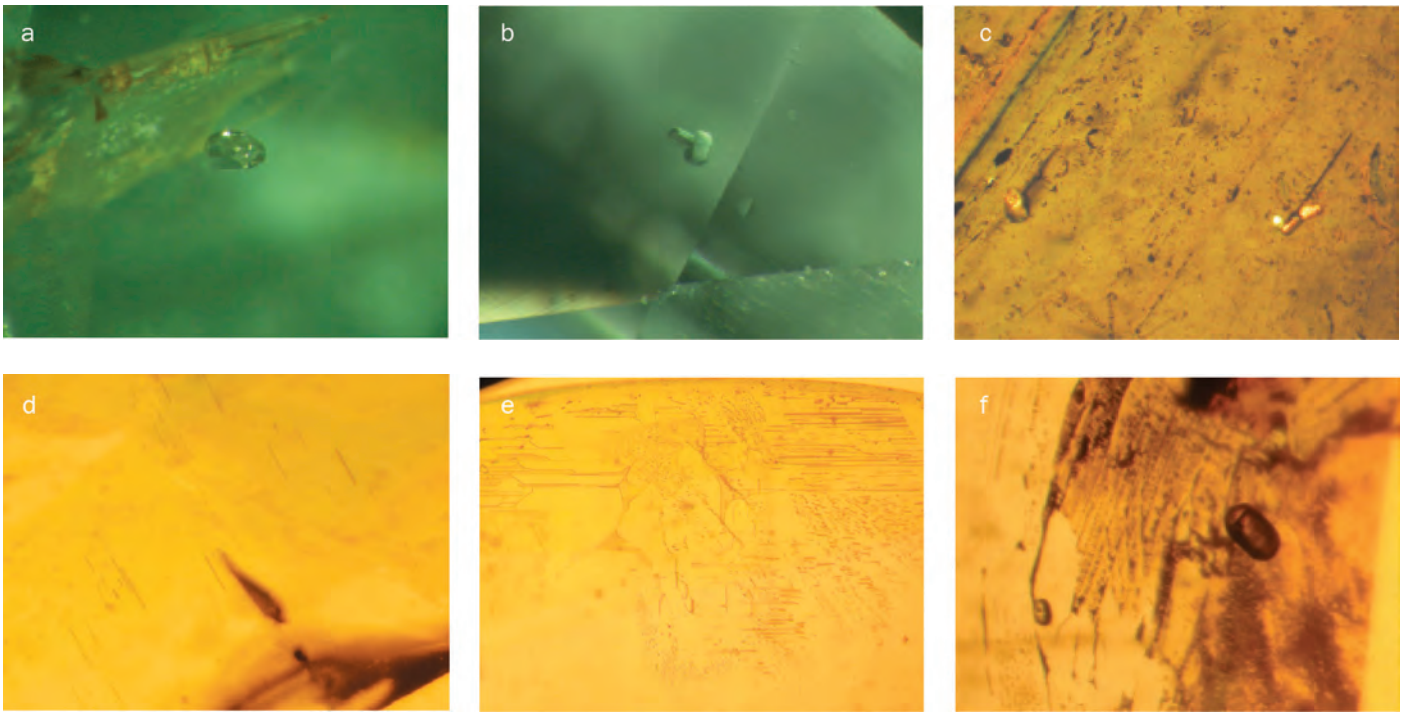

Figure 17: Inclusions seen in V-bearing chrysoberyl from Tunduru (a–e) and Ilakaka (f). Shown here are (a) apatite, (b) apatite next to a cavity, (c) apatite crystals associated with growth tubes oriented parallel to the c-axis, (d) growth tubes running parallel to the c-axis, (e) a partially healed fracture, and (f) apatite. (a,b) Fibre-optic illumination, field of view 1.6×1.2 mm; (c) immersion, crossed polarizers, 3.1×2.3 mm; (d,e,f) immersion, 2.3×1.8 mm, 2.8×2.1 mm, 2.0×1.5 mm, respectively. Photos by M.S. Krzemnicki (a,b) and K. Schmetzer (c–f).

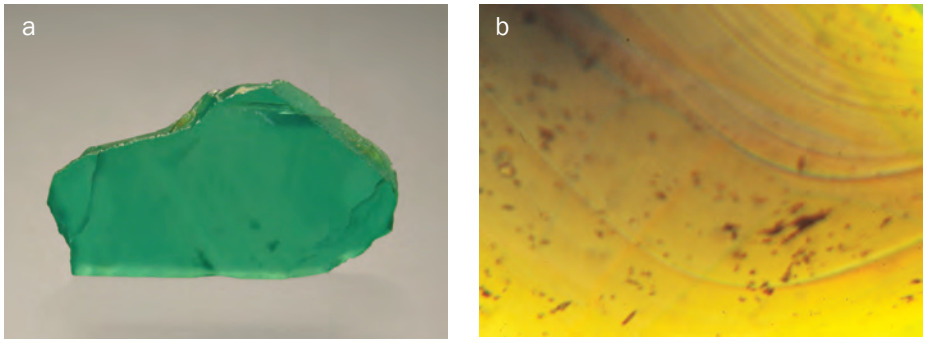

Figure 18: Vanadium-bearing synthetic chrysoberyl grown by the HOC technique in Novosibirsk, Russia. (a) Slice of 1.5 mm thickness, 19.3×10.8 mm; (b) irregularly curved growth striations; immersion, field of view 2.0×1.5 mm. Photos by K. Schmetzer

V contents (1.8 wt.% V_2O_3). Irregularly curved growth striations *(Figure 18b)* suggested this material was produced by the HOC technique. Recently, it was confirmed that a limited quantity of V-bearing synthetic chrysoberyl was grown by this method in Novosibirsk in the 1990s and released into the gem trade (V.V. Gurov, pers. comm., 2012).

Schmetzer *et al*. (1996) examined numerous flux-grown Russian synthetic alexandrites and a few samples were analysed that showed traces of V (up to 0.29 wt.% V_2O_3) in addition to Cr. One such sample even contained more V than Cr. All of the samples with relatively high V contents showed the same twinning, growth structures and inclusions (mostly various forms of residual flux) as observed in the Cr-dominant samples with lower V contents. Extremely high amounts of germanium (up to several wt.% GeO_2) are a characteristic chemical property that can be used to identify this type of synthetic alexandrite and V-bearing chrysoberyl.

Figure 19: Light yellowish green or greenish yellow chrysoberyls such as this 2.44 ct gem (9.7×5.3 mm) typically contain — in addition to some Fe — small amounts of V and/or Cr (in this instance, microprobe analyses showed 0.77 wt.% Fe_2O_3, 0.02 wt.% V_2O_3, and 0.01 wt.% Cr_2O_3). Photo by K. Schmetzer.

Chemical properties of samples from Tunduru reflect two different types: Type 1 is almost Cr-free and contains Sn, while Type 2 contains somewhat greater amounts of Cr (with V>>Cr) but no Sn was detected in some of those samples. These data are consistent with the literature (Johnson and Koivula, 1996; Mayerson, 2003). The trace-element pattern of V-bearing chrysoberyl from Ilakaka is similar to Type 1 Tunduru material. The few samples examined from Sri Lanka showed traces of both V and Cr, as well as unambiguous X-ray emissions of Sn. The samples from Mogok showed relatively high V and Cr contents, but no Sn. All natural samples with the exception of chrysoberyl from Mogok showed distinct Fe and characteristic X-ray lines of Ga were detected in stones from all localities. In contrast, the Kyocera synthetics contained little or no Cr and Fe, and neither Ga nor Sn was detected.

The majority of the natural V-bearing chrysoberyl displayed diagnostic growth patterns that were clearly observable in immersion. Some of the natural samples also contained characteristic inclusions such as apatite (occasionally associated with cavities or growth tubes), K-feldspar, calcite and negative crystals. The Kyocera synthetics showed no growth structures or mineral inclusions.

The absorption spectra of V-bearing chrysoberyl from three localities show dominant maxima due to V^{3+} (Tunduru and Ilakaka) or mixed V^{3+} and Cr^{3+} (Sri Lanka), as well as the characteristic absorption lines of Fe^{3+}, which were not present in the synthetic chrysoberyl grown by Kyocera.

Consequently, a combination of microscopic, spectroscopic and chemical features provide a clear distinction of natural V-bearing chrysoberyl from its known synthetic counterparts.

Conclusions

Since its discovery in Tunduru, Tanzania, in the mid-1990s, 'mint' green V-bearing chrysoberyl has remained a rare gem material. Despite the demand for this attractive gem, only small quantities have been produced from the known deposits at Tunduru, Ilakaka, Sri Lanka and Mogok.

Until now, the more yellowish green material from Sri Lanka containing relatively higher Fe contents and V>Cr have not been separated from green chrysoberyl from Sri Lanka with Cr>V. This also applies to chrysoberyl from other sources containing both V and Cr in variable but low amounts. Several chrysoberyls from various sources, typically with high Fe contents and low V and/or Cr (<0.04 wt.% oxide) have been analysed by the present authors. Such stones (see, e.g., *Figure 19*) are consistently light yellowish green or greenish yellow, and no separation of these gemstones according to colour or colour cause (i.e., V:Cr ratio) is presently done by the trade.

The two intense bluish green samples examined by the present authors came from Mogok to collections in the UK in the 1970s, and additional samples produced during this time may exist in other private or museum collections. The rediscovery of the original source in the Mogok area of these magnificent, bright gems would certainly cause excitement.

The separation of natural from synthetic V-bearing chrysoberyl can be successfully accomplished by a combination of microscopic, spectroscopic and chemical criteria, provided the gemmologist has an awareness of the different types of natural and synthetic materials produced in the past. Characteristic microscopic features that may help identify natural materials are inclusions and growth structures, while the synthetics contain no inclusions or

may reveal curved growth structures, gas bubbles or residual flux inclusions (depending on the growth technique used). Spectroscopic and chemical data are useful for indicating the presence and ratio of various colour-causing trace elements (V, Cr and Fe). Natural chrysoberyls contain traces of Ga and usually Sn, which are both absent from synthetic material.

Acknowledgements

Most of the V-bearing chrysoberyl samples examined in this study were obtained from the H.A. Hänni collection at SSEF. For the loan of additional samples, the authors are grateful to Dr R. Hochleitner (Bavarian State Collection for Mineralogy, Munich), P. Tandy (Department of Earth Sciences at the Natural History Museum, London) and Dr E. Fritsch (University of Nantes, France). In addition, natural V-bearing chrysoberyls were kindly supplied for the present study by C. Cavey (London), D. Gravier (Poncin, France) and S. Hanken (Waldkraiburg, Germany), from their collections or company stock. Thanks go also to Dr W. Balmer (Unterseen, Switzerland) for performing colorimetric measurements. Dr V.V. Gurov (Institute of Geology and Mineralogy, Russian Academy of Sciences, Novosibirsk) provided information about the Russian production of synthetic chrysoberyl and alexandrite in the past.

References

Bank, H., Henn, U., and Milisenda, C.C., 1997. Mintgrüner Chrysoberyll aus Tansania. *Gemmologie: Zeitschrift der Deutschen Gemmologischen Gesellschaft,* **46**(2), 63

Bukin, G.V., Eliseev, A.V., Matrosov, V.N., Solntsev, V.P., Kharchenko, E.I., and Tsvetkov, E.G., 1980. The growth and examination of optical properties of gem alexandrite. In: A.V. Sidorenko *et al.,* Eds., *Inhomogeneity of Minerals and Crystal Growth.* Proceedings of the XI General Meeting of IMA, Novosibirsk, 04-10 Sept. 1978, publ. in Moscow in 1980, pp. 317–28 (in Russian)

Cline, C.F., and Patterson, D.A., 1975. Synthetic Crystal and Method of Making Same. U.S. Patent 3,912,521, assigned to Creative Crystals Inc., Oct. 14

Farrell, E.F., and Newnham, R.E., 1965. Crystal-field spectra of chrysoberyl, alexandrite, peridot, and sinhalite. *American Mineralogist,* **50**(11–12), 1972–81

Hänni, H.A., 2010. Chrysoberyl: A gemstone with many faces. *Australian Gemmologist,* **24**(3), 68–70

Johnson, M.L., and Koivula, J.I., Eds., 1996. Gem News: Nonphenomenal vanadium-bearing chrysoberyl. *Gems & Gemology,* **32**(3), 215–6

Johnson, M.L., and Koivula, J.I., Eds., 1997. Gem News: Update on vanadium-bearing synthetic chrysoberyl. *Gems & Gemology,* **33**(2), 148–9

Koivula, J.I., Kammerling, R.C., and Fritsch, E. Eds., 1994. Gem News: New production facility inaugurated in Siberia. *Gems & Gemology,* **30**(3), 200

Krzemnicki, M.S., and Kiefert, L., 1999. Bluish green, light green, and pink synthetic chrysoberyl. *Gems & Gemology,* **35**(3), 175

Machida, H., and Yoshihara, Y., 1980. Synthetic single crystal for alexandrite gem. U.S. Patent 4,240,834, assigned to Kyoto Ceramic Co. Ltd., Dec. 23

Machida, H., and Yoshihara, Y., 1981. Synthetisches Einkristall für einen Alexandrit-Edelstein. Published Patent Application DE 29 35 330 A1, assigned to Kyoto Ceramic Co. Ltd., April 2

Malsy, A.-K., and Armbruster, T., 2012. Synthetic alexandrite — growth methods and their analytical fingerprints. *European Journal of Mineralogy,* **24**(1), 153–62

Mayerson, W.M., 2003. Gems News International: Chrysoberyl, non-phenomenal vanadium-bearing. *Gems & Gemology,* **39**(2), 144–5

McClure, S.F., 1998. Lab Notes: Chrysoberyl, dark green. *Gems & Gemology,* **34**(3), 212–3

Nishigaki, Y., and Mochizuki, S., 1998. Green chrysoberyl synthetic single crystal. Published Patent Application JP 10-045495 A, assigned to Kyocera Corporation, Feb. 17 (in Japanese)

Ottemann, J., 1965. Gallium und Zinn in Alexandrit. *Neues Jahrbuch für Mineralogie, Monatshefte,* **1965**(2), 31–42

Ottemann, J., Schmetzer, K., and Bank, H., 1978. Neue Daten zur Anreicherung des Elements Gallium in Alexandriten. *Neues Jahrbuch für Mineralogie, Monatshefte,* **1978**(4), 172–5

Pfenninger, S., 2000. Mineralogische und Gemmologische Untersuchungen an Chrysoberyllen aus Tunduru (Tansania). Diplomarbeit, Universität Basel, 82 pp (unpublished)

Schmetzer, K., 2011. Measurement and interpretation of growth patterns in chrysoberyl, including alexandrite. *Journal of Gemmology,* **32**(5–8), 129–44

Schmetzer, K., and Bosshart, G., 2010. Colorimetric data of Russian alexandrite and yellowish green to green chrysoberyl. In: K. Schmetzer, *Russian Alexandrites.* Schweizerbart Science Publishers, Stuttgart, Germany, pp 107–20

Schmetzer, K., and Malsy, A.-K., 2011. Alexandrite and colour-change chrysoberyl from the Lake Manyara alexandrite-emerald deposit in northern Tanzania. *Journal of Gemmology,* **32**(5–8), 179–209

Schmetzer, K., Peretti, A., Medenbach, O., and Bernhardt, H.-J., 1996. Russian flux-grown synthetic alexandrite. *Gems & Gemology,* **32**(3) 186–202

Schmetzer, K., Hainschwang, T., and Bernhardt, H.-J., 2002. Gem News International: Yellowish green and green chrysoberyl from Ilakaka, Madagascar. *Gems & Gemology,* **38**(3), 261

Schmetzer, K., Bernhardt, H.-J., Bosshart, G., and Hainschwang, T., 2009. Colour-change garnets from Madagascar: Variation of chemical, spectroscopic and colorimetric properties. *Journal of Gemmology,* **31**(5–8), 235–82

Schmetzer, K., Bernhardt, H.-J., and Hainschwang, T., 2012. Flux-grown

synthetic alexandrites from Creative Crystals Inc. *Journal of Gemmology,* **33**(1–4), 49–81

Schmetzer, K., Bernhardt, H.-J., Balmer, W.A., and Hainschwang, T., 2013a. Synthetic alexandrites grown by the HOC method in Russia: Internal features related to the growth technique and colorimetric investigation. *Journal of Gemmology,* **33**(5–6), 113–29

Schmetzer, K., Bernhardt, H.-J., and Cavey, C., 2013b. Vanadium- and chromium-bearing chrysoberyl from Mogok, Myanmar — an examination of two historical samples. *Australian Gemmologist,* **25**(2), 41–5

The Authors

Dr Karl Schmetzer
85238 Petershausen, Germany
email: SchmetzerKarl@hotmail.com

Dr Michael S. Krzemnicki FGA
Swiss Gemmological Institute SSEF, CH-4001 Basel, Switzerland
email: gemlab@ssef.ch

Thomas Hainschwang FGA
GGTL Laboratories, Gemlab (Liechtenstein)/GemTechLab, FL 9496 Balzers, Liechtenstein/CH 1227 Geneva, Switzerland
email: thomas.hainschwang@ggtl-lab.org

Dr Heinz-Jürgen Bernhardt
ZEM, Institut für Geologie, Mineralogie und Geophysik, Ruhr-University, 44780 Bochum, Germany
email: Heinz-Juergen.Bernhardt@rub.de

Tracing cultured pearls from farm to consumer: A review of potential methods and solutions

Henry A. Hänni and Laurent E. Cartier

Abstract: This article reviews various methods that could be used to determine the geographic origin of cultured pearls, potentially allowing a consumer to trace them back to the farm. Chemical marking using different substances is possible due to the porosity of the nucleus and nacre. It is also possible to affix a logo marker to the nucleus that can later be imaged using X-radiography. In addition, radio-frequency identification chips are today so small that they can be housed within the nucleus of a cultured pearl. Also discussed is the potential of using trace-element chemistry to differentiate mollusc species and pearling regions. Carbon and oxygen isotopes could also be useful given that they reflect the waters in which a cultured pearl grew, and DNA testing may offer options in the future.

Keywords: cultured pearl branding, cultured pearl traceability, LA-ICP-MS, RFID chips, shell and cultured pearl DNA

Introduction

Branded jewellery products are more successful than non-branded goods (Kapferer and Bastien, 2009). There is continued demand from jewellery consumers for branded goods and increasing desire for traceability of products (Conroy, 2007; Ganesan *et al.,* 2009). Cultured pearls are an interesting case study where some products are branded (e.g., *Figure 1*), but traceability to source is something that is difficult to verify independently at present. A cultured pearl strand with a branded tag does not provide a clear guarantee of origin for the end consumer, given that individual cultured pearls can easily be exchanged or strands re-strung. At the same time, there is a growing interest in tracing cultured pearls through the supply chain, so that an end consumer knows which farm their cultured pearls came from. Producers who operate responsibly are investigating ways of marking their cultured pearls so that provenance can be guaranteed to the end consumer.

Any method used to trace cultured pearls must largely be invisible so as to maintain the commercial value of the end products. Cultured pearls are produced both with a nucleus (e.g., Akoya, South Sea and Tahitian) and without a nucleus (e.g., Chinese freshwater beadless products); for general reviews, see for example Gervis and Sims (1992) and Southgate and Lucas (2008). Different labelling/traceability approaches may be required for these two types of cultured pearls, based on their internal structure. This article reviews a wide range of methods — chemical, physical and biological — that potentially could be used in tracing cultured pearls through the supply chain.

Chemical marking

Pearls consist of fine polycrystalline calcium carbonate ($CaCO_3$) crystals and traces of organic matter. The mother-of-

Figure 1: A branded necklace of South Sea cultured pearls (12 mm in diameter) produced by Atlas Pearls in northern Bali and West Papua (Indonesia). Photo courtesy of Atlas Pearls, Claremont, Western Australia.

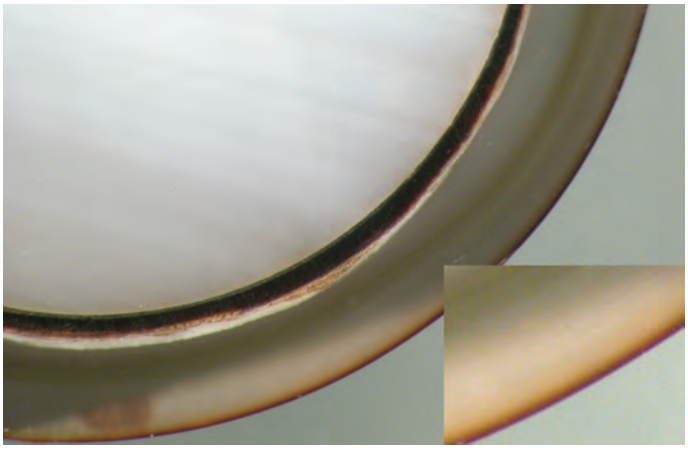

Figure 2: Cross-section of a 'chocolate' beaded cultured pearl. The light-coloured bead (i.e., nucleus) and the darker overgrowth are clearly visible. It is evident in the enlarged image at the bottom right that the brown colour has been artificially added. This demonstrates the porosity of a cultured pearl and its potential for absorbing chemically doped or colour-doped solutions. The colour has penetrated approximately 0.5 mm. Photo by H. A. Hänni.

pearl (also called nacre) surface of pearls is made up of aragonite tablets. A pearl's porous structure means that it has a good potential for absorbing chemically doped or colour-doped solutions. A good example of this are dyed cultured pearls (e.g., *Figure 2*), which can be found in many different colours (Hänni, 2006; Strack, 2006). In a similar way, cultured pearls from selected producers could be marked using a colourless doped solution — that is unique to a pearl producer — after harvest. If chemically doped, these pearls could later be identified in a gemmological laboratory using EDXRF spectroscopy (Hänni, 1981). However, the applicability of this approach is limited given that EDXRF spectroscopy is not in widespread use in the jewellery industry.

Alternatively, rather than marking the cultured pearl after harvest, one could mark the nucleus before insertion using a specific solution. However, if the nacreous overgrowth is too thick, it may not be possible to identify the chemical signal from the nucleus. Another approach would be to remove a tiny amount of nucleus material from a drilled cultured pearl for chemical analysis.

The authors have experimented with the diffusion of fluoroamine (NH_2F) into a cultured pearl, something a pearl farmer could easily do. The subsequent detection of fluorine could then be linked back to that farm. Fluorine is a relatively light element that is not detectable by EDXRF spectroscopy, but is best analysed by nuclear magnetic resonance (NMR). However, NMR is cost-intensive and the instrument's sample chamber is typically smaller than the diameter of a cultured pearl.

If only a limited number of pearl farms are involved in such chemical marking of their cultured pearls, it could be viable to supply each of them with different cost-effective and nontoxic chemicals that could be detected in a gemmological laboratory.

Labelling the nucleus or the surface of a cultured pearl

Initial experiments using physical labels affixed to a cultured pearl nucleus were carried out in 2010 by author HAH. Thin (0.05 mm) rings consisting of gold wire were affixed to several Mississippi shell nuclei (the nucleus material commonly used in the pearl industry) and used to produce cultured pearls. The aim was to investigate the possible rejection of labelled nuclei by the molluscs and to see whether this gold label (or the associated adhesive) would influence cultured pearl growth. Results after six months showed that the labelling materials (gold and glue) had no influence on cultured pearl production and this spurred further efforts to investigate the production of nucleus logos.

Any such logo marker must be extremely thin, be composed of noble metal (and therefore be resistant to corrosion) and have the same convex shape as the nucleus to ensure that the resulting cultured pearl is also round. However, the production of such round metal labels, generally 3–4 mm wide and 0.05 mm thick, is relatively expensive. Different label production techniques were tested, such as galvanic production, pressing, etching and cutting with a

Figure 3: Silver logo labels (3 mm in diameter) for a pearl farm. These can be affixed onto the bead prior to insertion and later be used to trace a beaded cultured pearl back to its farm. Photo by H. A. Hänni.

laser or water jets; these are widely used techniques in manufacturing (Schultze and Bressel, 2001). The water jet technique was most precise for cutting the contours of the logo, but still considered too expensive.

Several dozen logo tags (e.g., *Figure 3*) were affixed to shell nuclei and sent to different marine farms to be tested in cultured pearl production. After the usual 12–18 month growth period, these 'tagged' cultured pearls were harvested and successfully examined with X-radiography *(Figure 4)*. Due to the position of the logo in the peripheral part of a cultured pearl, there is only a statistically small chance of the logo being damaged during drilling.

The production of such logo markers is relatively expensive, even if produced in large quantities. In addition, these cultured pearls need to be tested using X-rays, which is relatively unfeasible for a jeweller. (X-rays used for medical purposes, such as in dentistry, are not strong enough to visualize all required details within a cultured pearl of, e.g., 10 mm.) Nevertheless, for beaded cultured pearls that use a nucleus (e.g., Akoya, South Sea and Tahitian), this method is an option. For beadless cultured pearls (e.g., Chinese freshwater cultured pearls), the introduction of a label together with the saibo (donor mantle tissue) would have the disadvantage of positioning the logo in the centre of the cultured pearl, resulting in a high likelihood of damage during the drilling process.

Another approach is to mark the surface of the cultured pearl rather than the nucleus. This could involve either laser engraving with a unique number (similar to laser inscriptions on diamonds) that can later be used to identify its source or embossing a hologram onto the surface of the cultured pearl that can be read with a suitable reader. Both of these methods are currently being investigated in French Polynesia ('Redonner ses Lettres…', 2013; 'Le Tahiti Pearl Consortium Disparaît', 2013). These methods are slightly destructive to a cultured pearl's surface and it remains to be seen if they are acceptable to the pearl trade.

Only the laser engraving method should have been described as slightly destructive.

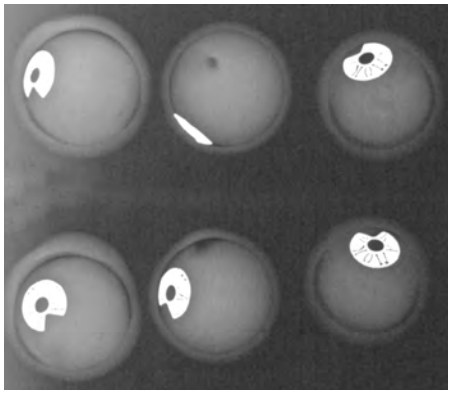

Figure 4: X-radiographs of three Tahitian cultured pearls with a branded nucleus. The farm-specific logos are in silver, which has a high density making it quite visible with X-rays. Three cultured pearls are shown in two slightly different orientations in this composite image. The diameter of the cultured pearls is approximately 8 mm and the width of the logos is 3 mm. Image by H. A. Hänni.

RFID – radio frequency identification

Radio frequency identification (RFID) technology has undergone rapid development in the past decade and is now a widely used method in many technology applications (Want, 2006). It is increasingly being employed in jewellery management solutions (Wyld, 2010). Through the miniaturization of RFID chips (transponders in millimetre sizes), the use of electromagnetic frequencies is a feasible option for the tagging/traceability of cultured pearls. Transponders are chips that contain relevant data which can be accessed with an RFID reader. These devices are inexpensive and they could be easily used in jewellery retail stores ('June HK Fair Special…', 2013). Information stored on the chips could include the production location, harvest date and details about the pearl farm. Additional information can be added to the RFID chip after a cultured pearl has been harvested, including its quality grade, inventory data and unique identification information that could be useful for theft recovery.

RFID chips have been introduced into commonly used Mississippi shell nuclei, which are currently being piloted by pearl farmers in the Pacific Ocean.

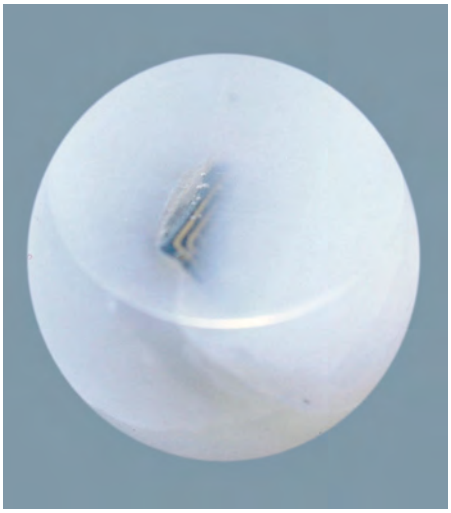

Figure 5: A composite shell bead that has been sliced and polished to show a small RFID chip (3 mm long) embedded within it. The information on such a chip can be accessed using an RFID reader. Photo by H. A. Hänni.

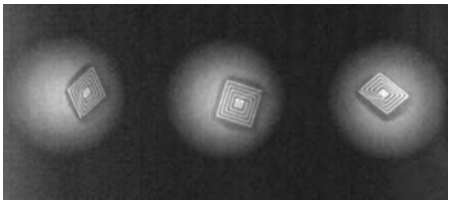

Figure 6: X-ray shadow images of bead nuclei (7.5 mm diameter) consisting of pieces of shell with embedded RFID chips. These are being marketed by Fukui Shell Nucleus Factory. Image by H. A. Hänni.

One nucleus manufacturer (Fukui Shell Nucleus Factory, Hong Kong) has already brought to market nuclei that contain RFID chips (see 'June HK Fair Special…', 2013). *Figure 5* shows such a 'micro-chip embedded nucleus' which, depending on its size, costs US$2–3 per piece. According to the manufacturer, these nuclei consist of two layers of shell material (i.e., laminated nuclei) and a 3 mm RFID chip that is located 1 mm below the surface of the nucleus *(Figure 5)*. *Figure 6* shows an X-ray shadow image of such chip-embedded nuclei.

One disadvantage of these nuclei is the relatively high cost of the chips, which would be wasted in cultured pearls of low quality. Also, the 3 mm size of the straight-edged chips is rather large when taking into account that the nucleus has a spherical shape. The size and position

*Table I: LA-ICP-MS analyses of cultured pearls and shells from various species and locations.**

Habitat		Saltwater														
Sample		*Pinctada maxima* (silver) shell			*Pinctada maxima* (gold) shell			*Pinctada radiata* shell			*Pinctada margaritifera* cultured pearl			*Pinctada margaritifera* cultured pearl		
Source		Indonesia			Philippines			United Arab Emirates (RAK)			Rangiroa, French Polynesia			Fiji		
CaO	wt.%	56.03	56.03	56.03	56.03	56.03	56.03	56.03	56.03	56.03	56.03	56.03	56.03	56.03	56.03	56.03
Na_2O	wt.%	0.91	0.91	0.88	0.84	0.84	0.86	0.97	0.92	0.95	0.75	0.75	0.74	0.90	0.86	0.93
Li	ppm	0.53	0.40	0.40	0.40	0.33	0.23	0.56	0.50	0.56	0.38	0.44	0.40	0.57	0.64	0.69
B	ppm	18.2	20.5	21.2	15.1	15.1	15.6	1.8	1.9	1.7	10.7	10.8	10.6	16.3	14.6	14.0
Mg	ppm	169	180	199	115	115	121	476	392	463	206	198	226	120	98	98
P	ppm	34.0	33.0	35.0	6.6	6.5	6.6	73.2	71.5	71.7	13.8	13.2	12.9	13.3	13.5	12.7
K	ppm	71.1	63.6	51.1	131	157	180	104	118	106	60.0	51.2	42.7	82.7	87.2	83.7
Cr	ppm	2.3	1.9	2.1	2.0	1.9	1.8	2.0	1.8	2.0	2.5	2.2	2.2	2.3	2.4	2.2
Mn	ppm	3.4	3.3	3.4	6.2	6.6	6.2	0.19	0.18	0.18	1.3	1.4	1.4	88.5	92.9	56.9
Fe	ppm	18.4	19.6	17.3	18.3	19.1	22.8	15.6	18.1	18.1	26.9	26.7	29.0	25.4	26.8	28.3
Cu	ppm	0.14	0.08	<0.06	0.09	0.11	0.10	0.26	0.35	0.29	0.11	0.10	0.06	0.04	0.08	0.07
Zn	ppm	<0.08	0.34	0.41	0.38	0.44	0.55	0.59	0.73	0.59	0.28	0.21	0.45	<0.05	0.31	0.12
Sr	ppm	1030	1070	1130	1040	1040	1080	802	775	795	166	169	163	964	138	113
Ba	ppm	0.35	0.49	0.43	0.28	0.26	0.30	0.17	0.15	0.23	0.28	0.37	0.30	0.19	0.39	0.23
Pb	ppm	0.12	0.10	0.10	3.0	3.6	14.9	0.13	0.13	0.12	0.06	0.05	0.05	0.05	0.05	0.04
Ag	ppm	<0.003	<0.004	<0.006	<0.005	0.01	0.01	<0.009	<0.009	<0.004	<0.004	<0.004	<0.004	<0.005	<0.005	<0.005

Habitat		Saltwater						Freshwater								
Sample		*Pteria sterna* shell			*Pteria penguin* shell			*Hyriopsis* shell			*Unio* shell			Ming cultured pearl		
Source		Mexico			Irian Jaya, Indonesia			China			Scotland			China		
CaO	wt.%	56.03	56.03	56.03	56.03	56.03	56.03	56.03	56.03	56.03	56.03	56.03	56.03	56.03	56.03	56.03
Na_2O	wt.%	0.97	0.95	0.88	0.67	0.66	0.70	0.28	0.28	0.28	0.25	0.25	0.25	0.34	0.34	0.35
Li	ppm	0.64	0.57	0.47	0.47	0.56	1.14	<0.07	0.12	0.09	<0.07	<0.09	<0.08	<0.03	0.07	<0.03
B	ppm	5.0	5.5	7.3	8.5	8.5	9.7	4.0	4.0	3.5	3.7	4.4	4.4	0.20	<0.13	<0.14
Mg	ppm	132	73	57	165	147	112	23.9	23.5	15.4	18.3	18.7	56.4	14.0	20.0	18.0
P	ppm	123	122	135	158	150	121	192	183	188	100	113	127	183	191	160
K	ppm	65.7	66.0	65.0	41.8	40.8	50.5	19.6	8.9	5.6	34.6	66.4	95.7	19.0	28.0	6.0
Cr	ppm	2.2	2.0	2.0	2.1	2.2	2.2	2.1	1.7	1.6	2.3	1.4	1.8	2.3	2.6	2.3
Mn	ppm	1.7	1.5	0.8	1.6	1.5	2.2	661	1580	861	519	501	477	133	268	137
Fe	ppm	11.6	13.4	12.8	12.4	12.4	13.7	13.3	12.3	15.1	14.9	16.3	16.3	28.0	29.8	32.4
Cu	ppm	0.10	0.10	0.07	0.06	0.05	0.05	0.17	0.20	0.22	0.33	0.25	0.38	0.25	0.41	0.38
Zn	ppm	0.41	0.40	0.56	0.43	0.33	0.30	0.29	<0.11	0.18	0.67	0.26	0.53	2.3	2.6	1.8
Sr	ppm	1000	908	923	1280	1320	1170	761	877	360	250	260	267	305	446	409
Ba	ppm	0.20	0.17	0.90	1.11	0.96	1.03	247	288	225	469	516	543	57.6	117.3	76.2
Pb	ppm	0.36	0.45	0.40	0.27	0.24	0.29	0.02	0.02	0.02	0.12	0.07	0.14	0.05	0.06	0.13
Ag	ppm	<0.003	0.005	<0.003	<0.002	<0.003	<0.003	<0.006	<0.003	<0.005	<0.004	<0.004	<0.005	<0.02	<0.02	<0.02

* CaO = 56.03 wt.% was used as an internal standard on the basis of the $CaCO_3$ formula for aragonite and calcite. Ag was measured to identify cultured pearls dyed black using silver nitrate. Iodine was analysed in all samples but could not be quantified for lack of an iodine standard. Be, Al, Sc, Ti, V, Co, Ni, As, Rb, Y, Cd, REEs (La, Ce, Nd, Tb, Yb and Lu), and Bi were measured at or just below the detection limit (sub-ppm). Each sample was analysed in three different spots, corresponding to the three columns for each sample.

of these chips within the nucleus means they may often be damaged during the cultured pearl drilling process. Rapid developments in RFID technology are promising, but we may need to await the further miniaturization of the chips before they become a feasible option for the cultured pearl industry.

Advanced fingerprinting of pearl and shell materials

Laser ablation–inductively coupled plasma–mass spectrometry (LA-ICP-MS) has become more widely used in the last few years in geosciences, even in gemmology (e.g., Saminpanya *et al.,* 2003; Abduriyim and Kitawaki, 2006). Many laboratories and researchers now employ it for the chemical characterization of gems because it has a low detection limit and can also detect light elements. With this method it is possible to carry out high-resolution spot analyses, which allows us to take into account possible chemical zoning in gem materials, including cultured pearls. The technique has been used for characterization of cultured freshwater pearls (Jacob *et al.,* 2006) and natural saltwater pearls from Australian *Pinctada maxima* molluscs (Scarratt *et al.,* 2012). To our knowledge, there are no published LA-ICP-MS data on a wider range of cultured pearls or shell samples from various mollusc species.

For this study, a preliminary LA-ICP-MS investigation of cultured pearls and shell material was undertaken at the University of Bern. The instrumentation used a 193 nm ArF laser, and synthetic glass (SRM612) was used as a standard for calibration before and after each round of measurements. This was also done to ensure the reproducibility of measurements and detect possible impurities in the chamber that might affect subsequent data. The pits produced on the surface of the samples during ablation had a diameter of 160 µm. As such, the technique is quasi-nondestructive.

Table I lists the results for the seven shell samples and three cultured pearls from different locations that were analysed. It is clear that further research is required to compile a useful LA-ICP-MS database that might permit origin determination of cultured pearls from different species.

Figure 7: The Atlas Pearl farms that produced the necklace shown in Figure 1 *are located in Bali (shown here) and West Papua, Indonesia. Giving consumers access to the origin of their cultured pearls may create additional value for pearl farmers. Photo by L. Cartier.*

Another possible (and nondestructive) method for chemically fingerprinting gem materials is particle-induced X-ray emission (PIXE), which has been applied to ruby and emerald (Calligaro *et al.,* 1999; Yu *et al.,* 2000). More recently, PIXE was used on cultured pearls (Murao *et al.,* 2013). Other studies have measured oxygen and carbon isotopic values of nacre and cultured pearls in an attempt to identify geographic origin (Yoshimura *et al.,* 2010). However, all these techniques remain academic and expensive, and they presently do not fulfil the requirements for a rapid and cost-effective tracing method for cultured pearls.

A final method that is very new but merits description is DNA fingerprinting of cultured pearls. Oyster shells and pearls have a biological origin and contain small amounts of organic matter between aragonite layers and in the form of organic pockets. A recently published study described how DNA can be extracted from this organic material in cultured pearls in a practically nondestructive manner (Meyer *et al.,* 2013). The DNA can be used to identify the oyster species of the cultured pearl and the authors also proposed that geographic origin determination might also be possible using next generation sequencing (NGS) techniques in the near future. A similar approach has been used for geographic origin and species determination of ivory (Wasser *et al.,* 2004).

Conclusion

The aim of this review is to show the range of currently available methods that potentially could be used to trace cultured pearls through the supply chain. Supply chain accountability and product traceability are becoming increasingly important issues in the jewellery industry. The branding strategies of various producers, wholesalers and jewellery companies would benefit from additional support through an efficient traceability method. Furthermore, there is a potential for responsible pearl farmers (e.g., *Figure 7*) to capture greater value for their products if they can be traced all

the way to the consumer, but the supply chain accountability and provenance need to be guaranteed (Conroy, 2005; Cartier 2012; Cartier and Ali, 2012). As technology continues to evolve, the search for methods to trace cultured pearls through the supply chain should be addressed in collaboration with the gemmological community and the focus should be on developing cost-effective solutions that are feasible for those at all levels of the supply chain (producer, wholesaler, retailer and consumer).

Acknowledgements

We are grateful to all the pearl farmers who were most generous with their time, advice and support of our research. Special thanks go to Arthur and David Wong (Fukui Shell Nucleus Factory, Hong Kong), who have been generous in sharing their knowledge of cultured pearl and nucleus traceability, as well as samples. We thank Prof. Thomas Pettke at the University of Bern (Switzerland) for performing LA-ICP-MS analyses. Finally, Damian Hostettler (Basel, Switzerland) is thanked for logistical assistance.

References

Abduriyim, A., and Kitawaki, H., 2006. Determination of the origin of blue sapphire using laser ablation inductively coupled plasma mass spectrometry (LA-ICP-MS). *Journal of Gemmology,* **30**(1/2), 23–36

Calligaro, T., Poirot, J.P., and Guerré, G., 1999. Trace element fingerprinting of jewellery rubies by external beam PIXE. *Nuclear Instruments and Methods in Physics Research Section B,* **150**(1), 628–34

Cartier, L.E., 2012. Challenges and opportunities in the black cultured pearl industry. *GIT Bangkok 2012 Proceedings,* 312–6

Cartier, L.E., and Ali, S.H., 2012. Pearl farming as a sustainable development path. *The Solutions Journal,* **4**(3), 30–4

Conroy M.E., 2005. Certification systems as tools for natural asset building: Potential, experience to date, and critical challenges. *Political Economy Research Institute Working Paper Series No. 100,* University of Massachusetts, Amherst, 27 pp

Conroy, M.E., 2007. *Branded!: How the 'Certification Revolution' is Transforming Global Corporations.* New Society Publishers, Galbriola Island, Canada, 335 pp

Ganesan, S., George, M., Jap, S., Palmatier, R.W., and Weitz, B., 2009. Supply chain management and retailer performance: Emerging trends, issues, and implications for research and practice. *Journal of Retailing,* **85**(1), 84–94

Gervis, M.H., and Sims, N.A., 1992. *The Biology and Culture of Pearl Oysters (Bivalvia: Pteriidae).* Overseas Development Administration of the United Kingdom (London) and International Center for Living Aquatic Resources Management (Manila, Philippines), ICLARM Studies and Reviews 21, 49 pp

Hänni, H.A., 1981. Energiedispersive röntgenfluoreszenz-analyse in der gemmologischen diagnostik. *Zeitschrift der Deutschen Gemmologischen Gesellschaft,* **30**, 207–9

Hänni, H.A., 2006. Update on 'chocolate' Tahitian cultured pearls. *Gems & Gemology,* **42**(4), 270–2

Jacob, D.E., Wehrmeister, U., Häger, T., and Hofmeister, W., 2006, Herkunftsbestimmung von Süsswasserzuchtperlen mit Laser Ablation ICP-MS (Provenance determination of freshwater cultured pearls using laser ablation ICP-MS). *Gemmologie: Zeitschrift der Deutschen Gemmologischen Gesellschaft,* **55**(1/2), 51–8

June HK Fair Special: Seminar on pearls with RFID tags, 2013. www.jewellerynewsasia.com/en/pearls/7983/june-hk-fair-special-seminar-on-pearls-with-rfid-tags.html, posted 19 June, accessed 05 Oct. 2013

Kapferer, J.-N., and Bastien, V., 2009. *The Luxury Strategy: Break the Rules of Marketing to Build Luxury Brands.* Kogan Page, London, 408 pp

Redonner ses Lettres de Noblesse à la Perle de Tahiti, 2013. *La Dépêche,* 23 Oct., 24

Meyer, J.B., Cartier, L.E., Pinto-Figueroa, E.A., Krzemnicki, M.S., Hänni, H.A., and McDonald, B.A., 2013. DNA fingerprinting of pearls to determine their origins. *PLOS ONE,* **8**(10), e75606

Murao, S., Sera, K., Goto, S., Takahashi, C., Cartier, L.E., and Nakashima, K., 2013. Optimization of PIXE quantitative system to assist the traceability of pearls and other gemstones. *PIXE 2013: 13th International Conference on Particle Induced X-Ray Emission,* Gramado, Brazil, March 3–8, 145

Saminpanya, S., Manning, D.A.C., Droop, G.T.R., and Henderson, C.M.B., 2003. Trace elements in Thai gem corundums. *Journal of Gemmology,* **28**(7), 399–415

Scarratt, K., Bracher, P., Bracher, M., Attawi, A., Safar, A., Saeseaw, S., Homkrajae, A., and Sturman, N., 2012. Natural pearls from Australian *Pinctada maxima*. *Gems & Gemology,* **48**(4), 236–61

Schultze, J.W., and Bressel, A., 2001. Principles of electrochemical micro- and nano-system technologies. *Electrochimica Acta,* **47**(1), 3–21

Southgate, P.C., and Lucas, J.S., 2008. *The Pearl Oyster.* Elsevier, Oxford

Strack E., 2006. *Pearls.* Ruhle-Diebener-Verlag, Stuttgart, Germany

Le Tahiti Pearl Consortium Disparaît, 2013. Tahiti Infos, www.tahiti-infos.com/Le-Tahiti-Pearl-Consortium-disparait_a77015.html, posted 20 June, accessed 13 Nov. 2013

Want, R., 2006. An introduction to RFID technology. *Pervasive Computing, IEEE,* **5**(1), 25–33

Wasser, S.K., Shedlock, A.M., Comstock, K., Ostrander, E.A., Mutayoba, B., and Stephens, M., 2004. Assigning African elephant DNA to geographic region of origin: Applications to the ivory trade. *PNAS,* **101**(41), 14847–52

Wyld, D.C., 2010. 24-karat protection: RFID and retail jewelry marketing. *International Journal of UbiComp,* **1**(1), 1–14

Tracing cultured pearls from farm to consumer: A review of potential methods and solutions

Yoshimura, T., Nakashima, R., Suzuki, A., Tomioka, N., and Kawahata, H., 2010. Oxygen and carbon isotope records of cultured freshwater pearl mussel *Hyriopsis sp.* shell from Lake Kasumigaura, Japan. *Journal of Paleolimnology,* **43**, 437–48

Yu, K.N., Tang, S.M., and Tay, T.S., 2000. PIXE studies of emeralds. *X-ray Spectrometry,* **29**(4), 267–78

The Authors

Prof. Dr Henry A. Hänni FGA
Professor Emeritus of Basel University and GemExpert GmbH, Postfach 921, CH-4001 Basel, Switzerland
email: h.a.haenni@gmail.com

Laurent E. Cartier FGA
Department of Environmental Sciences, University of Basel, Bernoullistrasse 30, CH-4056 Basel, Switzerland
email: laurent.cartier@unibas.ch

Abstracts

Diamonds

The Ellendale diamond field: exploration history, discovery, geology and mining.
A.L. Ahmat. *Australian Gemmologist,* 24(12), 2012, 280–8.
This article concentrates on the history and geology of this significant hard-rock diamondiferous region. Regarded as a source of high-value fancy yellow diamonds, a summary of recent mining production is included along with an expected life span. L.G.

The Kimberley Diamond Company Ellendale diamond collection at the Western Australian Museum.
P.J. Downes, A.W.R. Bevan and G.L. Deacon. *Australian Gemmologist*, **24**(12), 2012, 289–93.

The authors describe a representative collection of yellow and colourless rough diamonds (38.06 carats total weight) in the Kimberley Diamond Company Ellendale diamond collection at the Western Australian Museum, from the operations at Ellendale in the West Kimberley region of Western Australia. History, geological setting and characteristics of diamonds from this region are outlined. L.G.

The Kimberley Process: it's a question of provenance, not origin.
H. Levy. *Gems&Jewellery,* **22**(7), 2013, 10–11.

The author outlines the beginnings of the Kimberley Process and its purpose, and questions whether in the future it can incorporate such issues as human rights. Perceptions of origin and provenance from inside and outside the gemmological community are compared and examples discussed. L.G.

Diamonds: not all is explained with clarity.
A. Matlins. *Gems&Jewellery,* **22**(7), 2013, 17.

The author and a reporter from ABC-TV follow up a previous investigation in New York regarding the disclosure of clarity-enhanced diamonds. Their experiences are documented and comparisons made to the industry eight years ago when the previous investigation on filled diamonds was carried out. L.G.

Lab Notes.
T.M. Moses and S.F. McClure (Eds). *Gems & Gemology,* **48**(4), 2012, 300–3.

A 1.04 ct round brilliant diamond was graded Fancy reddish brown. Whilst the colour appeared natural, it was obviously attributed to heavy irradiation and annealing. UV-Vis-NIR absorption spectroscopy yielded additional interesting features.

A 15.01 ct cushion-cut diamond was graded as Fancy Intense yellow. The stone had previously been submitted and had then been graded Fancy Light yellow. Additional strengthening of the H3 and H4 optical centres was detected by infrared absorption spectroscopy; previously only moderate concentrations were observed in spectra at liquid nitrogen temperatures. The results suggested that artificial treatment had been carried out to strengthen the colour.

Two crystal inclusions, a green diopside and a reddish pyrope, in contact with one another were seen in a 2.34 ct cape Fancy yellow diamond. DiamondView images suggested that the inclusions were formed during the diamond's growth. In a peridotite environment, singular and binary inclusions can be useful in calculating the equilibrium pressure and temperature of diamond formation, although post-growth events may alter the preservation of these conditions.

A 2.03 ct Fancy yellow-green diamond contained inclusions of greyish blue omphacite in contact with orange garnet. This was the first time this assemblage was seen in the Carlsbad laboratory. C.M.

Lab Notes.
T.M. Moses and S.F. McClure (Eds). *Gems & Gemology,* **49**(1), 2013, 44–7.

Thirty unusual 'buff-top' round-cut diamonds weighing 0.25–1.50 ct were graded. Their cut style made grading challenging. The cutting methods were considered.

An unusually large HPHT-treated Fancy pink diamond of 20.32 ct displayed no secondary colours that are common in HPHT-treated diamonds, making this a rare case. Interference colours observed with crossed polars were associated with HPHT treatment. The diamond demonstrates improvements in the HPHT technique.

A 1.53 ct heart-shaped Fancy Intense pinkish orange diamond showed an absorption band at 550 nm, which is usually associated with pink-to-red coloration. The reason for the unusual colour was not fully understood.

A near-colourless 0.70 ct round brilliant diamond displayed subtle cuboctahedral growth structure with the DiamondView, which usually indicates HPHT-grown synthetic diamond. Small cuboctahedral forms can be found in nature but are very rare. Microscopic observation confirmed the diamond to be natural.

A Fancy Deep green 3.17 ct round brilliant diamond was examined. Microscopic observation revealed it had been coloured by radioactive salts, rarely

Abstracts (continued)

encountered today. Unusual surface coloration was seen in diffused light.

A 4.72 ct Light blue rectangular-cut diamond showed an extremely strong 579.9 nm emission centre and lattice dislocations that were the strongest yet observed in the laboratory. C.M.

Gems and Minerals

Experiences on the South Australian Mintabie opal fields – past and present.
P. Blythe, M. Novelli and T. Coldham. *Australian Gemmologist,* **25**(2), 2013, 46–54.

A brief history of the Mintabie opal field is outlined. The area was listed as a gem field in 1933 and substantial recovery began during the 1960s. The experiences and photographs of miners Peter Blythe and Max Novelli are documented through the rest of the paper as they lived and worked in the field spanning from the early 1980s until today. L.G.

New developments in cultured pearl production: use of organic and baroque shell nuclei.
L.E. Cartier and M.S. Krzemnicki. *Australian Gemmologist,* **25**(1), 2013, 6–13.

In this detailed paper the authors discuss the context, composition, process and application of organic nuclei for the production of baroque cultured pearls. Expansion of this organic material allows large cultured pearls to be produced. Varying generations of cultured pearls with different nuclei are examined and their appearance, identification features and properties compared using both standard and laboratory equipment. L.G.

Violet and pink coated opals.
G. Choudhary. *Australian Gemmologist,* **25**(2), 2013, 55–7.

Since the discovery of opal in the Wollo province of Ethiopia, a variety of colours of treated opal have appeared on the market. The author studies two beads of violet and pink coated opals, using both standard and laboratory equipment. As well as identifying the source of the coloration, the author makes the surprising discovery that the base material is different from that of the Wollo province. L.G.

Echte Perlen und Zuchtperlen: ein Grundkonzept und seine Variationen. (Natural and cultured pearls: a basic concept and its variation.)
H.A. Hänni. *Gemmologie. Z. Dt. Gemmol. Ges.,* **62**(1/2), 2013, 3–18.

Natural pearls are the results of an injury to the mollusc's mantle tissue in which some cells are displaced to form a cyst. Natural pearls are not formed by grains of sand, as these cannot drill themselves into the mantle. To produce cultured pearls there are a number of options: non-beaded cultured pearls are usually mantle-grown in freshwater mussels. Beaded cultured pearls are usually gonad-grown in saltwater oysters. There are minor variations which lead to the great number of different products available on the market today. The author describes in detail the operation performed on the oyster or mussel to produce a cultured pearl as well as the materials inserted, which can vary from mother-of-pearl beads to natural or cultured pearls of poor quality. E.S.

Highlights from the Giazotto mineral collection.
R. Hansen and L. Rennie. *Australian Gemmologist,* **24**(12), 2012, 302–3.

This article shows some spectacular well-formed 'museum sized' crystal specimens from the more than 500 minerals displayed at the Museo di Storia Naturale in Florence, Italy. Collected over some 50 years, they include 'The Emperor of India', a 9.8 kg prismatic aquamarine that is 32 cm high, and clusters of 'blue cap' tourmaline from Lavra da Sapo, Minas Gerais, Brazil. L.G.

Gemmologische Kurzinformationen. Gelber transparenter Opal aus Mali. (Yellow transparent opal from Mali.)
U. Henn. *Gemmologie. Z. Dt. Gemmol. Ges.,* **62**(1/2), 2013, 46–8.

A yellow transparent opal from a region near Kayes in western Mali was found to be similar to material found in Mexico and Brazil, with RIs = 1.446–1.453 and SG = 2.05. The yellow colour is due to inclusions of iron hydroxides. E.S.

Infrared spectroscopic study of filled moonstone.
Jianjun Li, Xiaofan Weng, Xiaoyan Yu, Xiaowei Liu, Zhenyu Chen and Guihua Li. *Gems & Gemology,* **49**(1), 2013, 28–34.

Twenty-two beads of plagioclase moonstone were studied. Infrared spectroscopy confirmed 15 of the 22 had been filled with material of a benzene structure, their composition having been identified as close to albite. Links are described between the strength and distribution of UV fluorescence with the filling. It is also noted how filler may be suspected using standard magnification and warns of this treatment now being found in gem materials other than the more well-known emerald. L.G.

Gemological characteristics of saltwater cultured pearls produced after xenotransplantation.
S. Karampelas and A. Lombard. *Gems & Gemology,* **49**(1), 2013, 36–41.

Cultured pearl samples grown by the xenotransplantation between bivalve species are considered. Spectroscopic techniques and X-radiography were used on 10 of these experimental cultured pearls of various colours and sizes, and the study allowed links between the host animal and the donor when creating cultured pearls to be further investigated. Interestingly, using spectroscopy the mantle donor species may be identified but not the host. The investigation further confirms previous research regarding whether the donor animal or the host will dictate coloration and nacre thickness of the resulting cultured pearl. L.G.

Cobalt-doped glass-filled sapphires: an update.
T. Leelawatanasuk, W. Atitchat, V. Pisutha-Arnond, P. Wattanakul, P. Ounorn, W. Manorotkul and R.W. Hughes. *Australian Gemmologist,* **25**(1), 2013, 14–20.

Updated information is provided regarding the latest generation of blue glass-filled sapphires. A short history

Abstracts (continued)

of the process is outlined along with properties of both earlier and newer material. It is concluded that standard gemmological equipment may be used to identify either material, with advanced tests able to provide more information. L.G.

Color origin of lavender jadeite: an alternative approach.
R. Lu. *Gems & Gemology,* **48**(4), 2012, 273–83.

The colour origin of lavender jadeite is examined using gemmological observation, UV-Vis spectroscopy and modern trace-element analytical techniques. Analysing high-quality single crystals of closely matched materials with laser ablation–inductively coupled plasma–mass spectrometry (LA-ICP-MS) provided detailed chemical compositions.

Nine natural jadeite slabs, 16 impregnated and/or colour-enhanced jadeites, plus three natural crystals of spodumene were tested. The spodumene was used since the properties of this pyroxene are similar to that of jadeite. Polycrystalline jadeite was found to be difficult to analyse.

Through analysis, confirmation was obtained that manganese and chromium are the causes of lavender and green coloration in jadeite, respectively. C.M.

Korunde mit blauem kobalthaltigem Bleiglas gefüllt. (Corundum with blue cobalt-bearing lead glass filling.)
C.C. Milisenda, K. Schollenbruch and S. Koch. *Gemmologie. Z. Dt. Gemmol. Ges.,* **62**(1/2), 2013, 19–24.

The article describes the gemmological properties of corundum which has been dyed blue and clarity enhanced with cobalt- and lead-bearing glass. There is concentration of blue colour in surface-reaching fissures and cavities, and bubble-like inclusions can also be seen. There is also the flash effect commonly seen in glass-filled rubies. Chemical analysis shows elevated lead and cobalt contents. The spectrum shows cobalt-related absorption lines at 530, 590 and 635 nm. This treatment can easily be identified with a 10× loupe. E.S.

Sammlersteine — Teil II. (Collectors' stones — part II.)
C.C. Milisenda, S. Koch and M. Wild. *Gemmologie. Z. Dt. Gemmol. Ges.,* **62**(1/2), 2013, 31–45.

This article describes gem specimens that were submitted to the German Gemmological Laboratory. Gemmological data is given for each specimen. Included are transparent, faceted brown axinites from Pakistan weighing 4.18 and 4.56 ct; a cut, blue opaque ceruleite from Chile; samples of iron-containing orthorhombic crystals of yellow-brown childrenite-eosphorite from Brazil and Pakistan; opaque, faceted davidite from Norway; a green, faceted, transparent actinolite and a transparent faceted yellow-green tremolite, both from Tanzania; a grey-blue 0.14 ct stone from the U.S.A. identified as lawsonite; a transparent faceted octagonal mellite from Hungary; a pale yellow octagon from Kazakhstan identified as preobrazhenskite; a transparent, yellow sellaite from Brazil; a transparent, orange-pink serandite from Canada; a round grey-blue faceted vesuvianite from Pakistan; an oval greyish white wardite from Austria as well as a pyrargyrite from Peru; an orange-pink bustamite from South Africa; and round faceted sphalerites from the Las Manforas mine in Cantabria, Spain, a well-known source of cuttable sphalerite. E.S.

Lab Notes.
T.M. Moses and S.F. McClure (Eds). *Gems & Gemology,* **48**(4), 2012, 303–4.

Two green stones were submitted for emerald origin reports. Unusually low SG readings of 2.43 and 2.37, a lack of chromium lines in the spectrum and strong fluorescence to long-wave UV radiation raised suspicions. Further tests including microscopic examination and Raman spectroscopy revealed a natural beryl top and core, with a polymer layer on the bottom.

The results are given of UV-Vis spectral readings on both the blue and red areas of a 14.60 ct bicoloured spinel with unusual colour zoning. This was the first bicoloured spinel seen by the Bangkok lab. C.M.

Pennies from heaven: a market for meteorites.
J. Ogden. *Gems&Jewellery,* **22**(6), 2013, 8.

The author discusses Steve Arnold's passion and profession as a meteorite hunter, and his travels worldwide to acquire specimens. A wide range of meteorites and associated minerals are listed from his inventory, and methods of tracking and recent imitations are given. L.G.

Spell bound.
J. Ogden. *Gems&Jewellery,* **22**(7), 2013, 20–1.

Nineteenth-century acrostic jewellery is discussed in which names and sentiments are conveyed through each gemstone's name. Early recorded French examples are examined through well-known pieces such as the 'regards ring' to more unusual political pieces of the 1920s. Complications involving alternative names are considered with the possibility that some secrets will never be revealed. L.G.

Dichromatism, the cause of the usambara and alexandrite colour change effect.
G.M. Pearson and D.B. Hoover. *Australian Gemmologist,* **25**(2), 2013, 62–70.

The authors first discuss and define the term dichromatism within minerals; adding a context of its different meanings within several branches of the sciences and a history documenting its discovery and research. The Beer-Lambert law is described in relation to dichromatism and hypothetical situations presented that would simulate the effect. Finally, a number of gemmological examples and their transmission spectra are examined, including Tanzanian chromium-vanadium dark green tourmaline, Brazilian rhodolite garnet and synthetic chrome spinel. L.G.

Big gem trend.
G. Roskin. *Gems&Jewellery,* **22**(6), 2013, 9–11.

The author considers the current trend for large and wearable gems, and discusses such stones seen at JCK Las Vegas Show in June. These pieces were more affordable and wearable than the described museum pieces, but they were still both rare and spectacular. L.G.

Abstracts (continued)

Natural pearls from Australian *Pinctada maxima.*
K. Scarratt, P. Bracher, M. Bracher, A. Attawi, A. Safar, S. Saesaw, A. Homkrajae and N. Sturman. *Gems & Gemology,* **48**(4), 2012, 236–61.

A history of natural pearling in Australia is given, comparing the properties of natural and cultured pearls from the area.

Early trading and diving methods for *Pinctada maxima,* values and expenditures are detailed, from the early writings of E.W. Streeter, Kornitzer and Gale through to modern-day literature. A table illustrates values of pearl shell recovered in 1889–1898 (from Gale, 1901).

Broome, Western Australia, has always played a large part in the industry and even today it continues as an important part of the cultured pearl market. In early times it was considered a 'wild west' town with high mortality due to sickness, natural disasters and the dangers of diving; attention is drawn to a cemetery with the graves of some 900 Japanese pearl divers.

The article considers the wane in popularity of the *Pinctada maxima* and its re-emergence, with major pearl finds, qualities and quantities from that area noted, including the 'Southern Cross' pearl which is mentioned in detail and was examined by one of the authors (KS).

Other products produced by *Pinctada maxima* are considered, i.e. utensils, inlays and edible meat.

Production regulations and harvesting methods are given briefly. Studies were done of wild unopened *Pinctada maxima* through microscopic observation, X-ray, LA-ICP-MS, UV-Vis-NIR, Raman and photoluminescence (PL) data at GIA's Bangkok laboratory. Results are provided through photos, graphs and tables.

In conclusion, "microradiographic structures previously used to distinguish between natural *Pinctada maxima* pearls and accidently cultured specimens are not conclusive" plus "the products of pearl sacs formed by nature within hatchery-reared shell are virtually indistinguishable from natural pearls and could not be identified as cultured". More samples are to be collected and examined and data provided in a future report. C.M.

Vanadium- and chromium-bearing chrysoberyl from Mogok, Myanmar.
K. Schmetzer, H.J. Bernhardt and C. Cavey. *Australian Gemmologist,* **25**(2), 2013, 41–5.

The two historic samples studied are examples of chrysoberyl of a bright bluish green colour rarely submitted to laboratories today for testing. Morphology, gemmological properties and microscopic features are described along with coloration, trace-element contents and spectroscopic properties. It is investigated why, despite their coloration and chromium content, these samples do not show a distinctive colour change between light sources. It is also speculated whether these may have come from the same Myanmar source as an intensely coloured crystal described by Payne in 1956 said to come from the collection of A.C.D. Pain. L.G.

Unusual organic gem materials — chitons.
S. Stocklmayer. *Australian Gemmologist,* **25**(2), 2013, 58–9.

The author discusses the use of an unusual type of decorative material. Chitons are marine creatures found worldwide in cold and tropical seas with an aragonite shell of eight articulated plates. Pendants containing these creatures' shells up to 50 mm in length were observed in Ushuaia, on the extreme south coast of Argentina. L.G.

Non-decorative jewels – with particular reference to watch jewel bearings and components.
J. Warner. *Australian Gemmologist,* **24**(12), 2012, 294–301.

Due to their hardness and inert properties, many gem materials have long been used in industrial applications as well as for decorative use. The author lists applications of these from the Stone Age to the present with emphasis upon development of their use within watches. L.G.

Hibonit aus Myanmar (Burma). (Hibonite from Myanmar [Burma].)
M. Wild and C.C. Milisenda. *Gemmologie. Z. Dt. Gemmol. Ges.,* **62**(1/2), 2013, 25–30.

The authors studied gem-quality hibonite from Myanmar consisting of a crystal weighing 0.10 g and two faceted yellowish brown and orangey brown specimens weighing 0.50 and 0.45 ct, respectively. Hibonite is a calcium-aluminium oxide, Mohs hardness = 7½–8, RI = 1.788–1.792, dichroic yellow-brown to orange-brown. Hibonite is fairly rare and seldom faceted above half a carat. It might be taken for phlogopite as the rough material looks very similar and is found in the same mine. E.S.

A comparison of modern and fossil ivories using multiple techniques.
Zuowei Yin, Pengfei Zhang, Quanli Chen, Chen Zheng and Yuling Li. *Gems & Gemology,* **49**(1), 2013, 16–27.

Samples of both fossil and modern ivory (mammoth and elephant) were examined using standard gemmological equipment, followed by laboratory equipment. These materials may look very similar, especially if the fossil ivory is only weakly weathered. Samples and their sources are described, with many being sliced for analysis and some ground to powder. Observation of 'Schreger lines' to distinguish them requires much caution as the angles can vary between layers as well as cutting direction and consequently overlap. High magnification proved useful, showing a differing structure between each material, and spectroscopy revealed distinct water and collagen contents. Trace elements may also indicate their differences. L.G.

Instruments and Techniques

Update on the identification of dye treatment in yellow or 'golden' cultured pearls.
Chunhui Zhou, Artitya Homkrajae, Joyce Wing Yan Ho, A. Hyatt and N. Sturman. *Gems & Gemology,* 48(4), 2012, 284–91.

Dye treatments in yellow or 'golden' cultured pearls have dramatically improved, leaving little surface evidence. The authors used routine observations, UV-Vis reflectance and Raman PL spectroscopy to analyse eight sample groups of the cultured pearls. The groups consisted of natural-coloured South Seas cultured pearls from the Philippines and

Abstracts (continued)

Myanmar, dyed South Sea and Akoya cultured pearls, dyed freshwater non-beaded cultured pearls and heat-treated yellow cultured pearls. Observational results are provided in a table and graphs illustrate the results of advanced testing.

Conclusions were drawn that many dyed yellow or 'golden' cultured pearls can still be easily detected using observational techniques. Those lacking any visible evidence of dye can be identified by nondestructive testing techniques. C.M.

Detecting HPHT synthetic diamond using a handheld magnet.
K. Feral. *Gems & Gemology,* **48**(4), 2012, 262–72.

The use of magnets is investigated for testing individual HPHT-grown synthetic diamonds, either loose or mounted in jewellery, down to melee-sized goods. The author tested five types of magnets, and a total of 85 HPHT synthetic diamonds of varying size and colour were studied. The direct method (dragged along a smooth dry surface), and flotation method (reducing friction therefore enhancing sensitivity) and pinpoint testing methods were applied. Results were classified according to weak, drag, pickup and strong diamagnetism (repelled). Magnet size and strength was considered and terminology of magnetism is provided for the reader.

As a control, 168 natural diamonds were also tested — with one containing inclusions large enough (over 0.5 mm and close to the surface) to be attracted to the magnet (using the flotation method). This is the first reported case of a facetable natural diamond attracted to a magnet due to minute inclusions. Also tested were 58 HPHT-treated natural diamonds, 48 natural diamonds in gold jewellery and 19 CVD-grown synthetic diamonds.

Although a significant percentage of HPHT-grown synthetic diamonds could be detected, CVD synthetics could not be separated using this method. Natural diamonds may contain ferromagnetic or paramagnetic inclusions either as inclusions or as contaminants from polishing and handling, but they are rarely detectable with a magnet.

The article concluded that N52-grade neodymium magnets achieved the highest rate of detection. C.M.

Miscellaneous

Auction houses, a powerful market influence on major diamonds and coloured gemstones.
R. Shor. *Gems & Gemology,* **49**(1), 2013, 2–15.

The article highlights the fact that today the highest-profile sellers of major diamonds are the world's two largest auction houses, Sotheby's and Christie's, being major competitors with traditional jewellery houses, influencing and increasing the prices and awareness of coloured diamonds. This trend commenced with the sale of the Wittelsbach Graff diamond in December 2008, with subsequent records being reached.

The histories of both auction houses are given, including observations of the market influence of 'celebrity' gem auctions commencing with what was to be the Taylor Burton. As a consequence, a new market channel known as the 'auction effect' on trade and retail markets stabilized in the early 1980s. The emergence of a strong relationship between luxury jewel houses, dealers and auction houses developed.

High-profile sales such as those of the Duchess of Windsor's jewels are considered as a 'watershed event', establishing auction houses as major players and strongly influencing prices and creating more consumers through media awareness. Cataloguing has become more detailed, including origin reports and treatment information.

Controversy over pricing and selling directly to clients and the legal consequences of such are reviewed.

In the early part of the 21st century, new ultra-wealthy markets were emerging in places such as Asia, creating a renewed demand. Important auctions are now being offered there and becoming market leaders, with fancy-colour diamonds playing an important role in the market over the past 15 years; price increases during this time are given and their reasons are discussed. C.M.

Synthetics and Simulants

Gemmologische Kurzinformationen. Synthetischer zweifarbiger Quarz. (Synthetic two-coloured quartz.)
U. Henn. *Gemmologie. Z. Dt. Gemmol. Ges.,* **62**(1/2), 2013, 49–51.

Bicoloured synthetic quartz is described that shows a blue and a green colour zone. The green is coloured by Fe with two absorption bands at 743 and 923 nm, while the blue is due to Co^{2+} with absorption bands at 547, 591 and 646 nm. E.S.

A mystery jewel.
J.G. Henry and T. Coldham. *Australian Gemmologist,* **25**(1), 2013, 21–5.

An unusual inclusion within a ring-mounted purple gem is examined. Under 40× magnification the inclusion transpires to be a microphotograph family portrait embedded in the 6.5×4.5 mm faceted sample. Methods of production and makers are speculated with a description of the inclusion and observations under magnification. L.G.

Follow up on the 'mystery jewel'.
J.G. Henry. *Australian Gemmologist,* **25**(2), 2013, 60–1.
This is a continuation from the article 'Mystery Jewel' that was published in the *Australian Gemmologist,* 25(1). Having received more information about the photograph, further thoughts are added regarding the caption upon the image and possible manufacturers. Upon a second viewing, the stone is identified as glass and, thanks to other specialists, the location, construction and date of the ring with its contents are revealed. L.G.

Gemmologische Kurzinformationen. Künstliches Glas als Diasporimitation. (Synthetic glass as diaspore imitation.)
C.C. Milisenda and S. Koch. *Gemmologie. Z. Dt. Gemmol. Ges.,* **62**(1/2), 2013, 52.

The authors studied loose and mounted stones that were sold in Turkey

Abstracts (continued)

as 'Zultanite', which is a trade name for the mineral diaspore. They were identified as light-rare-earth–doped artificial glass. E.S.

Lab Notes.
T.M. Moses and S.F. McClure (Eds). *Gems & Gemology,* **48**(4), 2012, 304–5.

Two HPHT-grown synthetic diamonds were tested, a 0.51 ct round brilliant Fancy Light blue and a 0.79 ct round brilliant Fancy Deep blue. DiamondView fluorescence images showed octahedral and cubic growth patterns typical for HPHT synthetics. PL emissions at 736.6 and 736.9 nm were recorded and attributed to the $[Si\text{-}V]^-$ centre common in CVD synthetic diamonds but believed to be rare in HPHT-grown synthetics. C.M.

Lab Notes.
T.M. Moses and S.F. McClure (Eds). *Gems & Gemology,* **49**(1), 2013, 47–50.

A 0.94 ct Fancy yellow-brown emerald-cut CVD synthetic diamond was examined. This was the first to be observed at GIA with aggregated nitrogen impurities that had not undergone additional HPHT treatment.

Three CVD synthetic diamonds were tested, a rectangular step cut of 0.93 ct, and two round brilliants of 0.52 and 0.57 ct. Different growth and/or treatment histories were detected by a combination of laboratory techniques. With the DiamondView, the 0.57 ct sample displayed a fluorescent colour combination not seen before in a GIA lab.

A CVD synthetic diamond of 2.16 ct was the largest seen by GIA so far. The stone indicates the rapid improvement of CVD growth technology.

A 2.58 ct yellow synthetic sapphire was reported, coloured by a trapped–hole mechanism. C.M.

Abstractors

C. Mitchell — C.M. E. Stern — E.S. L. Gleave — L.G.

Book reviews

HPHT-Treated Diamonds
Inga A. Dobrinets, Victor G. Vins and Alexander M. Zaitsev, 2013. *Springer Series in Materials Science,* Volume 181. Springer-Verlag, Berlin and Heidelberg, Germany, 257 pages, http://link.springer.com/book/10.1007/978-3-642-37490-6. ISBN 978-3-642-37489-0 (print, US$139.00) and 978-3-642-37490-6 (online, US$179.00).

This is the first book that attempts to describe the process of high-pressure, high-temperature (HPHT) treatment of diamonds and the characteristics of diamonds so treated. The objective of HPHT treatment is the reduction or removal of the undesirable brown colour, frequently found in natural diamonds, to produce more valuable colourless, near-colourless or fancy-colour diamonds. Following the first announcement of this treatment, the then-president of GIA, Bill Boyajian, wrote in 2000 that HPHT treatment was "arguably one of the most serious challenges the diamond industry has ever faced". Even today, the identification of HPHT-treated diamonds remains a major and complex task for gemmological laboratories, and the authors make clear in the preface that the main aim of this book is to aid those dealing with potentially HPHT-treated diamonds in their identification.

All three authors began their scientific careers in Russia, and each has been engaged in diamond research for many years. Dr Inga Dobrinets is now at RUBION, an ion beam and radionuclide research facility at Ruhr-Universität Bochum, Germany, having previously been employed as a gemmologist at EGL New York. Prof. Alexander Zaitsev is now in the Engineering Science and Physics Department of the College of Staten Island, New York. Prof. Zaitsev is best known for his data handbook, *Optical Properties of Diamond* (2001), which attempts to provide a comprehensive list of all optical spectroscopic features found in diamond. Dr Victor Vins is the only one of the three still in Russia where, in Novosibirsk, he runs his own business, VinsDiam Ltd, a company that carries out irradiation and HPHT treatment of both natural and synthetic diamonds. He is therefore able to provide interesting insight into both the technological and commercial aspects of the HPHT treatment of diamonds.

Brown colour in natural diamonds is believed to be due to clusters of vacancies that form following the interaction of dislocations that were introduced by plastic deformation during their geological history. The very high temperatures used in HPHT treatment, typically 1900–2300°C, with the application of high pressure to avoid graphitization, lead to the breakup of the vacancy clusters with a loss of

Book reviews (continued)

brown colour, and the formation of various defects such as isolated nitrogen and nitrogen-vacancy defects if nitrogen is present in sufficient concentrations. As the authors point out, the precise details of the changes induced by HPHT treatment depend upon the defects that are present in the starting material and the temperature, pressure and duration of the treatment. Treatments are often carried out for only a few minutes and this can result in highly non-equilibrium concentrations of defects, which complicates understanding of what is going on during treatment. In some cases, HPHT-treated diamonds are subsequently irradiated and heated to somewhat lower temperatures than used in HPHT treatment to produce, for instance, high concentrations of nitrogen-vacancy defects that give rise to the so-called 'Imperial Red' colour. The nature of the features present or absent in HPHT-treated diamonds is extremely complex so identification can be challenging in some cases. This is especially the case when treaters deliberately reintroduce features destroyed during treatment with the sole intention of concealing the treatment.

The book describes the characteristics of the various kinds of diamonds that may be subjected to HPHT treatment and how these may change upon treatment. The main body of the book, some 100 pages, follows the format of Zaitsev's earlier handbook in listing the optical absorption and photoluminescence spectroscopic features that may be relevant to identification of HPHT-treated diamonds. Some of this data comes from the authors' own research but most has been carefully gleaned from the published literature. Some of the references that they have found are extremely obscure and it is very valuable that they have brought them to light. Several of the optical features listed are thought to be due to nickel-related defects found in HPHT synthetics and, occasionally, in some natural diamonds. Whilst it is okay that these defects are included for completeness, it is unlikely that many will be encountered in a gemmological laboratory in the context of HPHT treatment identification. The authors clearly expect the book to be used as a reference handbook rather than as a textbook, and have attempted to make each section stand on its own. The result is a great deal of repetition. It might have been better if specific points had been explained clearly and completely once rather than explained briefly several times. A reader who is unfamiliar with concepts such as radiation damage or nitrogen aggregation in diamond may find the explanations given in this book rather confusing.

The book, unfortunately, has not been well edited. Some references are missing or incomplete, and one or two figures are missing or referred by the wrong number in the text. Whilst one accepts that none of the authors is a native English speaker, it is a pity that several grammatical and spelling mistakes have not been corrected (e.g., the frequent absence of the definite article can be irritating, and the word 'peak' is written as 'pick' in several instances). However, this does not really detract from the comprehensibility of the text.

The list of optical features is very comprehensive but there are a few instances where the information given is not altogether accurate. One example is the discussion of the line-width of the zero-phonon line of the GR1 centre, where the authors say that this "cannot be practically used for recognition of HPHT treatment (Fisher et al 2006)." In fact, this reference does indicate how the line-width might be used for this purpose. In another case, the authors do not distinguish between a line seen in photoluminescence at 648 nm, found in untreated type IIb diamonds, and a line at 649 nm, which is found in some HPHT-treated diamonds as well as some untreated diamonds.

Those engaged in identifying HPHT-treated diamonds will find this book a useful reference but it will need to be used with caution. Leading gem testing laboratories have developed their identification criteria over many years by careful research and observation of many thousands of stones. Much of this data remains unpublished for the simple reason that gem laboratories want to avoid assisting those who might seek to undermine their identification criteria. Consequently, this kind of material has not been available to the authors for inclusion in their book.

Dr C.M. Welbourn

The Handbook of Gemmology
Geoffrey Dominy, 2013. Amazonas Gem Publications, Vancouver, British Columbia, Canada, 652 pp, http://handbookofgemmology.com, ISBN 978-0-9918882-0-7. US$39.95 per digital download or US$49.95 for a DVD containing all formats.

This book is the latest addition to the electronic arsenal of the gemmologist, picking up and covering areas previously neglected by other commercially available software. *The Handbook* offers all the information found in traditional reference books, but in a new and more versatile format. The 'deluxe' edition comes packaged in several formats, covering a wide range of devices and platforms (iPad, iPhone, Android, e-reader, Mac and Windows). For this review, *The Handbook* was tested using Windows 8, iPad, iPhone and Android devices.

The program itself is relatively intuitive and runs well, without problems or hitches, even while other programs are running in Windows 8. On iPad and iPhone, *The Handbook* runs equally well, with the functionality being maintained. Despite the smaller screen it works well on a smartphone, although only sections of each page can be viewed at a readable size at any time. The search function works effectively, displaying a list of results for the location of any word within the entire *Handbook*, and each links back to the relevant section, enabling cross reference of data. There is also a bookmark facility, enabling key sections to be marked for quick access, which can be combined with a note function, enabling the user to record their own findings or thoughts wherever desired. Highlighter and zoom functions complete the set of available tools, and these should keep even the most gadget-minded gemmologist happy. The zoom functionality is especially helpful for smartphone users, as it allows sections of a page to be enlarged whilst maintaining

Book reviews (continued)

the quality of the original. Once enlarged, the viewing area can be moved around the page fluidly.

Thumbing through *The Handbook* in any of its non-PDF formats is reminiscent of a true paper book, with a page turn setup that works responsively and provides a good user interface.

Split into the 30 sections listed below, covering 652 pages, *The Handbook* sets out to systematically cover the key areas that any gemmologist or student would need to know:

1. What is a gemstone?
2. The chemical nature of gemstones
3. Physical, chemical and optical properties
4. Basic crystallography
5. The absorption of light and the spectroscope
6. The 3 Rs — reflection, refraction and the refractometer
7. Polarized light and the polariscope
8. Pleochroism, the dichroscope and colour filters
9. Specific gravity
10. Luminescence
11. Magnification and thermal conductivity
12. Imitation and assembled stones
13. Synthetic gemstones
14. Gemstone enhancements
15. Gem mining
16. Gem cutting and grading
17. Gem identification

18–27. Identifying gems, based on their colour

28. Identifying phenomenal and unusual gemstones
29. Natural, cultured and imitation pearls
30. Advanced gem testing techniques

Appendices

Each of these sections outlines the necessary and relevant information in an easy-to-read and visual style, accompanied by numerous colour photographs and diagrams throughout. Students would find the section on the refractometer of particular use, as it sets out in simple terms how to use and interpret the results (which many find difficult when first studying gemmology).

The sections on enhancements, imitations and synthetics are extensive, and cover the vast range of these materials available. Synthesis covers all the current commercial and historic techniques, as well as lesser known methods (e.g., ultrasound cavitation), giving an overview of what is potentially in the market. The same applies to treatments, giving a good grounding for any gemmologist, and making the reader aware of the potential pitfalls that can arise from the misidentification of features.

Sections 18 to 27, which cover the identification of gem materials based on their colour, is probably of greatest benefit to students (as it offers a useful reference basis), but for the more advanced gemmologist, or those who realize that colour isn't always the key, a full listing of gem materials ordered by descending RI is included in the Appendices, as well as a full alphabetical listing, with all the usual values and constants at your fingertips.

Sections 11 and 30 give a basic overview of the more equipment-driven aspects of gemmology, covering thermal conductivity and advanced testing. For diamonds, only individual testers (thermal or electrical) are covered, although the majority of people nowadays use combination testers. Minor omissions such as this do not, however, detract from the overall appeal of the book. The description of such advanced techniques as Raman, LIPS (LIBS), EDXRF and LA-ICP-MS (although only briefly), makes this an all-round useful reference.

Overall, *The Handbook* is very well presented and thought-out, covering all necessary and relevant aspects of gemmology, and providing a reference work at your fingertips, no matter where you are. This is truly a gemmology text for the 21st century, and although the digital format is probably not to everyone's liking, it does fit in with the modern lifestyle of today's gemmologist and student, whether used on desktop computer, tablet or smartphone.

A.S. Fellows

Conference reports

Hong Kong Jewellery & Gem Fair

Held 11-17 September, this enormous show organized by UBM Asia featured more than 3,600 exhibitors from 48 countries and regions. There were numerous educational opportunities, and those attended by this author are reported here.

The Gemstone Industry and Laboratory Conference (GILC), organized by the International Colored Gemstone Association, took place on 12 September and featured four speakers. **Chris Smith** (American Gemological Laboratories Inc., New York) described the history, properties and nomenclature of cobalt-coloured lead-glass-filled blue sapphires. The treatment debuted in 2007, and in 2012 Mr Smith noted significant improvements in the appearance of this material due to more careful selection of rough by the treaters and refinements in the process. The main identification features are wispy colour concentrations following fractures, gas bubbles within larger volumes of glass, and surface inhomogeneities seen in reflected light; flash-effect colours are subtle, unlike those seen in lead-glass-filled rubies. The treatment can also be revealed by UV-Vis, IR or EDXRF spectroscopy. **Prof. Dr Henry Hänni** (GemExpert, Basel, Switzerland) reviewed potential methods for tracing cultured pearls from the farm to the consumer (see article on pp 239–45 of this issue). **Prof. Mimi C. M. Ou Yang** (Hong Kong Institute of Gemmology) surveyed the value factors, mineralogical composition and nomenclature of Burmese jade. She recommended calling such material by the trade name *Fei Cui* together with mineral modifiers (jadeite, omphacite or kosmochlor) to designate specific varieties according to the most abundant constituent. **Dr John Ho Chun-Wah** (Hong Kong Accreditation Service [HKAS]) explained the process and benefits of accreditation in support of the gem and jewellery industry. HKAS follows a three-part process for evaluating gem laboratories in Hong Kong: testing, inspection and certification. Accredited laboratories enjoy improved acceptance and consumer confidence. At the conclusion of the programme, **Richard Hughes** (Sino Resources Mining Corp. Ltd., Hong Kong) was invited to give an update on his recent visit to Mogok, Myanmar. He described efforts by local diggers to prevent large mechanized mining projects from rapidly exploiting the area's gem deposits and depriving them of their way of life.

On 14 September, **Robert Weldon** (Gemological Institute of America [GIA], Carlsbad, California) gave a GIA GemFest presentation on gem and jewellery photography. He suggested photographing light-coloured gems on a dark background and vice versa. In addition, he recommended using a light-coloured neutral background to best show a transparent gem's coloration. Lighting is of paramount importance, and techniques should be adjusted according to the requirements of the stones/metals being photographed (e.g., *Figure 1*).

Also taking place on 14 September, the International Gemological Conference organized by the Asian Gemmological Institute and Laboratory Ltd. (AGIL), Hong Kong, featured 11 speakers. **Prof. Dr Henry Hänni** discussed value factors, treatments and sources of ruby. He pointed out that 'silk' inclusions in ruby can remain unaffected by treatment involving glass filling since the process is done using glass that has a relatively low melting temperature. **Manfred Eickhorst** (Eickhorst & Co., Hamburg, Germany) explained the benefits of using LED lighting in gemmological instruments, including monochromatic illumination for refractometers and high-intensity darkfield lighting in microscopes. **Prof. Lijian Qi** (China University of Geosciences, Wuhan) described the detection of irradiated HPHT-treated diamonds, in colours ranging from yellow-to-green, blue and pink. **Dr Hyun-Min Choi** (Hanmi Gemological Institute, Seoul, Korea) reported using ESR spectroscopy to detect gamma irradiation of South Sea cultured pearls, by looking for enriched amounts of CO_2^- radicals in their nacre. In his experience, the dark colour of such cultured pearls faded after five months' exposure to light. **Alan Hodgkinson** (Ayrshire, Scotland) described the use of top-lighting with the refractometer to observe RI values slightly greater than 1.81 and for obtaining more accurate RI measurements of small gems. **Prof. Dr Zhili Qiu** (Sun Yat-Sen University, Guangzhou, China) explained how to differentiate jadeite from Myanmar, Guatemala, Russia and Kazakhstan. Compared to jadeite from the other localities, the material from Myanmar shows the largest colour variety, is available in the finest quality, and has the lowest rare-earth element content and highest amount of the jadeite molecule in its composition. **Lin Sung Shan** (World Gem Identification and Study Center, Taoyuan City, Taiwan) surveyed jewellery markets in Taiwan and mainland China. He said that compared to the 'mature' market in Taiwan, the emerging market in China

Figure 1: The challenge in photographing this tourmaline pendant from Frank Heiser was to illuminate the tourmaline crystals (55 and 71 mm long) while also inducing the cat's-eye effect in the cabochons. This required two types of lighting: fibre-optic for the cabochons and diffused illumination for the crystals; these lighting techniques also worked well for the melee diamonds in the piece. Photo © Robert Weldon.

holds unlimited opportunities for the jewellery industry. Diamond is the most popular gemstone in China, and although smaller sizes make up the majority of the market, in recent years he noted a 15% annual increase in the demand for stones weighing 1–3 ct. **Dominic Mok** (AGIL, Hong Kong) described the use of advanced gem testing equipment to tackle gemmological challenges in his laboratory. In one instance, he used portable Raman spectroscopy to identify a large (80 kg) black carving as jadeite. **Ted Themelis** (Gemlab Inc., Bangkok, Thailand) illustrated his experiments with the treatment of white opaque corundum from Madagascar using blue cobalt-coloured lead glass. The procedure involves opening voids and channelways in the material with hydrofluoric acid pre-treatment, and then glass filling at 1,200–1,300°C in oxidizing conditions (i.e., in air) for several hours. Approximately 25% of the material showed satisfactory results and the remainder was re-treated under different conditions. **Dr Taijin Lu** (National Gems & Jewelry Technology Administrative Center, Beijing, China) described Hetian jade (nephrite) pebbles from Xinjiang Province in China. He determined that microscopic pits on the surface of the pebbles are caused by the dissolution of carbonate by chemical etching during alluvial transport. The microscopic characteristics of these pits are helpful in separating natural nephrite pebbles from various imitations in the Chinese marketplace. **Branko Deljanin** (Canadian Gemological Laboratory, Vancouver) summarized the properties of natural and synthetic diamonds. He noted that most natural diamonds show stronger fluorescence to long-wave UV radiation than to short-wave UV, while the opposite is the case for synthetics (both HPHT- and CVD-grown). Also, natural diamonds are most commonly type Ia (with rare type Ib, IIa and IIb stones), whereas HPHT-grown synthetics are mostly type Ib (less commonly type IIb and rarely type IIa) and CVD synthetic diamonds are mostly type IIa or possibly type IIb.

A launch seminar for the Gübelin Academy took place on 16 September and featured two presentations. **Dr Lore Kiefert** (Gübelin Gem Lab, Lucerne, Switzerland) showed video footage from visits by Dr Edward Gübelin to the famous Mogok Valley in Myanmar. Simple mining methods depicted in a 1962 video were similar to those seen during a recent (July 2013) visit to Mogok by Dr Kiefert and colleagues. She also reported that ruby mining is currently taking place at several primary deposits, including Dattaw (reopened recently after being closed for eight years), Yadanar Shin and Baw Lone Gyi. Sapphires are being mined from both primary (e.g., Baw Mar) and secondary deposits (e.g., in the Pyaunggaung area). Then **Dr Daniel Nyfeler** (Gübelin Gem Lab, Lucerne, Switzerland) explained the importance of undertaking field research in support of geographic origin determinations by his laboratory. Currently his lab does origin reports for ruby, sapphire (blue and fancy coloured), emerald, spinel (red and pink), alexandrite and Cu-bearing tourmaline. As more deposits have been discovered, some yielding gems with overlapping properties, origin determination has become more challenging—particularly for blue sapphires, for which Dr Nyfeler estimated 20–30% of his lab's reports in the last two years have indicated unknown origin.

Brendan M. Laurs

33rd International Gemmological Conference (IGC)

This biennial conference was held 12–16 October 2013 in Hanoi, Vietnam, and was attended by invited delegates, observers and Vietnamese honorary attendees. It was organized by Vietnam National University and DOJI Gold & Gems Group (both located in Hanoi). There were 41 talks and 16 posters presented. The conference abstracts are published in a 182 pp proceedings volume that can be downloaded at www.igc-gemmology.org.

A pre-conference excursion took place on 10–12 October to Halong Bay. The group first visited the retail showroom of VietPearl, where they were given a brief presentation on pearl culturing in Halong Bay and then saw cultured pearls and jewellery from both saltwater *(Figure 2)* and freshwater farms in Vietnam. The following morning they boarded a ship for an overnight tour of the bay including visits to a pearl farm *(Figure 3)* and a large limestone cave. The farm reportedly produces 10 kg annually of akoya-type cultured pearls from *Pinctada martensii* molluscs (or a related hybrid). The shell bead nuclei *(Figure 4)* are typically 5–6 mm in diameter, and they are left in the molluscs for 18 months before harvesting the cultured pearls.

Conference reports

Figure 2: The akoya-type cultured pearls from Halong Bay in this necklace are 13 mm in diameter. Photo by B.M. Laurs, © Gem-A.

Figure 3: This pearl farm in Halong Bay was visited as part of the IGC pre-conference excursion. It is a popular stop for tourists, and houses an active pearl culturing area and a showroom. Photo by B.M. Laurs, © Gem-A.

The opening programme of the conference included an informative overview of Vietnam's gemstone industry by **Dr Do Minh Phu** (DOJI Gold & Gems Group). He indicated that although gems were only discovered two decades ago in Vietnam, the revenue from the jewellery industry totals more than US$3.5 billion/year. The most important gem material produced in Vietnam is heat-treated pink sapphire in 1–3 mm calibrated sizes.

In diamond presentations, **Dr Emmanuel Fritsch** (University of Nantes and Institut des Matériaux Jean Rouxel, France) reviewed the morphology of natural and synthetic diamonds. He noted some particular aspects of natural diamonds that he has yet to properly document: hopper growth, true cube faces and signs of dissolution that occurred during growth. **Thomas Hainschwang** (GGTL Gemlab–Gemtechlab Laboratory, Balzers, Liechtenstein) discussed the origin of colour and properties of natural type Ib diamonds (i.e., those containing isolated nitrogen, or C centres, detectable with infrared spectroscopy). Although the C centre is known to be a strong producer of yellow colour, the vast majority of natural type Ib diamonds show combinations of yellow, orange, brown, grey and 'olive' green that are caused by variable C centre contents together with related defects. **Dr Hiroshi Kitawaki** (Central Gem Laboratory, Tokyo, Japan) examined numerous natural and synthetic diamonds with the DiamondView and noted the following general trends: colourless natural type Ia diamonds have blue-white luminescence, commonly with octahedral growth sectors; yellow natural type Ib diamonds display greenish yellow luminescence and mosaic patterns; HPHT synthetics show yellow or blue luminescence with cross-shaped intersections of {111} and {100} growth sectors; and CVD synthetics display layered growth striations. **Dr James E. Shigley** (GIA, Carlsbad, California) summarized observations of CVD-grown synthetic diamonds seen in GIA's laboratory. Most of the colourless CVD synthetics were G–J colour, VVS clarity, and inert to long- and short-wave UV radiation. Of the fancy-coloured CVD synthetics, pink was the most common hue, with the majority having Fancy Vivid,

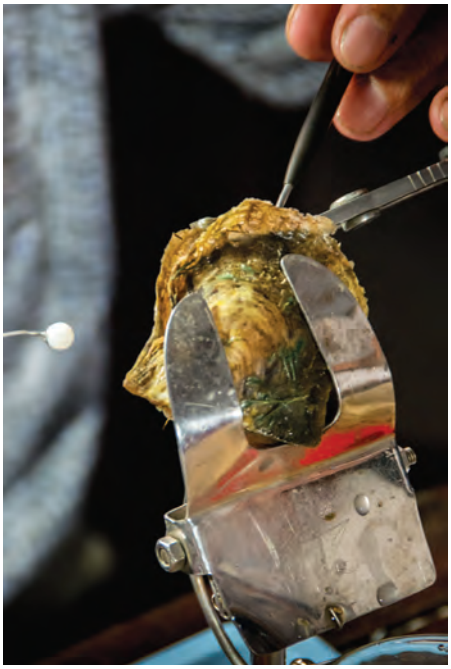

Figure 4: A shell bead (~6 mm in diameter) is inserted into a mollusc at the pearl farm in Halong Bay. Photo by B.M. Laurs, © Gem-A.

Conference reports

Fancy Intense and Fancy Deep colour grades, VS clarity, and orange fluorescence to long- and short-wave UV radiation.

There were several presentations on gem corundum. **Dr Dietmar Schwarz** (AIGS Lab, Bangkok, Thailand) reviewed the geology and gemmology of ruby and sapphire from Kenya and Tanzania. The main deposit areas are Lake Baringo (basalt-related) and Mangari (micaceous lenses and veins cutting serpentinite) in Kenya, and Longido (metamorphic 'anyolite'), Umba (desilicated pegmatitic veins in serpentinite), Winza (amphibolite dikes) and Tunduru-Songea (alluvial deposits) in Tanzania. **Hpone-Phyo Kan-Nyunt** (Gübelin Gem Lab, Hong Kong; delivered by co-author Dr Stefanos Karampelas) provided an update on the mining and characteristics of sapphires from the Baw Mar deposit near Mogok, Myanmar. The sapphires formed at the contact between syenite and gneiss, and the mine workings reach a depth of 40 m. About 300 people are mining and processing the material, which is faceted on site (typically in 0.5–4 ct sizes). They are relatively free of inclusions and have high iron contents, making them distinct from 'classic' Burmese sapphires. **Hai An Nguyen Bui** (University of Nantes, France) discussed the challenges and limitations of determining the geographic origin of Kashmir sapphires. Stones from Kashmir, Sri Lanka, Madagascar and Myanmar may show similar or overlapping characteristics, and in her opinion a Kashmir origin can be determined with satisfactory confidence in only 20% of cases. **Gamini Zoysa** (Mincraft Co., Mount Lavinia, Sri Lanka) reviewed some sapphire deposits of Sri Lanka. He focused on alluvial deposits in the Hasalaka area near the town of Mahiyangana in central Sri Lanka, as well as eluvial-primary deposits discovered in 2012 near Tammanawa village (Kataragama, southern Sri Lanka). **Dr Jayshree Panjikar** (Panjikar Gem Research & Tech Institute, Pune, India) characterized bicoloured yellow-blue sapphires from Chinnadharapuram, southern India. Their most common inclusions are apatite, mica, zircon, feldspar, ilmenite, 'silk', negative crystals and corundum crystals. These sapphires show similarities to those from Garba Tula, Kenya. **Dr Pornsawat Wathanakul** (Gem and Jewelry Institute of Thailand, and Kasetsart University, Bangkok) reported that sapphires associated with the Denchai basalt in Phrae Province, northern Thailand, are concentrated in both placer and residual deposits derived from at least two basaltic episodes. The alluvial deposits consist of both recent and older gravel beds related to point-bar and terrace deposits. **Dr Nguyen Ngoc Khoi** (DOJI Gold & Gems Group; delivered by co-author Dr Nguyen Thi Minh Thuyet) explained the geology of gneiss-hosted corundum deposits from the Tan Huong–Truc Lau area in northern Vietnam. Exploration guides include corundum and associated minerals (spinel, sillimanite, ± garnet) in heavy mineral concentrates in streams, lakes and soils; aluminous rocks within high-grade metasedimentary sequences; and the contacts of migmatized pegmatoid bodies with surrounding mafic and ultramafic rocks or marbles. **Maxim Viktorov** (Gemological Center, Lomonosov Moscow State University [MSU], Russia) described sapphires from the Koltashi deposit in the Ural Mountains, Russia. Discovered in deeply weathered soil in 1999, the sapphires are mostly colourless with blue zones and rarely pink. Although none are gem quality as found, they do respond to heat treatment (1600°C for two hours in a reducing atmosphere). **Dr Hanco Zwaan** (National Museum of Natural History [Naturalis], Leiden, The Netherlands) studied alluvial sapphires from Montana (mostly Rock Creek) and found a mineral inclusion assemblage indicative of a complex geological history involving incompatible elements (e.g., alkali magmas or carbonatites). **Kentaro Emori** (Central Gem Laboratory, Tokyo, Japan) used LA-ICP-MS to measure the concentration of beryllium in more than 1,000 samples of untreated and treated corundum. He found the highest amounts in Be-diffused yellow sapphires (9.2–11.4 ppmw). Traces of Be were also detected in untreated sapphires from Cambodia, Laos and Nigeria, together with various combinations of Nb, Ta, Zr, Hf, Th and other elements. **Shane McClure** (GIA, Carlsbad) documented Ti-diffused synthetic sapphires submitted for lab reports that were free of inclusions and therefore presented difficulties in determining natural or synthetic origin. Initial LA-ICP-MS analyses gave unexpected results, and further studies of a sliced sample showed that Ga and Mg (and, in places, Be) were associated with Fe, Ti and V in a diffused layer that was thicker than typically seen. This raises the question of whether treaters are using additional elements to help facilitate the diffusion into corundum of relatively immobile elements such as Ti.

There were three talks covering beryl. **Dr Jürgen Schnellrath** (Centro de Tecnologia Mineral, Rio de Janeiro, Brazil; delivered by co-author Stefanos Karampelas) described a new emerald occurrence from the Itatiaia mine near Conselheiro Pena, Minas Gerais, Brazil. The emeralds were discovered in 2010 in biotite-phlogopite schist near a gem-bearing pegmatite, and initial mining in 2012 produced a limited amount of gem-quality material that was cut into stones weighing up to ~2 ct. These emeralds typically show light green to slightly bluish green colour, and are notable for their enriched Cs content. **Prof. Dr Jean-Marie Dereppe** (University of Louvain, Belgium) used EPR spectroscopy to separate untreated Maxixe beryls from irradiated Maxixe-type beryl which has a more unstable colour. EPR was useful for differentiating the colour centres in each type of beryl (NO_3 groups in Maxixe and CO_3 groups in Maxixe-type beryl). **Dr Le Thi-Thu Huong** (Vietnam National University, Hanoi) presented preliminary data on previously unrecognized features recorded using Raman and infrared spectroscopy that may prove useful for separating natural from synthetic emerald. Specifically, natural emeralds have a Raman band at 1072–1068 cm^{-1}, while in synthetics this band is shifted slightly to 1068–1067 cm^{-1}. Infrared spectra recorded on K-Br pellets show a shoulder adjacent to a band at ~1200 cm^{-1} in natural emeralds, while no such shoulder is present for synthetic emeralds.

Conference reports

In presentations on other coloured stones, **Edward Boehm** (RareSource, Chattanooga, Tennessee, U.S.A.) reviewed the inclusions in spinel from various localities. He indicated that inclusions are of more use for simply identifying a stone as spinel, rather than indicating a spinel's geographic origin. **Dr Tobias Häger** (Johannes Gutenberg–Universität Mainz, Germany) examined the causes of colour in natural untreated spinels from Vietnam, and compared them to flame fusion– and flux-grown synthetics. Various combinations of the chromophores Fe^{2+}, Co^{2+}, Cr^{3+} and V^{3+} are responsible for the different colours. **Dr Karl Schmetzer** (Petershausen, Germany) studied the effect of vanadium and titanium on the coloration of natural and synthetic chrysoberyl and alexandrite. (For details of this research, see pp 223–8 of this issue, and pp 137–48 of *Journal of Gemmology,* **33**(5–6), 2013). **Prof. Dr Henry Hänni** (GemExpert, Basel, Switzerland) documented traces of rare-earth elements (REE) in 'mint' green grossular from Merelani, Tanzania. The element with the greatest abundance was dysprosium (up to ~20 ppm by LA-ICP-MS). Although not enough REE were present to produce absorptions visible with the spectroscope, Raman analysis showed a series of photoluminescence peaks that are not typically seen in grossular. **Dr Jaroslav Hyršl** (Prague, Czech Republic) used UV-Vis-NIR spectroscopy to separate chrome pyrope from various localities. In addition to a small Cr peak at 685 nm that is seen in chrome pyrope from all localities, samples from both of the important Czech sources (Podsedice and Vestřev) show just one absorption peak at 575 nm, while those from Arizona, Tanzania and Yakutia have two peaks at 445 and 575 nm. **Prof. Mimi C. M. Ou Yang** (Hong Kong Institute of Gemmology) used cathodoluminescence to examine the zonal texture of jadeite. Growth zoning was indicated by differences in luminescence intensity and/or colour within individual grains. The luminescence hue varied according to the colour of the jadeite analysed: blue with pink zones in white jadeite, pink with blue zones in lavender material, and green to yellow-green (and orange in some samples) in the Hte Long Sein variety of chromian jadeite. **Masaki Furuya** (Japan Germany Gemmological Laboratory, Kofu) performed electron-irradiation and annealing experiments on Imperial topaz from Ouro Preto, Brazil. Orange-red or violetish pink samples became more orange after electron irradiation and annealing to 350°C by increasing Cr^{4+} absorption. However, the colour of yellow-to-orange topaz (i.e., without a reddish component) was not enhanced by the treatment. **Dr Ulrich Henn** (DSEF German Gem Lab, Idar-Oberstein) surveyed the many colours seen in quartz and explained their causes (i.e., colour centres, inclusions and optical effects). He noted that some 'greened amethyst' is produced by the gamma irradiation of colourless quartz (not amethyst) from Brazil's Rio Grande do Sul State. It shows a 610 nm absorption feature and fades when heated to just 120–150°C (vs. natural prasiolite, which has a 720 nm absorption and is colour-stable to at least 600°C). **Dr Claudio C. Milisenda** (DSEF German Gem Lab, Idar-Oberstein) characterized pale greyish greenish brown zoisite from Pakistan. Internal features include hollow tubes, actinolite needles, growth zoning and healing planes. Absorption spectra are dominated by Fe^{3+}, and heating to 850°C had no effect on coloration. **Willow Wight** (Canadian Museum of Nature, Ottawa) examined the history and coloration of Canadian labradorite. The two main localities of labradorite in Canada are Newfoundland (Nain) and Labrador, and the most unusual colour in the material is purple. **Elisabeth Strack** (Gemmologisches Institut Hamburg, Germany) examined three jewels from the Veliki Preslav treasure in Bulgaria and suggested the emeralds in the pieces may have an Egyptian source. Also, purple stones that were thought to be amethyst turned out to be mostly garnets and one sapphire. **Anette Clausen** (Ministry of Industry and Mineral Resources, Nuuk, Greenland) reviewed gem materials from Greenland, including the unusual materials greenlandite, tugtupite and nuumite, as well as ruby and pink sapphire. The latter materials are being investigated by True North Gems and another venture called Moxie Pictures. True North has completed a pre-feasibility study and they plan to start infrastructure developments in 2014. **Michael Gray** (Coast-to-Coast Rare Stones, Fort Bragg, California, U.S.A.) surveyed gem mining in the United States during the past 10 years. While some mines closed or ceased operation (i.e., for red beryl and benitoite, as well as spessartine from the Little 3 mine in Ramona, California, and sapphire from Yogo Gulch in Montana), others saw renewed activity (Mt. Mica in Maine for tourmaline, Hiddenite in North Carolina for emerald and hiddenite, Jackson's Crossroads in Georgia for amethyst, and the Oceanview mine in Pala, California, for spodumene, tourmaline and beryl). Other gems were mined continuously during this period (sunstones in Oregon, aquamarine at Mt. Antero in Colorado, and diamonds in Arkansas). **Dr Karen E. Fox** (Waterloo, Canada) performed optical spectroscopy of iron in sodium silicate glasses, and indicated that natural high-silica glass (i.e., fulgurite) shows no evidence of non-bridging oxygens in the structure since any iron impurities take on the role of a network former.

In pearl presentations, **Shigeru Akamatsu** (Japan Pearl Promotion Society, Tokyo) described current efforts to produce high-quality akoya cultured pearls at two new farms near Aino-shima island in Japan. The farms use the latest technology to monitor ocean conditions and conduct genetic analyses, while also protecting the environment and conserving oyster resources in the area. **Terry Coldham** (Gemmological Association of Australia, Sydney) documented the harvesting (10 years ago) of natural 'pipi' pearls from *Pinctada maculata* molluscs in Tongavera Atoll, Cook Islands. Of the 600 shells collected from coral heads in the lagoon, only 17 contained pearls or blisters. **Laurent Cartier** (Swiss Gemmological Institute SSEF, Basel; delivered by Prof. Dr Henry Hänni) provided an update on Galatea cultured pearls from French Polynesia. This product line contains bead nuclei

Conference reports

composed of coral, synthetic opal, amethyst and other gem materials, which are partially exposed by carving various patterns through the nacre. Some of the 'turquoise' beads used in these cultured pearls were later identified as barium sulphate that had been pressed and dyed; the company is actively disclosing this. **Dr Stefanos Karampelas** (Gübelin Gem Lab, Lucerne, Switzerland) reported the current status of pearl cultivation at Guaymas (Sonora) Mexico, using *Pteria sterna* molluscs. Over the past 10 years, both the success rate of the harvesting and the average size of the cultured pearls have increased. In 2012 approximately 4,000 gem-quality cultured pearls were produced, and the goal is to reach 10,000 per year. Pearls cultured from *Pteria sterna* are commercially produced only in Mexico, and they can be easily identified with diffuse reflectance spectroscopy by their lack of absorption at 700 nm. **Steve Kennedy** (The Gem & Pearl Laboratory, London) described the history and characteristics of The Pearl of Asia. The large blister pearl, estimated to weigh 155 g, is mounted together with pink tourmaline, jadeite, opal and synthetic ruby. X-radiography showed it to be a hollow blister pearl containing what appear to be pieces of shell and metal that were apparently added to give it the proper heft. **Sutas Singbamroong** (Dubai Gemstone Laboratory, United Arab Emirates) showed how to use a digital SLR camera to observe and record the X-ray luminescence of pearls. He placed the camera in a conventional Faxitron X-ray cabinet (with no viewing window) and used the timer to photograph the luminescence after the door was closed. A reference pearl was included in each photo to provide a consistent colour and strength of luminescence. The best camera settings were found to be a 30 second exposure with an aperture of *f*3.2 and a sensitivity of 6400 ISO. **Abeer Al-Alawi** (Ministry of Industry & Commerce, Manama, Bahrain; delivered by co-author Stefanos Karampelas) compared the characteristics of cavities in natural vs. beadless cultured saltwater pearls. Features seen in X-radiographs or micro-CT scans were compared to the appearance of the corresponding cavities after the samples were sliced in half.

Three talks addressed the application of new technology to gemmology. **Menahem Sevdermish** (Gemewizard Ltd., Ramat Gan, Israel) described further research into the digital analysis and communication of colour in gemmology using the Gemewizard software package. The newest developments include the GemePro for obtaining the 'colour DNA' from the photo of a gem, GemePrice for allocating wholesale prices to diamonds and coloured stones, GemeFancy for evaluating the colour of fancy diamonds, GemeEdu for establishing colour borders according to gem name (e.g., ruby vs. pink sapphire) and teaching colour grading, GemeMatch for finding gems of a desired colour, and GemeShare for locating suppliers for those stones. **S. Sivovolenko** (OctoNus Software, Tampere, Finland; delivered by co-author R. Serov) explored cut optimization technology for fancy-colour diamonds. A case study for a yellow piece of rough showed that the highest cutting yield did not correlate to the greatest stone value, due to differences in the depth of face-up colour showed by various stone shapes. **Dr Yuri Shelementiev** (MSU Gemological Center, Russia) demonstrated digital microscopy applications in gemmology. Advantages include three-dimensional viewing of gems and their inclusions (with suitable software and 3D glasses) and image enhancements (e.g., contrast and high dynamic range).

Poster presentations covered a wide range of subjects, particularly gem corundum. **Gagan Choudhary** (Gem Testing Laboratory, Jaipur, India) studied inclusions in rubies from various localities (covering five states) in India. Most of the inclusions were of similar type, pattern and appearance, and no definitive locality-specific features were noted. Some minerals were identified only in rubies from one locality, such as hematite (from Chhattisgarh), chromite and green mica (from Orissa), and apatite and yellow spinel (from Tamil Nadu). **Dr Christoph A. Hauzenberger** (Karl-Franzens-Universität Graz, Austria) investigated the genesis of corundum crystals with spinel coronas from Truc Lau and Kinh La in northern Vietnam. Colourless sapphire or ruby may be surrounded by brown Al-Mg spinel or dark hercynite ($FeAl_2O_4$) overgrowths, which formed in metacarbonate and Fe-rich gneiss, respectively. **Natthapong Monarumit** (Kasetsart University, Bangkok, Thailand) applied dielectric constant values to differentiating rubies from Mong Hsu, Myanmar, and Montepuez, Mozambique. The average dielectric K values measured for Mong Hsu and Montepuez rubies were greater 20 and less than 12, respectively. **Aumaparn Phlayrahan** (Kasetsart University, Bangkok, Thailand) documented changes in structural OH groups in the FTIR spectra of rubies from Mong Hsu and Montepuez, before and after heat treatment. The spectra revealed differences in the 3400–3100 cm^{-1} range that probably relate to the dehydration of hydrous aluminium-phase inclusions in the presence of certain trace elements. **Y. Shelementiev** (MSU Gemological Center, Russia) studied the alteration of zircon, boehmite and kaolinite inclusions in corundum during heat treatment. Systematic changes were noted in the visual appearance and Raman spectra of the zircon, and in the FTIR spectra of the boehmite and kaolinite due to dehydration of those phases.

Several poster presentations dealt with the treatment of gems other than corundum. **Chanikarn Sanguanphun** (Kasetsart University, Bangkok, Thailand) used atomic force microscopy to detect the electron irradiation of faceted diamonds. After treatment, the surfaces of the irradiated green and bluish green diamonds showed increases in the calculated values of step height and root mean square (RMS) roughness. **Prof. Dr Panjawan Thanasuthipitak** (Chiang Mai University, Thailand) performed heat treatment experiments on aquamarine and morganite from Madagascar. The experiments were done in a reducing atmosphere (using Ar gas), and the optimum temperature for intensifying the blue colour of aquamarine was 400°C, while 350°C was sufficient for

Conference reports

Figure 5: Miners search for spinel after washing soil through a sieve at this small mine on the edge of a rice paddy near Luc Yen. Photo by B.M. Laurs, © Gem-A.

Figure 6: IGC participants search for spinel in tailings at the Cong Troi mine near Luc Yen. The active mining face is obscured by clouds. Photo by B.M. Laurs, © Gem-A.

enhancing the pink colour of morganite. **Dr Shang-i Liu** (Hong Kong Institute of Gemmology) used EPR spectroscopy in a preliminary study to investigate the causes of colour in untreated and irradiated green spodumene. EPR data showed that an untreated hiddenite from North Carolina contained Cr^{3+} in octahedral coordination (and no colour centres), whereas a laboratory-irradiated spodumene showed a Cr^{3+} signal overlapping with a related colour centre, and a naturally irradiated spodumene contained only colour centres. **Dr Somruedee Satitkune** (Kasetsart University, Bangkok, Thailand) compared the heat treatment of reddish brown zircon from Ratanakiri, Cambodia, and Kanchanaburi, Thailand. The Cambodian samples turned blue after heating to 1000°C for 1 hour in a reducing atmosphere, due to the absorption of U^{4+} at 653 nm. In contrast, the Thai samples became colourless after heating.

Other posters covered various issues related to coloured stones. **Dr Arūnas Kleišmantas** (Vilnius University, Lithuania) investigated 17th- and 18th-century garnet-garnet doublets imitating rubies in liturgical objects from Lithuania. These doublets are particularly convincing because they have an empty space at the glue-garnet interface that reflects light and gives them greater brilliance. **Elizabeth Su** (Gemsu Rona, Shanghai, China) examined the classification of jadeite by deposit type, colour, texture, transparency and composition. **John M. Saul** (ORYX, Paris, France) proposed three origins for foul odours emitted by gem-bearing host rocks from southeast Kenya and northeast Tanzania when they are struck or crushed. The gases may come from (1) materials of primordial origin, (2) mobilization of evaporites, and/or (3) serpentinization of ophiolites, producing hydrogen gas and hydrocarbons. **Dr Nguy Tuyet Nhung** (Vietnam Gemstone Association, Hanoi) surveyed gem materials from the Luc Yen pegmatite in Vietnam. Tourmaline is most important and a relatively small amount of green orthoclase feldspar also has been polished. Large blocks of purple lepidolite have been produced but not used for display purposes. **Dr Nguyen Thi Minh Thuyet** (Hanoi University of Science, Vietnam) reported the gemmological characteristics and chemical composition of peridot from southern Vietnam. No systematic differences were noted in their properties compared to peridot from other sources that are hosted by xenoliths within basalt flows. **Sora Shin** (Hanyang University, Seoul, Korea) compared the characteristics of the colourless gems phenakite, petalite, pollucite and goshenite. **Chakkrich Boonmee** (Kasetsart University, Bangkok, Thailand) characterized Thai ivory from Lampang Province using SEM-EDS and LA-ICP-MS.

A post-conference excursion on 17–19 October took participants to Luc Yen in the Yen Bai Province of northern Vietnam to visit the Cong Troi mine and the local gem market. Cong Troi is a primary deposit that is worked mainly for mineral specimens of pink-to-purple spinel crystals embedded in white marble. The mine was reached by walking for about two hours through rice paddies and jungle. Along the way participants passed a small secondary deposit *(Figure 5)*. The miners washed the soil in a sieve using water pumped from a nearby pond. The spinel they found that day consisted only of non-gem-quality material. At the Cong Troi mine no activity was taking place due to the rainy weather. The deposit is worked by blasting or sawing blocks of spinel-bearing marble from a large open-cut at the top of the mountain. In the extensive tailings pile *(Figure 6),* some fieldtrip participants found samples of marble containing spinel associated with colourless forsterite, orange clinohumite and/or green pargasite. None was of gem quality, but they made attractive mineral specimens. Such pieces were offered for sale in the local gem market in Luc Yen *(Figure 7)* and also seen in numerous shops around town.

The next IGC conference will take place in Lithuania in 2015.

Brendan M. Laurs

Conference reports

Figure 7: At the gem market in Luc Yen, these local vendors offer ruby, sapphire, spinel, yellow tourmaline, green feldspar, citrine and tektite. Photo by B.M. Laurs, © Gem-A.

2013 GIC International Gems and Jewellery Conference

The annual Gemological Institute of China (GIC) conference was held on 13 October at the China University of Geosciences campus in Wuhan. A total of 102 delegates from the United Kingdom, Hong Kong, Taiwan and from 11 provinces in China participated in the conference. There were 17 oral presentations and a post-conference field trip. A proceedings volume is planned for publication in *The Journal of Gems and Gemmology* later this year.

Two of the talks addressed gemmological education in China, focused on a formal academic environment. Four presentations were on jewellery art and design. Five talks examined the gem and jewellery business and markets in mainland China and Hong Kong, covering the following topics: integrating ISO standards with jewellery branding; high-end jewellery market strategy; diamond investment in 2013–2014; the impact of the internet on traditional jewellery business; and research on consumer psychology. The other six talks covered new research in gemmology and precious metals, as described below.

Prof. Ren Lu (Institute of Gemology, China University of Geosciences) presented his recent study on the colour origin and identification of lavender jadeite using UV-Vis spectroscopy and LA-ICP-MS. Through an analogous study on another pyroxene mineral (kunzite), he firmly established Mn as the trace element that is responsible for the lavender colour in jadeite.

Baozheng Tian (Hunan Provincial Gem Testing Center, Changsha, China) described a new dark violet-blue jade called *zimo xiangyu* from the Liuyang area of Hunan Province that is composed of cryptocrystalline cordierite-biotite amphibolite.

Guolong Yao (Enyu Jewellery, Haikou, Hainan Province, China) surveyed various imitations of sea tortoise shell, in which he showed hundreds of slides comparing natural tortoise shell to different imitations (such as plastic) and assembled materials.

This author explored applications of LA-ICP-MS analysis to gemmology, including instrument development and techniques for evaluating Be-diffused sapphires, chrome chalcedony treatment and peridot country-of-origin determination.

The field trip took place on 14 October, when over 80 delegates visited a freshwater pearl farm near Ezhou in Hubei Province. The delegates were shown procedures for producing the cultured pearls *(Figure 8)* and they had a chance to purchase the local products.

Prof. Andy H. Shen
(ahshen1@ymail.com)
Institute of Gemology
China University of Geosciences
Wuhan, China

Figure 8: Technicians at a pearl farm in Hubei Province demonstrate the insertion of tissue nuclei into mussels used for producing freshwater cultured pearls. Photo by Xiong Ni.

Conference reports

2013 China Gems & Jewelry Academic Conference

This annual conference took place on 30 October in Beijing *(Figure 9)*, organized by the National Gems & Jewelry Technology Administrative Center (NGTC, Beijing) and the Gems & Jewelry Trade Association of China. The attendees consisted of nearly 400 gemmologists, researchers, educators, leading industry representatives and students, as well as Chinese government officials. The programme encompassed 21 talks selected from 85 short research articles published in a special issue of *China Gems* (September–October 2013; mostly in Chinese with English abstracts). The topics included diamond, coloured stones, organic gems, nephrite and other jade varieties, precious metals and their testing techniques, and jewellery appraisal, marketing and design. Highlights of some of the research presented at the conference are given here.

Prof. Mark Newton (University of Warwick, Coventry) explained how electron paramagnetic resonance (EPR) can be applied to the study of treated and synthetic diamond. His talk concentrated on three aspects: (1) the importance of EPR spectroscopy for studying the electronic structure of crystal defects; (2) how to identify HPHT-treated type IIa and IaB brown diamond by analysing nitrogen aggregation with EPR; and (3) how to identify HPHT- and CVD-grown synthetic diamonds by detecting defects that are absent from natural diamonds.

Prof. Guanghai Shi (China University of Geosciences, Beijing) examined the mineral composition and structure of Myanmar jade and its nomenclature. He showed a variety of mineral compositions and textures, and demonstrated how the study of these characteristics are important not only for understanding the genesis of jadeite jade, but also for the proper naming and quality evaluation of this complex material.

Prof. Jongwan Park (Hanyang University, Seoul, Korea) described his study of 12 Madagascar tourmaline samples that were irradiated by an electron beam. The treatment modified their colours to various degrees, which he correlated to features recorded in their UV-Visible and IR spectra. The tourmalines' original colours were restored by heating to 550°C for three hours.

The afternoon talks expanded into two conference rooms. **Prof. Zuowei Yin** (China University of Geosciences, Wuhan) investigated fossil mammoth ivory. He discussed differences between mammoth and modern ivories using gemmological testing, IR spectroscopy (to analyse molecular water- and collagen-related absorptions) and X-ray diffraction (to study the crystallization of hydroxyapatite).

Prof. Zhili Qiu (Sun Yat-Sen University, Guangzhou, China) examined the development of modern Chinese jade carving arts, with an emphasis on the driving forces for the divergence and subsequent convergence of art styles. **Prof. Shiqi Wang** (Peking University, Beijing, China) discussed the visual characteristics of tremolite in nephrite jade from several localities: China (Xinjiang, Qinghai and Liaoning), Russia and Korea. He suggested that these jades can be distinguished by their colour, lustre, transparency, texture and structure.

Prof. V.K. Garanin (Moscow State University, Russia) compared kimberlitic diamonds from Russia's two major deposit areas: Yakutia and Arkhangelsk. Mineralogical and gemmological research were presented on diamonds from both localities.

Prof. Lijian Qi (Tongji University, Shanghai, China) reported that some 'insect amber' and 'dark amber' currently on the market are produced from copal resin using heat and pressure. In addition, imitation amber is made by treating copal powder. The identification of treated copal with gemmological testing and IR and EPR spectroscopy was described, and absorption characteristics of amber from various global deposits were presented.

Dr Taijin Lu (NGTC) examined tarnish spots on the surface of high-purity gold jewellery (99.9% Au). He correlated the spots with silver and sulphur impurities in the gold, and indicated that they might be prevented by using improved cleaning processes during gold manufacturing.

Figure 9: The 2013 China Gems & Jewelry Academic Conference was recently held in Beijing. Here, the audience listens to Prof. Mark Newton's presentation. Photo by R. Lu.

Tao Chen (summerjewelry@163.com)
and Prof. Ren Lu
Institute of Gemology
China University of Geosciences
Wuhan, China

Conference reports

Gemological Research in the 21st Century: Characterizing Diamonds and other Gem Minerals

The Geological Society of America (GSA) held its annual meeting on 27–30 October in Denver, Colorado. While this venerable organization celebrated its 125th Anniversary with a record number of submitted abstracts and a high attendance drawn from all segments of the geological sciences, gemmologists may also find reason for celebration in that their science was represented for the very first time in the history of GSA as a session all its own. Session conveners Dona Dirlam and Dr James E. Shigley of GIA (Carlsbad, California) organized and moderated the session's presentations, which were held over two days in both oral and poster formats. Both were well attended and received positive comments from the participants (for details see 'Gemology bears triumphant tidings', www.palagems.com/gem_news_docs/GSA_Gemology_Session.pdf). The abstracts of the presentations may be accessed at http://gsa.confex.com/gsa/2013AM/webprogram (in the Final Session Number box, type T216), and below is a listing of the titles.

- Geochemical methods to address the challenges facing modern gemological research (Prof. Georg e R. Rossman)
- Recent advances in the understanding of the distribution, origin, age and geological occurrences of diamonds (Prof. Steven B. Shirey)
- Comparison of luminescence lifetimes from natural and laboratory irradiated diamond (Dr Sally Magana)
- Identification of green colored gem diamonds: An on-going challenge (Dr Christopher M. Breeding)
- Chemical characterization of gem tourmaline (Prof. William B. Simmons)
- Crystal-filled cavities in granitic pegmatites: Bursting the bubble (Prof. David London)
- Trace element comparison of ancient Roman intaglios and modern samples of chromium chalcedony: An archaeogemological provenance study (Dr Cigdem Lule)
- Country-of-origin determination of modern gem peridots from LA-ICPMS trace-element chemistry and linear discriminant analysis (LDA) (Prof. Andy Shen, Dr Troy Blodgett, Dr James E. Shigley)
- Precisely identifying the mines from which gemstones were extracted: A case study of Columbian emeralds (Catherine E. McManus)
- Sapphire — a crystal with many facets (Dr Jennifer Stone-Sundberg)
- Gem pargasite from Myanmar: Crystal structure and infrared spectroscopy (David Heavysege, Dr Yassir A. Abdu and Prof. Frank C. Hawthorne)
- Comparison of surface morphology of Montana alluvial sapphires by SEM (Dr Richard B. Berg)
- Investigation of gem materials using 405 nm laser spectroscopy (Prof. Henry L. Barwood)
- Provenance determination of rubies and sapphires using laser-induced breakdown spectroscopy and multivariate analysis (Kristen Kochelek, Prof. N.J. McMillan, Catherine McManus, and Prof. David Daniel)
- Reversible color modification of blue zircon by long wave ultraviolet radiation (Nathan D. Renfro)
- Scholarly treasure: The role of gems in a university setting (Elise A. Skalwold and Prof. William A. Bassett)
- Spatial distribution of boron and PL optical centers in type IIb diamond (Troy Ardon)
- Trace element and chromophore study in corundum – application of LA-ICP-MS and UV-visible spectroscopy (Prof. Ren Lu).

Elise A. Skalwold
Ithaca, New York, U.S.A.

Gem-A Conference 2013

This annual conference took place 1–6 November in London and featured a diverse line-up of 13 speakers. A variety of seminars and museum visits were arranged to coincide with the conference (see page 265 of this issue).

David Callaghan (Harrow) recounted the history of the London Gem Lab, mostly using notes made by Basil Anderson. Of particular importance was the development of the endoscope in 1926–7, which was critical to addressing the trade's need to confidently identify natural vs. cultured pearls.

Dr Emmanuel Fritsch (University of Nantes and Institut des Matériaux Jean Rouxel, France) described luminescence in gemmology. Luminescence is the emission of visible light caused by some type of excitation, and it should be described according to its strength, turbidity and zonation. Two types of luminescence spectroscopy — excitation and time-resolved — are expected to have increasing applications to solving gemmological problems in the future.

Dr James Shigley (GIA, Carlsbad, California) chronicled the evolving challenges of gem identification, particularly those due to treatments. He predicted that future concerns will involve treated and synthetic melee diamonds, ceramic materials, and high-tech coatings.

Martin Rapaport (Rapaport Diamond Corp., New York, U.S.A.) discussed the overall state of the diamond industry, commenting that mining companies are responsible for driving up the price of rough to unsustainable levels, artisanal diamond miners (particularly in West Africa) are not benefitting from their work, and synthetic diamonds are not being disclosed properly in the trade (especially in melee sizes).

Gary Roskin (Roskin Gem News, Exton, Pennsylvania, U.S.A.) examined some challenges in diamond grading. For evaluating clarity, he stressed the need to consider the following aspects of diamond inclusions: colour and relief, location, nature, number, and size in relation to the stone. He also had suggestions for successfully grading colour in the D–Z range: have master stones re-graded in a lab, move the master stones further away from the light source and use magnification.

Conference reports

Sonny Pope (Suncrest Diamonds, Orem, Utah, U.S.A.) discussed the multi-step treatment of diamonds using high-pressure, high-temperature (HPHT) processing and irradiation. Of the diamonds on the market, only some stones have the potential to be treated to various colours (approximately 30% yellow, 50% green, 20% orange and 2% colourless), so the starting material is carefully pre-screened using infrared spectroscopy. The treatment is done on faceted stones (therefore requiring some post-treatment repolishing), in weights ranging from 2 points to 60 ct.

Arthur Groom (Arthur Groom & Co., Ridgewood, New Jersey, U.S.A.) surveyed emerald clarity enhancements on the market today. He said that the main challenges are seen in emeralds from Brazil and Colombia, which are being enhanced as rough material with 'permanent' methods such as Gematrat resin (which expands as it hardens). Only about 5% of the emeralds he encounters are treated with cedarwood oil, and repeated treatment with this oil (involving heating without prior cleaning) can result in yellow staining within fractures.

Dr John Emmett (Crystal Chemistry, Brush Prairie, Washington, U.S.A.) explained how various chromophores (i.e., Fe^{3+}, V^{3+}, Cr^{3+}, Fe^{2+}-Ti^{4+} and trapped hole centres involving Fe, Cr and Mg) affect the colour of corundum. The coloration depends on their concentration and absorption cross section (or strength of imparting coloration), as well as the optical path length through a stone. He also showed how padparadscha colour is produced by a combination of Cr^{3+} and trapped hole centres involving Cr.

Dr Jack Ogden (Striptwist Ltd., London) described the Cheapside Hoard, which dates to the 1640s and was discovered in 1912 under the floor of a former goldsmith's shop in London. The jewellery in the Hoard contains a variety of coloured stones (but only one diamond), and several imitations have also been identified such as foil-backed glass to imitate emerald, ruby and sapphire, and quench-crackled quartz that was stained red (now faded to orange) to imitate spinel.

Chris Sellors (C W Sellors Fine Jewellery, Ashbourne, Derbyshire) focused on two English gemstones: Blue John and Whitby jet. Mined for centuries in Derbyshire, Blue John consists of banded purple and colourless fluorite that is locally iron-stained. The deposit is located within a national park, and only one-half ton of the material can be mined each year. Whitby jet is the fossilized wood of the monkey puzzle tree *(Araucaria araucana)*, and the material is gathered from beaches after it erodes from cliffs near the town of Whitby in Yorkshire. Cabochons of both Blue John and Whitby jet are now being manufactured into higher-end jewellery with gold and diamonds.

Brian Jackson (National Museums Scotland, Edinburgh) provided an overview of Scottish gem materials, which include jet, amber, freshwater pearls, smoky quartz, aquamarine, topaz, tourmaline, garnet, sapphire, agate, prehnite, ammolite, zircon and serpentinite. The diversity of these materials results from the variety of rock types that underlie Scotland. Overall there is not enough Scottish gem production to make a sustained commercial impact on the market.

Shelly Sergent (Somewhere In The Rainbow™, Scottsdale, Arizona, U.S.A.) described the Somewhere In The Rainbow™ gem and jewellery collection, which was founded in 2008 and became an educational resource in 2012. The collection, which is still growing, consists of high-quality examples of coloured stones and pearls that are loose or mounted in jewellery (e.g., *Figure 10*).

Figure 10: This pendent, which features a 13.57 ct tsavorite from the Komolo mine in Tanzania, is one of many jewellery pieces that was on display during the Gem-A conference. The stone was mined in 1979 by Campbell Bridges, and the pendent was designed in 2013 by Shelly Sergent and Harry Tutunjian of Goldbench Jewelers, Scottsdale, Arizona. Courtesy of Somewhere In The Rainbow™; photo by B.M. Laurs, © Gem-A.

John Bradshaw (Coast-to-Coast Rare Stones, Nashua, New Hampshire, U.S.A.) examined some rare and collector stones on the market. Of the approximately 200 mineral species (out of more than 4,000) that have been faceted, only about 20 are common in jewellery. The remainder are important for the collector market, particularly benitoite, sphene, rhodochrosite, apatite, fluorite and sphalerite.

Brendan M. Laurs

Proceedings of the Gemmological Association of Great Britain and Notices

Gem-A Conference 2013

The 2013 Gem-A Conference, in celebration of the centenary of the Gemmology Diploma and the 50th anniversary of the Diamond Diploma, was held on Saturday 2 and Sunday 3 November at Goldsmiths' Hall in the City of London. The weekend also included an Anniversary Dinner and Graduation Ceremony.

Speakers were John Bradshaw, David Callaghan, Dr John Emmett, Dr Emmanuel Fritsch, Arthur Groom, Brian Jackson, Dr Jack Ogden, Sonny Pope, Martin Rapaport, Gary Roskin, Chris Sellors, Shelly Sergent and Dr James Shigley. Highlights of the presentations are given in the Conference Reports, pages 263–264.

Delegates were able to view a number of exhibits and demonstrations during the breaks, including those by Somewhere In The Rainbow™, C.W. Sellors, the Institute of Registered Valuers, GemmoRaman and Alan Hodgkinson, President of the Scottish Gemmological Association.

Conference Events

A programme of seminars, workshops and visits over a period of six days was arranged to coincide with the Conference. These started on Friday 1 November with half-day seminars presented by Richard Drucker, Arthur Groom and Craig Lynch.

On Monday 4 November visits were arranged to the Pearls exhibition at the Victoria & Albert Museum and to view the Cheapside Hoard at the Museum of London. On Tuesday 5 November a guided tour of the Mineral Galley at the Natural History Museum was held and on Wednesday 6 November there was a private viewing of the Crown Jewels at the Tower of London with David Thomas.

A full report of the Conference and events was published in the November/December 2013 issue of *Gems&Jewellery*.

Conference Sponsors and Supporters

The Association is most grateful to the following for their support:

MAJOR SPONSOR

Jewelry Television (JTV)
www.jtv.com

SPONSORS

Fellows Auctioneers
www.fellows.co.uk

GemmoRaman
www.gemmoraman.com

SUPPORTERS

Marcus McCallum FGA
www.marcusmccallum.com

Gemworld
www.gemguide.com

National Association of Goldsmiths' Institute of Registered Valuers
www.jewelleryvaluers.org

ASSOCIATE SUPPORTERS

Apsara Gems
www.apsara.co.uk

Gemfields
www.gemfields.co.uk

British Jewellers' Association
www.bja.org.uk

T.H. March, Insurance Brokers
www.thmarch.co.uk

We would also like to thank DG3 Diversified Global Graphics Group for sponsoring conference materials.
www.dg3.com

Anniversary Dinner

An Anniversary Dinner was held at Goldsmiths' Hall on Saturday 2 November. The evening commenced with a drinks reception sponsored by Somewhere In The Rainbow™ held in the Drawing Room. Those who attended were welcomed to the event by the music of harpist Zuzanna Olbryś as they made their way up the magnificent staircase.

This was followed by dinner in the candlelit Livery Hall, attended by over 180 members and guests from around the world. Speeches were given by Gem-A CEO James Riley and President Harry Levy. Katrina Marchioni, President of Gemmological Association of Australia, also gave a speech and presented Gem-A with a ceremonial plaque of prasiolite mounted on Australian gumtree sap.

The evening finished with a raffle, and the Association is most grateful to those who generously donated the prizes.

Harpist Zuzanna Olbryś, a student at the Guildhall School of Music and Drama, playing at Goldsmiths' Hall. Photo by Miles Hoare. © Gem-A.

Graduation Ceremony

Martin Rapaport giving the address at the Graduation Ceremony at Goldsmiths' Hall. Photo courtesy of Photoshot.

The Graduation Ceremony and Presentation of Awards was held at Goldsmiths' Hall on Sunday 3 November. Cally Oldershaw, Chairman of the Gem-A Council, welcomed those present which included graduates from Australia, Canada, China, India, Japan, Madagascar, Sri Lanka, Taiwan, Thailand and the U.S.A., as well as well as those from Europe and the UK.

James Riley, Gem-A CEO, then introduced the guest speaker, Martin Rapaport, who presented the diplomas and awards. Special mention was made of Charlotte Leclerc of Paris, France, whose excellent answers in the examinations qualified her for all the Gemmology Diploma prizes — the Anderson-Bank Prize, the Read Practical Prize and the Christie's Prize for Gemmology, as well as the Tully Medal.

Following the presentations to the graduates, in recognition of their enormous contribution in their own fields of gemmology, Dr Emmanuel Fritsch of Nantes, France, and Martin Rapaport of New York, U.S.A., were awarded an Honorary Fellowship and Honorary Diamond Membership, respectively.

Three members were awarded Fellowship status in recognition of their high level of expertise and who had made a significant contribution to the field of gemmology for no less than 10 years were presented with Fellowship diplomas. They were Ronnie Bauer of Glen Iris, Victoria, Australia, Brendan Laurs of Encinitas, California, U.S.A., and Tay Thye Sun of Singapore.

Life membership was awarded to Leonard Baker of Ferndown, Dorset, the longest-standing Fellow of the Association, who had qualified for his Diploma in 1948. Life memberships were also awarded to David C.B. Jones of Adligenswil, Switzerland, Douglas M. Leake of Nuneaton, Warwickshire, John F. Marshall of Sutton Coldfield, West Midlands, William Richard H. Peplow of Worcester, Sarah A. Riley of Strensham, Worcestershire, and John M.S. Salloway of Lichfield, Staffordshire, all of whom qualified in the first Diamond Diploma examinations held in 1963. David Jones and Sarah Riley were present to receive their certificates of life membership.

Martin Rapaport gave an enthusiastic and stimulating address, congratulating the graduates on their great achievement and emphasizing that theirs was an industry with the highest moral and ethical codes. He encouraged them not to rest with the knowledge that they had qualified in their examinations but now to "strive to be excellent".

Charlotte Leclerc receiving the Tully Medal from Harry Levy, President of Gem-A. Photo courtesy of Photoshot.

The vote of thanks was given by Harry Levy, Gem-A President.

The ceremony was followed by a reception for graduates and guests in the Drawing Room.

Gifts and Donations to the Association

The Association is most grateful to the following for their gifts and donations for research and teaching purposes:

Leonard Baker FGA, Ferndown, Dorset, for a selection of crystal models, handheld gem equipment and a Moe gauge, and a large pearl oyster shell with pearl colour testing blotting paper.

John Bradshaw, Coast-to-Coast Rare Stones, for 32 rare and collectors' stones.

Elaine Branwell, Wellington, Somerset, for a selection of treated, imitation and synthetic stones.

Terry Coldham, Sydney, New South Wales, Australia, for a bag of small rough blue spinel from Vietnam.

Andrew Fellows FGA DGA, Gem-A, London, for four doubly terminated apatite crystals and one sharply terminated tourmaline crystal.

The Gemmological Association of Australia for a ceremonial plaque of prasiolite mounted on Australian gumtree sap.

Denis Ho, Myanmar, for a set of seven diamond simulants, a set of A, B, C and B+C jades, and three rough and three cut chrome tourmalines.

Brendan Laurs FGA, Gem-A, Encinitas, California, U.S.A., for a pearl oyster shell and cultured pearl from Halong Bay, Vietnam; a pearl oyster shell with a shell-shaped blister pearl from Halong Bay; also rough spinel-bearing marble and a bag of spinel-bearing gem gravel from the Cong Troi mine, Luc Yen, Vietnam.

Dominic Mok FGA DGA, AGIL, Hong Kong, for pre-treated and treated rough and faceted samples of corundum, showing the stages of cobalt-infused lead-glass-filled blue sapphire. A sample card displaying rough crystals of gemstones of Burma.

Tawee Khankaew, Bangkok, Thailand, for a small parcel of lead-glass-filled sapphires.

Ted Themelis, Bangkok, Thailand, for pre-treated and treated rough and faceted samples of corundum, showing the stages of cobalt-infused lead-glass-filled blue sapphire.

Gem-A Photographic Competition

2013 Competition winners

Overall winner and winner of Natural category

Michael Hügi FGA

Gilalite aggregates in rock crystal (Medusa quartz) from Brazil. Gilalite is a rare hydrous copper silicate. (Polarization filter used on the microscope objective to eliminate blurring of the image due to the double refraction of quartz. Magnified approximately 25×.)

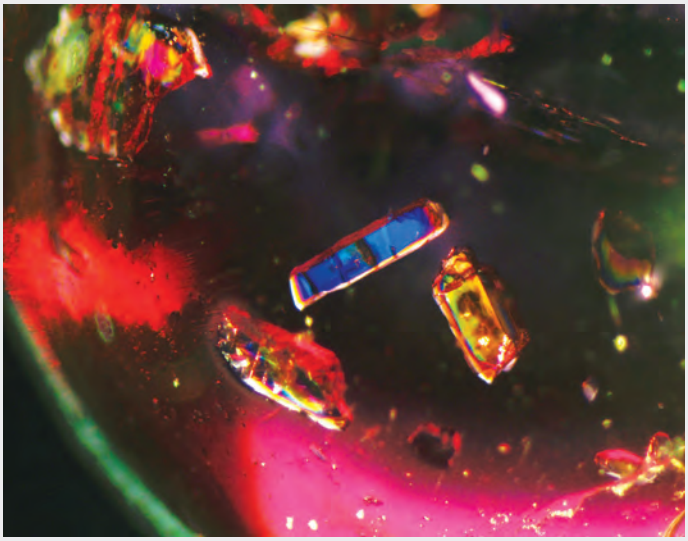

Winner of Treated category

Edward Ferder FGA DGA

Almandine seen with crossed polars. The photomicrograph shows vivid interference colours of doubly refractive crystal inclusions. (Magnified approximately 50×.)

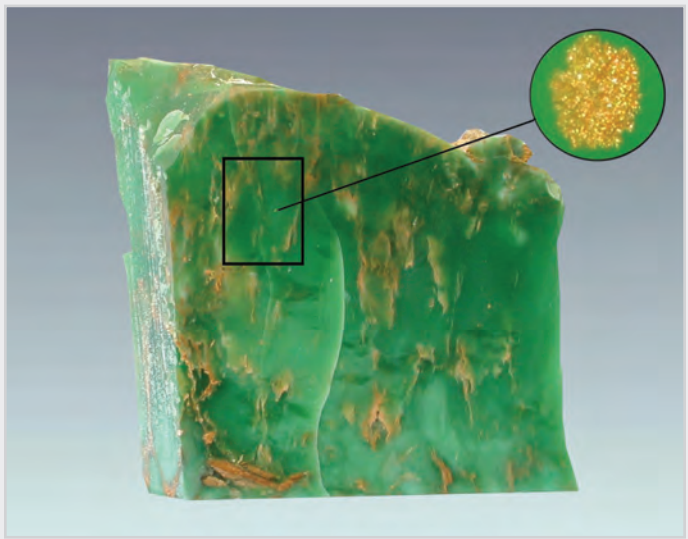

Winner of Synthetic category

John Harris FGA

A polished section of Australian variscite (2.6 cm across) with a microscopic surface-reaching inclusion of gold (inset, magnified approximately 200×).

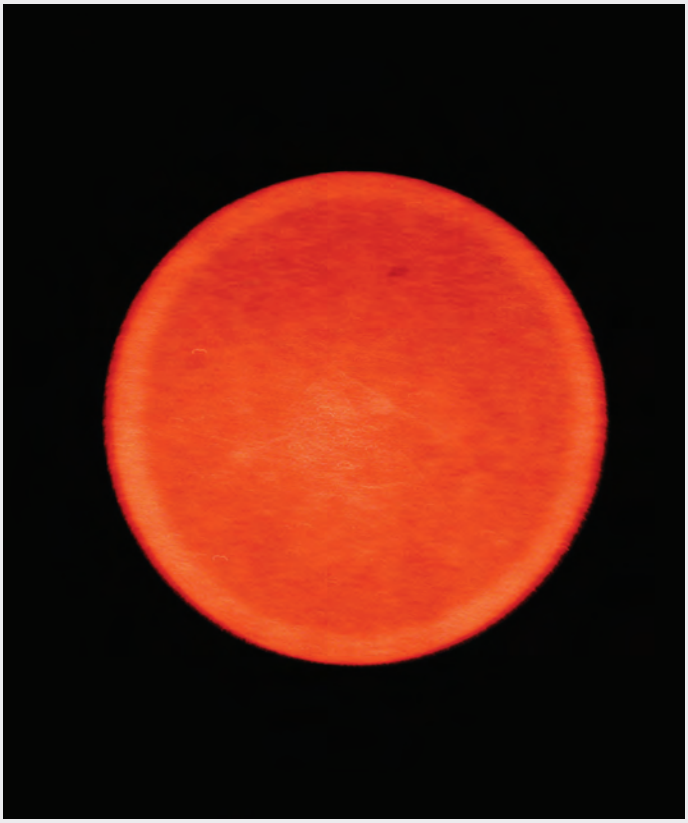

Winner of Melange category

John Harris FGA

A ground glass diffusion filter capturing the polarized extraordinary ray from an orangey pink sapphire giving an impression of solar energy.

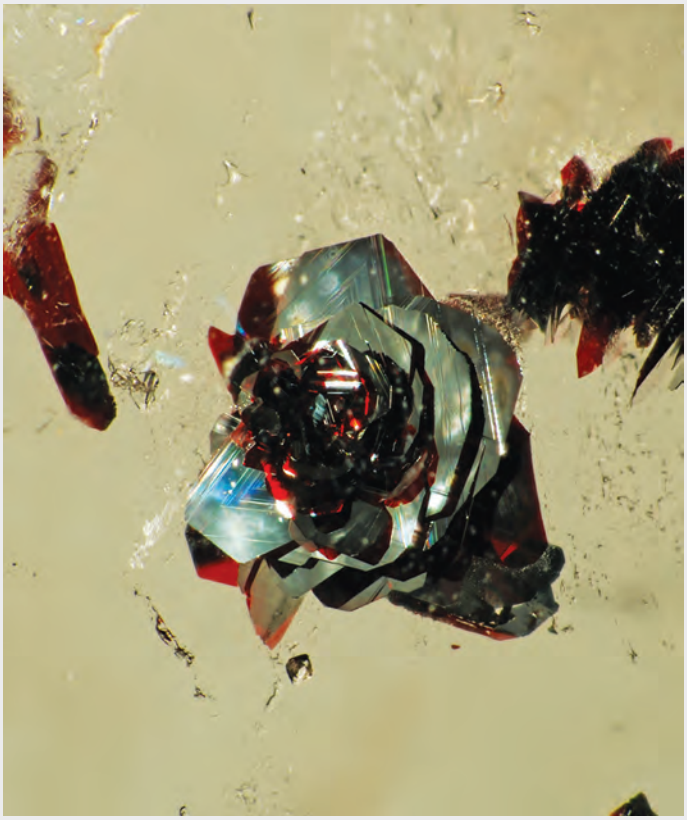

Honourable mention

Conny Forsberg FGA

Hematite rose in quartz from Brazil. (Magnified approximately 70×.)

The 2014 Competition is now open!

All Gem-A members are invited to participate. Once again there are four categories in which an image may be submitted:

1 **Natural**
Digital photograph (or photomicrograph) with minimal post-production work (may include basic cropping, contrast and minor hue/saturation adjustments).

2 **Treated**
Digital photograph (or photomicrograph) with significant post-production work (such as background manipulation, HDR and contrast masking).

3 **Synthetic**
Computer-rendered 3D models of gemstones, crystals, crystal structures, images from microtomography, etc.

4 **Melange**
This category includes any gem-related image that doesn't fit in the above and may include such things as photos of a spectrum, a scanning electron microscope image, mining, cutting, etc.

The entries will be judged by an industry panel on the basis of gemmological interest, inspiration, artistic quality and, in the case of categories 2 and 3, computer skills and ingenuity. A prize will be awarded in each category and, depending on submissions and at the judges' discretion, an additional prize for the most humorous or unusual image might also be awarded. All prize winners will receive their image within a frameable mount. In addition there will be one overall winner who will receive a free Gem-A membership for the following year.

To enter

Please send a low resolution version of your photo to editor@gem-a.com. Entry forms and full details of the competition, including copyright information and Rules of Entry, can be accessed at www.gem-a.com/membership/photographic-competition.aspx or call Amandine Rongy at +44 (0)20 7404 3334.

Closing date: 30 June 2014

Winning entries will be announced at the 2014 Gem-A Conference and be featured in *Gems&Jewellery*.

Gem-A Awards

In the Gem-A examinations held in June 2013, 177 students qualified in the Gemmology Diploma Examination, including nine with Distinction and 23 with Merit, and in the Foundation Certificate in Gemmology Examination 276 qualified. In the Gem Diamond Examination 78 qualified, including 11 with Distinction and 12 with Merit.

In the Gemmology Diploma examination, the Tully Medal is awarded to the candidate who submits the best set of answers which, in the opinion of the Examiners, are of sufficiently high standard. The Christie's Prize for Gemmology is awarded to the best candidate of the year, the Anderson Bank Prize for the best set of theory papers and the Read Practical Prize (sponsored for 2013 by DeeDee Cunningham of Toronto, Canada) for excellence in the practical examination. The **Tully Medal**, the **Christie's Prize for Gemmology**, the **Anderson Bank Prize** and the **Read Practical Prize** were awarded to **Charlotte Leclerc** of Paris, France.

In the Foundation Certificate in Gemmology examination, the **Anderson Medal** for the candidate who submitted the best set of answers which, in the opinion of the Examiners, were of sufficiently high standard, and the **Hirsh Foundation Award** for the best candidate of the year, were awarded to **Nicole Mouralian** of Montreal, Quebec, Canada.

In the Gem Diamond Diploma examination, the **Bruton Medal** for the best set of theory answer papers of the year was awarded to **Li Ziyue** of Zhuhai, Guangdong, P.R. China.

The **Deeks Diamond Prize** for the best candidate of the year was awarded to **Stefanus Salomon Weyers** of Brandhof, Bloemfontein, South Africa.

The **Diamond Practical Prize** for excellence in the Diamond Practical Examination, sponsored by Dominic Mok from AGIL, Hong Kong, was awarded to **Caroline R. Marcus** of Oxford.

The names of the successful candidates are listed below.

Examinations in Gemmology

Gemmology Diploma

Qualified with Distinction

Blake, Andrea Renae, Chevy Chase, Maryland, U.S.A.
Bosshard Schreckenberg, Astrid, Zurich, Switzerland
Caruel, Maxime, Antananarivo, Madagascar
Choquette, Carolyne, Laval, Quebec, Canada
Leclerc, Charlotte, Paris, France
Saeseaw, Sudarat, Bangrak, Bangkok, Thailand
Suthiyuth, Ratima, Bangrak, Bangkok, Thailand
Walker, Megan G., Edinburgh
Yao Shun, Beijing, P.R. China

Qualified with Merit

Chen Yang, Wuhan, Hubei, P.R. China
Corbin, Marie-Hélène, Montreal, Quebec, Canada
Floch, Edouard, Paris, France
Haeringer, Manuelle, Marseille, France
Howard, Naomi Victoria Georgina, Brussels, Belgium
Huang Lilin, Beihai, Guangxi, P.R. China
Jiang Huiyue, Punan, Shandong, P.R. China
Li, Timothy, Idle, Bradford, West Yorkshire
Li Pengfei, Kuytun, Xinjiang, P.R. China
Lindt, Yulia, Vaucluse, New South Wales, Australia
Massot, Marie-Caroline, Ambatobe, Antananarivo, Madagascar
Miao Ruiyuan, Liaocheng, Shandong, P.R. China
Rafalimanana, Laza Andriamizaka, Antsirabe, Antananarivo, Madagascar
Raynaud, Victoria, Grilly, France
Ren Qianqian, Nanyang, Henan, P.R. China
Rodrigues, Silvio, Geneva, Switzerland
Steele, Sarah Caldwell, Nether Poppleton, North Yorkshire
Wang Xiaodi, Beijing, P.R. China
Zhang Bailu, Beijing, P.R. China
Zhang Yingxin, Foshan, Guangdon, P.R. China
Zhao Qiannan, Beijing, P.R. China
Zhao Yijia, Shaoxing, Zhejiang, P.R. China
Zheng Yi, Wenzhou, Zhejiang, P.R. China

Qualified

Armin, Leonie, Edinburgh
Assemmar, Soundouss, Montreal, Quebec, Canada
Au Siu Tong, Kowloon, Hong Kong
Bai Fangfang, Heze, Shandong, P.R. China
Bai Yuxutao, Anda, Suihua, Heilongjiang, P.R. China
Baker, Jan L., Rockhampton, Queensland, Australia
Ban Yuansheng, Nanning, Guangxi, P.R. China
Berros, Laura, Montigny-lès-Cormeilles, France
Billot, Nathalie, Marseille, France

Proceedings of the Gemmological Association of Great Britain and Notices

Boucher, Edouard, Isle, France
Bouts, Antonia, Amsterdam, The Netherlands
Cai Changhua, Ziyuan, Guangxi, P.R. China
Caussinus, Alice, Beausoleil, France
Cha Liwen, Funing, Jiangsu, P.R. China
Chan Ngai Man, Tsing Yi, Hong Kong
Chang Hsueh-Pin, Taipei, Taiwan, R.O. China
Chao Ting, Taipei, Taiwan, R.O. China
Chen Chun-Wen, Taipei, Taiwan, R.O. China
Chen Jingli, Liuzhou, Guangxi, P.R. China
Chen Lingyu, Shanghai, P.R. China
Cheng Pei-Ling, Taipei City, Taiwan, R.O. China
Chong, Ronald R.K.K., Amsterdam, The Netherlands
Chou Chia Chia, Taipei, Taiwan, R.O. China
Chow Man Man, Shatin, Hong Kong
Chui Chun Hin, Shatin, Hong Kong
Coert, Edward James, Amsterdam, The Netherlands
Dai Qin, Shanghai, P.R. China
Deng Heng, Guilin, Guangxi, P.R. China
Devlin, Janet, Belfast, Northern Ireland
Dishington, Megumi, Shizuoka, Shizuoka Pref., Japan
Elazzouzi Louraoui, Celine, Ile de la Reunion, France
Fan Yun, Beijing, P.R. China
Fang Qiaoling, Hangzhou, Zhejiang, P.R. China
Faure, Florian, Versailles, France
Feng Wei, Guangzhou, Guangdong, P.R. China
Ferder, Edward, Lyndhurst, Hampshire
Fredolin, Christophe, Jurançon, France
French, Lucy, London
Fu Siyi, Beijing, P.R. China
Gauthier, Danielle, Laval, Quebec, Canada
Gellini, Roberta, Nice, France
Geng Yuxin, Huangshi, Hubei, P.R. China
Guo Jing, Shanghai, P.R. China
Guo Mengyan, Hebi, Henan, P.R. China
Guo Yikai, Jieyang, Guangdong, P.R. China
Hammarqvist, Susanne E., Stockholm, Sweden
Harris, Natalie, Merstham, Surrey
Hasselrot, William Anders, Stockholm, Sweden
He Huishi, Zhuji, Zhejiang, P.R. China
Ho Wai Fun, Margaret, Tseung Kwan O, Hong Kong
Homkrajae, Artitaya, Bangrak, Bangkok, Thailand
Hou Hongxi, Hangzhou, Zhejiang, P.R. China
Hou Lu, Montreal, Quebec, Canada
Hu Yue, Shenzhen, Guangdong, P.R. China
Huang Hui Meng, Kaohsiung City, Taiwan, R.O. China
Huang Jen Yu, Taipei City, Taiwan, R.O. China
Huang Shengling, Hepu, Guangxi, P.R. China
Huang Zi-Ning, London
Hughes, Erin Billie, Bangrak, Bangkok, Thailand
Ibison, Hannah, Bowgreave, Lancashire
Jendoubi, Faouzi, Paris, France
Kennedy, Ramona, Brunswick, Victoria, Australia
Kikkawa, Tomomi, Kofu, Yamanashi Pref., Japan
Kitcharoen, Kunakorn, Taling Chan, Bangkok, Thailand
Kuroda, Makiko, Hirakata City, Osaka, Japan
Kwong San Fong, Cathy, To Kwa Wan, Hong Kong
Lai Ruoyun, Lanxi, Zhejiang, P.R. China
Lau Man Wa, Eukice, Mong Kok, Hong Kong
Levy, Elsa, Boulogne-Billancourt, France
Li Jia, Beijing, P.R. China
Li Man Kit, Shatin, Hong Kong
Li Pingting, Wuhan, Hubei, P.R. China
Li Xiaofeng, Lianjiang, Fujian, P.R. China
Li Xin, Kaifeng, Henan, P.R. China
Li Xuemeng, Zhengzhou, Henan, P.R. China
Li Zhidong, Haifeng, Guangdong, P.R. China
Liang Zixin, Dongwan, Guangdong, P.R. China
Lin Jih Hsiang, Taipei City, Taiwan, R.O. China
Ling Yu, Beijing, P.R. China
Liu Jiatong, Lianyungang, Jiangsu, P.R. China
Liu Nianchuan, Yangzhou, Jiangsu, P.R. China
Liu Xiaotong, Zhengzhou, Henan, P.R. China
Liu Yingjiao, Beijing, P.R. China
Lo Yi-Ting, Luzhu Township, Taiwan, R.O. China
Ludlam, Louise, Birmingham, West Midlands
McKenzie, Troy, Greenslopes, Queensland, Australia
Matetskaya, Samantha, Pokrov, Vladimir Oblast, Russia
Matur, Fabienne, Lambesc, France
Mendes, Isabella, Dagnall, Hertfordshire
Meridoux, Marion, Saint-Gervais-les-Bains, France
Ming Lu, Shenzhen, Guangdong, P.R. China
Moore Laja, Sarah Elizabeth, Austin, Texas, U.S.A.
Mukamucyo, Marie-Claire, Montreal, Quebec, Canada
Muyal, Jonathan Daniel, Bangrak, Bangkok, Thailand
Norris, Edward, London
Ouyang Huiping, Shenzhen, Guangdong, P.R. China
Peshall, Jessica Monica Eyre, Pimlico, London
Pino, Loredana, Sestri Levante, Genova, Italy
Qin Yayun, Yulin, Guangxi, P.R. China
Qiu Yun, Conan, Zetland, New South Wales, Australia
Ramanasse, Anthony Heritiana, Ampandrianomby, Antananarivo, Madagascar
Randrianarivony, Cedric Dimakias, Antananarivo, Madagascar
Robinson, Molly, Quenington, Gloucestershire
Rodriguez, Faritza, London
Rongy, Amandine, London
Ryalls, Lucy, Birmingham, West Midlands
Saengbuangamlam, Saengthip, Bang Khun Thian, Bangkok, Thailand
Sang Miao, Taiyuan, Shanxi, P.R. China

Shen Yi, Changzhou, Jiangsu, P.R. China
Sheung Si Lai, Tin Hau, Hong Kong
Siritheerakul, Piradee, Bangrak, Bangkok, Thailand
Skinner, Jasmine Georgina, Birmingham, West Midlands
So Sau Man, Bernadette, Tsing Yi, Hong Kong
Street, Neil, Wilton, Connecticut, U.S.A.
Sun Lin, Wuhan, Hubei, P.R. China
Sun Ruijie, Korla, Xinjiang, P.R. China
Tan Cuiying, Shenzhen, Guangdong, P.R. China
Teissier, Virginie, Marseille, France
Thierrin-Michael, Gisela, Porrentruy, Switzerland
Thompson, Noah, Chiddingfold, Surrey
Tin Zaw Win, May, Pabedan Township, Yangon, Myanmar
Tjioe, Ay Djoen, Montreal, Quebec, Canada
Tsalis, Nicholas Alexander, Wellington, New Zealand
Tseng De-Luen, Taipei, Taiwan, R.O. China
van Gulik, Barbara Sophie, Edam, The Netherlands
Wang Jing, Beijing, P.R. China
Wang Chenfei, Qingyang, Gansu, P.R. China
Wiriya, Songserm, Chiangmai, Thailand
Wong Ying Ha, Kwai Chung, Hong Kong
Wu Yuqi, Xining, Qinghai, P.R. China
Yan Chi Kit, Nicholas, Sai Kung, Hong Kong
Yang Jiong, Tai'an, Shandong, P.R. China
Yang Nan Nan, Beijing, P.R. China
Yang Yilun, Shenzhen, Guangdong, P.R. China
Yoda, Takahiro, Ota-ku, Tokyo, Japan
Yuan Yihao, Wuhan, Hubei, P.R. China
Zhang Ruxiang, Shanghai, P.R. China
Zhang Sisi, Nanyang, Henan, P.R. China
Zhang Yiling, Montreal, Quebec, Canada
Zhang Yingjian, Xiamen, Fujian, P.R. China
Zhao Junlong, Wulumuqi, Xinjiang, China
Zhao Junlong, Beijing, P.R. China
Zhao Yanglan, Beijing, P.R. China
Zheng Juanjuan, Laibin, Guangxi, P.R. China
Zheng Qiuting, Beijing, P.R. China
Zhou Yonghang, Jinhua, Zhejiang, P.R. China
Zhu Lanling, Beijing, P.R. China

Foundation Certificate in Gemmology

Qualified

Adenaike, Bosun, Stevenage, Hertfordshire
Ahlstrom, Shawn, Bordon, Hampshire
Amoaku, Emefa, Ruislip, Greater London
Angel, Natalie, Redditch, Worcestershire
Aubert, Lea, Ivry-sur-Seine, France
Baggott, Sophie, Plymouth, Devon
Bai Xiao, Beijing, P.R. China
Battocchi, Francesca, Nairobi, Kenya
Belahlou, Fatima, Castelnau-le-Lez, France
Berros, Laura, Montigny-lès-Cormeilles, France
Boucher, Edouard, Isle, France
Cao Ri, Bangbu, Anhui, P.R. China
Caplan, Candice, Geneva, Switzerland
Carter, Nicole, Leeds, West Yorkshire
Caruel, Maxime, Ambohidratrimo, Antananarivo, Madagascar
Cazanescu, Cristina, Genova, Italy
Chai Jing, Beijing, P.R. China
Chaisinthop, Yodying, Suan Luang, Bangkok, Thailand
Chan Hang Cheung, Central, Hong Kong
Chen Lei-An, Taichung, Taiwan, R.O. China
Chen Miaofen, Chenxi, Guangxi, P.R. China
Chen Ming-Hsueh, I-Ian Hsien, Taiwan, R.O. China
Chen Qian Ran, Beijing, P.R. China
Chen Qianyu, Guangzhou, Guangdong, P.R. China
Chen Silei, Shanghai, P.R. China
Chen Xiao Ai, Dalian, Liaoning, P.R. China
Cheng Pei Fen, Tai Kok Tsui, Hong Kong
Cheng Qian, Shanghai, P.R. China
Cheng Tsz Yan, Repulse Bay, Hong Kong
Cheng Tze Kin, David, Shatin, Hong Kong
Cherrak, Djamila, Paris, France
Cheung Hoi Fun, Ho Man Tin, Hong Kong
Cheung Lok Yu, Hung Hom, Hong Kong
Cheung Tak Yee, Tseung Kwan O, Hong Kong
Choi Lai Kiu, Kwun Tong, Hong Kong
Choquette, Carolyne, Laval, Quebec, Canada
Chung Yu-Chen, Taichung, Taiwan, R.O. China
Clark, Bryan, Old Saybrook, Connecticut, U.S.A.
Cole, Stephanie, Bournemouth, Dorset
Convert, Nicolas, Mantes-la-Jolie, France
Dai An, Beijing, P.R. China
Dai Li Li, Beijing, P.R. China
De Lamberterie, Isabelle, Ambohidratrimo, Antananarivo, Madagascar
Delaye, Aline, Singapore
Dias Da Rosa, Caroline, Dublin, R.O. Ireland
Disner, Emilie, Geneva, Switzerland
Dray, Marine, Allauch, France
Du Hua Ting, Beijing, P.R. China
Duffy, Alex, Sutton Coldfield, West Midlands
Dunn, Lauren, Trowbridge, Wiltshire
Elazzouzi, Celine, Ile de la Reunion, France
Ellis, Angela, Hamilton, New Zealand
Fan Jing, Beijing, P.R. China
Fang Tzu-Liang, Hualien City, Taiwan, R.O. China
Fang Yi Bin, Beijing, P.R. China
Farmer, Jane, Stratford-upon-Avon, Warwickshire
Fayyer, Irina, Jersey City, New Jersey, U.S.A.

Fiebig, Jim, West Des Moines, Iowa, U.S.A.
Föge, Kerstin, Dijon, France
Forster, Helen, Stanley, County Durham
Fuchs, Alice, Vaud, Switzerland
Fujiki, Otoe, Shibuya, Tokyo, Japan
Gao Manmengxi, Wuzhou, Guangxi, P.R. China
Gaudion, Tina, Gagny, France
Gibson, Jane, Durham, County Durham
Gichonge, Stephen, Kalimoni, Juja, Kenya
Gordon-Finlayson, Camilla Rose, Singapore
Griffon, Denise, Montreal, Quebec, Canada
Guo Bi Jun, Beijing, P.R. China
Gyde, John, Abingdon, Oxfordshire
Hagbjer, Sarah, Lannavaara, Sweden
Hall, Claire-Louise, Newcastle-upon-Tyne, Tyne and Wear
Han Jie, Beijing, P.R. China
Han Ying Hui, Beijing, P.R. China
Hancock, Nancy, London
Harper, Kate, Edgbaston, West Midlands
Hoi Mou Lin, Southern District, Hong Kong
Holland, Katherine, Liverpool, Merseyside
Hon Pui Yee, Kwai Chung, Hong Kong
Hopkins, Gary, East Grinstead, West Sussex
Hou Lu, Montreal, Quebec, Canada
Howard, Naomi, Brussels, Belgium
Hsu Ching Tang, New Taipei City, Taiwan, R.O. China
Hsu Wei Lun, Taipei City, Taiwan, R.O. China
Hsu Yu Lan, Taipei City, Taiwan, R.O. China
Hu Yizhi, Shanghai, P.R. China
Huang Hui-Min, Taichung, Taiwan, R.O. China
Huang Jiajun, Guangzhou, Guangdong, P.R. China
Huang Qiong, Liuzhou, Guangxi, P.R. China
Huang Yong, Beijing, P.R. China
Huang Yu Chih, New Taipei City, Taiwan, R.O. China
Huang Yue, Nanning, Guangxi, P.R. China
Huang Yue, Suzhou, Jiangsu, P.R. China
Hubley, Kate, Pointe-Claire, Quebec, Canada
Hughes, Erin Billie, Bangkok, Thailand
Indorf, Paul D., Chester, Connecticut, U.S.A.
Ip Sui Yee, Bianca, Wan Chai, Hong Kong
Jenner, Kelly, Birmingham, West Midlands
Jiamanusorn, Siriwat, Bangkok, Thailand
Jiang Chen, Beijing, P.R. China
Jiang Wen Hao, Beijing, P.R. China
Jiang Yi Lun, Harbin, Heilongjiang, P.R. China
Kanevskij, Aleksandr, London
Katwal Maygha, Yangon, Myanmar
Kitcharoen, Kunakorn, Bangkok, Thailand
Kitching, Laura, Northampton
Knuckey, Samantha, Prestbury, Cheshire
Korcia, Sandrine, Marseille, France
Kotiranta, Karina, Helsinki, Finland
Kuo Hsin, Taipei, Taiwan, R.O. China
Kwok Hei Tung, Hung Shui Kiu, Hong Kong
Kwok Lai Kwan, Kwai Chung, Hong Kong
Kwong Yiu Pan, Tuen Mun, Hong Kong
Lai Yi-Ying, Taichung, Taiwan, R.O. China
Lam Ching Fei, Sha Tin, Hong Kong
Lam Ka Wang, Tuen Mun, Hong Kong
Lancaster, Sonya, Sutton, Surrey
Langlet, Anna, Stockholm, Sweden
Lau On Ni, Tuen Mun, Hong Kong
Law, Suang See, Singapore
Lee, Elizabeth, London
Lee Chun Man, Godman, Lam Tin, Hong Kong
Lee Tak Yan, Tsing Yi, Hong Kong
Li Chen Xi, Beijing, P.R. China
Li Guo Yi, Beijing, P.R. China
Li Lihui, Shanghai, P.R. China
Li Qiu Cen, Shenzhen, Guangdong, P.R. China
Li Wen Xin, Beijing, P.R. China
Li Ying, Guilin, Guangxi, P.R. China
Liang Lu, Taiyuan, Xian, P.R. China
Liao Chiang-Ching, Erlun Township, Yunlin County, Taiwan, R.O. China
Liao Yi Yi, Beijing, P.R. China
Lim Eng Cheong, Singapore
Lin Zay Yar, Yangon, Myanmar
Lineker-Mobberley, Maryanne, Bridgnorth, Shropshire
Liu Chen Pu, Beijing, P.R. China
Liu Chung Ki, Tin Shui Wai, Hong Kong
Liu Wing Yi, Shatin, Hong Kong
Liu Yun Juan, Beijing, P.R. China
Lloyd, Samantha, Leicester
Lou Xue Cong, Hami City, Xinjiang, P.R. China
Lu Xiao, Beijing, P.R. China
Lutumba, Salomon, Coventry, West Midlands
Ma Kam On, Ma On Shan, Hong Kong
MacLeod, Jennifer, Mint Hill, North Carolina, U.S.A.
Maillard, Celine, Ampandrianomby, Antananarivo, Madagascar
Mak Ho Kwan, Tin Shui Wai, Hong Kong
Mariaud, Jeanne, Marseille, France
Marleau, Diane, Ville Mont-Royal, Quebec, Canada
Marshall, Elizabeth, Hitchin, Hertfordshire
Marshall, Theodora, Weston, Hertfordshire
Mason, Miles, Penryn, Cornwall
Massot, Marie Caroline, Ambatobemore, Antananarivo, Madagascar
Matetskaya, Samantha, Pokrov, Vladimir, Russia
Matthews, Timothy, Knoxville, Tennessee, U.S.A.
Mazouz, Rina, Marseille, France

Middleton, Julie, Lichfield, Staffordshire
Miller, Mona, Portland, Oregon, U.S.A.
Millet, Angélique, Ville d'Avray, France
Mo Hongyan, Nanning, Guangxi, P.R. China
Montmayeur, Bob-John, Ratnapura, Sri Lanka
Moon, Heather, Birmingham, West Midlands
Moore, Anneka, London
Moore Laja, Sarah, Austin, Texas, U.S.A.
Moorhead, Lisa, London
Morris, Charlene, Pyrton, Oxfordshire
Mouralian, Nicole, Montreal, Quebec, Canada
Mukamucyo, Marie-Claire, Montreal, Quebec, Canada
Murphy, Deidre, New Ross, County Wexford, R.O. Ireland
Nakanishi, Masaki, Tochigi Pref., Japan
Nijzink-Brandt, Saskia, Arnhem, The Netherlands
Nunoo, Barbara, Carshalton, Surrey
Occhipinti, Virna, Paris, France
Olie, Caroline, Sainte-Foy-lès-Lyon, France
Oo Hein Naing, Yangon, Myanmar
Ootani, Wakana, Setagaya, Tokyo, Japan
Oz, Iryna, Crimea, Ukraine
Palliyaguruge, Menaka, Battaramulla, Sri Lanka
Papandreou Davakis, Dimitrios, Nea Ionia, Greece
Pasakarnyte, Gintare, Bournemouth, Dorset
Petrou, Natasha, Laval, Quebec, Canada
Platis, Alexandros, Nafpaktos, Greece
Posey, Tina, London
Qin Wenjie, Shanghai, P.R. China
Qu Qi, Paris, France
Rafalimanana, Laza Andriamizaka, Antsirabe, Madagascar
Ramanasse, Anthony Heritiana, Ampandrianomby, Antananarivo, Madagascar
Raynaud, Victoria, Grilly, France
Recchi, Jean, Marseille, France
Rentzias, Alexandros, Trikala, Greece
Rexworthy, Simon, Market Drayton, Shropshire
Rigaud, Matthieu, Bayonne, France
Rimmer, Heather, Lichfield, Staffordshire
Rivens, Lucie, Marseille, France
Rodrigues, Silvio, Geneva, Switzerland
Ruddie, Elaine, London
Saengbuangamlam, Saengthip, Bangkok, Thailand
Saito, Mari, Itabashi, Tokyo, Japan
Sampson, Suzanne, Leicester
San Thinzar Soe, Yangon, Myanmar
Sapault, Jordan, Antony, France
Schoettel, David, Ramatuelle, France
Senior, Lauren J., Leeds, West Yorkshire
Shaw, Stephanie, London
Shekhar, Aarti, New Delhi, India
Shi Xue, Beijing, P.R. China
Shi Yang, Guilin, Guangxi, P.R. China
Shum Tsui Ting, Kwai Chung, Hong Kong
Sim Hwa San, Singapore
Slootweg, Peter, Nootdorp, The Netherlands
Smith, Jennifer, Stourport-on-Severn, Worcestershire
So Yuk Mei, Tuen Mun, Hong Kong
Soe Hnin Wutyi, Yangon, Myanmar
Springham, Melvin, Berlin, Germany
Steventon, Rebecca, Badsey, Worcestershire
Stott, Kelly, Carshalton, Surrey
Sugawara, Naoyuki, Saitama, Japan
Sun Xiyuan, Zhuozhou, Hebei, P.R. China
Sun Xue Ying, Anqing, Anhui, P.R. China
Suttichot, Yuwaluk, Pattani, Thailand
Swaving, Christine, The Hague, The Netherlands
Sze-To On Kiu, Quarry Bay, Hong Kong
Takebayashi, Maya, Yokohama-City, Kanagawa Pref., Japan
Tang Tse Shan, Sai Kung, Hong Kong
Tang Ying, Shanghai, P.R. China
Teissier, Virginie, Marseille, France
Thu Tun Kyaw, Yangon, Myanmar
Tiainen, Heli, Helsinki, Finland
Timms, Andrew, Lancaster
Tsang Kim Po, Tai Kok Tsui, Hong Kong
Tsang Yu Nam, Tin Shui Wai, Hong Kong
Tsang Yuk Tin, Jessica, Yuen Long, Hong Kong
Tseng Yen-Chun, Changhua, Taiwan, R.O. China
Tung Yu-Ying, Taichung, Taiwan, R.O. China
Van Eerde, Christa, London
Wall, Rebecca, London
Wan, Jacqueline, Ho Man Tin, Hong Kong
Wang Jiafen, Shanghai, P.R. China
Wang Yan, Beijing, P.R. China
Wang Yue, Beijing, P.R. China
Wiriya, Songserm, Chiang Mai, Thailand
Wong Chee Po, Sai Wan Ho, Hong Kong
Wong Ling Sum, Olivia, Tuen Mun, Hong Kong
Woodman, Jonathan, Harrogate, North Yorkshire
Wormack, Michael, London
Wu Pin Hua, Taipei City, Taiwan, R.O. China
Wu Wei Ran, Beijing, P.R. China
Wu Zhe, Beijing, P.R. China
Xie Ting Ye, Beijing, P.R. China
Xu, Danbei, London
Xu Jing, Hangzhou, P.R. China
Xu Ting, Shaoxing, Zhejiang, P.R. China
Xu Yan, Beijing, P.R. China
Xue Cen, Shanghai, P.R. China

Yamazaki, Junichi, Kamihei, Iwate Pref., Japan
Yao Junjie, Shanghai, P.R. China
Yeh Hai-Yin, Taichung, Taiwan, R.O. China
Yeung Pui Lam, Choi Wan, Hong Kong
Yokoo, Rie, Ichikawa, Chiba Pref., Japan
Yu Duojia, Qingdao, Shandong, P.R. China
Yuan Yi Rong, Beijing, P.R. China
Yuen Wan Fung, Tai Po, Hong Kong
Zandy, Farhad, Tehran, Iran
Zhang, Jielu, London
Zhang Cheng, Beijing, P.R. China
Zhang Guoqing, Nanning, Guangxi, P.R. China
Zhang Jia, Guilin, Guangxi, P.R. China
Zhang Yiling, Montreal, Quebec, Canada
Zhang Yun, Beijing, P.R. China
Zhang Zhen, Beijing, P.R. China
Zhao Hong, Beijing, P.R. China
Zhao Jia Hui, Beijing, P.R. China
Zhong Chunyu, Shenzhen, Guangdong, P.R. China
Zhou Si Si, Beijing, P.R. China

Diamond Diploma Examination

Qualified with Distinction

Attwood, Amanda, Offenham, Worcestershire
Drouin, Claude, Loughborough, Leicestershire
Evans, Richard H., Harlow, Essex
Gilbert, Tanya, London
Hardy, Sarah, Holyhead, Gwynedd
Ilich, Helen, Haymarket, New South Wales, Australia
Matthews, Timothy, Knoxville, Tennessee, U.S.A.
Shannon, Rebecca, London
Simon, Gowry Raji, Wolverhampton, Staffordshire
Weyers, Stefanus Salomon, Brandhof, Bloemfontein, South Africa
Woodrow, Gillian, Wokingham, Berkshire
Wyndham, Jessica, London
Yuen Lung Hon, Yuen Long, Hong Kong

Qualified with Merit

Barton, Emma, London
Batchelor, Richard, London
Berridge, Jason, Knutsford, Cheshire
Chan Wai Ling, Tin Shui Wai, Hong Kong
Dunn, Lauren, Trowbridge, Wiltshire
Hughes, Beata, Sutton Coldfield, West Midlands
Hunt, Glynis, Knights Enham, Andover, Hampshire
Lally, Jo, Southampton, Hampshire
Marcus, Caroline R., Oxford
Wang Siyu, Beijing, P.R. China
Yang Xiao, Zibo, Shandong, P.R. China
Yuen Shui Ping, Central, Hong Kong

Qualified

Acklam, Sharon E., Hull, East Yorkshire
Barrows, Michael James, Kidderminster, Worcestershire
Beales, Wayne Michael, Hampsthwaite, North Yorkshire
Bragg, Caitlin Louise, Bristol
Brown, Debra, Great Sutton, Cheshire
Burton, Amy Louise, London
Burton, Guy Christopher, London
Chan Yuen Lam, Lucia, Lam Tin, Hong Kong
Choi Yuen Mei, Natalie, Tseung Kwan O, Hong Kong
Chow Tsz Tung, Elizabeth, Shatin, Hong Kong
Duffy, Alexander, Four Oaks, West Midlands
Ferder, Edward, Lyndhurst, Hampshire
Fortunato, Claudio, Erith, Kent
Green, Bradley Giles, Handsacre, Staffordshire
Hancock, Elizabeth Ann, Leatherhead, Surrey
Horst, Kirsti, Trier, Germany
Huang Zi-Ning, London
Karlsson, Patrik, Lidingö, Sweden
Kozhisseril Abdul Haque, Hisana, Arookutty, Kerala, India
Lai King Fung, Tai Po, Hong Kong
Lai Shuk Yu, Kwun Tong, Hong Kong
Lam Koon Fung, Fannade, Wan Chai, Hong Kong
Lam Ming Chi, Sau Mou Ping, Hong Kong
Lee Chi Wing, Sheung Shui, Hong Kong
Lee Man Yu, Tuen Mun, Hong Kong
Liu Ruyi, Beijing, P.R. China
Ma Sin Yue, Kwun Tong, Hong Kong
Ning Pengfei, Harbin, Heilongjiang, P.R. China
Poon Tsz Yan, Tuen Mun, Hong Kong
Reimi, Olesja, Tallinn, Estonia
Rice, Max, Camerton, East Yorkshire
Riley, James, Knutsford, Cheshire
Russell, Lucy, Kidderminster, Worcestershire
Shalyshkin, Alexei, Vancouver, British Columbia, Canada
Shang Qi Qi, Kay, Taipa, Macau
Smith, Jennifer, Astley Burf, Worcestershire
Surensoy, Zubeyde, London
Tan Sifan, Beijing, P.R. China
Timms, Andrew Gibson, Hest Bank, Lancaster

Tsang Ka Kei, Kowloon, Hong Kong
Tsang Wing Hang, Wong Tai Sin, Hong Kong
U Wai Fan, Kowloon, Hong Kong
Wang Anyi, Beijing, P.R. China
Wang Jingying, Southsea, Hampshire
Wang Pengfei, Beijing, P.R. China
Willmott, Karra Jane, Croydon, Surrey
Wong Shuk Yi, Kowloon, Hong Kong
Wong Tik Hin, Tin Shai Wai, Hong Kong
Yam Man Hung, Tseung Kwan O, Hong Kong
Ye Fei Yan, To Kwa Wan, Hong Kong
Yuen Ching Chi, Kowloon, Hong Kong
Yuen Chui Shan, Kau Wa Keng, Hong Kong
Zhang Yuanling, Guangzhou, Guangdong, P.R. China

Membership Subscriptions 2014

The 2014 subscription for Fellow, Diamond and Associate members is £125 and that for Corporate and Gold Corporate members £275. Members paying by direct debit (UK bank accounts only) may take a £25 discount.

James Heatlie
1937–2013

It is with great sadness that I report the death of James (Mac) Heatlie FGA DGA BSc (Hons). He will be forever remembered as a stalwart of the Scottish Gemmological Association (SGA). Mac was a man of few words; he had little regard for 'blethering' and tended to summarize everything he said.

The study of science was his great passion and he took a Degree in Chemistry and Physics at St Andrews University. After university Mac was employed as a Research Scientist with Imperial Chemical Industries and later at Edinburgh Pharmaceuticals Ltd. Following a teacher training course at St Margaret's Training College, Mac taught his beloved sciences at Broughton School and after a few years settled into a role at Telford College, becoming a senior lecturer teaching physics, computing, photography and even hair science with the hairdressing students!

Mac enjoyed sharing his knowledge and interest for the sciences, but his real passion was for gemmology, particularly the study of diamonds. This held his interest for 25 years. Mac did manage to teach gemmology at Telford for a couple of years before he retired in 1994 through ill-health. Exposure to chemicals was one of the key causes of his unusual serious medical condition: doctors only expected him to live six months, a year at the most. Although surviving against the odds, Mac never returned to full health again.

Mac was one of the founding members of the SGA, attending monthly lectures, the annual conference and going on field trips to discover hidden gems. Mac loved the field trips and even when battling with ill-health, he still took to the hills. He was the first to sign up for the SGA field trip to Russia.

Mac spent many hours volunteering at the National Museums of Scotland, identifying minerals from around the world and providing information for the collection. He also tutored and lectured on gemmology — the Gemmology Diploma and the Diamond Diploma courses.

Mac set about making his own gemmological instruments, and those who participated in the gold panning field trip that was part of the 2013 SGA Conference will remember his 'sookers', an essential aid for sucking up gold-bearing gravel.

Shortly after the conference Mac became ill and suddenly but peacefully died at home on Sunday 23 June, aged 76 years.

Mac, you will be remembered for your vast knowledge on so many subjects and your many years of sharing your expertise with students, friends and colleagues. You never let your illness knock you down and showed your strength until the end.

I would like to share with you a line from the *Colour of Magic* by Terry Pratchett, from the Discworld series which Mac loved: "And there were all the stars, looking remarkably like powered diamonds spilled on black velvet, the stars that lured and ultimately called the boldest towards them..."

Our thoughts and sympathy go out to his widow Katalin and son Andrew.

Brian Jackson

Mac Heatlie at the Karkodino demantoid mine, Ural Mountains, Russia. Photo by Maria Alferova.

Gem-A

THE GEMMOLOGICAL ASSOCIATION
OF GREAT BRITAIN

Achieve your potential

Gem-A Gemmology and Diamond Courses

A strong knowledge of gemstones and diamonds will increase customer confidence and boost your sales. Gain that knowledge by studying with the world's longest established educator in gemmology. Graduates may apply for election to Fellowship or Diamond membership of the Association enabling them to use initials FGA or DGA after their name.

GEM-A COURSES

- Gemmology Foundation*
- Gemmology Diploma*
- Diamond Diploma

* Course notes are also available in Simplified and Traditional Chinese, Japanese and French.

STUDY OPTIONS

As well as attending day or evening classes at our headquarters in London, students may study worldwide with the following study options:

- Open Distance Learning (ODL) – Study online with a wealth of online resources
- Accredited Teaching Centres (ATC) – Study at one of our ATCs
- Gem-A Approved Practice Providers (GAPP) – ODL students may visit a GAPP for practical lab classes
- Blended Learning – Online and on-site at our London headquarters

Full details of all courses are given at www.gem-a.com/education.aspx, or call +44 (0)20 7404 3334 or email education@gem-a.com.

Understanding Gems™

Visit www.gem-a.com

The Journal of
Gemmology
2013 / Volume 33 / Nos. 7–8

Contents

Cover Picture: A pair of ancient cameo carvings in garnet. The Hellenistic pyrope-almandine carving on the left (19.1×12.9 mm), probably Queen Arsinoë II of Egypt, is one of most beautiful examples of glyptic art produced in the Classical world and is one of the earliest dated extant cameo carvings in gem garnet. On the right is a pyrope cameo of the head of Eros encircled by a plaque (11.7×9.5 mm). This motif was popular in Roman glyptic of the 1st century BC to 1st century AD. Inv. nos. 81.AN.76.59 (left) and 83.AN.437.42 (right, gift of Damon Mezzacappa and Jonathan H. Kagan). The J. Paul Getty Museum, Villa Collection, Malibu, California. Photo by Harold and Erica Van Pelt. (See 'Greek, Etruscan and Roman Garnets in the antiquities collection of the J. Paul Getty Museum', pages 201–22.)

The Gemmological Association of Great Britain

21 Ely Place, London EC1N 6TD, UK
T: +44 (0)20 7404 3334 **F**: +44 (0)20 7404 8843
E: information@gem-a.com **W**: www.gem-a.com

Printed by DG3 (Europe) Ltd
ISSN: 1355-4565